ISAS - INTERNATIONAL SCHOOL
FOR ADVANCED STUDIES

A Thesis submitted for the Degree of

"Doctor Philosophiae"

Studies on the Large–Scale Structure of the Universe

Candidate

Roberto Scaramella

Supervisor

Professor *D.W. Sciama*

Theoretical Astrophysics Sector

Academic Year 1987/1988

November 1988

TRIESTE

SISSA - SCUOLA
INTERNAZIONALE
SUPERIORE
I STUDI AVANZATI
TRIESTE
Strada Costiera 11

... *"What is the sound of a single hand ?"*

Studies on the Large–Scale Structure of the Universe

Acknowledgments

First I want to acknowledge the people I collaborated with on the work presented in this thesis.

In order of appearance they are: N. Vittorio (who relentless tried to amend my habit of a stochastic renormalization of real numbers, i.e. $4\pi \rightarrow 1$), P. de Bernardis and S. Masi (who tried to help my understanding of the experimental details), F. Occhionero (who is mostly responsible for my working in the field), S. Bonometto (who introduced me to a correlated Universe), and finally G. Baiesi, G. Chincarini, G. Vettolani and G. Zamorani (who, especially the latter two, helped me to get better acquainted with the 'real' Universe).

I want to acknowledge my supervisor D.W. Sciama, for many interesting discussions and insights on various arguments, especially for stressing to me the importance of the Cosmic Microwave Background, and for having given to me the maximum freedom in choosing my topic(s) of research and allowing me to pursue the necessary collaborations.

Many thanks are also due to G.F.R. Ellis, for having brought to my attention the importance of fundamental questions and for having greatly improved the readability of my writing. I want to acknowledge M. Calvani (the 'guru–TEX') for having always been ready to help in all possible ways our student life and research.

I thank the SISSA staff for their helpfulness, as well as my fellows of the astro–group (i.e. my roomate V. Antonuccio, and all other students, post–docs, and visiting professors) for their having made a lively environment and for the patience they have shown in finding a computer terminal always occupied by me. Thanks also to the GM^2/R group (i.e. G. Giuricin, M. Mezzetti, F. Mardirossian, and M. Ramella), for the friendly hospitality they always offered me and the many interesting discussions and collaborations we had. Last, but not least, it is opportune to mention that part of this work stems from the knowledge I acquired through my studies at Cornell: I thank E. Salpeter, S. Shapiro, S. Teukoslky, and I. Wasserman from who I learned so much.

Table of contents

I. Introduction.

I.1 Outline of the thesis' contents.

We have decided to try to have almost self–contained chapters, in each of which there is presented a specific framework together with our contribution to the particular area and to its discussion, because we got interested in several different, albeit related, projects (some of which, not fully exploited, are not presented here). Also, a large part of the work which won't show up directly is the large number of computer codes which have been developed. Numerical work played a very significant part in the present work, although as a tool and not as an end for future applications, as often happens in numerical theses. Hence we will not usually give the details of the computer programs, but only their principles when they are useful. Nevertheless we remark that it often took endless hours to produce a single figure or a single number which is buried in the text.

We have organized the presentation of material according to the cosmological 'clock' (i.e. for different values of the redshift, z): we will discuss first events which refer to an almost primordial epoch (i.e. to the last scattering surface of the Cosmic Microwave Background (CMB), with a redshift, for the effect which is of concern to us, of $z \sim 10^3$), then we pass on to intermediate epochs, those of possible formation of galaxies and clusters of galaxies ($z \sim \mathcal{O}(1)$), and we will end with a discussion concerned with superclusters (SC) at very recent epochs ($z \ll 1$).

Of the following chapters, two (Chap. II and Chap. III) are concerned in detail with the study of possible Large–Scale (LS) fluctuations of the CMB. This topic is of paramount importance to the whole field and to cosmology at large, and indeed these two chapters constitute the core of our thesis' work.

In Chap. II we first discuss the effect we will be concerned with (the Sachs–Wolfe effect) and then develop a new formalism which takes into account, in an exact way, the fact that different experiments get different results even if they are measuring the same fluctuation, because of different sizes of the experimental beams used. This point, which might seem to be trivial, has important consequences. We then present the first meaningful comparison between present results on the LS anisotropies of the CMB.

In Chap. III we pursue further the study of LS CMB anisotropies and implement and enlarge the formalism. We first give a discussion of the effect of the beamsize on observations of possible cosmological hotspots. Then we discuss the results of a recent experiment, and also clarify the validity range of the new results we obtain by a direct application of the results of Chap. II to the data, through a Likelihood Ratio method. We continue with a discussion of how to derive meaningful confidence levels on upper limits for cosmic density fluctuations, from experimental upper limits on CMB LS fluctuations that are quoted in the literature. Then, through Monte–Carlo simulations of different realizations of the CMB last scattering surface, we obtain upper limits on the amplitude of density fluctuations (for the scale invariant spectrum) which are almost one order of magnitude more stringent than those obtainable from the limits on the quadrupole component of the temperature fluctuations. We conclude the Chapter with a discussion of effects which could have caused a recently reported 'bump' in the CMB sky.

In Chap. IV we show the impact that different perturbation spectra, obtained in 'hybrid' models, have on the mass-multiplicity function, evaluated with the Press–Schechter formalism and with approximate formulæ for the peak number density. We then discuss the possible effect of an increase of the amplitude of the galaxy spatial two–point correlation as a function of the limiting intrinsic luminosity of the sample. An explanation of this effect is tentatively given in terms of the theory of biased galaxy formation.

In Chap. V we present and discuss present catalogues of clusters of galaxies

and then concentrate on an analysis of the most recent available one. We discuss the problems of distance estimates through apparent magnitudes, and then derive a relationship with which we obtain distance and density estimates for this new catalogue. We also discuss percolation algorithms including the one we devised and have applied to this recent data. We then pass on to discuss the problem of LS peculiar velocities, which is one of the 'hottest topics' at the moment in this field, and review recent results and methodologies which try to get estimates for the value of Ω_0. We close the chapter and the thesis with a discussion of the most interesting SC we found by our analysis. The interest comes from the fact that this SC is close to us (on a cosmological scale) and is in a very particular position. Being close, this SC can be studied more easily than others which are much further away, and therefore be a source of a wealth of cosmological information. On the other hand, not only is its radial distance of interest, but also its direction: this SC *could* in fact be mostly responsible for the observed peculiar velocity of our Local Group (LG) of galaxies.

I.2 A 'not so large' overview (seeded with comments and afterthoughts).

We will give here only a brief overview of the general framework, having already given in the previous section an outline of the topics discussed in detail in the following chapters.

We first outline some aspects of the Large Scale Structure and its current problems. We prefer not to give detailed references to general problems mentioned in the following, both because of the overwhelming number of references involved and the extremely fast evolution of the topic itself. Therefore we advise the interested reader to start getting acquainted with this field through the many summaries which appear in recent congresses and seminars like, for instance IAU 104–117–124–130, ESO/CERN 1^{st}–2^{nd}–3^{rd}, Texas meetings, and review papers which appear in *Nature*, in *Ann.Rev.A.A*, and in the proceedings of dedicated Enrico Fermi Schools, Erice Schools, and Saas-Fee Schools. At the moment, the only

widely used book which is dedicated to this topic is still Peeble's *The Large Scale Structure of the Universe*†. Problems with this book are the fact that is hardly pedagogical (although it includes almost all the basics) and that it is becoming dated in parts (it is from 1980).

We assume that the reader knows the basics of the cosmological framework that we will always adopt, i.e. the Friedmann–Robertson–Walker (FRW) models (see any book on Cosmology), so we spare ourselves and the reader such discussion and, to fix the notation, just say we adopt the convention $a(t) \propto (1+z)^{-1}$ for the expansion parameter. Usually everything is normalized to the present epoch, so that $a(t) = (1+z)^{-1}$.

The basic problem to start with is how to identify structure: already at this first point there is no clear or definite answer. What is meant by 'structure' ? and what by 'large' ? We do not want to get involved here with such formidable questions, so we will simply say that the topic is the study of inhomogeneities in the 'spatial' distribution of astronomical objects. We put the word spatial between quotes because of what we consider to be is a real problem: most of the available information is tied to our past light cone, therefore we have (and expecially in future will have) to try to take into account evolutionary processes of the possible tracers of Large–Scale structure, as we consider ever larger volumes of space. This problem is, of course, most severe for redshifts of one or more, where the information comes at the present from quasars and Ly_α clouds, although a galaxy has recently been seen at $z \gtrsim 3$!

The main goal of the whole field is to find plausible mechanisms which are capable of generatimg the observed structures, starting from a general cosmological framework, usually that of FRW models. These models are preferred because they are aesthetically simple, but mainly because they find very strong experimental support from the presence and the smoothness of the CMB background (in conjunction with nucleosynthesis arguments). On the other hand these models

† see also *The Structure and Evolution of the Universe* by Zel'dovich and Novikov)

imply (in the synchronous gauge) a complete homogeneity for equal time hypersufaces: in a FRW model the universe is currently described as a continuous fluid with the same composition and temperature everywhere (strictly speaking, the same temperature for each background component on its own when not in thermal equilibrium), which is expanding with a pure Hubble flow. The reality, our reality, is of course very different from this description. Therefore having to work in a definite background (i.e. the assumed FRW models), one is led to the following questions: 'How did departures from the FRW homogeneity arise ? How did these departures lead to the observed objects ? How well can a FRW model describe a situation very different from a homogeneous one ?'

We will be concerned with the part of the second question which refers to epochs which range from after nucleosynthesis up to the present time. The first question is addressed by those working in inflation and other theories concerning the early universe. We will be passive users of the main proposed types of small fluctuations which perturb the original FRW smoothness, and that should grow to the present structures. The third question is still to be fully investigated, and is not even (yet) a pressing problem for most workers in the field. We just want to say here that in our opinion the question: 'Above which scale –if any at all– can the observed universe be approximated as homogeneous ?', deserves the greatest consideration.

As noted above, one could try to say that a structure is defined by the positions of the objects that we use as tracers. Leaving aside for the moment evolutionary and completeness problems, we would like to have the full kinematical description of these tracers in order to try to describe also their dynamics. This means that one would like to know at least six quantities for each tracer, so as to have its position in phase space (i.e. the three components of its position and momentum vectors).

Unfortunately, already at this basic level, we are confronted with great, indeed almost insurmountable , difficulties. Leaving aside for the moment the problem of the mass of the tracer (i.e. going from phase to configuration space), what

fraction of the 'minimal' information is one usually able to achieve ? Most of the information comes from optical catalogues and, ignoring for our purposes the problems that arise in some circumstances (e.g. error boxes on X–ray sources), we can say that the position on the sky is well determined. Hence we have 1/3 of the minimal information. Then, one can sometimes measure a redshift for the object (emission lines, or absorption lines on its own continuum or when it is illuminated from behind). So, under the assumption of a pure Hubble flow, one would get the full minimal information needed, because under this hypothesis redshift→distance (neglecting H_0–value problems) and every object has zero peculiar velocity. Unfortunately, when one goes into some detail the latter assumption breaks down, and one is faced with a decrease of a factor of two in the known fraction of minimal information: this now is only 1/2 (i.e. two position coordinates plus the radial velocity). With great effort and large errors in some cases it is possible to get estimates of the radial distance which are independent of the redshift, so that one attains 2/3 of the minimal information (i.e. the position plus the radial velocity). This, however, seems to be the maximum information than one can reach when the assumption of pure Hubble flow is dropped: what is needed is some method which can directly measure transverse peculiar velocities of galaxies. A more detailed discussion of the topic of peculiar velocities can be found in Chap. V.

Another tremendous problem is that of completeness of the catalogues: most of the time observations have not been made with the explicit purpose of treating large volume of space with the same procedure, so that very often people try to understand something from data which comes from different bands, different depths, and has been obtained by different techniques, so that they have different uncertainty and precision. Hence large amounts of homogeneously taken data, are badly needed. We point out that a large effort in this direction has been made at CfA, whose optical catalogues at $m_{lim} = 14.5$ and $m_{lim} = 15.5$ (at the moment 'the slice') have been milestones in this kind of studies. The same comment applies to Abell's catalogue of clusters of galaxies (more on this in Chap. V).

This is fine, but where is the structure ? What has been observed (especially from optical surveys with measured redshifts) is that galaxies do not fill

the available volume uniformly (in a Poisson sense). This was well known as was the presence of aggregates (i.e. clusters) of the order of hundreds galaxies. Nevertheless, up to a few years ago, say late seventies–early eighties, the large scale structure did not emerge in its full glory. The common picture most people had in mind was that of an almost uniform 'sea' of galaxies, in which were embedded a few clusters, scattered around. This picture suffered dramatic changes when observations showed what theory did not even hint at: the universe is structured on almost all scales for which we have a fair amount of data. The more redshifts became available, the more prominent structures showed up. Giant voids (better: underdense regions) of size several tens of Mpc, filaments in the cluster distribution of size hundreds of Mpc, bubbles in the galaxy distribution with typical diameters of tens of Mpc, detailed radial structure in deep pencil–beam surveys, clustering of quasars and Ly_α clouds, and peculiar velocities of ten percent of the Hubble flow over several tens of Mpc are all phenomena discovered and partly discussed in very recent times (e.g. J.Oort, 1988, *P.A.S.J.* **40**, 1).

One real problem is how to get quantitative measures of the presence of structure, so as to pass from visual descriptions (notorious 'artist's impressions') to solid numbers. This problem has been addressed with a variety of techniques, like filament statistics, Likelihood Ratios, percolation, fractals, multifractals, void probability functions, spanning trees, genus of surfaces, cluster analysis, and correlation functions.

Among these techniques the one most applied, most studied, and the one which has led to the present greatest disputes, is evaluation of the two–point correlation functions (spatial, $\xi(r)$, and angular, $w(\theta)$ with θ sky separation angle; a related discussion can be found in Chap. IV). Observationally it is found that the two–point correlation function is well–described by a power law over a wide range of scales. It is worth noting that, at present, the various arguments about the measured values of the amplitude and slope of the two–point correlation function give an idea of our poor 'understanding + available data', especially because this function should in principle be the most easy to determine. Indeed the two–point correlation function by itself carries very little information, compared to the infor-

mation one needs to fully describe the system (e.g. that obtainable through the void probability function or multifractals). This function is in fact only the first of a hierarchy of functions, which has a height proportional to the number of objects under examination. Only when the distribution of objects is strictly Gaussian, or when some scalings apply among the hierarchy, does the two–point correlation function give an amount of information sufficient to describe the system. This fact can be easily seen by comparing some outputs from N–body codes which simulate different types of collisionless dark matter (e.g. 'hot' and 'cold' types, which at the beginning of the simulation have respectively large and negligible peculiar velocity dispersions). These outputs have the same slope for the two–point correlation function (the amplitude is obtained by rescaling coordinates), but describe strikingly different situations (e.g. filaments, pancakes and large underdensities vs. a hierarchy of finely distributed groups of simulation particles).

This is just to give a feeling for the great uncertainties that theorists are confronted with and which are responsible for the large proliferation of models which attempt (so far unsatisfactorily) to give a vague picture of the processes which led to the formation of what we see (note the 'see').

In fact, for instance, we do not know: the specific value of the basic parameters of the FRW model (i.e. $1/2 \lesssim H_0/(100\,h\,km/s/Mpc) \lesssim 1$, $0.1 \lesssim \Omega_0 h^2 \lesssim 1-3$, $\Lambda =?$), the amount and the type of the main matter components (we have only bounds on the baryonic fraction, $10^{-3} \lesssim \Omega_0 h^2 \lesssim 0.2$ from standard nucleosynthesis calculations), what are/have been the main mechanism(s) of galaxy/cluster formation and which of these two kind of objects formed first (chicken or egg ?), wheter the universe has been completely reionized at late epochs, what produced the cosmic X–ray background (CXB; there is also the recently claimed Infrared one), what is the dark matter which seems to influence dynamics, what is responsible for the lack of neutral intergalactic hydrogen, and lots of other important questions. This level of uncertainty leaves room for very ingenious proposals of different pictures, which sometimes are quite different from each other.

In the literature several examples can be found of tables in which the suc-

cesses and failures of different models are summed up with various marks awarded (a variable number of plusses or minuses according to the authors' taste), so we think it is instructive to present at the end of this Chapter one of the latest (Peebles and Silk, 1988, preprint), as an example of the maze of different classes of theories (each with its own subclasses) which appear in the literature today.

We want then just to sketch the basic strategies in the game: one starts with a given assumption for a density perturbation spectrum (sometimes already with primordial 'objects') and a given composition for the universe contents (the only component which is invariably present is the baryons, but in different percentages and with varying dynamical importance). Then the evolution of such perturbations is followed by use of linear theory, with a particular stress on the possible consequences for temperature fluctuations in the CMB. After this, one enters the no man's land of nonlinear phases, that are usually tentatively tackled with the use of massive N–body computations (which only in recent times achieved the degree of sophistication necessary to –almost– reliably describe a self–gravitating system, and are still very far from being capable of describing the hydro–gravitational coupling really needed). Through these outputs, plus results obtained from the use of semi–linear approximations or linear theory wherever these approaches are still applicable, one then tries to squeeze the original parameters so as to be able to obtain agreement with various observables. If the conflict with some major observational result (and we already noted how these are usually pretty uncertain) is too large, an opportunely different set of initial parameters is then tried with the hope of a better outcome, repeating the whole process.

The large scale structures and measurements constitute a very hard constraint on these theories, essentially because of the large scales, large times, and large amounts of matter involved: it is not easy to move around masses of the order of those involved in superclusters, even in an Hubble time. And this should be done without perturbing the CMB.

It is worthwhile mentioning here a brilliant tactic for circumventing this problem: biased galaxy formation. Roughly speaking, according to this theory, the

high degree of structure that is observed is not completely 'real': the observations give the distribution of the light, not necessarily that of the mass. Therefore, if some process exponentially amplified the light production per unit mass in some particular regions, we would see the bottom of an 'inverse iceberg': a lot of smoke with almost no flames. Hence, paying for the introduction of an additional degree of freedom with a great uncertainty in the possible mechanisms (one could also have anti–bias), one could reconcile the gross inhomogeneities by saying that these, for the most part, are apparent (another bonus is an explanation of the observed differences in clustering amplitudes of galaxies and clusters of galaxies).

On the other hand, there is a fundamental difference in the overall picture: if there is severe biased galaxy (and cluster) formation, the universe should today be pretty unperturbed on large scales, hence with small peculiar velocities. If this were not the case, then, by a mere application of the continuity equation, huge amounts of matter are moving around and have non–negligible peculiar velocities. The latter issue is very important at the present moment (we would say a red–hot issue) and is studied in detail in Chap. V.

We conclude here the 'cubist' picture we sketched above with a general remark on this area of Cosmology–Astrophysics. The field is still in its infancy and this partly explains the high degree of uncertainty which permeates almost all its aspects, but makes it very promising and exciting to work in. On the other hand, we feel it is important also that, while waiting for new, surprising observational results, people who enter this field (including ourselves) should make every possible effort, whenever it is feasible, to go beyond the order–of–magnitude–minded approach which is sometimes taken as an end point instead a starting point. At the same time also more efforts should go into exploring and fully clarifying the basic, fundamental questions that we mentioned above.

A cosmic book

The Cosmological model

1) $\Omega_0 \sim 0.1$ and	
a) zero space curvature	$\mathcal{E}$
b) $\Lambda = 0$	$\mathcal{E}$
2) $\Omega_0 = 1$ with dominant mass in	
a) exotic particles	$\mathcal{E}^2$
b) baryons	$\mathcal{E}^3$
3) New physics:	
a) failure of the inverse square law, a 7^{th} force, ...	$\mathcal{E}^3$

The seeds for galaxies

4) Primeval adiabatic fluctuations	
a) Gaussian and scale–invariant	$\mathcal{E}^2$
b) a specifically tuned power spectrum	$\mathcal{E}^4$
5) Primeval isocurvature fluctuations	$\mathcal{E}^3$
6) Massive cosmic string loops	
a) $G\mu$ needed to make something	$\mathcal{E}^2$
b) $G\mu$ needed for gravitational accretion	$\mathcal{E}^3$
7) Primeval magnetic fields	$\mathcal{E}^2$

The development of galaxies

8) Gravitational instability	$\mathcal{E}$
9) Explosive amplification	$\mathcal{E}^2$

The models

Baryonic adiabatic (2b, 4b, 8)	$\mathcal{E}^8$
Canonical Cold Dark Matter (2a, 4a, 8)	$\mathcal{E}^5$
Cosmic strings loops (2a, 6b, 8)	$\mathcal{E}^6$
Magnetized strings (2a, 6b, 7, 9)	$\mathcal{E}^9$
Baryonic isocurvature (1a, 5, 8)	$\mathcal{E}^5$

$\mathcal{E} < 1$ is an 'a priori', subjective theoretical unit of probability (Peebles and Silk, 1988, preprint). The larger its power, the less likely is the scenario.

II CMB : Large Scale Anisotropies.

II.1 Temperature fluctuations and the Sachs-Wolfe effect.

As already mentioned in the previous chapter, detection of possible anisotropies in the CMB would provide a great wealth of information on the mechanisms which originated the present structure.

On the other hand, notwithstanding almost 30 years of experimental efforts, no cosmological anisotropy in the CMB has been firmly detected, with the exception of a dipole signal. The latter signal, though, is widely believed to be extrinsic and due to our peculiar motion with respect to a uniformly expanding 'cosmic frame', which could be defined in terms of the mean state of motion of the matter at great distances (or in terms of the reference frame in which the CMB itself appear to be uniform at a level just above the current upper limits on intrinsic anisotropies). The reason is that the dipole signal is at a level $((\Delta T/T_b)_{dip} \simeq 10^{-3}$, see Lubin and Villela, 1986) which is almost two order of magnitudes greater than current limits on the quadrupole amplitude and no theory so far seems to be able to account for such a disparity between the amplitudes of these contiguous harmonics. Of course this dipole signal and our inferred peculiar motion are also of great interest to the large scale problems and will be discussed in detail in Chap. IV.

We now return our attention to the intrinsic anisotropies of the CMB, which can broadly be divided in two general, overlapping groups, according to their angular coherence scale on the sky, i.e. on large and small scales.

The Fig. II.1 , taken from a recent excellent review paper (Kaiser and Silk, 1986) illustrates the main features of the problem. From this we can summarize the main properties of the fluctuations which are of interest to us here. The

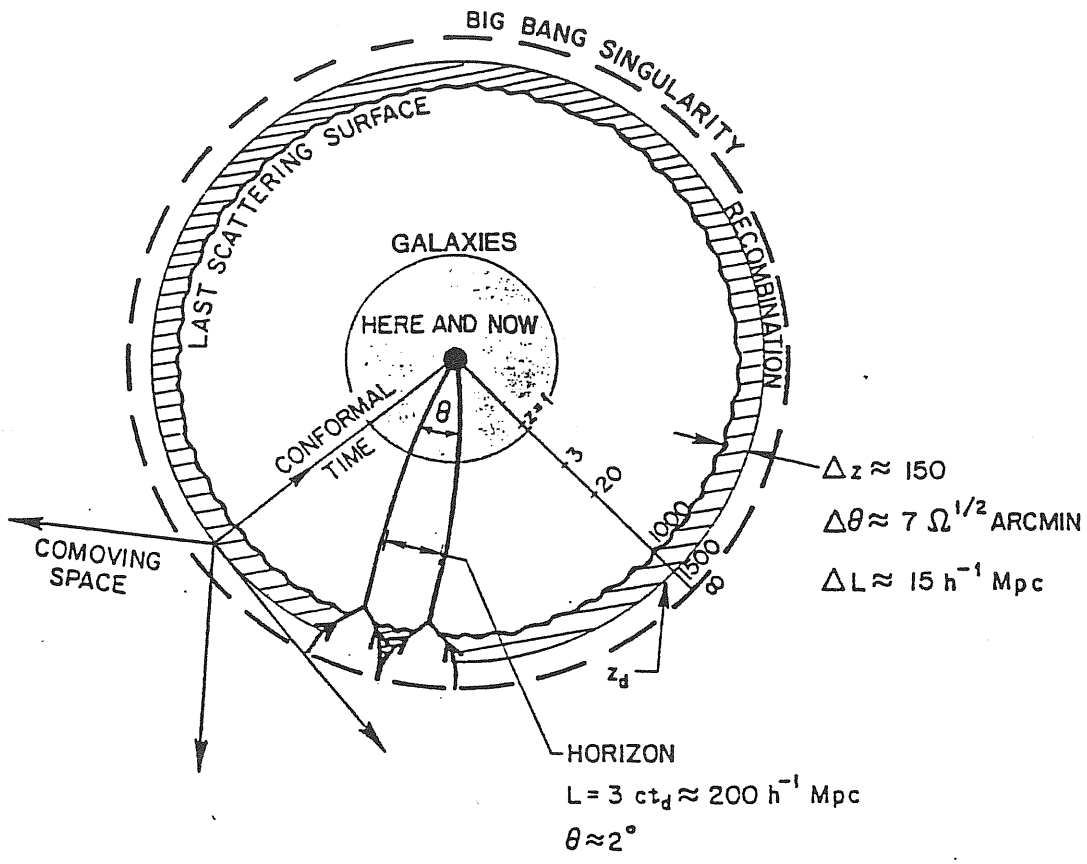

Figure II.1. *A schematic diagram of the standard Big Bang (adopted from Kaiser and Silk, 1986).*

path of most of cosmic photons is assumed to be free after they have left the last scattering surface, composed of ionized and recombining atoms. Because of the finite duration of the recombination process the last scattering surface has a finite depth and, because of photon diffusion, any signal on this scale ($\Delta L \approx 15\Omega_0^{-\frac{1}{2}}\, h^{-1}\, Mpc$, which corresponds to an angular scale of $\Delta\theta \lesssim 8\,\Omega_0^{\frac{1}{2}}\, arcmin$) is washed out (Kaiser and Silk, 1986). The other interesting angular scale is that of the causal horizon at the last scattering epoch, z_d, which is of order $\approx (\Omega_0/z_d)^{\frac{1}{2}}$ and translates to $\Delta\theta_{hor} \sim 2^o$ for $z_d \sim 10^3$. Therefore any temperature anisotropy on scales larger than the latter one should carry information which completely bypasses the effects of possible nonlinear processes, limited by the causal horizon, and can then be directly ascribed to true primordial fluctuations. The angle above which this should hold is however dependent on the actual value of z_d: a possible

energy injection sufficient to ionize again the cosmic baryons ('reheating') and consequently cause the cosmic optical depth τ to again reach unity, would lower accordingly the value of z_d and increase that of $\Delta\theta_{hor}$. In the most extreme case though one would have (Kaiser and Silk, 1986) $z_d \gtrsim 30$ and $\Delta\theta_{hor} \gtrsim 10^o$. Such a scenario would itself cause other temperature perturbations below such scales (Vishniac, 1988). Nevertheless, as long as $z_d > \Omega_0^{-1}$, as occurs in the usual scenarios, a given comoving region of size l_0 essentially subtends the same angle on the last scattering surface (Hogan *et al.*, 1982): $\theta(l_0) \approx (\Omega_0/2c) l_0 H_0$ (a good rule of thumb is that a linear scale of $\sim 100\, Mpc$ subtends $\sim \Omega_0 h$ degrees). Also of importance is the angle subtended by the possible spatial curvature radius, $\Delta\theta_{curv} = \Omega_0/(2(1-\Omega_0)^{\frac{1}{2}})$.

Up to this moment we have not discussed the mechanisms of possible temperature anisotropies because, over the years, dozens of physical effects have been proposed and scrutinized in detail by scores of theorists. Many good reviews on the subject have been written and we dare not give even a mere (probably incomplete) list of these effects. We want just to point out a majority of these effects involve causal processes at recent redshifts, so if we stick to large angular scales we can ignore them for the reasons mentioned in the previous paragraph (some possible exceptions will be discussed at the end of Chap. III).

We therefore will discuss the gravity-induced anisotropies in the context of the standard FRW model and show that even this well studied framework can still give new, interesting results.

We give a brief summary of the general framework, which is that of the study of perturbations of the FRW metric. This approach, pioneered by Lifshitz (1946), consists, as usual in physics, in expressing the perturbed quantities as the unperturbed ones plus a correction, assumed to be small. For instance the perturbed metric is usually written as $g_{\mu\nu} = g^{(0)}_{\mu\nu} + h_{\mu\nu}$, where $g^{(0)}_{\mu\nu}$ is the unperturbed FRW and the perturbation tensor $h_{\mu\nu}$ has negligible components with respect to that of the unperturbed metric tensor in an appropriate reference frame (it is difficult to define the 'smallness' of a perturbation of the metric tensor: see Wald,

1984). Problems can arise because of the possible choices of gauge, resulting in non-physical smoothness or irregularity (Press and Vishniac, 1980). This can be avoided by using the elegant gauge-free approach by Bardeen (1980) (for specific applications to the CMB case, see Abbott and Schaefer, 1987, and Panek, 1987) or by consistently using the time-orthogonal coordinates (Peebles, 1980, sect. 81). The perturbations themselves (e.g. combinations of $h_{\mu\nu}$) can be divided according to their behaviour under coordinate transformation into scalar, vector, or tensorial perturbations (Landau and Lifshitz, 1979). In most scenarios the scalar perturbations are the dominant ones and we will restrict ourselves to these in the present discussion (further information on the other types can be found in Starobinsky, 1983; Abbott and Schaefer, 1987; Fabbri *et al.*, 1987; Linder, 1988).

On large angular scales, for an observer with zero peculiar velocity (cf. the above discussion), the anisotropy is essentially of gravitational origin: cosmic photons from different directions, which leave the last scattering surface from regions that have different gravitational potentials, will suffer a slightly different amount of redshift. This results in their still having black-body spectra (no spectral distortions are induced by gravity alone) but with slightly different temperatures. This effect, introduced by Sachs and Wolfe (1967 henceforth SW), simply amounts to the difference in peculiar potential and its order of magnitude is simply given by $\Delta T/T_b \approx \frac{1}{3}\,\delta\,(\ell/r_0)^2$, where $\delta \equiv \delta\rho/\rho$ is the density perturbation of comoving scale ℓ and and $r_0 \equiv ct_0$ is the present horizon length scale (Kaiser and Silk, 1986); in a flat universe $r_0 = (2c)/(3H_0) \simeq 2000\,h^{-1}\,Mpc$.

We want also to point out that Traschen (1984), and Traschen and Eardley (1986) discussed possible modifications to the canonical approach we will use. These modifications with respect to the SW results, mainly consist in a reduction of the predicted level of temperature fluctuations (for the same amplitude of density pertubations), due to the implementation of general relativistic causal constraints. We will leave to future work the applications of the formalism we develop below to this latter case.

The derivation of the exact SW expression is given by Peebles (1980, sect. 93),

who also neatly summarized the hypotheses under which the following equation is valid (Peebles, 1983):

$$\frac{\delta T(\hat{\gamma}_{12})}{T} = \frac{G\rho_i a_i^2}{3} \int \frac{d^3x}{x} \left[\delta_i(\mathbf{x_2} - \mathbf{x}) - \delta_i(\mathbf{x_1} - \mathbf{x})\right] , \qquad \text{(II.1)}$$

where a is the expansion factor ($a \propto (1+z)^{-1}$), $\hat{\gamma}_{12} = \theta$ is the angle between the directions of the points 1 and 2, separated by $x_{12} \sim 2c\theta/(\Omega_0 H_0 a_0)$, $\mathbf{x}$ are the observer comoving coordinates, ρ is the background density, and the subscripts $i, 0$ denote, respectively, some starting redshift z_i and the present time. The above expression for the SW relation assumes (Peebles, 1983):

a) The optical depth for scattering since z_i is negligibly small.

b) Non-gravitational forces on the scale x_{12} may be neglected.

c) Linear perturbation theory is a good approximation (reasonable because $\delta T/T \sim 10^{-4}$).

d) Initial temperature fluctuations on the starting hypersurface at $z = z_i$ are negligible (indeed $(\delta T/T)_i \sim \delta_i \ll (\delta T/T)_0 \sim \delta_i (a_i x_{12}/t_i)^2$ because the term in the last parenthesis is much greater than unity for $\theta > \Delta\theta_{hor}$).

e) $1 + z_i \gg |\Omega_0^{-1} - 1|$ so that the expansion rate at z_i is well described by the Einstein-de Sitter model.

f) The separation of the two lines of sight is smaller than the radius of curvature of space, so $\theta \ll \Delta\theta_{curv}$.

g) The primeval perturbations are adiabatic.

Concerning the last item we note that the adiabatic assumption is a quite a common scenario, although many others have been considered: for instance a scenario with isocurvature perturbations would simply give a fluctuation ~ 5 times higher than the corresponding adiabatic one with same δ_i, (Efstathiou and Bond, 1986), while isothermal fluctuations with *ad hoc* initial conditions or pure baryonic isocurvature models would give no temperature perturbations on large scales.

It is common practice to Fourier-expand the primordial density perturbation field with respect to comoving wavevectors $\mathbf{k}$ and then solve the linearized equations for the single modes. With this prescription the transform of the peculiar potential for a given $\mathbf{k}$, $\phi_\mathbf{k}$, becomes simply proportional to that of the density perturbation at the same $\mathbf{k}$ (cf. Poisson equation): $\phi_\mathbf{k} \propto \delta_\mathbf{k}/k^2$. Therefore we can

write for the temperature fluctuation along a given line of sight (Peebles, 1980):

$$\Delta(\theta,\phi) \equiv \frac{T(\theta,\phi)}{T_b} - 1 = -B \sum_{\mathbf{k}} \frac{\delta_{\mathbf{k}}}{k^2} e^{i\,\mathbf{k}\cdot\mathbf{r_0}} , \qquad \text{(II.2)}$$

where $|\mathbf{r_0}| \equiv 2c/H_0$, θ and ϕ are angles of direction on the sky, and $B \equiv 2/r_0^2$. It is useful to expand Δ in spherical harmonics:

$$\Delta(\theta,\phi) \equiv \sum_{\ell,m} a_\ell^m \, Y_\ell^m(\theta,\phi) . \qquad \text{(II.3)}$$

Being primarily interested now in the angular dependence we can define the operator $\mathrm{S}_{\mathbf{k}} \equiv -B \sum_{\mathbf{k}} k^{-2} \delta_{\mathbf{k}}$, obtaining $\Delta = \mathrm{S}_{\mathbf{k}}\, e^{i\,\mathbf{k}\cdot\mathbf{r_0}}$ and find an expression for the coefficient of the expansion of Eq. (II.3) by integrating over all possible directions of $\mathbf{r_0}$ (we will drop the subscript from r_0 for the remaining part of the section):

$$a_\ell^m = \int d\Omega_{\mathbf{r}}\, Y_\ell^{m*}(\Omega_{\mathbf{r}})\, \Delta(\Omega_{\mathbf{r}}) = \mathrm{S}_{\mathbf{k}} \int d\Omega_{\mathbf{r}}\, Y_\ell^{m*}(\Omega_{\mathbf{r}})\; e^{i\,\mathbf{k}\cdot\mathbf{r}} . \qquad \text{(II.4)}$$

Now $\mathbf{k}\cdot\mathbf{r} = |k|\,|r|\,\cos\gamma$, where $\gamma = \widehat{\Omega_{\mathbf{k}}\,\Omega_{\mathbf{r}}}$, so we can use the expansion

$$e^{i\,z\,\cos\gamma} = \sum_{n=0}^{\infty} (2n+1)\, e^{i\,\frac{n\pi}{2}}\, j_n(z)\, P_n(\cos\gamma) , \qquad \text{(II.5)}$$

where $j_n(z)$ and $P_n(\cos\gamma)$ are respectively the spherical Bessel function and the Legendre polynomial of order n. Substituting the previous expression in that for a_ℓ^m we get

$$a_\ell^m = \mathrm{S}_{\mathbf{k}} \sum_{n=0}^{\infty} (2n+1)\, e^{i\,\frac{n\pi}{2}}\, j_n(kr) \int d\Omega_{\mathbf{r}}\, Y_\ell^{m*}(\Omega_{\mathbf{r}})\, P_n(\cos\gamma) . \qquad \text{(II.6)}$$

By expanding the Legendre polynomials in spherical harmonics, $P_n(\cos\gamma) = \frac{4\pi}{(2n+1)} \sum_{m=-n}^{n} Y_n^{s\,*}(\Omega_{\mathbf{k}})\, Y_n^s(\Omega_{\mathbf{r}})$, we can take advantage of the orthonormality of spherical harmonics, $\int d\Omega_{\mathbf{r}}\, Y_\ell^{m\,*}(\Omega_{\mathbf{r}})\, Y_n^s(\Omega_{\mathbf{r}}) = \delta_{\ell\,n}\delta_{m\,s}$, and get rid of the last two sums, so find (Peebles, 1980):

$$a_\ell^m = 4\pi\, i^\ell \, \mathrm{S}_{\mathbf{k}} \; j_n(kr) \;\; Y_\ell^{m*}(\Omega_{\mathbf{k}}) . \qquad \text{(II.7)}$$

II.2 Power law spectra and a sketch of the linear theory.

We can pass now from the discrete to the continuous Fourier transform ($\sum_{\mathbf{k}} \rightarrow \int d^3k\,/(2\pi)^3$) and make an important assumption about the primeval density perturbations: that these are described (on spatial hypersurfaces at constant time) by a 3–D Gaussian random field, resulting in a Gaussian distribution for the given Fourier component, which then has a phase totally independent of the other ones. The latter assumption, which has been continuously used over the years, can find its justification from speculations on possible processes which can have generated such fluctuations: it would not be so easy to introduce correlations and phase dependences over scales which exceed the present horizon. On the other hand, the inflation scenario can give possible coherence before or during the inflationary phase to perturbations on such scales (Ortolan *et al.*, 1988 and references therein). The 'standard' proposed mechanism for the generation of these perturbations (Starobinsky, 1982 Guth and Pi, 1982; Bardeen *et al.*, 1983) is zero–point oscillations of the inflaton field and results again in random Gaussian fluctuations.

We note that to take the volume average is equivalent to taking the mean value over the ensemble constituted by all the possible 'fiducial' cosmic observers. This is an important point which will be expanded in Chap. III, where we will discuss in detail the distribution over such an ensemble of the physical quantities which are relevant for the present work.

With the assumption of random phases for the Fourier components, the cross-product of different Fourier components average to zero (Peebles, 1980, sect 46) so that the ensemble average of the square of modulus of Eq. (II.7) becomes

$$\left\langle |a_\ell^m|^2 \right\rangle = (4\pi B)^2 \int \frac{d^3k}{(2\pi)^3} \frac{|\delta_{\mathbf{k}}|^2}{k^4} \left[j_\ell(kr_0)\right]^2 \left|Y_\ell^m(\Omega_{\mathbf{k}})\right|^2 . \qquad \text{(II.8)}$$

It is then convenient to define the average harmonic component as

$$a_\ell^2 \equiv \frac{1}{(2\ell+1)} \sum_{m=-\ell}^{\ell} \left\langle |a_\ell^m|^2 \right\rangle , \qquad \text{(II.9)}$$

and with $(2\ell+1)^{-1} \sum_{m=-\ell}^{\ell} |Y_\ell^m(\Omega_{\mathbf{k}})|^2 = (1/4\pi)$ we get

$$a_\ell^2 = 4\pi B^2 \int_0^\infty \frac{d^3k}{(2\pi)^3} \frac{|\delta_{\mathbf{k}}|^2}{k^2} \left|j_\ell(kr_0)\right|^2 . \qquad \text{(II.10)}$$

The above equation gives the relationship between the average harmonic coefficient and the density perturbation field: once the latter is known, one can easily compute the rms temperature fluctuation, $\Delta^2_{rms} \equiv \langle \Delta^2 \rangle^{\frac{1}{2}}_{\Omega}$, by averaging over the sky the square of Eq. (II.3) (more about this later). So we are led to return our attention to the fluctuation spectrum, $\delta_{\mathbf{k}}$. As noted earlier, as long as the perturbation approach maintains its validity, the Fourier components evolve independently from each other, so that one can write $\delta_{\mathbf{k}}(z) = T(k,z)\,\delta_{\mathbf{k}}(z_1)$, where z_1 is a suitably high initial redshift and the physical details of the model (e.g., component's composition, law of growth for the given mode) are contained in the 'transfer function' $T(k,z)$ (of course $T(k,z_1) \equiv 1$). The latter function is usually computed numerically and brings us back to the problem of the initial conditions, $\delta_{\mathbf{k}}(z_1)$. One of the widest and more commonly adopted choice for initial conditions is to assume them to be scale-free (i.e. without a 'built-in' length scale) and to be described by a power-law spectrum of index n:

$$|\delta_{\mathbf{k}}|^2 = A\ k^n\,, \tag{II.11}$$

where A is an overall normalization constant of fundamental importance to be determined from observable quantities, in that is the main tool to be used in discriminating among models which belong to this class. Possible values for the exponent n are usually taken to be $|n| \lesssim 3$, in order to avoid serious divergences of physical quantities (see for instance the discussion by Peebles, 1980). While gravitational interaction (and momentum conserving processes) can develop a k^4 'tail' (Peebles, 1980; Carr and Silk, 1983), of particular importance is the case $n = 1$, the 'scale-invariant' or Harrison-Zel'dovich spectrum. This initial spectrum has the simple and very nice property of causing the fluctuations to have the same amplitude when they cross the causal horizon (i.e when the physical wavelength of the given mode is comparable to the horizon scale): from this property comes the denomination scale-invariant (although Peebles also proposed this spectrum on the basis that is the one with the smallest degree of divergence, namely logarithmic, Peebles and Yu, 1970)

We now make a crucial, albeit trivial, remark: as shown above the final density field (and related quantities), to be compared with the observations, de-

pends also on the transfer function which is itself a function of the wavevector. Therefore, if still a power law, the final spectrum will have an 'effective' power dependence, n_{eff} on scales of interest which is different from the primordial one, n, and will depend heavily on specific details of the composition of the component of the models, thereby giving very little information on n . We can circumvent this difficulty, however, if we consider only very large scales (small k): these uniformly experienced uninterrupted growth, so that the transfer function is no longer wavevector-dependent but is a function of time only, $T(k,z) \rightarrow T(z)$. This is exactly the case in which the Sachs-Wolfe effect takes place, so from the study of large scale temperature fluctuations in principle we can get informations on *both* the primordial spectral index, n, and the normalization amplitude, A. With such information, as noted above, one can cross-check with the normalization amplitude which is derived from smaller scales (i.e. number counts, peculiar velocities, correlation amplitudes) according to the specific models.

With the above assumption for the spectrum, substituting Eq. (II.11) in Eq. (II.10) , we obtain

$$a_\ell^2 = \frac{B^2\, A\, r_o^{1-n}}{2\pi^2} \int_0^\infty dx\; x^{n-2}\;\; |j_\ell(x)|^2 \;. \tag{II.12}$$

Now, because

$$\int_0^\infty dx\; x^q\;\; [j_\ell(x)]^2 \;\; = \;\; \pi\, 2^{q-2}\; \frac{\Gamma(3-q)}{\left[\Gamma\left(\frac{4-q}{2}\right)\right]^2}\; \frac{\Gamma\left(\frac{2\ell+q-1}{2}\right)}{\Gamma\left(\frac{2\ell+5-q}{2}\right)}\,, \tag{II.13}$$

if we substitute for B its definition, we can finally write (Fabbri *et al.*, 1987; Bond and Efstathiou, 1987)

$$a_\ell^2 = \frac{2^{n-1}\, A}{r_0^{(n+3)}}\; \frac{\Gamma(3-n)}{\left[\Gamma\left(\frac{4-n}{2}\right)\right]^2}\; \frac{\Gamma\left(\frac{2\ell+n-1}{2}\right)}{\Gamma\left(\frac{2\ell+5-n}{2}\right)}\,. \tag{II.14}$$

II.3 The temperature fluctuation autocovariance and the effect of beam smoothing.

As will be discussed in the next section, anisotropy experiments adopt subtraction techniques to detect temperature fluctuations: what is actually measured is the

temperature difference of two separate directions on the sky, then repeated and averaged on (ideally) all the points of the sky which have the same angular separation. We therefore need from the theory a prescription to compute such a value, which is obviously a function of the separation angle.

To this end it is very important to consider the function $C(\alpha)$, the temperature fluctuation autocorrelation function (henceforth acf), which also completely describes the statistical properties of the temperature field because of its Gaussian distribution. We can then define the acf as

$$C(\alpha) \equiv \left\langle \frac{\Delta T}{T_b}(\hat{\gamma}_1) \cdot \frac{\Delta T}{T_b}(\hat{\gamma}_2) \right\rangle \ , \tag{II.15}$$

where $\alpha = \cos^{-1}(\hat{\gamma}_1 \cdot \hat{\gamma}_2)$ and the average is here taken over the whole sky and over the ensemble constituted by all the possible realizations of last scattering surfaces. We will discuss in the next chapter the effects of dropping the latter assumption (i.e. the ensemble average). We note also that $C(0) = \Delta^2_{rms}$.

It is now necessary to derive the relationship between $C(\alpha)$ and the density field. The direct way is to use the results from the previous section, expressing $C(\alpha)$ in terms of the a_ℓ^m's. First we can expand the acf in Legendre polynomials and we will adopt here the definition commonly used in the current literature: we will not consider the monopole term, unobservable by difference experiments, nor the dipole term which is commonly assumed to be of extrinsic origin (cf. discussion in Sect. II.1). Therefore we define:

$$C(\alpha) \equiv \sum_{\ell=2}^{\infty} c_\ell \ P_\ell(cos\,\alpha) \ . \tag{II.16}$$

We now express the coefficients $\{c_\ell\}$ in terms of the $\{a_\ell^m\}$. By the orthogonality of Legendre polynomials we have that

$$c_j = \frac{(2j+1)}{2} \int_{-1}^{1} d(\cos\alpha) \ P_j(cos\,\alpha) \ C(\alpha) \tag{II.17}$$

which can be rewritten by substituting for Eq. (II.3) and for Eq. (II.15) as

$$\begin{aligned} c_j = \frac{(2j+1)}{2} \int_{-1}^{1} d(\cos\alpha)\, P_j(\cos\alpha) \ \times \\ \times \left\langle \sum_{\ell\geq 2,m} a_\ell^m\, Y_\ell^m(\Omega_1) \sum_{n\geq 2,p} a_n^p{}^*\, Y_n^p{}^*(\Omega_2) \right\rangle \ , \end{aligned} \tag{II.18}$$

where Ω_i denotes the angles of the vector γ_i and we use the condition $\alpha = \cos^{-1}(\hat{\gamma}_1 \cdot \hat{\gamma}_2)$. One can expand further the expression above through $P_j(\cos\alpha) = \frac{4\pi}{(2j+1)} \sum_{s=-j}^{j} Y_j^s(\Omega_1) Y_j^{s\,*}(\Omega_2)$ and note that here the average reduces to $< \; > \rightarrow \int d\Omega_1 \int d\Omega_2 \, /(4\pi)^2$. Taking then repeated advantage of spherical harmonics properties one can derive the very simple result (Peebles 1982b):

$$c_\ell \; = \; \frac{1}{4\pi} \sum_{m=-\ell}^{\ell} \left\langle |a_\ell^m|^2 \right\rangle \; = \; \frac{1}{4\pi} \, (2\ell+1) \, a_\ell^2 \; , \tag{II.19}$$

and then get the general expression for the *theoretical* acf (different from the observed one, discussed below):

$$C(\alpha) = \frac{1}{4\pi} \sum_{\ell=2}^{\infty} \, (2\ell+1) \, a_\ell^2 \; P_\ell \, (cos\, \alpha \,) \; . \tag{II.20}$$

which, by Eq. (II.14) , can be rewritten in a compact way showing its dependence on n:

$$C(\alpha, n) = f(n) \; \sum_{\ell \geq 2} \; g(\ell, n) \, (2\ell+1) \; P_\ell \, (cos\, \alpha \,) \; , \tag{II.21}$$

where we have defined $a_\ell^2 \equiv 4\pi \, f(n) \, g(\ell, n)$ so that

$$f(n) \equiv \frac{2^{n-1} \, A(n)}{4\pi \, r_0^{3+n}} \; \frac{\Gamma(3-n)}{\left[\Gamma\left(\frac{4-n}{2}\right)\right]^2} \; , \tag{II.22}$$

where, having in mind the need to confront with observations, we have shown also the dependence on n of the normalization factor A, and

$$g(l, n) \equiv \; \frac{\Gamma\left(\frac{2\ell+n-1}{2}\right)}{\Gamma\left(\frac{2\ell+5-n}{2}\right)} \; . \tag{II.23}$$

Before discussing the issue of the possible formal divergence of the quantity $C(\alpha)$ as derived above, we want to point out that a closed form for Eq. (II.21) can be found for a particular value of n, luckily for the scale-invariant case, $n = 1$ (Starobinsky 1983). In fact we have that $g(\ell, 1) = (\ell - 1)!/(\ell + 1)! = 1/[\ell(\ell + 1)]$ and therefore

$$C(\alpha, n = 1) = f(1) \; \sum_{\ell=2}^{\infty} \; \left[\frac{1}{\ell+1} + \frac{1}{\ell} \right] \; P_\ell \, (cos\, \alpha \,) \; . \tag{II.24}$$

Now we can add and subtract the appropriate monopole and dipole components to complete the sum and take advantage of formula 8.926 in Gradshteyn-Ryzhik (1980) to get

$$C(\alpha) = -\frac{3}{\pi}\, a_2^2 \left\{ ln\left[\sin\left(\frac{\alpha}{2}\right)\right] + \frac{3}{4}\cos\alpha + \frac{1}{2} \right\}, \qquad \text{(II.25)}$$

where we expressed the normalization in terms of the average quadrupole component, a_2^2 (cf. Eq. (II.14)). Indeed this is a common practice and we see that here the quadrupole value is simply proportional to the value of the acf at π lag:

$$C(\pi) = \frac{3}{2\pi}\, a_2^2 \,. \qquad \text{(II.26)}$$

We want now to have a closer look at the expression for $C(\alpha, n)$. For large ℓ the product $(2\ell+1)g(\ell,n) \propto \ell^{n-2}$ so it easy to see that the sum in Eq. (II.21) diverges for $n > 1$ and there is a logarithmic divergence for the scale-invariant case. Of course this nasty behaviour just reflects the divergence present in the power-law assumption for the spectrum. Nevertheless physically there is no need for some sort of renormalization or a modification to the spectrum itself to be applied: there is in fact a natural cutoff which is due to the observing process. Indeed the noted divergent behaviour happens when $\ell \to \infty$: this translates to an ever increasing resolution, $\theta \to 0$ (the zeros of a Legendre polynomial of order ℓ are separated by $\sim 1/\ell$). But only an ideal, perfect detector would be able to record ever increasing angular details: real detectors do not. Real detectors have a given resolution which of course averages out such details. Formally the recorded signal is the convolution of the 'true' intrinsic signal and the detector response function (cfr. discussion in the last section of Chap. III): the ideal detector has a Dirac's delta as response function so that the observed signal and the true one coincide. In the cases considered here (microwave differential bolometers; for a complete review see Partridge, 1988) the detector response function is well described by a 2–D Gaussian function of dispersion σ.

This fact has been considered considered and applied to the CMB first by Doroshkevich *et al.*, (1978), and by Wilson and Silk, (1981), to obtain an expression for the *observed* acf. The former authors gave an approximate solution in integral

form, which we will discuss below, and the latter also gave an (almost) exact integral expression which had then to be numerically integrated. Consequently, because of the integration burden, many authors applied a sort of rule-of-thumb correction which consists in truncate the sum in Eq. (II.16) beyond $\ell_{max} \simeq 1/\sigma$, roughly mimicking the attenuation of harmonics which have many zeros within the beamsize (e.g. Lukash, 1987;Lukash and Novikov, 1987; or Fabbri *et al.*, 1987, who estimate the uncertainty due to this procedure to be at most a factor 2).

We want to show now another solution to the above problem, which will have useful and far reaching consequences.

We will take as a starting point the expression (Wilson and Silk, 1981) for the 'smoothed' acf:

$$C(\alpha,\sigma) = \int_0^\infty \frac{\phi\, d\phi}{2\,\sigma^2}\; C(\phi)\; I_0\left(\frac{\alpha\,\phi}{2\sigma^2}\right)\; \exp\left\{\left[-\left(\frac{\alpha^2+\phi^2}{4\,\sigma^2}\right)\right]\right\} \qquad \text{(II.27)}$$

where I_0 is a modified Bessel function and has been obtained by expanding as far as possible the analytic integration of the double convolution of a Gaussian response function of dispersion $\sigma \ll 1$ with the unsmoothed acf, $C(\alpha)$ (the upper limit of integration was extended from the original 2π to infinity because of the effective cutoff given by the Gaussian which makes the integrand completely negligible much before 2π: usually σ is at most few degrees). If we now expand the unsmoothed $C(\alpha)$ through Eq. (II.20) we can swap the integral and the sum operation because of the uniform convergence of the latter sum to get

$$C(\alpha,\sigma) = \frac{1}{4\pi}\sum_{\ell\geq 2}^{\infty}\; (2\ell+1)\;\; a_\ell^2\;\; w_\ell(\alpha,\sigma)\;, \qquad \text{(II.28)}$$

where we defined

$$w_\ell(\alpha,\sigma) \equiv \int_0^\infty \frac{\phi\, d\phi}{2\,\sigma^2}\; P_\ell(\cos\phi)\; I_0\left(\frac{\alpha\,\phi}{2\sigma^2}\right)\; \exp\left\{\left[-\left(\frac{\alpha^2+\phi^2}{4\,\sigma^2}\right)\right]\right\}\;. \qquad \text{(II.29)}$$

The above integral looks (and is) impressive from a numerical point of view, because of the presence of the highly oscillatory Legendre polynomial (from arguments above we expect in typical situations to have to consider quite high orders, most times larger than $\ell = 50$). The presence of the function I_0 retards only

slightly the Gaussian decrease (its asymptotic behaviour is $I_0(x) \sim e^x$ for large x but $x \approx \phi/\sigma$ because in most cases $\alpha/\sigma \sim$ a few, while the argument of the Gaussian is of course $\sim -x^2/2$).

We tried with little success to evaluate this integral with the use of standard, robust methods (Press *et al.*, 1987), which did not reliably converge even for values of ℓ much smaller than ℓ_{max}. We then implemented a self-made integration routine with an adaptive step size, capable therefore of handling also very rapidly varying integrands and of computing with little error the weights $w_\ell(\alpha, \sigma)$ up to values of $\ell \gtrsim 60 - 70$. Evident, but really time-consuming because of the large number crunching involved ($\sim 30 - 40$ minutes of CPU time on a Vax 8800 for a typical run), is the fact that the weights numerically computed in this way are valid for *given* values of the pair of angles α and σ. This fact would have caused an insurmountable difficulty for the rest of the work, which, as we shall see, required *many* different evaluations of $C(\alpha, \sigma)$.

Hence we tried to fit some interpolating function of α and σ, beginning with the simplest case, e.g. $\alpha = 0$ for which $I_0 \equiv 1$ in the integrand (note that still $P_\ell \neq 1$), and found that a good but not quite perfect representation was the Gaussian form $w_\ell(0, \sigma) \simeq \exp[-(\ell\sigma)^2]$ as could be guessed from the expected behaviour for large ℓ and the dominant part of the integrand (one can rethink the formula as $w_\ell(0, \sigma) \simeq \exp[-(\ell/\ell_{max})^2]$). On the other hand, no simple modifications of the Gaussian seemed to give a good representation of the behaviour of $w_\ell(\alpha, \sigma)$ for $\alpha > 0$.

After several unsuccessful further fitting attempts we tried to look for a modification in the type of approach and used the approximation $P_\ell(\cos\phi) \simeq J_0[2(\ell + 1/2)\sin(\phi/2)]$, which holds for large ℓ (Gradshteyn-Ryzhik, 1980, Eq. 8.722.1), and simply reduces to $P_\ell(\cos\phi) \simeq J_0[(\ell + \frac{1}{2})\phi]$ for $\phi \ll 1$ (cf. Peebles, 1980, sect. 46). This approximation was the key to the problem: we found first an analytical solution for the special case $\alpha = 0$, which is obtained through Eq. 6.631.4 in Gradshteyn-Ryzhik (1980), $w_\ell(0, \sigma) = \exp\{-[(\ell + \frac{1}{2})\sigma]^2\}$ and then the general solution as $w_\ell(\alpha, \sigma) = J_0[(\ell + \frac{1}{2})\alpha]\ \exp\{-[(\ell + \frac{1}{2})\sigma]^2\}$ through Eq. 6.633.4 of

Gradshteyn-Ryzhik (1980). This is very nice, provided that the former approximations are fully satisfied in our situation: indeed this is the case because of the dominance by the Gaussian of the integrand, which becomes negligible for $\phi \gtrsim 4\sigma \ll 1$. Nevertheless we checked this solution against the weights computed directly through the expression of Eq. (II.29) fitting as parameters the arguments in the derived functional forms: the result of the fitting gave an excellent agreement (e.g. fitting as argument $a + b\ell$ gave $a = 1/2$ and $b = 1$ in both the arguments of the Bessel function and the Gaussian with $\alpha > 0$). Such an agreement was maintained when we substituted back the Bessel function with the appropriate Legendre polynomial (another independent confirmation came from the subsequent appearance of the paper by Bond and Efstathiou, 1987, in which was given a similar expression, obtained through different approximations, which agrees with the one discussed here in the large ℓ limit –without the factor 1/2 in the argument of the Gaussian). Therefore we have the following relationship:

$$w_\ell(\alpha, \sigma) = P_\ell(\cos\alpha)\ e^{-[(\ell+\frac{1}{2})\sigma]^2}\ . \qquad \text{(II.30)}$$

With the previous relationship we then obtain *the general expression for the smoothed acf* as

$$C(\alpha, \sigma) = \frac{1}{4\pi} \sum_{\ell=2}^{\infty} \sum_{m=-\ell}^{\ell} \left\langle |a_\ell^m|^2 \right\rangle\ P_\ell(cos\,\alpha)\ e^{-[(\ell+\frac{1}{2})\sigma]^2} \qquad \text{(II.31)}$$

which is valid for arbitrary a_l^m: it does not depend at all on the fact that we are studying a given set of models of anisotropies. The *only* assumptions we made in its derivation are that of a Gaussian beam of dispersion $\sigma \ll 1$ and that $\left\langle a_\ell^m a_p^{s\,*} \right\rangle = \delta_{\ell p}\delta_{ms} \left\langle |a_\ell^m|^2 \right\rangle$.

Although we are completely satisfied with the above formula Eq. (II.30) , which agrees with the direct computations better than a few parts in ten thousands for the relevant values of ℓ (within the estimated precision for the integral computation) and is supported by the analytic solution for the J_0, we had (and still have) the feeling there should exist a complete analytic proof which connects *directly* the integral of Eq. (II.29) with the solution we found. We searched the

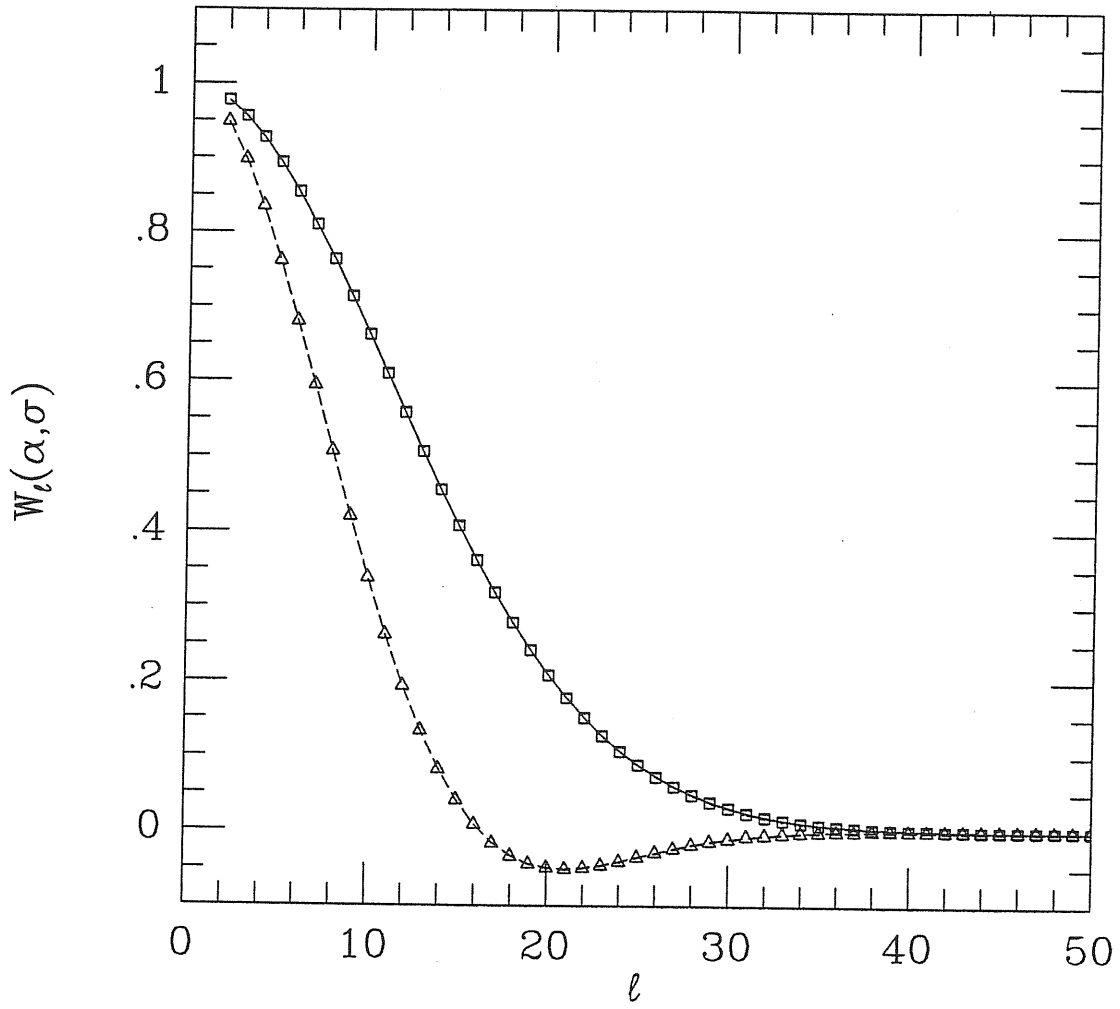

Figure II.2. *The weights $w_\ell(\alpha,\sigma)$ computed from direct integration of Eq. (II.29) , points, are confronted as a function of ℓ, with their simple expression from Eq. (II.30) , lines, for two typical angles and dispersion $\sigma = 3.5°$. Squares and solid line: $\alpha = 0°$, triangles and dashed line, $\alpha = 8°$.*

literature in the hope of finding such a proof without success. For instance, noting that use of the above approximation of the P_ℓ by the J_0 before swapping the integral and sum in Eq. (II.27) gave something similar to a Schlömilch sum was of no use as were similar tentative attempting at further refinements through peering at various tables of transforms (e.g. Hankel transforms).

We therefore did not invest further time on this secondary issue and proceeded to the applications of Eq. (II.30) exploiting its power: the CPU time required for the computation of $C(\alpha,\sigma)$ for a given couple of values α and σ dropped by almost four orders of magnitude and this fact allowed for most of the

results presented in the remaining part of the present Chapter and also most of the next one.

In our particular case of power law density spectra, the general solution given in Eq. (II.31) becomes:

$$C(\alpha,\sigma,n) = f(n) \sum_{\ell\geq 2} g(\ell,n)\,(2\ell+1)\;P_\ell(\cos\alpha)\;\exp\{-[(\ell+\tfrac{1}{2})\sigma]^2\} \qquad \text{(II.32)}$$

which is the form that will be used for the rest of the Chapter.

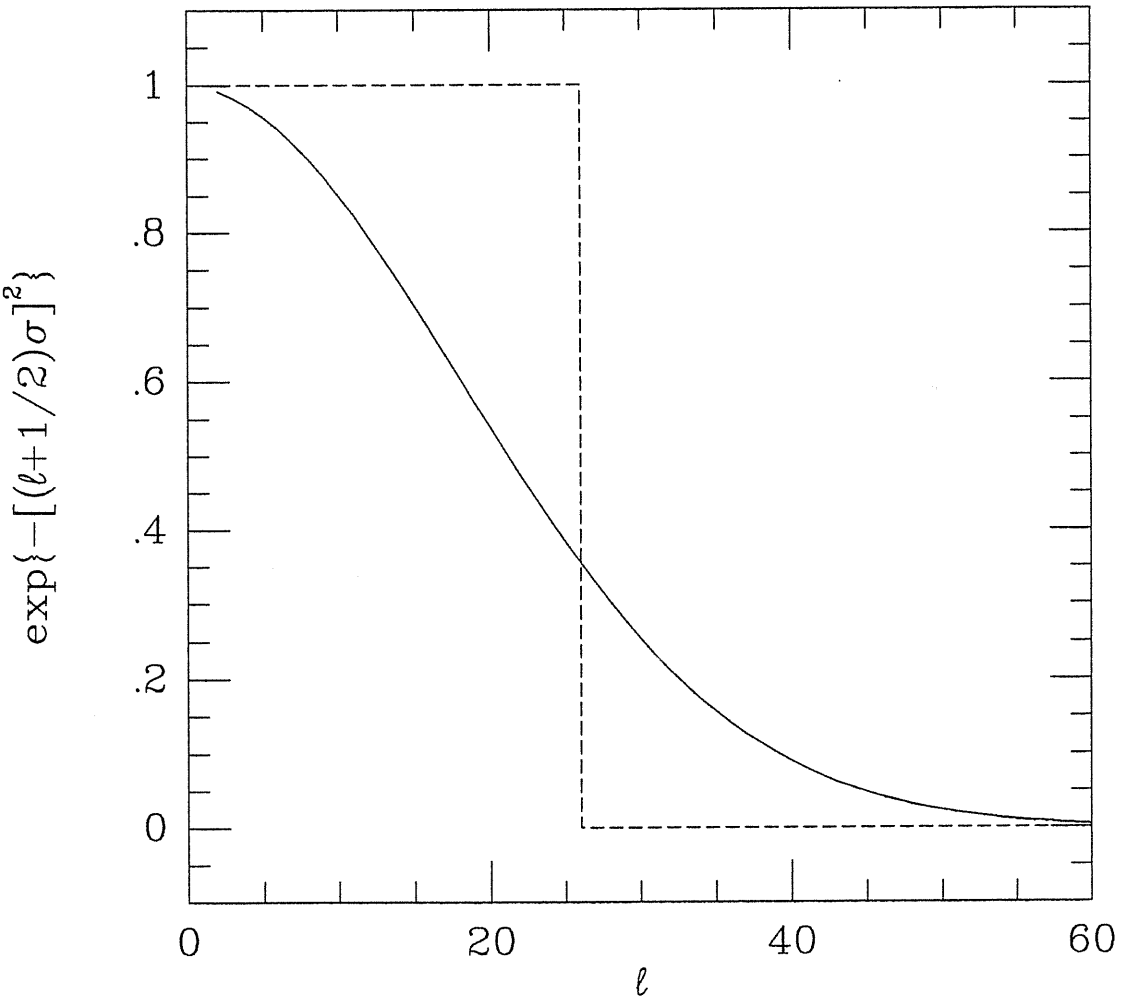

Figure II.3. *The exact weighting (solid line) as a function of the harmonic order, ℓ, is confronted with the rule-of-thumb weighting (dashed line). Here $\sigma = 2.2^o$.*

We want now to confront the solution we obtained for $C(\alpha,\sigma)$ with those appearing in the literature. The rule-of-thumb translates in our formalism into

considering $w_\ell^{r.o.t.}(\alpha,\sigma) = \tilde{\theta}(\ell_{max} - \ell)P_\ell(\cos\alpha)$ where $\tilde{\theta}$ here is the step function. therefore it is sufficient to confront the behaviour of $\exp\{-[(\ell + 1/2)\sigma]^2\}$ as a function of ℓ with a step function up to $\ell = 1/\sigma$ for a typical value, e.g. $\sigma = 2.2^o$. This is shown in Fig. II.3 . The difference is evident, but reflects itself in a inaccuracy which increases with the increase of the assumed spectral index, n. As we already noted above, the ℓ-dependent part of the unsmoothed $C(\alpha)$ (cfr. Eq. (II.21)) goes roughly as $\sim \ell^{2-n}$. Therefore the beam smoothing is not very important for $n \lesssim 0$ and completely uninfluential for $n \to -3$ when only the quadrupole a_2^2 matters. The opposite of course happens for n larger and larger.

We now pass to examine the approximate solution of Doroshkevich *et al.*, (1978). These authors gave the following solution for the smoothed acf in the case $\alpha \ll 1$:

$$C^{(D)}(\alpha,\sigma) = \left(\frac{1}{4\pi}\right) \int_0^\infty k^2\,dk \int_{-1}^{1} d\mu \;\; |i_\gamma|^2 \;\; e^{-(\zeta\sigma)^2} \;\; J_0(\zeta\alpha)\,, \qquad \text{(II.33)}$$

where $\mu \equiv \cos\alpha$, $\zeta \equiv kr_0\sqrt{1-\mu^2}$ (r_0 the same as in Sect. II.2), and in our case the perturbed photon intensity is $|i_\gamma|^2 \propto |\delta_{\mathbf{k}}|^2/k^4 = Ak^{n-4}$. Therefore we have:

$$C^{(D)}(\alpha,\sigma,n) \propto \left(\frac{2A}{4\pi}\right) \int_{-1}^{1} d\mu \int_0^\infty dk \;\; k^{n-2} \;\; e^{-k^2(\xi\sigma)^2} \;\; J_0(\alpha\xi k)\,, \quad \text{(II.34)}$$

where we clearly showed the k dependence by simply putting $\xi = \zeta/k$. The first thing to note is that the above integral is well defined (i.e. converges) only for $1 < n < 3$. For the scale-invariant spectrum one finds again at the origin the logarithmic divergence, as we discussed earlier, that would arise were ℓ not a discrete variable but a continuous one allowed to go to zero (one can make a 'parallel' between the behaviour with respect to the spatial transform, k, and that with respect to the angular transform, ℓ, because the only scale involved, r_0, is a constant). We are then led to consider, for instance, the two cases $n = 2$ and $n = 3$ (the divergence of the latter case can be circumvented as shown below). For this purpose are useful the equations 6.631.5, 6.618.1, and 6.631.4 of Gradshteyn–Ryzhik (1980), with which we solve the second integral of Eq. (II.34) .

It is convenient to consider the smoothed a.c.f. normalized at zero angular

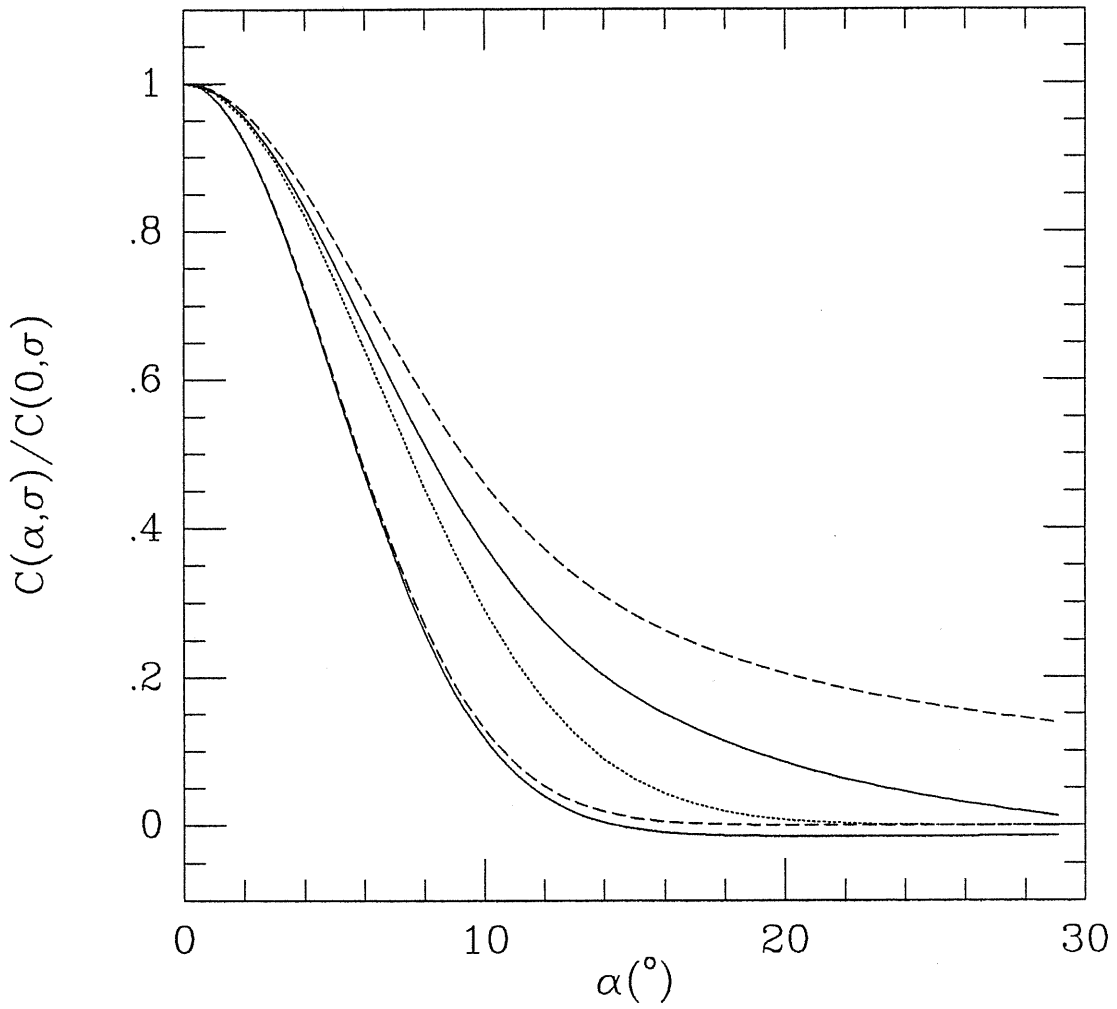

Figure II.4. *The smoothed acf, normalized to zero lag and with $\sigma = 3.5°$, is plotted for the Doroshkevich et al. approximate solution (dashed lines) and the solution from the present work (solid lines); $n = 2$ upper curve, $n = 3$ lower curve. The dotted line is the acf assumed by Davies et al. (see next sections).*

separation:

$$R(\alpha,\sigma) \equiv \left[\frac{C(\alpha,\sigma)}{C(0,\sigma)}\right] . \tag{II.35}$$

Having defined $\theta \equiv 2\sigma$, for the $n = 2$ case we find:

$$R^{(D)}(\alpha,\sigma,n=2) = I_0\left[\frac{\alpha^2}{2\theta^2}\right] \exp\left\{-\left[\frac{\alpha^2}{2\theta^2}\right]\right\} , \tag{II.36}$$

and for the $n = 3$ case:

$$R^{(D)}(\alpha,\sigma,n=3) = \exp\left\{-\left[\frac{\alpha^2}{\theta^2}\right]\right\} . \tag{II.37}$$

In the latter case a logarithmic divergence is present coming from the integral in $d\mu$ which, once solved that in dk, does not depend on the angle α and therefore cancels out from the ratio R.

We can now check the validity range of the Doroshkevich *et al.* approximate solution, by comparison of the $R^{(D)}$ for the above two cases with that obtained from our solution through a direct summation of Eq. (II.32) . This is shown by plotting R in Fig. II.4 as a function of the angle α. The approximate solution is indistinguishable from the correct one in the neighbourhood of the origin, $\alpha = 0$, but, surprisingly, breaks down quite early in the more interesting case $n = 2$, for $\alpha \gtrsim 10 - 20^{\circ}$ (a factor of two of difference for $\alpha = 20^{\circ}$), while we would have rather expected a larger range of validity (even for small values of α, we expect very large discrepancies for $n \gtrsim 1$).

We now can finally show the behavior of $C(\alpha, \sigma, n)$ for different n. This is shown in Fig. II.5 and can be understood by remembering that, for $\ell \gg 1$, $a_\ell^2 \sim \ell^{n-3}$. Hence, for negative n the sum in Eq. (II.32) is dominated by the first few terms. In this case the correlation function is significantly non zero even for large separations, since it is dominated by the low order harmonics and the effect of the finite antenna beam is negligible. On the contrary, for $n > 1$, high order harmonics dominate the sum. The correlation is then very steep, it goes rapidly to zero because of the cancelling contributions of P_ℓ's for large ℓ, and the antenna beam is crucial in introducing a coherence angle in the otherwise scale–free temperature distribution, which would diverge at the origin.

II.4 Currently available experimental results.

We refer to the recent review of Partridge (1988) as the today's best available source of information regarding experiments on the CMB and the inherent difficulties and will limit ourselves to a brief outline of those experiments which are of importance to our discussion.

As noted above, anisotropy measurements are made through *differential* tech-

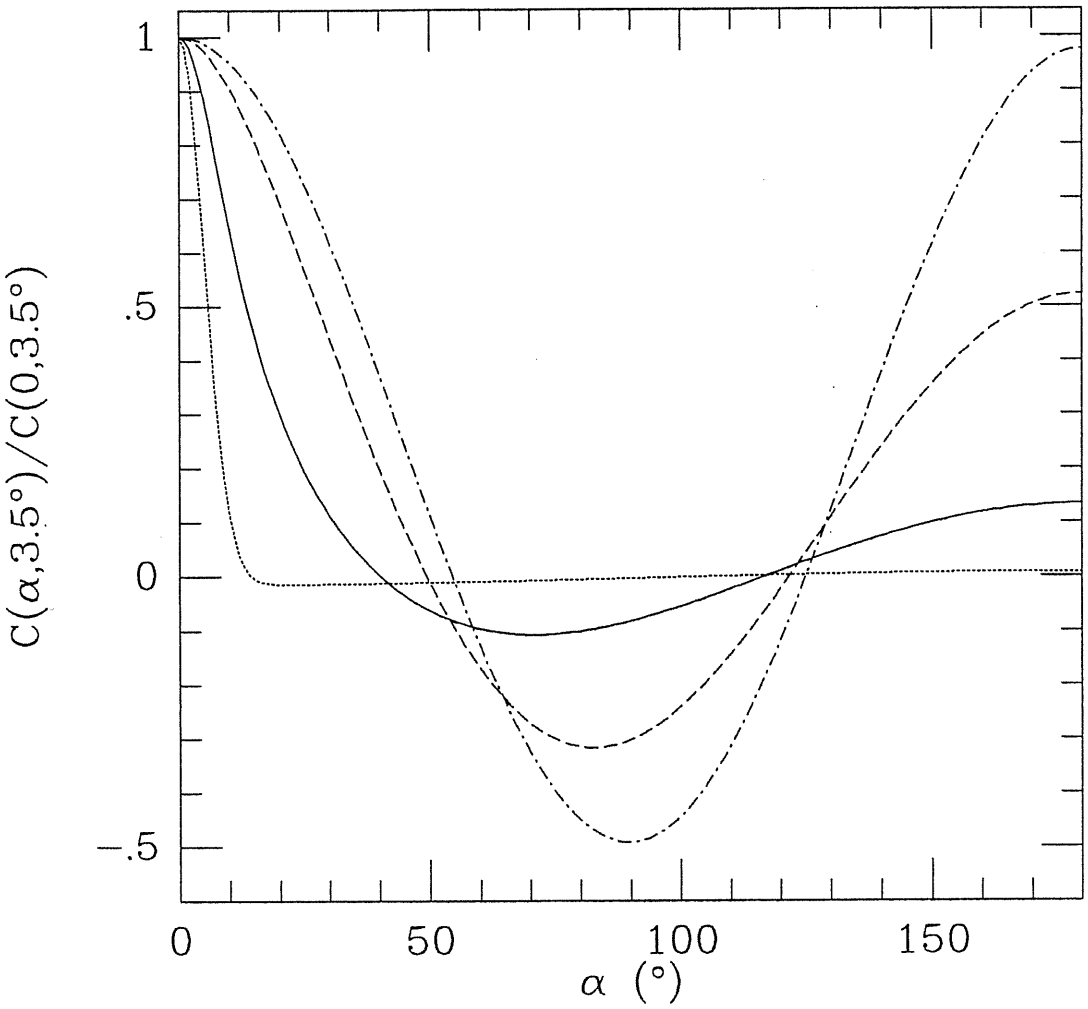

Figure II.5. *The smoothed autocorrelation function, normalized to zero lag, as a function of the sky separation is plotted for different primordial spectral index n; $n = 3$, dotted line; $n = 1$, solid line; $n = -1$, dashed line; $n = -2.9$, dotted-dashed line. Here $\sigma = 3.5^o$.*

niques: through opportune wobbling of mirrors and phase switching the signal from a direction in the sky is compared to that coming from one (or two) other directions.

Two main configurations have been used for large scale anisotropy studies, see Fig. II.6 , which will be referred to as 'single' or 'double beam' subtraction and 'double' or 'triple beam' subtraction respectively (caveat reader from possible confusion !). The double beam subtraction measures the first difference of two directions separated by an angle α on the sky, i.e. simply records the signal $\Delta T = T_A - T_B$ (or viceversa). The triple beam configuration instead subtracts

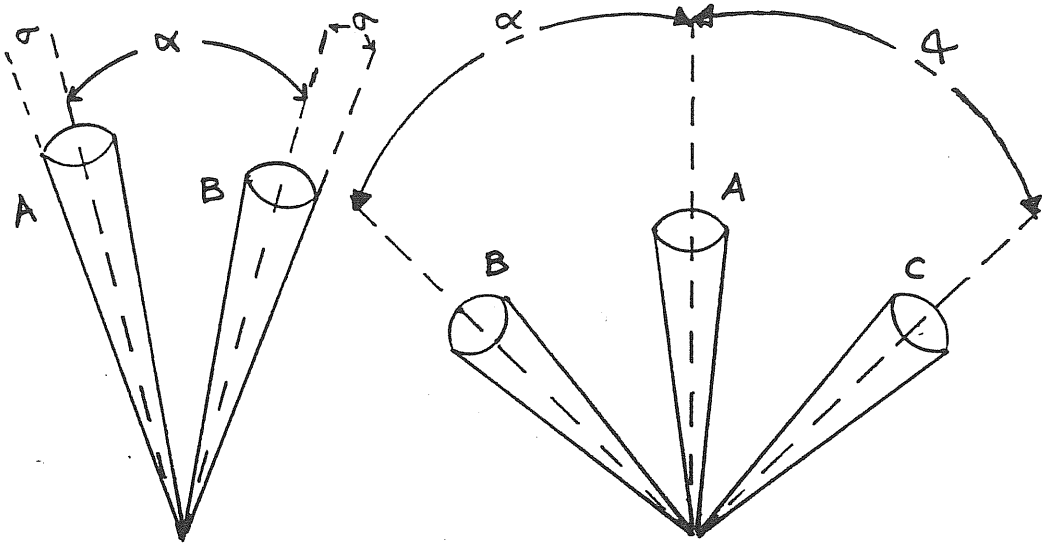

Figure II.6. *A sketch of common experimental configurations: double beam subtraction (left), triple beam subtraction (right). The beamtrough (separation) is α and the beamsize (dispersion) is σ.*

from the signal of the central beam the average of the sum of the signals coming from the two lateral directions, each of which is separated by α from the mid one, so that the recorded signal is the second difference: $\Delta T = T_A - \frac{1}{2}(T_B + T_C)$. It is then trivial, by the use of Eq. (II.15) , to express the squared sky average of temperature fluctuations, Δ^2_{rms} (cf. Sect. II.1), as a function of $C(\alpha)$: for a single subtraction experiment we have

$$\Delta^2_{rms} = 2\ [C(0) - C(\alpha)]\ , \tag{II.38}$$

and for a double subtraction experiment

$$\Delta^2_{rms} = \frac{3}{2}C(0) - 2C(\alpha) + \frac{1}{2}C(2\alpha)\ . \tag{II.39}$$

Therefore, remembering that, by definition, $C(0) = \Delta^2_{rms}$ and with the definition of Eq. (II.35) we can derive the value of the smoothed acf at zero lag directly from the observed temperature fluctuations. In fact, for a single subtraction experiment, we have

$$C(0,\sigma) \ = \ \frac{1}{2}\left(\frac{\Delta T}{T}|_{obs}\right)^2 \cdot [1 - R(\alpha,\sigma)]^{-1} \tag{II.40}$$

or, for a double subtraction experiment,

$$C(0,\sigma) = \left(\frac{\Delta T}{T}|_{obs}\right)^2 \cdot \left[\frac{3}{2} - 2\,R(\alpha,\sigma) + \frac{1}{2}\,R(2\alpha,\sigma)\right]^{-1} . \qquad \text{(II.41)}$$

These relationships are of great importance: they will allow us to relate directly results obtained in experiments which differ, e.g., in the subtraction technique and/or the values of α and/or σ.

We now pass to summarize the experimental data. Because of the experimental difficulties and the sophisticated equipment which is needed, there are not many available observations of the CMB angular distribution on the intermediate and large angular scales.

Fabbri etal (1980) reported a positive detection of CMB temperature fluctuation, which has been commonly considered as an upper limit because of the uncertainties in possible galactic contamination. The experimental configuration involved a single beam subtraction with $\alpha = 6°$ and $\sigma = 2°.2$. The deduced upper limit (Melchiorri *et al.*, 1981, hereafter M)) is, at the 90% confidence level, $\Delta_{rms} < 4 \cdot 10^{-5}$.

More recently, Davies *et al.* (1987, hereafter D) reported also a positive detection of CMB temperature fluctuations. The experimental configuration involved a triple beam subtraction, with $\alpha = 8.2^o$ and $\sigma = 3.5^o$. After applying the Likelihood Ratio method, a value of $C(0,\sigma)^{1/2} = 0.10\,mK/T_b$ was obtained. A Likelihood Ratio analysis requires an explicit guess for the functional form of the temperature correlation function and, due to the Bayesian approach used, it is not straightforward to give confidence levels to the quoted value: this issue will be discussed in great detail in Chap. III. D assumed $C(\alpha,\sigma) = C(0,\sigma)\cdot\exp\left\{-\alpha^2/\left[2\left(2\sigma^2+\theta_c^2\right)\right]\right\}$, with a sky intrinsic coherence angle of $\theta_c \simeq 4^o$. In principle the likelihood results could depend strongly on the assumed functional form for the a.c.f. For example, in the gravitational instability scenarios, for an initial scale free power spectrum (i.e., $|\delta_k|^2 = Ak^n$), at least for $n > 1$ the CMB temperature fluctuation should not exhibit any intrinsic coherence angle. According to the acf assumed by D, we get the value $\Delta_{rms}(8.2^o, 3.5^o) \cong 3.0 \cdot 10^{-5}$ (cfr. Eq. (II.38)).

Experiments with large sky coverage give upper limits on the quadrupole anisotropy. The Berkeley and Princeton groups (hereafter BPG) set $a_2 < 1.1 \cdot 10^{-4}$ at the 90 % confidence level (see , e.g., Lubin and Villela, 1986, for a recent review). Here we take into account the proportionality between a_2^2 as defined here and the $\tilde{Q}_{rms}^2$ used by BPG. According to the Berkeley convention used by these groups, the quadrupole of the temperature fluctuations, which in our notation is $\Delta_2 \equiv \sum_{m=2}^{2} a_2^m Y_2^m$, is written as $\Delta_2 \equiv \sum_{k=1}^{5} \tilde{Q}_k X_k$, where the basis functions $\{X_k\}$ form an orthogonal, but not orthonormal set (here we adimensionalize the coefficients: $\tilde{Q}_j \equiv Q_j^{Berk}/T_b$). These functions are (Smoot and Lubin, 1979): $X_1 \equiv \frac{3}{2}\sin^2\delta - \frac{1}{2}$; $X_2 \equiv \sin 2\delta \cos\alpha$; $X_3 \equiv \sin 2\delta \sin\alpha$; $X_4 \equiv \cos^2\delta \cos 2\alpha$; $X_4 \equiv \cos^2\delta \sin 2\alpha$ (α is the Right Ascension and δ the Declination). By the orthogonality it follows that $\langle \Delta_2^2 \rangle = \sum_{k=1}^{5} \tilde{Q}_k^2 X_k^2$, which, by our definitions, is also $Q_2^2 \equiv \langle \Delta_2^2 \rangle = 5a_2^2$. Expressing therefore the $\{X_k\}$ as linear combination of the $\{Y_2^m\}$ and, taking advantage of the orthonormality of the latter in averaging the squares, one can find that $\langle \Delta_2^2 \rangle = \frac{16\pi}{15}[\frac{3}{4}\tilde{Q}_1^2 + \tilde{Q}_2^2 + \tilde{Q}_3^2 + \tilde{Q}_4^2 + \tilde{Q}_5^2]$ (see also Peebles, 1981). The coefficient $\tilde{Q}_1$ was not actually measured in the quoted upper limit on the average component, so that we have $a_2^2 = \kappa \left\langle \tilde{Q}^2 \right\rangle$, with $\kappa = \frac{4}{5}\frac{16\pi}{15}$.

The Princeton Group (Fixsen *et al.*, 1981, hereafter F) placed also an upper limit on the acf itself : $C(\alpha, 2.9°) < 1.4 \cdot 10^{-9}$ for $10° < \alpha < 180°$.

More recently, the RELIC satellite borne experiment (as quoted by Lukash and Novikov, 1987, hereafter R) set $C(20°, 2.4°) < 5.5 \cdot 10^{-10}$ and $Q_2 < 1.1 \cdot 10^{-4}$ at the 95 % confidence level (there is a factor 4π between our and R's definition of Q_2^2). Assuming $n = 1$ in the fitting procedure makes the latter limit even more severe: $Q_2 < 7.1 \cdot 10^{-5}$.

II.5 The first meaningful comparison of different experiments for various spectral indices.

From the formalism developed in the preceding sections we can see how different experimental configurations can give *different outputs even if they are testing the*

same underlying fluctuations. Indeed often in the literature the figures from different experiments have been taken at face value and compared together, as if they were homogeneous quantities or 'scalar' ones: for instance one would have drawn (as did many workers in the field) the conclusion that the M result, $\Delta_{rms} \sim 4{\cdot}10^{-5}$, was 'above' the D result, $\Delta_{rms} \sim 3{\cdot}10^{-5}$ (note that also several authors mistakenly quote the value $3.7 \cdot 10^{-5}$ for Δ_{rms}, a value which refers instead to the $C(0,\sigma)$ derived according to the D assumed acf !), and similarly that the R acf limit, $C \sim 5.5 \cdot 10^{-10}$, was much 'below' and hence much 'better' (by a factor of ~ 2 !) than the F one, $C \sim 1.4 \cdot 10^{-9}$.

In our opinion this approach is too coarse and can give highly misleading conclusions. Indeed we can think of the *measured* temperature fluctuations as if they were a kind of 'vector' quantity whose numerical value is strongly dependent on the environment (i.e. the experiment) in which the measures were taken. *Meaningful comparisons among results from different experiments can only be made after having reduced these quantities to a common yardstick.* Also, in order to relate fluctuations observed on a given angular scale to those observed on a different one, the assumption of a given law for the autocorrelation properties of the underlying fluctuations field is of fundamental importance. It is obvious therefore that the conclusions which can be drawn have a range of validity which is limited by the latter assumption. For instance, the results of the following discussion can hardly have any meaning but for the assumed power law spectra and could not be applied to others in which, say, primordial processes produced 'kinks' or cutoffs on scales comparable to the one of interest here. On the other hand, whatever the power spectrum, the devised formalism and the related procedures can still be applied quite easily, once a relationship (e.g. some scaling law) among different harmonic coefficients $\{|a_\ell^m|^2\}$ is derived (we will leave for future work possible extensions to non-Gaussian fluctuation cases; the interested reader can find this issue treated by Bonometto *et al.*, 1986, for the 3-D case and by Coles and Barrow, 1987, Coles, 1988, for the CMB case).

Therefore, in order to have a first comparison among the different experiments mentioned in the previous section, we proceed as follows. We assume, for

the time being, that our CMB large scale fluctuations are well described by the $C(\alpha, \sigma)$ obtained through ensemble averaging as in Eq. (II.9) (we will present a more general, proper statistical treatment in Chap. III).

In the following, the comparisons were made through numerical evaluation, by direct summation, of various ratios of the type $C(\alpha', \sigma', n')/C(\alpha, \sigma, n)$.

By using Eq. (II.40) for a given n, we convert the M upper limit on Δ_{rms} to an upper limit on $C(0, 2.2^o)$. Then, using Eq. (II.40) , we evaluate, again for a given n, $C(0, 3.5^o)$, the result that M would have had with a larger beam. Then we take the F upper limit on $C(10^o, 2.9^o)$ and, again through Eq. (II.40) , we evaluate $C(0, 3.5^o)$.

The same procedure is then applied to the R limit on the a.c.f. Similarly, we obtain the same quantity from Δ_{rms}, obtained above for the D experiment and Eq. (II.41) . We have then for each n four values of $C(0, 3.5^o)$: three upper limits (M, F, and R) and one 'detection' (D).

Within our assumptions the comparison between these different experiments (see Fig. II.7) implies that the D 'detection' is consistent with the F and R upper limits only if $n > 1$. The M upper limit implies a rms temperature value *smaller* than the one implied by the D experiment (cf. the naive above conclusions ! –the same is true in the C case for large n). Also, it is more stringent than the F and R upper limits for $n > 1$ (for $n < 1$ the opposite holds). In the same figure is also plotted $C(0, \sigma = 2^o.1)$ obtained from the D result. This curve should predict the result of an ongoing experiment of the same group, carried on with the same α (and double subtraction) but a different σ (FWHM= 5°), under the assumption that the D experiment really provides a positive detection of primordial fluctuations of the type considered here.

The comparison shown in Fig. II.7 is fairly independent on the density parameter Ω_0. In fact, also for $0.2 \lesssim \Omega_0 < 1$, all the curves would have the same relative amplitude. In fact the angles involved are smaller than that subtended by the possible space intrinsic curvature, $\Delta\theta_{hor}$ in Sect. II.1 (Peebles, 1981, 1982a),

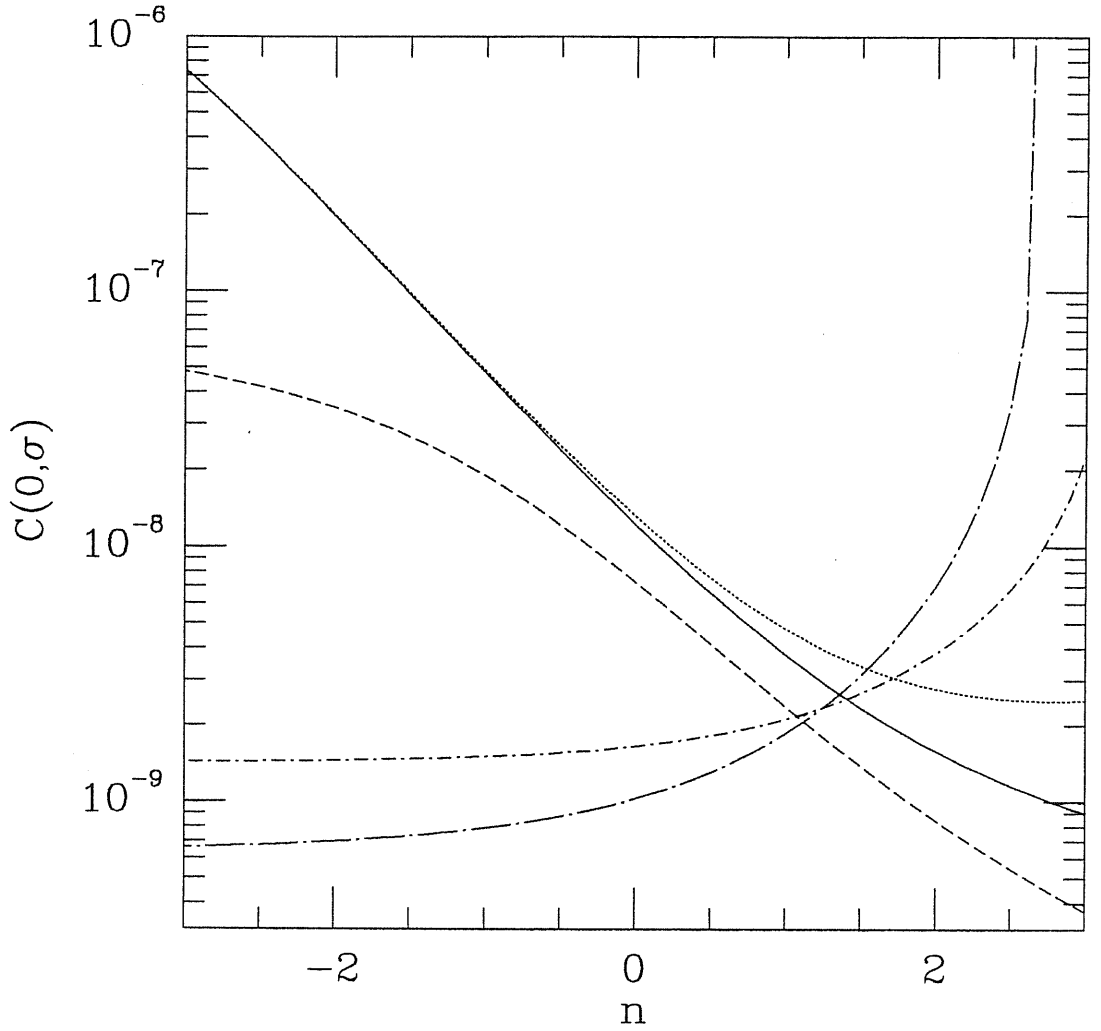

Figure II.7. *The values of* $C(0, \sigma = 3.5°, n)$ *derived from the M (dashed line), D (solid line), F (short dash-dotted line), and R (long dash-dotted line) experiments are plotted vs. the spectral index* n. *The dotted line shows the predicted value* $C(0, \sigma = 2.1°, n)$ *for the new, ongoing D experiment.*

which would accordingly limit the α range of validity of curves in Fig. II.5 .

Another comparison among different experiments can be made by predicting the quadrupole anisotropy implied by the values of $C(0, \sigma)$ deduced from the M, F, and D experiments. The predictions have the meaning of upper limits, except for the one deduced from the D experiment. The $a_2(n)$ derived with the above methods are shown in Fig. II.8 , where we also plot the direct observational upper limits on the quadrupole anisotropy.

The M 'upper' quadrupole is lower than that derived from the D experiment, for any value of the spectral index n. Both curves are consistent with the BPG

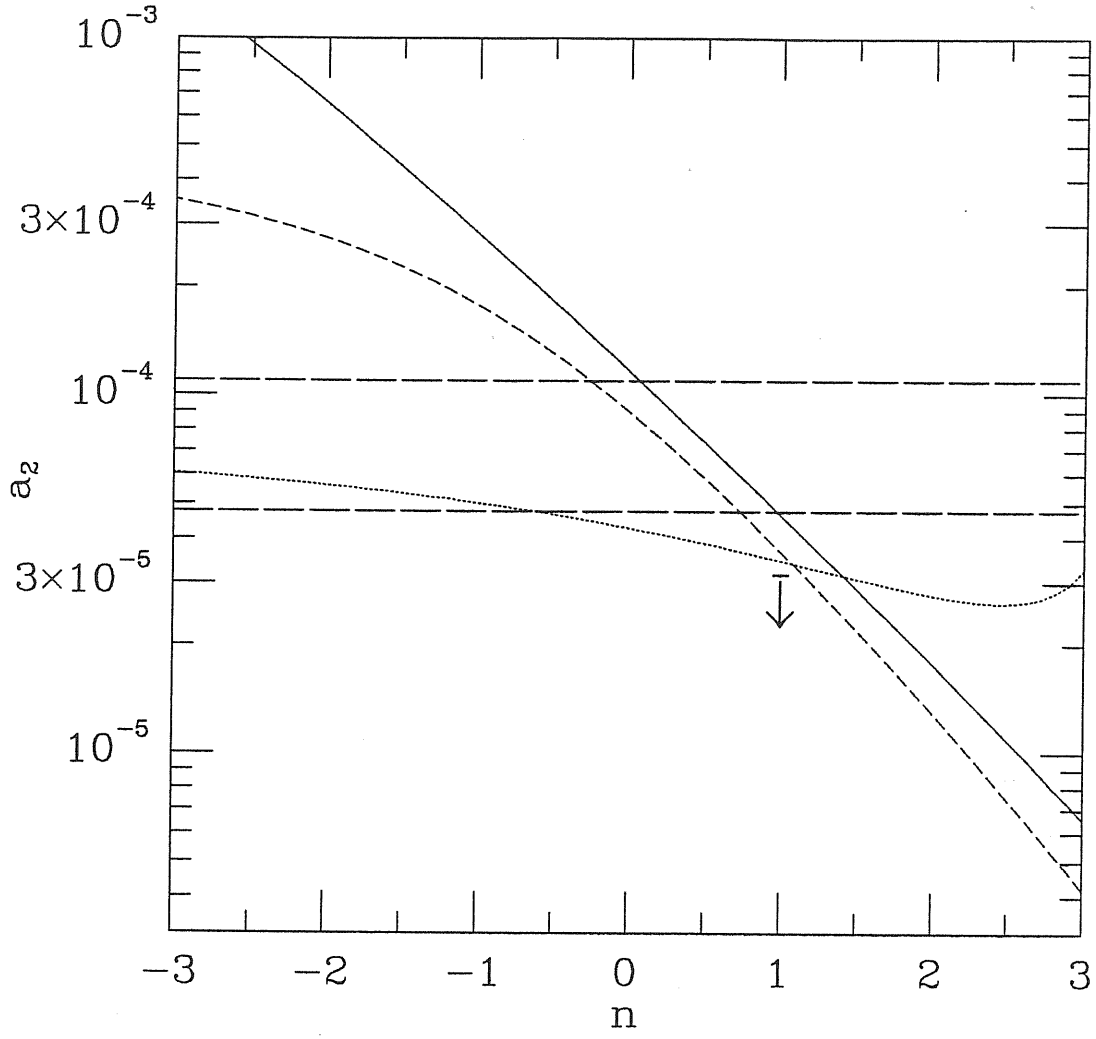

Figure II.8. *The rms quadrupole component derived from the D experiment (solid line) and the 'upper' inferred from M (dashed line) and F (dotted line) experiments are plotted vs. the spectral index n (b, right panel). The direct observational upper limits from the BPG (upper dot-dashed line), and the R (lower dot-dashed line) experiments are also shown. The upper limit set by the R experiment if* $n = 1$ *is shown by the arrow.*

upper limit for $n \gtrsim 0$. Also, the M 'upper' quadrupole is lower than the F 'upper' quadrupole for $n > 1$. The D 'predicted' quadrupole anisotropy is consistent with the R upper limit and with the F 'upper' quadrupole only if $n > 2$ and if $n > 1.5$, respectively.

The comparisons made in Fig. II.8 are valid only for a flat universe: if indeed $\Omega \neq 1$ there is no longer a simple correspondence between the fitted a_2 and the theoretical one as given in Eq. (II.9) because of different relations among the a_l themselves (Wilson, 1982, 1983; Traschen and Eardley, 1986; Abbott and

Schaefer, 1986).

II.6 Brief summary of the chapter.

In this chapter we described a general method which, starting from the analytical expression for the smoothed CMB temperature autocorrelation function, allows one to make several predictions and to check against different experimental results.

We provided a discussion of the dependence of the large scale fluctuations of the CMB on the primordial spectral index n.

From the theoretical point of view, the value $n = 1$ is highly motivated from the standard inflationary scenario (see Turner, 1987, for a review). However, the possibility of having values different from unity for the primordial spectral index should be kept in mind and may arise, for example, in power law inflationary scenarios (see, e.g., Vittorio *et al.*, 1988, and references therein).

If the D experiment really provides a measure of the primordial CMB temperature fluctuations and the RELIC result sets a realistic upper limit on the quadrupole anisotropy we have indications that n should be greater than 1.

This conclusion is also hinted at from a comparison of the $C(0,\sigma)$'s derived from F and D experiments and is then fairly independent of the assumed value of the density parameter Ω_0. We defer a more detailed discussion of the statistical relevance of the latter point on specific cosmological models (Scaramella and Vittorio, 1989), but here we want just to point out that the large scale power implied by the D result would be in contrast with the standard cold dark matter scenario (the disagreement would be even greater for a scenario with positive bias).

All the discussion presented here is independent of the detail of the components of the universe (i.e., presence of dark matter, type of dark matter, etc.). In fact, the intermediate and large scale CMB temperature fluctuations are determined by scales which experienced uninterrupted growth, preserving the primordial spectrum. The assumptions we made are that of a Gaussian, adiabatic,

scale-free initial density fluctuation spectrum and that we live in a typical region of the Universe which is well described by ensemble averages.

Part of the contents of this Chapter have been presented at a meeting held in Trieste (Scaramella and Vittorio, 1988a), and published in the *Astrophysical Journal* (Scaramella and Vittorio, 1988b).

References to Chapter II

Abbott, L.F., and Schaefer, R.K., 1986, *Astrophysical Journal* **308**, 546.

Bardeen, J.M., 1980, *Physical Review D* **22**, 1882.

Bardeen, J.M., Steinhardt, P.J., and Turner, MS., 1983, *Physical Review D* **28**, 679.

Bond, J.R., and Efstathiou, G., 1987, *Monthly Notices of the Royal astronomical Society* **226**, 655.

Bonometto, S.A., Lucchin, F., and Matarrese, S., 1987, *Astrophysical Journal* **323**, 19.

Boynton, P.E., and Partridge, R.B., 1973, *Astrophysical Journal* **181**, 243.

Ortolan, P., Lucchin, F., and Matarrese, S., 1988, *Physical Review D* **38**, 465.

Carr, B.J., and Silk, J., 1983, *Astrophysical Journal* **268**, 1.

Coles, P., 1988, *Monthly Notices of the Royal astronomical Society* **231**, 125.

Coles, P., and Barrow, J.D., 1987, *Monthly Notices of the Royal astronomical Society* **228**, 407.

Davies, R.D., Lasenby, A.N., Watson, R.A., Daintree, E.J., Hopkins, J., Beckman, J., Sanchez–Almeida, J., and Rebolo, R., 1987, Nature **326**, 462.

Doroshkevich, A.G, Zel'dovich, Ya.B., and Sunyaev, R.A., 1978, *Soviet Astronomy (Letters)* **22**, L523.

Efstathiou, G., and Bond, J.R., 1986, *Monthly Notices of the Royal astronomical Society* **218**, 103.

Fabbri, R., Guidi, I., Melchiorri, F., and Natale, V., 1980, *Physical Review Letters* **44**, 1563.

Fabbri, R., Lucchin, F., and Matarrese, S., 1987, *Astrophysical Journal* **315**, 1.

Fixen, D.J., Cheng, E.S., and Wilkinson, D.T., 1980, Phys.Rev.Lett. **44**, 1563.

Gradshteyn, Rhyzik, 1980, *"Table of integrals, series and Products,"*, Academic Press.

Guth, A.H., and Pi, S.Y., 1982, *Physical Review Letters* **49**, 1110.

Hogan, C.J., Kaiser, N., and Rees, M.J., 1982, *Phil.Trans.R.Soc.Lond.A* **307**, 97.

Kaiser, N., and Silk, J., 1986, Nature **324**, 529.

Landau, L.D, and Lifshitz, E.M., 1979, *"Classical Theory of Fields,"*, 4^{th} ed.,

Pergamon Press.

Linder, E.V., 1988, *Astrophysical Journal* **326**,, 517.

Lifshitz, E.M., 1946, *ZhETF* **16**, 587.

Lubin, P., and Villela, T., 1986, in *Galaxy Distances and Deviations from Universal Expansion*, Madore, B.F., and Tully, R.B., eds. D.Reidel Pub. Co.

Lukash, V.N. 1987, I.A.U. Symp. **114**, Kormendy, J., and Knapp, G.R. (eds.), D.Reidel Pub. Co.

Lukash, V.N., and Novikov, I.D., 1987, I.A.U. Symp. **127**, Hewitt *et al.* (eds.), D.Reidel Pub. Co.

Melchiorri, F., Melchiorri, B.O., Ceccarelli, C., and Pietranera, L., 1981, *Astrophysical Journal (Letters)* **250**, L1.

Panek, M., 1986, *Physical Review D* **34**, 416.

Partridge, R.B., 1988, *Rep.Progr.Phys.* **51**, 647.

Peebles, P.J.E., 1980, *"The Large-Scale Structure of the Universe,"*, Princeton University Press.

———————1981, *Astrophysical Journal (Letters)* **243**, L119.

———————1982a, *Astrophysical Journal* **259**, 442.

———————1982b, *Astrophysical Journal (Letters)* **263**, L1.

———————1983, *"The Origin and Evolution of Galaxies,"*, Jones, B.T.J., and Jones, J.E. eds., Reidel Pub. Co.

Peebles, P.J.E., and Yu, J.T., 1970, *Astrophysical Journal* **162**, 815.

Press, W.H., and Vishniac, E.T., 1980, *Astrophysical Journal* **239**, 1.

Press, W.H., Flannery, B.P., Teukolsky, S.A., and Vetterling, W.T., 1986, *"Numerical Recipes,"*, Cambridge University Press.

Sachs, R.K., and Wolfe, M.A., 1967, *Astrophysical Journal* **147**, 73.

Scaramella, R., and Vittorio, N., 1988a, *"Large-Scale Structure and Motions in the Universe,"*, Giuricin, G. *et al.* eds., in press.

Scaramella, R., and Vittorio, N., 1988b, *Astrophysical Journal (Letters)* **331**, L53.

Scaramella, R., and Vittorio, N., 1989, in preparation.

Smoot, G.F., and Lubin, P.M., 1979 *Astrophysical Journal (Letters)* **234**, L83.

Starobinskii, A., 1982, *Physics Letters* **117B**, 175.

———————1983, *Soviet Astronomy (Letters)* **9**, L305.

Traschen, J., 1984, *Physical Review D* **29**, 1563.

Traschen, J., and Eardley, D.M., 1986, *Physical Review D* **34**, 1665.

Turner, M.S., 1987, in *Observational Cosmology: confrontation between theory and experiment*, E. Fermi school proceedings, in press.

Vishniac, E.T., 1988, *Astrophysical Journal* **322**, 597.

Vittorio, N., Matarrese, S., and Lucchin, F., 1988, *Astrophysical Journal* **328**, 69.

Wald, R.M., 1984, *"General Relativity,"*, Univ. of Chicago Press.

Wilson, M.L., 1982, *Astrophysical Journal (Letters)* **273**, L2.

_____1983, *Astrophysical Journal* **273**, 2.

Wilson, M.L., and Silk, J., 1981, *Astrophysical Journal* **243**, 14.

III CMB : Further developments.

III.1 Beam smoothing and sky temperature pattern.

In this Chapter we will show others applications of the formalism developed in the previous Chapter.

In this section we want to extend results given in the literature for the theoretical sky pattern, to obtain the observable pattern which would result from such theoretical skies.

As discussed in Sect. II.2 , the common assumption that the density fluctuation are a Gaussian field in 3-D, will result in a 2-D Gaussian fluctuation field for the CMB sky intensity. Therefore in these models an ideal map of the sky will be pretty rough, showing peaks and troughs of the signal with respect to the average, probably interlaced in a complex pattern. These peaks and troughs are usually nicknamed 'hot' and 'cold' spots, respectively. Now, because of the differential type of anisotropy measurements (see Fig. II.6 and Sect. II.4), it could happen that we receive a signal much higher than the average rms fluctuation: in a single subtraction experiment, for instance, in which the 'left' beam output is subtracted from the 'right' output, the result from a 'lucky' situation, in which the 'left' beam is scanning a, say, $-3\ \Delta_{rms}$ through and at the same time the 'right' beam is scanning a $+2\ \Delta_{rms}$ peak, would be a net total of a $+5\ \Delta_{rms}$ signal amplitude ! This fact is obviously of great importance in trying to exploit the maximum detection probability for a given experiment, by opportunely choosing the best experimental configuration (i.e. type of subtraction, beamthrow and beam dispersion).

The attention on this kind of cosmological hotspots (we will briefly discuss different kinds of spots arising in anisotropic cosmological models in the last sec-

tion of this Chapter) has been first drawn by Zabotin and Nasel'skii (1985) and Sazhin (1985). Then, Vittorio and Juszkiewicz (1987, hereafter VJ) and Bond and Efstathiou (1987) developed this subject further and discussed in detail the quantities of interest for the theoretical sky, i.e. the unsmoothed fluctuation field. On the other hand, both the experiment sensitivity and characteristics are crucial in determining the effective possibility of detecting such spots.

In our case we will discuss the effect of smoothing by the beam only, assuming a comparison among equipment with the same sensitivity. Indeed, a non-detection of high level spots by an experiment with large beam dispersion would not necessarily rule out their existence: a too large beam could have simply averaged out adjacent hot and cold spots because of the poor resolution, completely missing them. This possibility is of course also a function of the shape and spatial frequency of the spots and therefore of the assumed fluctuation spectrum.

Hence, with the previously derived information on the acf, following VJ, we can evaluate the large scale pattern of the CMB temperature distribution, as observed with an antenna of resolution σ, for different primordial spectral indices. All we need (see VJ) is, besides $C(0,\sigma)$, the values of the second and fourth derivative of the acf with respect to α, evaluated at zero lag. These can be calculated from Eq. (II.32) through the approximation (Gradshteyn-Rhizyk; formula 8.722.1), valid for $\phi \ll 1$:

$$P_m(cos\phi) \cong J_0(\eta) + \sin^2\left(\frac{\phi}{2}\right) \left[\frac{J_1(\eta)}{2\eta} - J_2(\eta) + \frac{\eta}{6}J_3(\eta)\right] , \qquad \text{(III.1)}$$

where $\eta \equiv (2m+1)\sin^2(\phi/2)$. Therefore, to compute the quantities (VJ)

$$\begin{aligned} t^2 \equiv & C(0,\sigma) \\ u^2 \equiv & \left(-\frac{d^2}{d\alpha^2}C(\alpha,\sigma)\right)\Big|_{\alpha=0} \\ v^2 \equiv & \left(\frac{d^4}{d\alpha^4}C(\alpha,\sigma)\right)\Big|_{\alpha=0} \end{aligned} \qquad \text{(III.2)}$$

we can expand up to IV$^{\text{th}}$ order in α Eq. (III.1) and substitute for Eq. (II.32) to

get:

$$
\begin{aligned}
t^2 &\propto \sum_{\ell \geq 2} (2\lambda)\, g(\ell, n)\, \exp[-(\lambda\sigma)^2] \\
u^2 &\propto \sum_{\ell \geq 2} (2\lambda)\, g(\ell, n)\, \lambda^2 \left(\frac{1}{2} - \frac{1}{8\lambda^2}\right) \exp[-(\lambda\sigma)^2] \\
v^2 &\propto \sum_{\ell \geq 2} (2\lambda)\, g(\ell, n)\, \lambda^4 \left(\frac{3}{8} - \frac{15}{16\lambda^2}\right) \exp[-(\lambda\sigma)^2] \,,
\end{aligned}
\tag{III.3}
$$

where $\lambda \equiv \ell + 1/2$. The ratios only of these three quantities suffice to determine the values of interest.

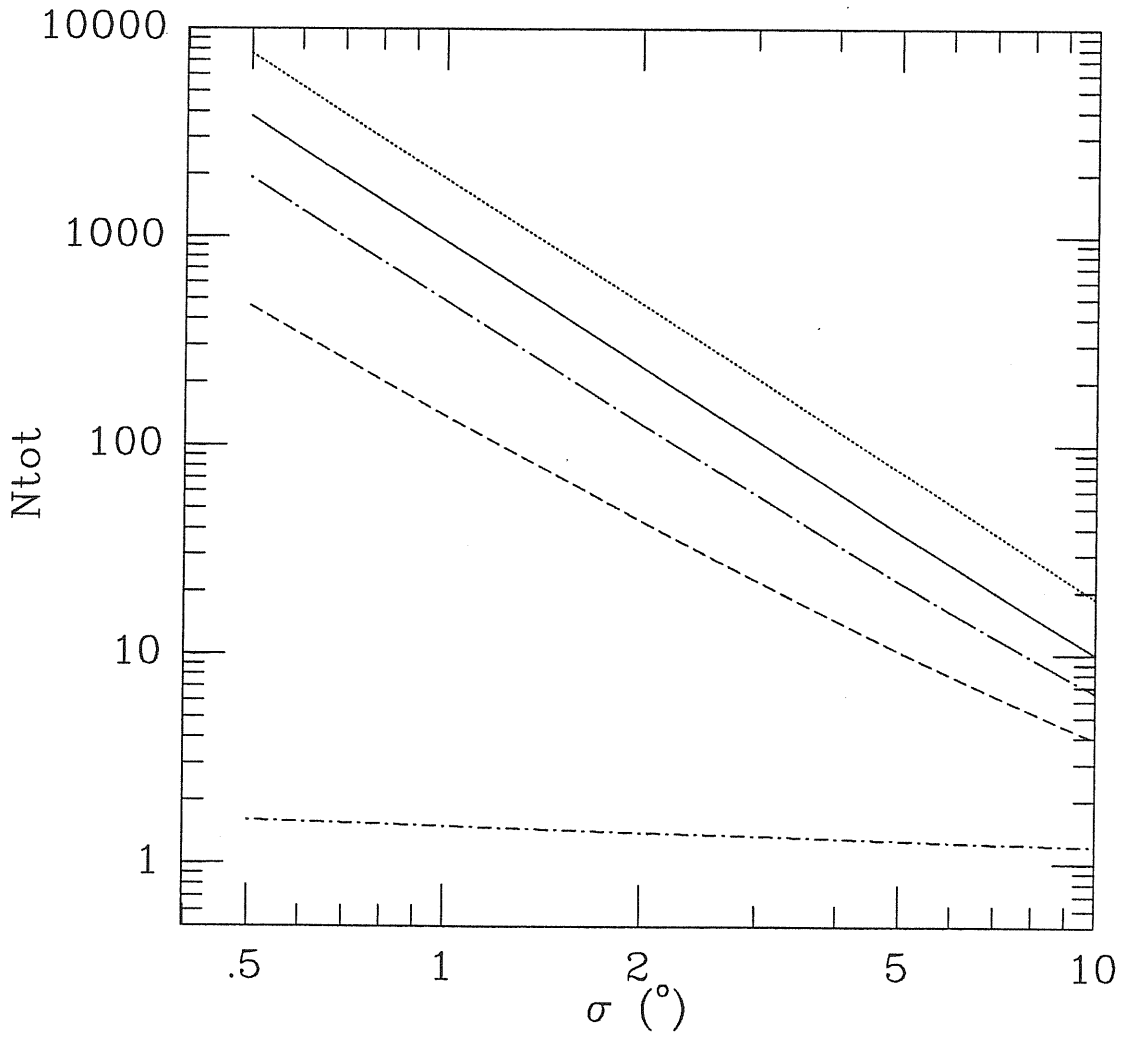

Figure III.1. *The total number of upcrossing regions N_{tot} is plotted as a function of the beamsize σ, for different primordial spectral index n; $n = 3$, dotted line; $n = 1$, solid line; $n = 0$, dotted-long dashed line; $n = -1$, dashed line; $n = -2.9$, dotted-dashed line.*

Then, we can evaluate the total number of maxima in the CMB temperature distribution, expected in all the sky as (VJ)

$$N_{tot} = \frac{2}{3\sqrt{3}} \left(\frac{v}{u}\right)^2 . \qquad \text{(III.4)}$$

This number is plotted in Fig. III.1 as a function of the antenna beam σ, for different values of the primordial spectral index n.

For $n < -2$ the quadrupole is the dominant harmonic and the number of maxima is slightly above 2 as it should exactly be for a pure quadrupolar pattern. For $-1 < n < 3$, the total number of detectable hot spots is to a very good approximation proportional to σ^{-2}, the resolution of the antenna. For these values of n, the temperature distribution is scale free and the only characteristic scale involved is the antenna beam size. As noted in VJ, this implies that the temperature fluctuations in the CMB due to the Sachs-Wolfe effect mimic unresolved sources: their number continuously increases on improving the antenna angular resolution.

From an observational point of view, however, one is interested in the number of regions in the sky where the temperature fluctuation is higher than the threshold ν times the rms temperature fluctuations [i.e., $t = C^{1/2}(0,\sigma)$ as from Eq. (III.2)]. If these regions are sufficiently abundant and large, one could look for rare but very hot spots in the sky. The number of hot spots is well approximated, for $\nu \gg 1$, by (see, VJ):

$$N_{up} \; = \; N_*(\sigma, n) \; \cdot \nu \; e^{-\frac{1}{2}\nu^2} . \qquad \text{(III.5)}$$

The function $N_*(\sigma, n)$ is plotted in Fig. III.2 , as a function of σ, for different values of the spectral index n. For $n > 2$, $N_*(\sigma, n) \propto \sigma^{-2}$. For smaller values of n, the dependence on σ is weaker and weaker. In fact, lowering n reduces the small scale (relative to the large scale) power and having a finite antenna beam becomes irrelevant. Eventually, only the quadrupole matters and N_* tends to 2. If only the quadrupole is present, however, $C^{1/2}(0) = \sqrt{\frac{5}{4\pi}}\, a_2$ (cfr. Eq. (II.20)). Then looking for regions with $\nu \gg 1$ (the limit in which Eq. (III.5) is valid) implies looking for very improbable values for the quadrupole anisotropy. Hence the actual number, N_{up} of hot spots tends to zero.

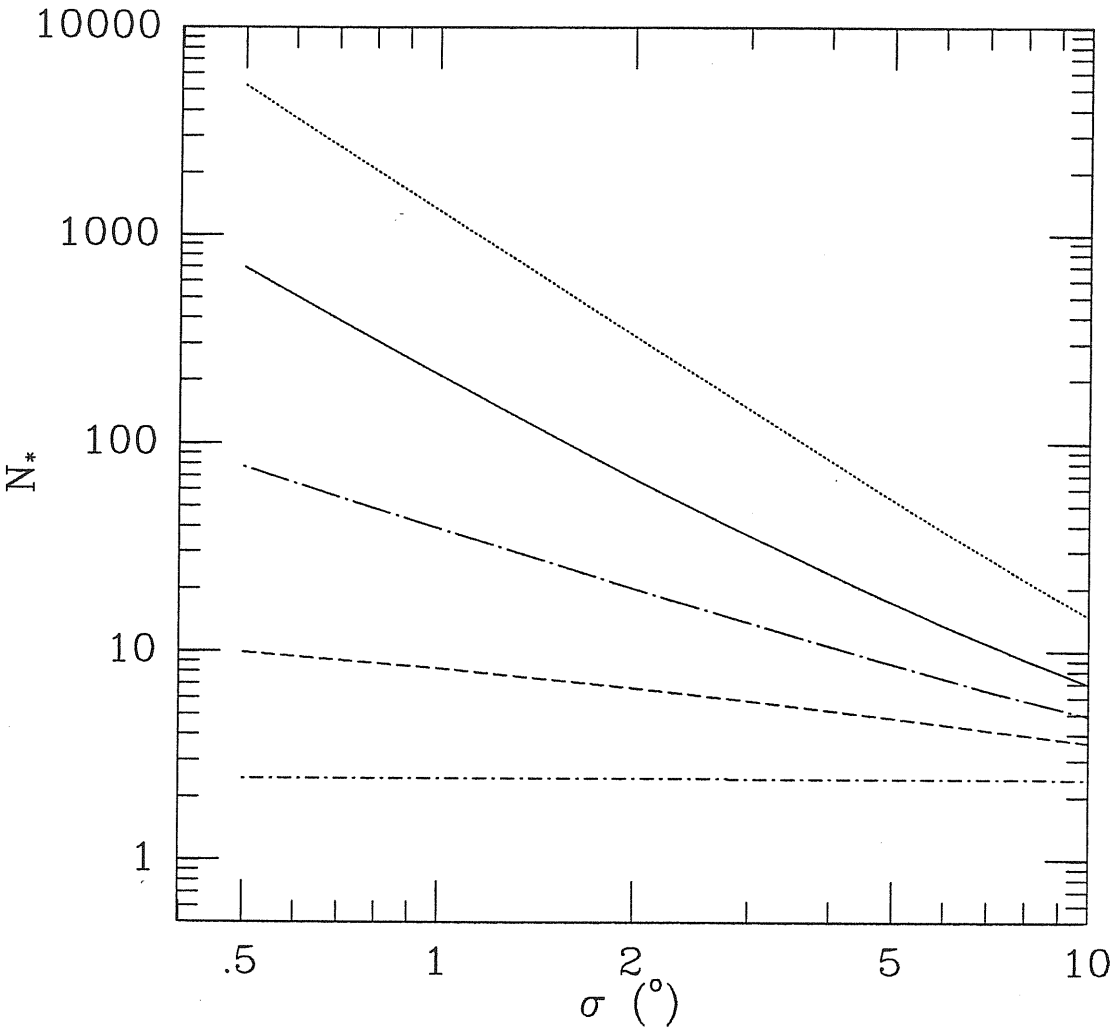

Figure III.2. *The quantity N_*, related to the total number of upcrossing regions N_{up}, is shown for different values of n as a function of σ. Line types as in Fig. III.1 .*

For moderate ν's, the temperature profile of the upcrossing regions is slightly steeper than the shape of the correlation function. If the temperature field is very correlated the profile is very flat and hence beam switching at an angular scale less than the typical hot spot angular diameter leads to the risk of a strong reduction in any detectable anisotropy, because of the differential technique.

Knowledge of the typical hot spot angular diameter can at least guide the design of the observational configuration, of course taking into account other trade–offs, such as atmospheric and ground emission. The expected angular diameter is

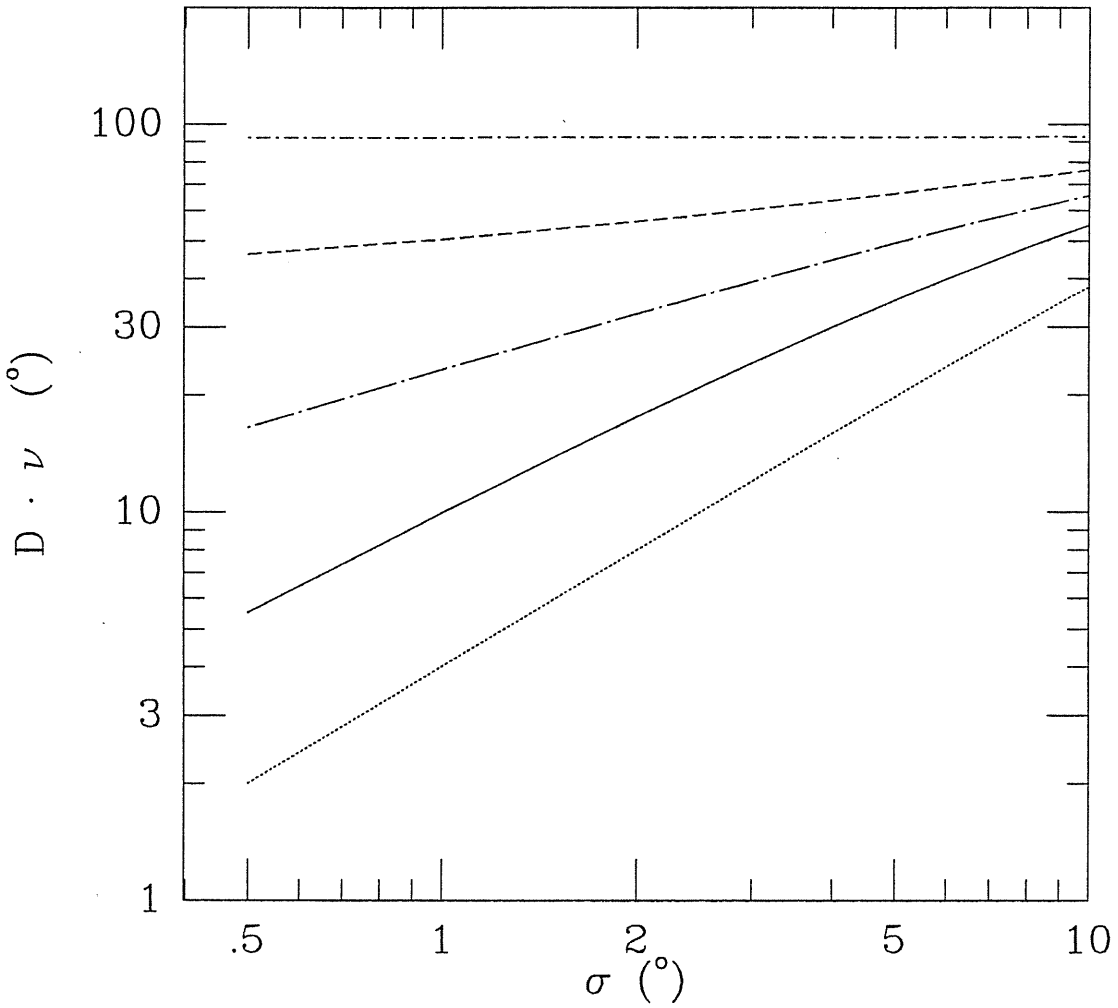

Figure III.3. *The average diameter D times the threshold ν. Line types as in Fig. III.1 .*

inversely proportional to the number of hot spots and depends on the threshold as ν^{-1} (for $\nu \gg 1$; see VJ). The quantity $D \cdot \nu$ is plotted in Fig. III.3 . For fixed ν, D increases linearly with σ for $n \simeq 3$, but flattens out to 90° (formally for $\nu = 1$) when only the quadrupole is dominant (i.e., $n < -2$). In this limit, however, the same comment applies that we made before: a quadrupole with amplitude much higher than $C^{1/2}(0, \sigma)$ is improbable.

As an example of the application of the above results to a practical situation, the angular diameter of a CMB temperature fluctuation, for $\sigma = 3°.5$ (as in the Davies *et al.* experiment), with $\nu = 2$ has an angular diameter of $\approx 13.5°$ if $n = 1$,

and of $\approx 21^o$ if $n = 0$. The expected angular diameter of the hot (or cold) spot is less than 8^o, the characteristic angular scale of the Davies *et al.*, experiment, only if $\nu > 3$ for $n = 1$, or if $\nu \gtrsim 1.7$ for $n = 2$.

We can also define the probability of measuring, e.g. in a triple beam experiment, a temperature fluctuation greater than or equal to the rms value (see VJ and Eq. (II.35)):

$$P[> rms] = erfc\left\{[3 - 4R(\alpha,\sigma) + R(2\alpha,\sigma)]^{-1/2}\right\} . \qquad \text{(III.6)}$$

If $\sigma = 3^o.5$ and $\alpha = 8^o.3$, this probability is $\sim 4\%$ if $n = 1$, but it can be $\sim 30\%$ if $n = 3$. This estimate is fairly independent of any assumption of the density parameter Ω_0 (see discussion at the end of previous Chapter). Eq. (III.6) does not depends on the actual value of $C^{1/2}(0,\sigma)$, as the probability is determined only by the pattern of the temperature field and by the geometry of the experimental configuration (i.e., double or single subtraction). It is of course necessary to specify a model in order to fix the actual level of rms sky temperature fluctuations, t. The latter quantity is then to be confronted with the sensitivity of the experiment in order to get the final estimate of the detection probability. We will leave this point to future work, as also the extension to non ensemble-average cases of the evaluations for the above interesting quantities.

III.2 Applications to the interpretation of a recent experiment.

Recently Davies *et al.* (1987; hereafter D) reported a possible positive detection of temperature fluctuations of the microwave sky. The experiment operated at 10.4 GHz and used a double subtraction technique (cfr. Sect. II.4), in order to minimize atmospheric contamination. The antenna beam size was $\sigma \simeq 3^o.5$ (corresponding to $8^o.3$ FWHM), and the beam switching angle was $\alpha = 8^o.2$.

The published data refer to a strip of the sky at constant declination ($\delta = 40^o$), in the RA range from 12^h to 17^h, avoiding the galactic plane. At a similar

angular scale, $\alpha = 6^o$ and $\sigma = 2^o.2$, a positive detection of the sky temperature fluctuation was also found in a far infrared balloon borne experiment (Melchiorri et al., 1981). Both these experiments may be contaminated by local effects, but, if confirmed, they will be fundamental in testing current ideas on galaxy formation and in providing a direct measure of the amplitude of the primordial density fluctuations.

The D data were analysed with the maximum likelihood method for estimating the intrinsic sky temperature fluctuation. This method may have some advantages (Kaiser and Lasenby, 1987) relative to the standard method (Boynton and Partridge, 1973) based on the Neyman–Pearson lemma.

This standard method consists in defining a χ^2-like statistics, such as $\chi^2 \equiv \sum_{i=1}^{N} D_i^2/S_{i,err}^2$, where $S_{i,err}^2$ are the instrumental variances, and $D_{o,i}^2$ are the recorded fluctuation data, assumed to be statistically independent and each $D_{o,i}^2$ is assumed to be drawn from a set of $\{D_i^2\}$. Then (Kaiser and Silk, 1986) the common procedure to determine an upper limit (UL) to the sky fluctuations (S_{sky}^2 is the sky variance, i.e. $C(0,\sigma)$), is to ask what is the value S_{UL}^2 such that, if $S_{sky} = S_{UL}$, a value of χ^2 as low as that observed, $\chi_o^2 \equiv \sum_{i=1}^{N} D_{o,i}^2/S_{i,err}^2$ would occur only a fraction $1-\epsilon$ of the time. The number S_{UL}^2 is then taken as upper limit on the sky variance at confidence level ϵ.

A possible problem with the above procedure (Kaiser and Silk, 1986; Kaiser and Lasenby, 1987) is that if the instrumental variance S_{err}^2 is overestimated then one would get a 'too good' (even negative one !) upper limit, S_{UL}^2, much smaller than the one obtainable from the sensitivity of the experiment ($\sim \mathcal{O}(S_{err}^2/N)$). As an example, consider the following situation (Kaiser and Silk, 1986): let $S_i^2 \equiv S_{err}^2$, assuming for simplicity the experimental errors to be always the same, so that $\chi^2 = \sum_{i=1}^{N} D_i^2/S_{err}^2$, and negligible or zero intrinsic fluctuations, $S_{sky}^2 \ll S_{err}^2$.

According to the above procedure, not knowing anything on the real level of sky fluctuations, one would have expected instead the rms value for the given fluctuation to be $\langle D_i^2 \rangle = S_{err}^2 + S_{sky}^2$. So $\langle \chi^2 \rangle = N(S_{err}^2 + S_{sky}^2)/S_{err}^2$ with variance $var(\chi^2) = \frac{2}{N} \langle \chi^2 \rangle^2$. Hence one wants to determine S_{UL}^2 such as to have

the following probability: $P[\chi^2(S_{UL}) < \chi^2_o] < \epsilon$.

For a large number of different observations, $N \gg 1$, the probability distribution function of the χ^2 tends to be Gaussian, so one can rewrite the condition on the probability as $\langle \chi^2(S_{UL}) \rangle - \chi^2_o = \theta_\epsilon [var(\chi^2)]^{\frac{1}{2}} = \theta_\epsilon \langle \chi^2(S_{UL}) \rangle \sqrt{2/N}$, where θ_ϵ is the appropriate 'number of sigmas' to get the confidence level $1 - \epsilon$ (e.g. $\theta_{\epsilon=0.05} = 1.65$). Hence, solving for S^2_{UL} one gets (Kaiser and Silk, 1986):

$$S^2_{UL} = S^2_{err} \left[\frac{\chi^2_o/N}{\left(1 - \theta_\epsilon \sqrt{\frac{2}{N}}\right)} - 1 \right] \cong S^2_{err} \left[\frac{\chi^2_o}{N} - 1 \right] . \qquad \text{(III.7)}$$

Now, in general, $\chi^2/N = 1 + \mathcal{O}(N^{-1/2})$, and as expected the upper limit is proportional to the sensitivity: $S^2_{UL} \sim S^2_{err} N^{-1/2}$. But in the present case $\chi^2_o \propto 1/S^2_{err}$, so that, if there is a systematic error in the estimate of the experimental error this reflects into the reliability of S^2_{UL}. More specifically, if there is an overestimate of S^2_{err} then the value for χ^2 becomes too low and $S^2_{UL} \cong \left[(\sum_{i=1}^{N} D^2_{i,o}/N) - S^2_{err} \right]$ is severely underestimated ('too good') with the possibility of having a negative value !

The other problem with the above method lies in its assumption of the statistical independence of data coming from different fields: this in general is not necessarily true and this assumption is wrong for the large angular scales in the general models we are studying here, as we saw in the previous Chapter (see Fig. II.5).

To circumvent the above mentioned problems of the χ^2 method use of the Likelihood-Ratio slightly different than the canonical one used by the Bayesian approach has been proposed (Davies *et al.*, 1987; and Kaiser and Lasenby, 1987). This approach consists in updating the *a-priori* ratio of probabilities for two different hypothesis, say H_0 and H_1, through the use of the Likelihood-Ratio to get:

$$\left. \frac{P(H_1)}{P(H_0)} \right|_{posterior} = \left[\frac{P(data|H_1)}{P(data|H_0)} \right] \left. \frac{P(H_1)}{P(H_0)} \right|_{prior} . \qquad \text{(III.8)}$$

In our situation, the main advantage of such an approach is that one is not limited by the assumption of zero correlations among experimental data, and that we have

to test just two simple competing hypotheses, i.e. zero or non-zero intrinsic sky fluctuations.

However, if it is true that the likelihood may exhibit a pronounced maximum for a certain choice of the model parameters, it is also true that the result depends strongly upon the model used.

D assume that the temperature fluctuations of the microwave sky have a Gaussian correlation function; taking into account the finite resolution of the antenna, they have:

$$C(\alpha,\sigma) = C_D \ \exp\left[-\frac{\alpha^2}{2\,(2\sigma^2+\theta_c^2)}\right] , \qquad \text{(III.9)}$$

where $\theta_c = 4^o$ is assumed to be an intrinsic coherence angle.

Although plausible as a choice, this function is not what one would expect in the framework of the gravitational instability scenarios, where the density fluctuation power spectrum is usually assumed to be a power law, with a spectral index n: $|\delta_k|^2 = Ak^n$. The acf for this case has been derived and fully discussed in the previous Chapter (see Sect. II.2 and Sect. II.3)

For this $C(\alpha,\sigma,n)$ (cfr. Eq. (II.32)), unlike the Gaussian correlation function, one expects anticorrelation on angular scales around $\pi/2$, for any reasonable choice of the spectral index n (see Fig. II.5). Also, the correlation can be larger than suggested by the Gaussian form on the angular scales of several degrees, which are of interest here (see Fig. II.4). In the rest of the section we will drop the explicit dependence of the acf on its arguments –σ is constant– and denote $C_0 \equiv C(0,\sigma)$.

The value to be determined from the experiment, C_0, is the variance of the CMB temperature fluctuations, as defined through an ensemble average taken over all the sky and all the possible realizations of last scattering surfaces.

Technically, the likelihood ($\mathcal{L}$), for Gaussian multivariate data, can be written as:

$$\mathcal{L} \propto \frac{exp[-\frac{1}{2}\sum \Delta_i S_{ij}^{-1} \Delta_j]}{|S|^{1/2}} . \qquad \text{(III.10)}$$

Here Δ_i and Δ_j are the temperature fluctuations measured in the $i-th$ and $j-th$ directions. The correlation matrix element, S_{ij}, relative to these directions, is $S_{ij} = S_{ij}^{th} + \sigma_{err}^2 \delta_{ij}$, where σ_{err} are the experimental errors at 1 standard deviation, and δ_{ij} is the Kroenecker symbol. The theoretical correlation matrix is:

$$S_{ij}^{th} = C_0 \left\{ \frac{3}{2} R[(i-j)\theta_0] - \Big(R[(i-j)\theta_0 - \alpha] + R[(i-j)\theta_0 + \alpha] \Big) + \right. \\ \left. + \frac{1}{4} \Big(R[(i-j)\theta_0 - 2\alpha] + R[(i-j)\theta_0 + 2\alpha] \Big) \right\}, \tag{III.11}$$

where θ_0 is the sampling angle interval, and α is the beam switching angle.

Using Eq. (II.32) , Eq. (III.10) and Eq. (III.11) , we have analysed the D published data. As a check, we assumed the Gaussian form for the correlation function, and we recovered the D result: $C_D^{1/2} = 0.10\ mK$. Then we used the correlation function expected for spectral indices $-3 < n < 3$. This wide range of values was taken to show the dependence of the result on different assumptions.

For each choice of the spectral index, we varied C_0 in order to find the value $C_{0,Max}$ which maximizes $\mathcal{L}$. For assessing a non-zero temperature fluctuation, we computed the Likelihood Ratio (LR) defined as $\mathcal{L}(C_0)/\mathcal{L}(C_0 = 0)$.

This quantity is a measure of the posterior confidence of having $C(0,\sigma) \neq 0$ (the greater the ratio the better the odds). In Fig. III.4 we plot $C_{0,Max}^{1/2}$ and LR_{Max} as a function of the spectral index. The values of $C_{0,Max}^{1/2}$ increase as n decreases. This is because the D experiment measures the second difference of the sky temperature fluctuations, Δ (see Sect. II.4).

In terms of correlation function, we have (Eq. (II.41)) $\Delta|_{rms}^2 = C_0[1.5 - 2R(\alpha,\sigma) + 0.5R(2\alpha,\sigma)]$. If the three beams are very correlated, the quantity in parenthesis is small, and tends to zero for a very flat correlation law (i.e., $R(\alpha) \rightarrow 1$), so that $C(0,\sigma)$ must increase in order to be consistent with a given set of data. For $n \rightarrow -3$, the correlation is indeed very flat on angular scales up to $\sim 10^o$.

The LR_{Max} shows a peak value ~ 10 for spectral indices between 0 and 1.

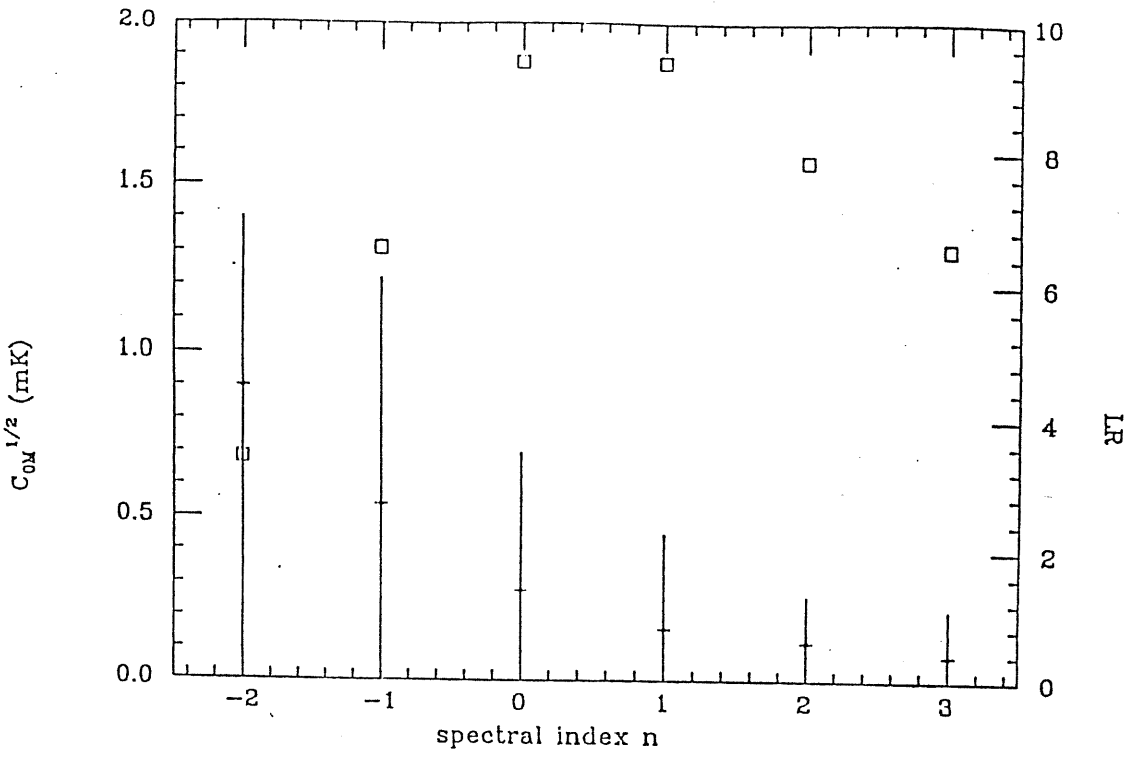

Figure III.4. *The quantities $C_{0,Max}^{1/2}$ (dots), and LR_{Max} (open squares) obtained by analysing the data of Davies et al. (1987) are shown as a function of the assumed perturbation spectral index. The amplitude of the error bars on the $C_{0,Max}^{1/2}$ values have been calculated imposing a* $\mathrm{LR} = 0.1\,\mathrm{LR}_{Max}$. *Scale invariant* ($n = 1$) *and white noise* ($n = 0$) *spectra show the larger values of maximum Likelihood Ratio.*

Thus a similar value for LR_{Max} was found analysing the D data with the Gaussian correlation function or a white noise or scale–invariant spectrum.

We investigated the stability of the above results for the $n = 1$ case through a 'jackknife'-type analysis (Efron, 1979). This kind of analysis consists in eliminating subsets of data, in order to test the stability of the results obtained using the complete data set. Since the D data are heavily oversampled (there are only seven truly independent data in the D data set) we need to eliminate at least 10 data around a given D data point. By changing this point, we built 61 pseudosamples of 60 data each.

We then applied the likelihood analysis to each of these pseudosamples and

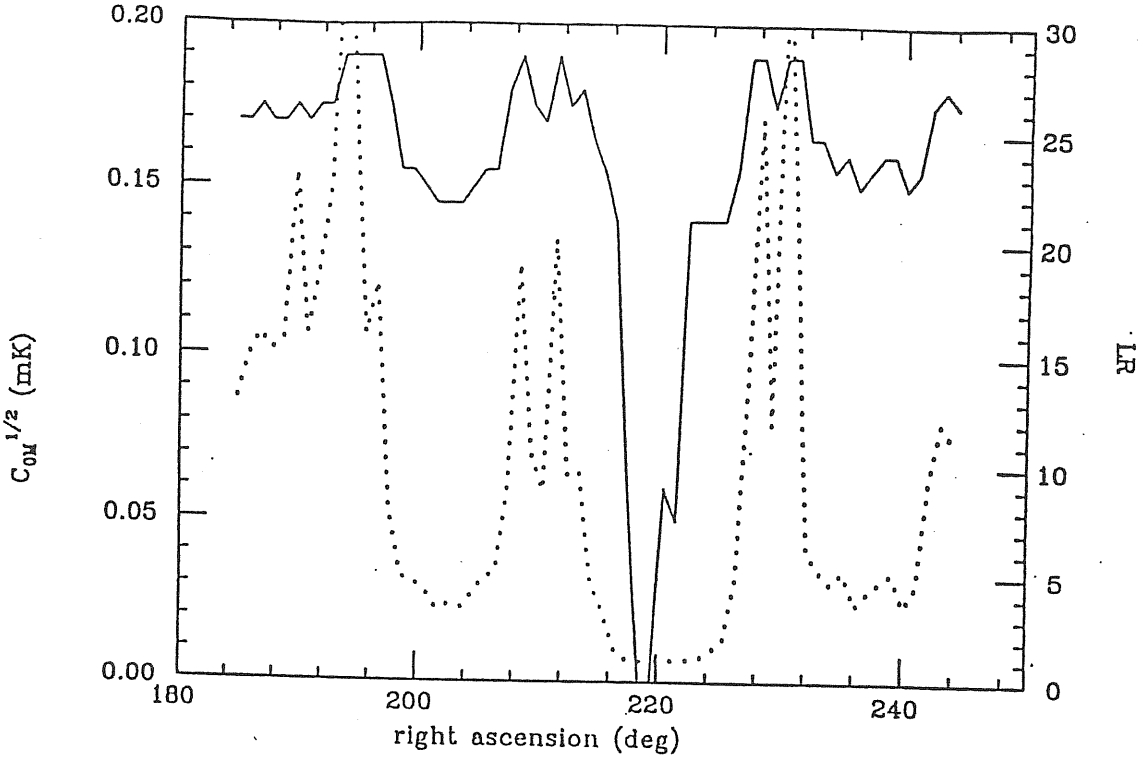

Figure III.5. *Results of the jack-knife analysis for the Davies et al. data. Continuous and dotted lines refer to* $C_{0,Max}^{1/2}$ *and* LR_{Max}*, respectively. The region around* $\alpha = 220°$ *shows a minimum in* LR_{Max} *and two null results for* $C_{0,Max}^{1/2}$.

accordingly derived the distributions for LR_{Max} and $C_{0,Max}^{1/2}$. The results of this analysis are shown in Fig. III.5 .

A null result for $C_{0,Max}^{1/2}$ is obtained around $\alpha = 219°$, with $\mathrm{LR}_{Max} \sim 1$. This suggests that most of the signal in the D data comes from that region (cfr. Watson *et al.*, 1988). Apart from this region, this analysis reveals a fair stability of the derived $C_{0,Max}^{1/2}$ ($\sim 0.16\ mK$), although the LR_{Max} strongly fluctuates.

In order to evaluate the statistical significance of the above likelihood result and in order to have a fair comparison between theory and observations, one must estimate the probability of detecting CMB temperature fluctuations in a given theoretical scenario and for a given experiment. This can be done by simulating observations of the theoretical sky, including effects such as noise (detector, atmo-

sphere, instrumentation, etc.), sky coverage, modulation geometry, beam pattern, data sampling, etc.

We simulated the D experiment in the following way. We generated 1000 random strips of the sky with a numerical algorithm described elsewhere (Vittorio, 1989). Each of these strips is $\sim 160^o$ wide and has a resolution of $\sim 0^o.8$. They are realizations of the theoretical microwave sky expected in a flat universe, where density fluctuations are Gaussian distributed, adiabatic, and scale–invariant (i.e., $n = 1$).

Then, by sampling each strip with the same density D had, we generated a data set of 70 points per strip. Each data point represents the result of a double subtraction, with a beam switching angle $\alpha = 8^o.3$ and with an antenna beam size $\sigma = 3^o.5$. To simulate the receiver noise, we added to the 'true' CMB temperature fluctuations at each point an uncorrelated Gaussian 'noise' of amplitude (rms) σ_{err}.

As an example, we plot in Fig. III.6 the original D data and one of the simulated data sets, extracted from a theoretical ensemble with $C_0^{1/2} = 0.16\ mK$ (the value found analyzing the D data for $n = 1$) and $\sigma_{err} = 0.22\ mK$ (the amplitude of the D error bars).

We carried out our numerical simulations for 6 different "signal to noise" ratios, SNR$\equiv C_0^{1/2}/\sigma_{err} =$ 0, 0.5, 0.75, 1, 1.5, 2. The analysis of each simulated data set provides two values for $C_{0M}^{1/2}$ and LR_{Max}. We have then, for each SNR, 1000 pairs of these values and we can plot the histogram of their frequency. It is easy to verify, using Eq. (III.10) , that the shape of the distribution depends only upon the value of SNR. Since the data Δ_i of each strip represent a realization of the theoretical ensemble, the value $C_{0,Max}$ which maximizes the likelihood in Eq. (III.10) is not expected to coincide with the ensemble average, $C(0, \sigma)$.

If SNR$\rightarrow$ 0, most of the simulated data sets provide a maximum Likelihood Ratio $1 < \mathrm{LR}_{Max} < 2$, some provide $\mathrm{LR}_{Max} \sim 5$, only 5 provide $\mathrm{LR}_{Max} \sim 10$. So, one would not infer any detections, if $\mathrm{LR}_{Max} \gtrsim 10$ is required for a statistically

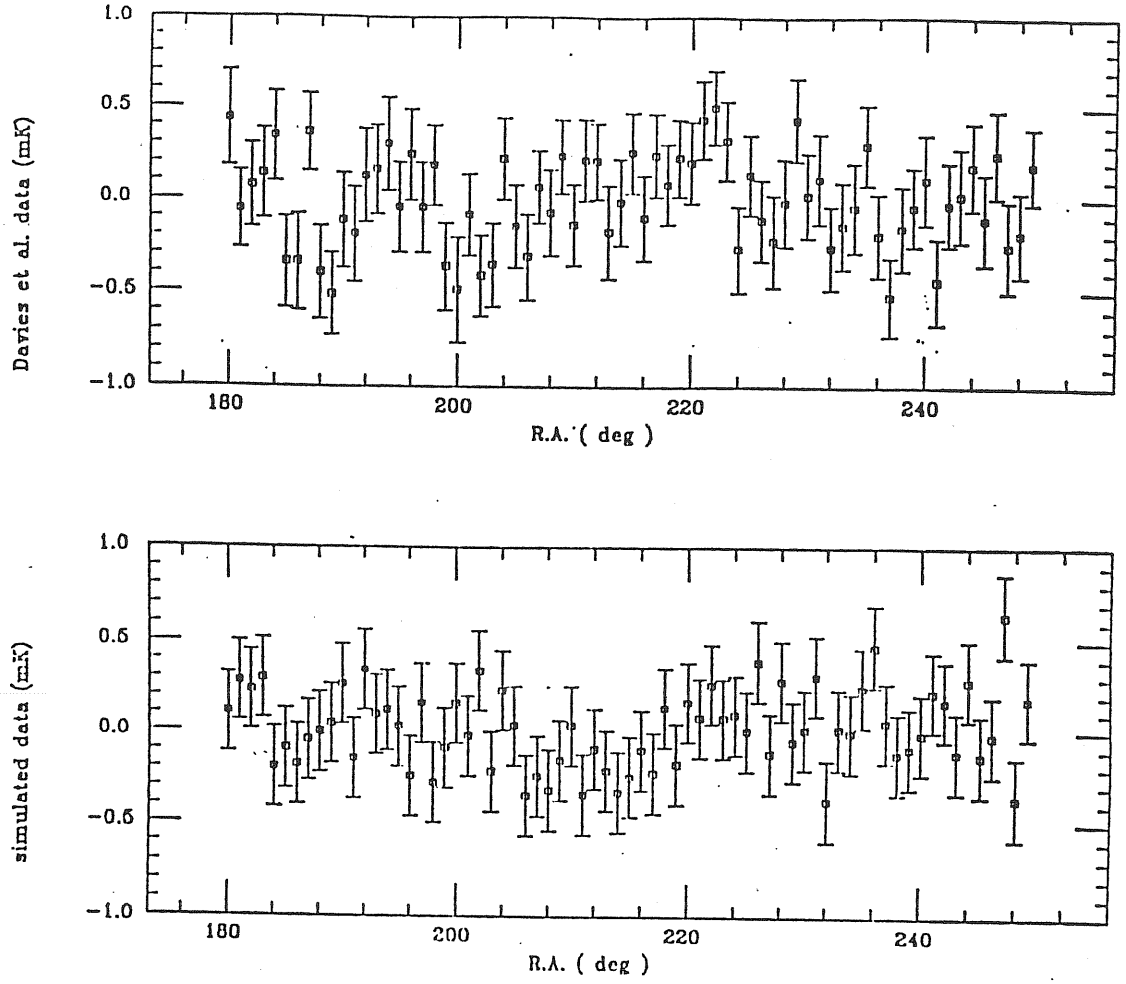

Figure III.6. *Comparison between the Davies et al. data (upper panel) and one simulated data set, similarly sampled, with* $C_0^{1/2} = 0.16\ mK$, $\sigma_{err} = 0.22\ mK$, *generated by scale-invariant density fluctuations (lower panel).*

significant detection.

The probability of having a $\mathrm{LR}_{Max} > 10$ (and $C_{0,Max}^{1/2} > 0$) continuously increases from $\sim 1\%$ to 11%, 22%, 43%, 83%, 94% for the SNRs we have considered. For small SNR, the distribution of cases with $\mathrm{LR}_{Max} \gtrsim 10$ is narrow and peaked around a value $C_1 > C_0$. In this case, in fact, only few realizations have temperature fluctuations significantly larger than the noise. Increasing the value of the SNR, maximum Likelihood Ratios $\gtrsim 10$ become quite common, $C_1 \to C_0$, and the C_{0M} distribution approaches the intrinsic theoretical one for the CMB

temperature fluctuations.

We can use our Monte Carlo simulations in order to state a firm upper limit on $C_0^{1/2}$ in the D data. In fact, we can test the hypothesis $H_0 : C_0 = 0$, against the hypothesis $H_1 : C_0 = C_0^*$ using as a test statistic the Likelihood Ratio LR_{Max}, whose distribution has been found via the Monte Carlo simulations. From these, we found that H_1 is preferred (i.e., the LR_{Max} is greater than the measured value $\mathrm{LR}_{Max} \simeq 10$) in 95% of the cases if the SNR is 2. This would imply $C_0^{*1/2} = 0.44\ mK$ if $\sigma_{err} = 0.22\ mK$ as in the Davies *et al.* experiment. On the contrary, if in fact $C_0 = 0$, we have that H_1 is preferred only in 1% of the cases. This means that $0.44\ mK$ is an upper limit on $C_0^{1/2}$ at a confidence level of 95%, with a power against the null hypothesis H_0 of 99% (a very significant upper limit !).

In the D experiment SNR= 0.75 ($C_0^{1/2} = 0.16\ mK$, $\sigma_{err} = 0.22\ mK$) and $\mathrm{LR}_{Max} \simeq 10$. The corresponding distribution (see Fig. III.7), obtained from the Monte Carlo simulations has a mean value of $0.22\ mK$, with a standard deviation of $0.04\ mK$ and is marginally consistent with the D result. In fact, only 5% of randomly placed observers would measure $LR \gtrsim 10$ and $C_{0M}^{1/2} \lesssim 0.18\ mK$, so the D result is in the 5% tail of the distribution. Increasing SNR to unity ($C_0^{1/2} = \sigma_{err} = 0.22\ mK$) does not change the previous conclusion. In fact, the mean value of the new distribution is $0.24\ mK$, and its standard deviation is $0.05\ mK$. The theoretical predictions are still marginally consistent with the D result, as only 5% of the realizations have $\mathrm{LR}_{Max} \gtrsim 10$ and $C_{0M}^{1/2} \lesssim 0.185\ mK$.

If the same level of CMB fluctuations (i.e. $C_0^{1/2} = 0.16\ mK$) were confirmed from data with smaller error bars, the consistency with the theoretical model would have a higher confidence. Lowering the simulated experimental noise to, e.g., $\sigma_{err} = 0.16\ mK$ (which corresponds to doubling the D integration time) implies comparing the D result with a theoretical distribution which has still SNR= 1, but $C_0^{1/2} = 0.16\ mK$. For such a distribution (see Fig. III.7) the probability of recovering the assumed level of fluctuations is higher. The mean value is now $0.17\ mK$, with a standard deviation $0.03\ mK$ and 5% (30%) of the realizations

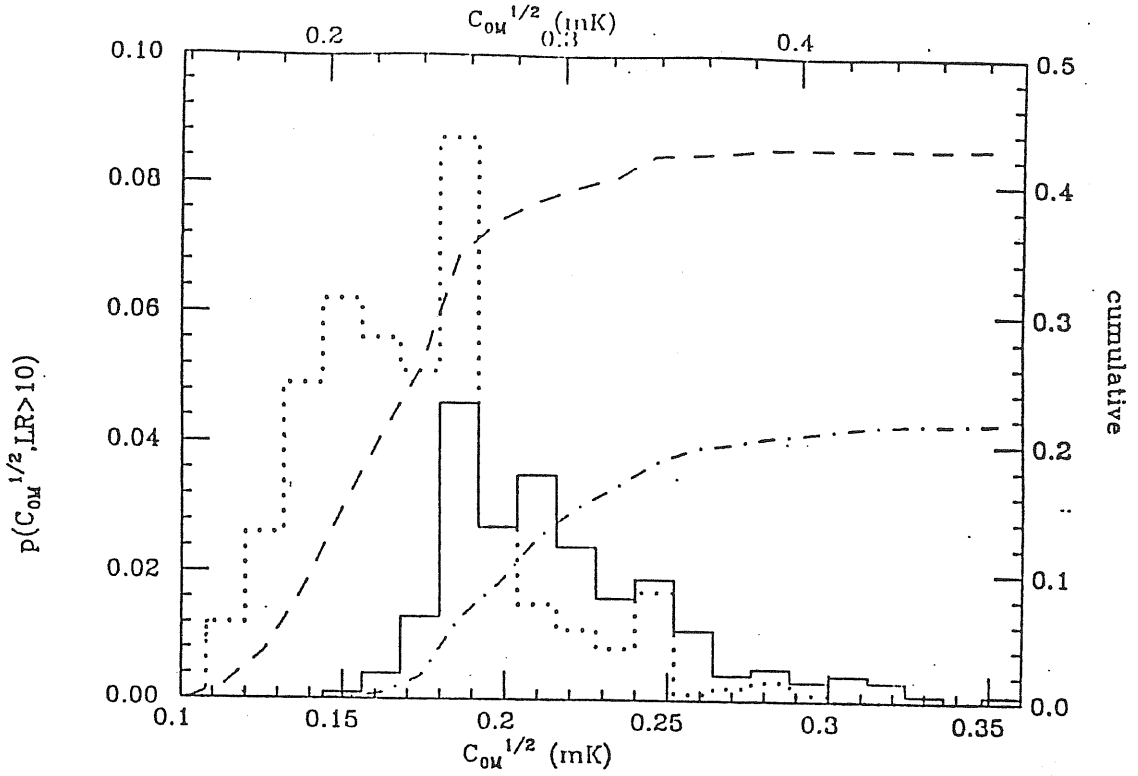

Figure III.7. *Histograms of the probability density,* $p(C_{0M}^{1/2}, \mathrm{LR}_{Max} > 10)$, *and the corresponding cumulative probability. Units are on the left and right axis, respectively. The continuous histogram and the dotted dashed cumulative correspond to simulations with SNR= 0.75: as in the Davies et al. experiment* $C_0^{1/2} = 0.16\ mK$ *and* $\sigma_{err} = 0.22\ mK$. *The dotted histogram and the dashed cumulative refer to SNR= 1: the lower scale holds for* $C_0^{1/2} = \sigma_{err} = 0.16\ mK$, *while the upper scale holds for* $C_0^{1/2} = \sigma_{err} = 0.22\ mK$.

have $\mathrm{LR}_{Max} \gtrsim 10$ and $C_0^{1/2} \lesssim 0.13\ (0.18)\ mK$.

Before concluding this analysis, we want to stress that the likelihood analysis provides only the best estimate of the model parameters, but not a confidence interval. Hence, it is necessary to check the $\mathcal{L}$ results using numerical simulations, which seems to be the only way to build up a probability distribution for the parameters. In this way, given our theoretical assumptions, we saw that in order to have a high confidence ($\sim$ 95 %) on the likelihood results, a SNR as high as two is needed.

We believe that this method of comparing theory and observations is very powerful and will become widespread, since it takes into account all the important experimental parameters, otherwise neglected in a purely theoretical analysis. Also, for a given model, this method can be used to define the best experimental configuration and observational strategy for detecting CMB temperature fluctuations.

III.3 Distribution functions for different cosmic observers.

Up to now, the discussion has been restricted to values obtained through *ensemble averaging*, that is taking the mean value of those that would have been measured by all the fiducial observers. This was accomplished by taking a spatial average over all the comoving positions (cfr. Eq. (II.8)), after having taken an angular average for each of these observers. The key point is that, due to differences of phases of the Fourier components of the density field, different observers will measure different amplitudes for the temperature fluctuations, because their last scattering surfaces will sample different parts of the density fluctuation field.

Because we are one such possible observer (i.e. we 'see' only one among the possible realizations of last scattering surfaces) it is of extreme importance to be able to estimate how far the actual values we observe can differ from those which could be measured by the other observers: we need the probability distribution function (hereafter pdf) for the quantities of interest. While in the case of small angular scales (e.g. a few arcseconds) because of the short-range correlations among the signals we can still have independent samples from different, well separated sky patches, and hence have several probes of the population from which the recorded values are drawn, here, because of the long range correlations, we can test only a single value (e.g. only a single value is measurable for the quadrupole) and therefore we are in a bad situation as far the statistical information is concerned.

This fact, as very well evidented by Sazhin (1985), makes dangerous to extrapolate to large scale situations the statistical methods used on small scales.

Hence, as noted also by Coles (1988), the only possible line of approach seems to be the derivation of the pdf by numerical Monte-Carlo simulations.

We already noted in Sect. II.3 that in our derivation of the expression for the smoothed acf (Eq. (II.28)) we did not make use of spatial averaging, just of sky averaging. Indeed, by the use of the definitions of Eq. (II.3) , of Eq. (II.15) , and of Eq. (II.18) we can write, *taking only angular averages* ($< > \rightarrow \int d\Omega_A/(4\pi) \int d\Omega_B/(4\pi)$) and with the condition of fixed sky separation α, between the directions $\hat{\gamma}_A$ and $\hat{\gamma}_B$:

$$
\begin{aligned}
c_j &= \frac{(2j+1)}{2} \int \frac{d\Omega_A}{4\pi} \Delta(\hat{\gamma}_A) \int \frac{d\Omega_B}{4\pi} \Delta^*(\hat{\gamma}_B) \times \\
&\times \int_{-1}^{1} d\mu \, P_j(\mu) \, 2\delta(\mu - \hat{\gamma}_A \cdot \hat{\gamma}_B) = \\
&= \frac{1}{4\pi} \sum_{p=-j}^{j} \int d\Omega_A \, \Delta(\hat{\gamma}_A) \, Y_j^{p*}(\hat{\gamma}_A) \int d\Omega_B \, \Delta^*(\hat{\gamma}_B) \, Y_j^p(\hat{\gamma}_B)
\end{aligned}
\qquad \text{(III.12)}
$$

(here $\mu = \cos\alpha$), and we recover the relation between c_ℓ and $\{a_\ell^m\}$ shown in Eq. (II.19) . We prefer to rewrite the relation Eq. (II.20) as

$$
C(\alpha) \;=\; \frac{1}{4\pi} \sum_{\ell \geq 2} Q_\ell^2 \, P_\ell(\cos\alpha) \,, \qquad \text{(III.13)}
$$

where the $\{Q_\ell^2\}$ differ only by a factor 4π from the $\{c_\ell\}$:

$$
Q_\ell^2 \;\equiv\; \sum_{m=-\ell}^{\ell} |a_\ell^m|^2 \,. \qquad \text{(III.14)}
$$

The important thing to note is that the $\{a_\ell^m\}$ are *stochastic variables*, Gaussianly distributed, all with the same expectation value (here the average is an ensemble average):

$$
\left\langle |a_\ell^m|^2 \right\rangle \;\equiv\; \Sigma_\ell^2 \,. \qquad \text{(III.15)}
$$

This follows directly from Eq. (II.7) and from the assumption that the field $\delta_{\rm k}$ has a Gaussian distribution. Note that $\langle a_\ell^m \rangle = 0$ and that Σ_ℓ^2 coincide with the previously considered a_ℓ^2.

Because of the randomness of the temperature distribution, a single realization of the microwave sky (e.g. our own universe) is then characterized by random values of the Q_ℓ^2's. The pdf of a given Q_ℓ^2 is that of χ_ν^2 with $\nu = 2\,\ell\,+1$ degrees of freedom (Abbott and Wise, 1984a,b, hereafter AB; see also the Appendix of Fabbri *et al.*, 1987 for a nice derivation). Hence expected value over the ensemble of possible observers is

$$\langle Q_\ell^2 \rangle \;=\; (2\,\ell + 1)\;\Sigma_\ell^2\;, \tag{III.16}$$

while its variance is

$$Var(Q_\ell^2) \;=\; 2\,(2\,\ell + 1)\;\Sigma_\ell^4\;. \tag{III.17}$$

It is then straightforward to obtain the same quantities for the acf because of the independence of different Q_ℓ^2's (AB, Bond and Efstathiou, 1987):

$$\langle C(\alpha) \rangle \;=\; \frac{1}{4\pi} \sum_{\ell=2}^{\infty} \langle Q_\ell^2 \rangle \;\; P_\ell(cos\alpha)\;, \tag{III.18}$$

$$Var\,(C(\alpha)) \;=\; \left(\frac{1}{4\pi}\right)^2 \sum_{\ell=2}^{\infty} Var(Q_\ell^2)\; P_\ell^2(cos\alpha)\;. \tag{III.19}$$

The above relations refer to intrinsic temperature fluctuations. Observing the sky with an antenna of finite resolution implies applying a low–pass filter, which strongly attenuates high order harmonics. Assuming a Gaussian beam of dispersion σ, this effect can be easily taken into account by opportunely weighting the terms of the above expansions, as shown in Sect. II.3 (that derivation still applies here). We can therefore restrict ourselves again to power law models and give the general expression for the acf (cfr. Sect. II.2) by writing

$$C(\alpha, \sigma, n) \;=\; \mathcal{A}(n) \cdot S(\alpha, \sigma, n)\;, \tag{III.20}$$

$$\mathcal{A}(n) \;\equiv\; \frac{2^{n-1}\,A}{4\pi\, r_0^{(n+3)}}\; \frac{\Gamma(3-n)}{\left[\Gamma\left(\frac{4-n}{2}\right)\right]^2}\;, \tag{III.21}$$

$$S(\alpha, \sigma, n) \;\equiv\; \sum_{\ell=2}^{\infty} X_\ell^2 \;\cdot\; W_\ell(\alpha, \sigma, n)\;, \tag{III.22}$$

where $\mathcal{A}(n)$ is an overall adimensional normalization factor ($\mathcal{A}(1) = A/(\pi^2\, r_o^4)$ for the scale-invariant case, $n = 1$), $X_\ell^2 \equiv Q_\ell^2 / < Q_\ell^2 >$ is a stochastic variable with a

normalized $\chi^2_{(2\ell+1)}$ pdf, and finally

$$W_\ell(\alpha,\sigma,n) \equiv (2\ell+1)\ \frac{\Gamma\left(\frac{2\ell+n-1}{2}\right)}{\Gamma\left(\frac{2\ell+5-n}{2}\right)}\ P_\ell\left(cos\,\alpha\right)\ \exp\left\{-\left[\left(\ell+\frac{1}{2}\right)\sigma\right]^2\right\}\ . \quad \text{(III.23)}$$

Having developed the formalism we can now proceed to implement it to the derivation of pdf's.

Before tackling the numerical part, though, we can get an idea of the amount of statistical uncertainty by considering the variance of the acf, from Eq. (III.19) we find that

$$Var(C(\alpha,\sigma,n)) = \mathcal{A}^2\ \sum_{\ell=2}^{\infty}\ \frac{2}{(2\ell+1)}\ W_\ell^2(\alpha,\sigma,n) \qquad \text{(III.24)}$$

Therefore, with the new definitions (cfr. Eq. (II.35))

$$\begin{aligned} \langle R(\alpha,\sigma,n)\rangle &\equiv \langle C(\alpha,\sigma,n)\rangle\ /\ \langle C(0,\sigma,n)\rangle\ , \\ \langle \Delta R(\alpha,\sigma,n)\rangle &\equiv [Var(C(\alpha,\sigma,n))]^{\frac{1}{2}}\ /\ \langle C(0,\sigma,n)\rangle\ , \end{aligned} \qquad \text{(III.25)}$$

we can obtain from the plots shown in Fig. III.8 a grasp of the possible variations of the acf for different observers and for different values of the primordial spectral index, n.

Before commenting on the plots of Fig. III.8 we note that the values plotted have been computed, and are fully valid, for different given values of the angle α as statistically independent quantities. The same argument *does not* apply to the acf function itself which, once the stochastic variables X^2_ℓ of Eq. (III.21) have assumed their particular values for the given realization, is completely and deterministically determined for all the values of α. Therefore the ± 1 s.e. band shown in Fig. III.8 must be in principle visualized for each value of α separately, although in practice it gives a very useful guide to the overall uncertainty.

The first thing evident in Fig. III.8 is the huge differences in standard deviation amplitudes for different values of n (note that the vertical scales are not the same for all the cases, to improve readability). These are due to the properties of scaling of the weights: $W_\ell(\alpha,\sigma,n) \propto \ell^{n-2}$ (cfr. Sect. II.2 and Sect. II.3).

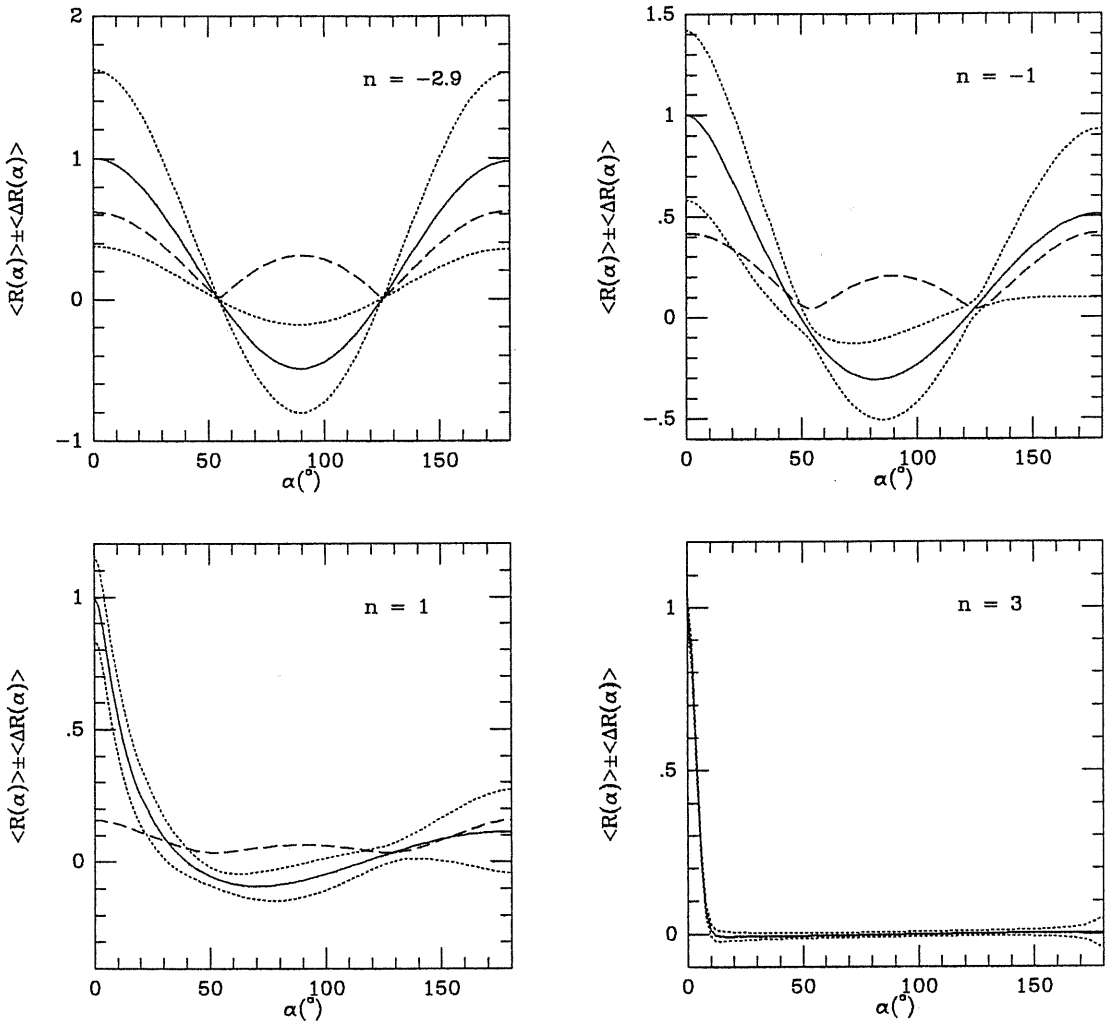

Figure III.8. *The ensemble average value for the acf (solid line), its standard deviation (dashed line), and the* ± 1 *s.e. band (region within the dotted lines) are shown as functions of the separation angle,* α*, and four values of the primordial spectral index,* n*.*

This fact influences the relative contributions and hence the statistical relevance of the stochastic variables X_ℓ^2's. For n very negative only the quadrupole component matters in the C sum (cfr. discussion in Sect. III.1) and therefore the pdf of C itself is that of a χ^2 with 5 degrees of freedom which is quite wide: $[var(\chi_5^2)]^{\frac{1}{2}} / \langle \chi_5^2 \rangle = \sqrt{2/5} \cong 63$ %. On the contrary, when other harmonics also enter into play, the C pdf starts to become narrower and narrower: for n large many harmonics contribute to the sum with no dominant ones and we find that the global variance much smaller as a percentage than in the other case because

it is the sum of many comparable variances, say N, and therefore is almost the variance of the average contributing term divided by N.

It is appropriate to make the technical remark that in our situation it is not possible to invoke the Central Limit theorem to infer that C, being a sum of many stochastic variables, has a nice Gaussian distribution: the validity of the theorem requires in fact not only the sum of several stochastic variables, but also that they have *comparable expected values*. Here this is not always the case and therefore we want to stress that, different from what many naively would have expected, *the pdf of the acf is not Gaussian.*

It is also important to note that, for small values of n, the minimum uncertainty happens to be near the zeros of the acf itself. The acf variance has its angular dependence through the square of the Legendre polynomials (note the symmetry with respect to $\pi/2$) and has nonzero minima (except for the case in which the quadrupole only matters) which are close to the values of α for which the acf has its zeros, this fact can have important consequences in determining the best experimental strategy for the detection of fluctuations. We note that, due to the different amplitudes for both the signal and the related uncertainty among different angles, the optimal choice for α is no longer necessarily the one, say $\tilde{\alpha}$, for which the average acf reaches its minimum, as has been generally considered up to now.

We will leave the detailed study of this point to future work, but we want here to just sketch the line of reasoning: it is true that, on average, at $\tilde{\alpha}$ the observable signal would be at maximum strength, but, because of the non minimum uncertainty at the same point, the observer would take the risk of a possible 'unlucky' situation in our last scattering surface, in which the different phases conspired to give at $\tilde{\alpha}$ a value for the acf much higher than the expected one, therefore diminishing the net observable signal (cfr. Eq. (II.38) ; of course one could have also the possibility of an opposite 'lucky' situation with an enhanced signal !). A different experimental choice could be that of playing more safely and choosing for α the one corresponding to the minimum uncertainty, and looking then for a level

of the signal which is in principle less profitable but more reliable.

We are therefore led to the task of simulating numerically many possible values for the acf (for different values of its parameters α, σ and n) to Monte-Carlo approximate its 'true' pdf.

We proceed as follow: by inspection of Eq. (III.20) and Eq. (III.21) we see that we need a general algorithm to generate pseudo-random numbers according to χ^2_ν distributions of different degrees of freedom (dof) ν. We then take advantage of the definition of a chi-square as a sum of squares of independent Gaussian variables: $\chi^2_\nu \equiv \sum_{i=1}^{\nu} z_i^2$, where the z_i are drawn from a Normal distribution with zero average and unit variance.

Numbers can be drawn according to a Normal distribution in an elegant way through the Box-Muller algorithm (see e.g. Press *et al.*, 1986). According to this algorithm one can obtain a couple of variables, z_1 and z_2, normally distributed as

$$\begin{aligned} z_1 &= (-2\ln\xi_2)^{\frac{1}{2}} \cdot \cos(2\pi\,\xi_1)\ , \\ z_2 &= (-2\ln\xi_2)^{\frac{1}{2}} \cdot \sin(2\pi\,\xi_1)\ , \end{aligned} \tag{III.26}$$

where $\xi_{1,2}$ are drawn from the uniform distribution on the interval $(0,1]$. It is then straightforward by the chi-square definition given above, to derive the following expression, which allows the computation of pseudo-random numbers with a chi-square pdf for an even or odd number of dof ν:

$$\begin{aligned} \chi^2_{2\nu} &= -2\,\ln(\xi_1\cdot\xi_2\cdot\xi_3\cdots\xi_\nu)\ , \\ \chi^2_{2\nu+1} &= -2\,\ln(\xi_1\cdot\xi_2\cdot\xi_3\cdots\xi_\nu) - 2\,\ln(\xi_{\nu+1})\cdot\cos^2(2\pi\,\xi_{\nu+2})\ . \end{aligned} \tag{III.27}$$

We can then use the above method to obtain a random set of $\{X^2_\ell\}$ and, with the *same* set of $\{X^2_\ell\}$ for all quantities, compute through Eq. (III.22) and Eq. (III.20) the values of interest for various angles α and smoothing σ. In this way we get a single realization of the sky. This procedure must then be repeated for a large number of times, in order to get a sufficiently accurate sampling of

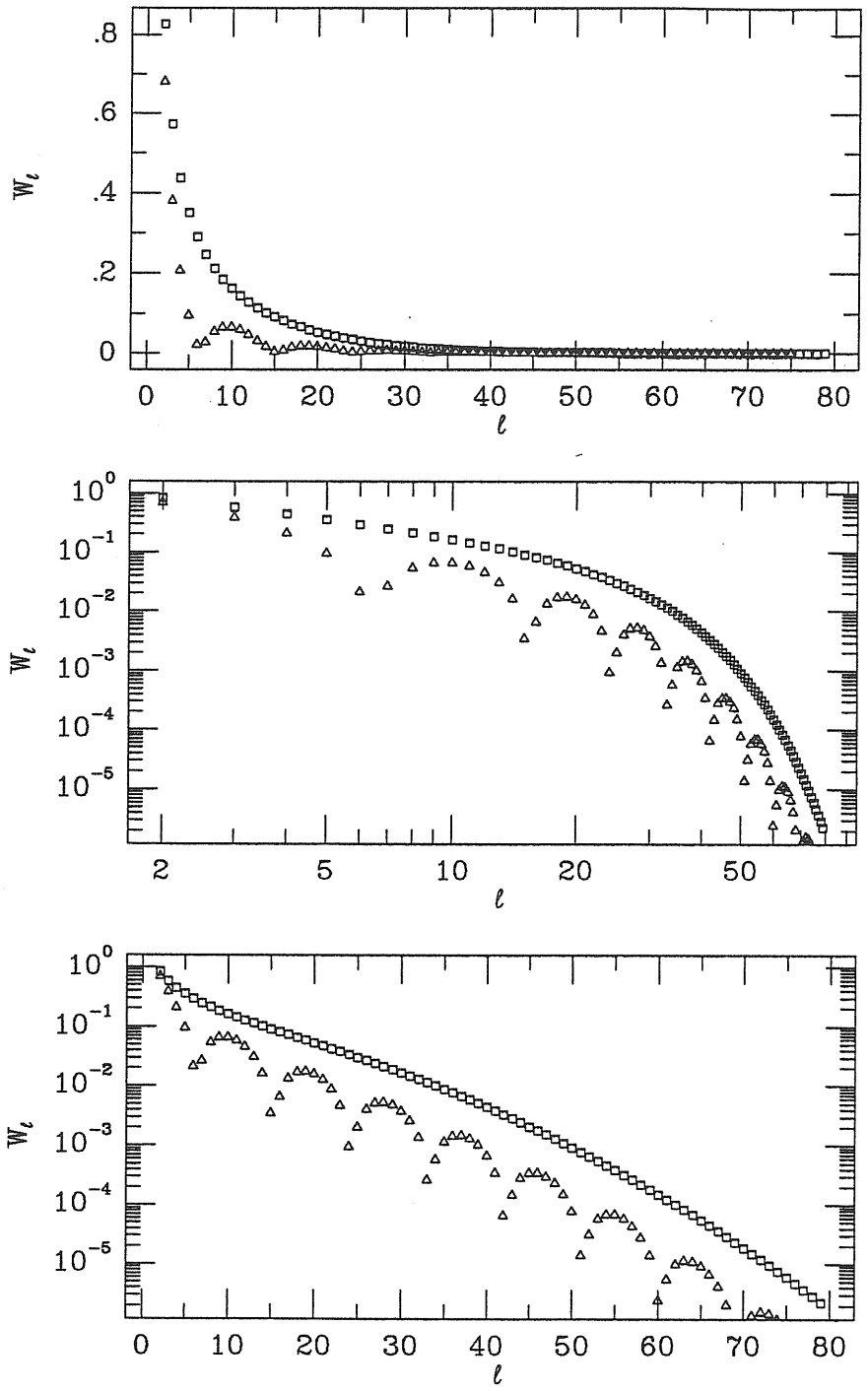

Figure III.9. *The modulus of the weights* $W_\ell(\alpha, \sigma = 2.4^\circ, n = 1)$ *for the case* $\alpha = 0^\circ$ *(squares) and* $\alpha = 10^\circ$ *(triangles) is plotted for different harmonic number,* ℓ.

the space of possible outcomes. As a good compromise between accuracy and computational cost (e.g. CPU time and memory disk space) we choose to have $N_{tot} = 10000$ realizations of last scattering surfaces. We will also limit the present discussion to the scale-invariant case, $n = 1$, which is the most interesting one from

a theoretical point of view.

In Fig. III.9 we plot the behaviour of the modulus of the weights from Eq. (III.23) for the cases $\sigma = 2^o.2$ and $\alpha = 0, 20^o$ with different choices of the axes scale to better show the interesting features. In the top panel we have a double linear scale which shows clearly that in practice high harmonics ($\ell \gtrsim 30 - 35$) contribute very little and that the dominant ones are for $\ell \leq 10 - 15$. In the mid and bottom panels are clearly seen the power law and the exponential decrease, respectively. Note also the typical oscillatory behaviour given by the Legendre polynomials for $\alpha \neq 0$.

It is important to have an idea of the effect of different realizations on the shape of the acf as a function of the angle α. In Fig. III.10 we show in the top panel five different realizations of the total weights at zero lag (e.g. $X_\ell^2 \cdot W_\ell(\alpha = 0, \sigma = 2^o.2)$) and their effect on the behaviour of the $C(\alpha, \sigma)$ in the bottom panel. Here $n = 1$. It is very interesting to note that for most ranges these curves differ little from the $\pm$ 1 s.e. band: the only exception is the dot-dashed line beyond $\sim 100^o$. This behaviour can be understood by a close inspection of the broken line with the same line-type in the top panel: in this particular realization the harmonics $\ell = 2, 4, 5$ happen to be greatly depressed with respect to that with $\ell = 3$ which then dominates the sum when the other harmonics interfere one with each other.

Having developed the necessary numerical tools we can now pass in the next section to one of their most interesting applications.

III.4 Upper limits to the amplitude of primordial density fluctuations.

As we discussed in Sect. II.1 and Sect. II.2 , one of the most interesting aspects of the large scale CMB anisotropies is that they can directly reflect the primordial fluctuations. Because no firm detection of such temperature fluctuations has been achieved, we will discuss in detail how to constrain the amplitude of the possible

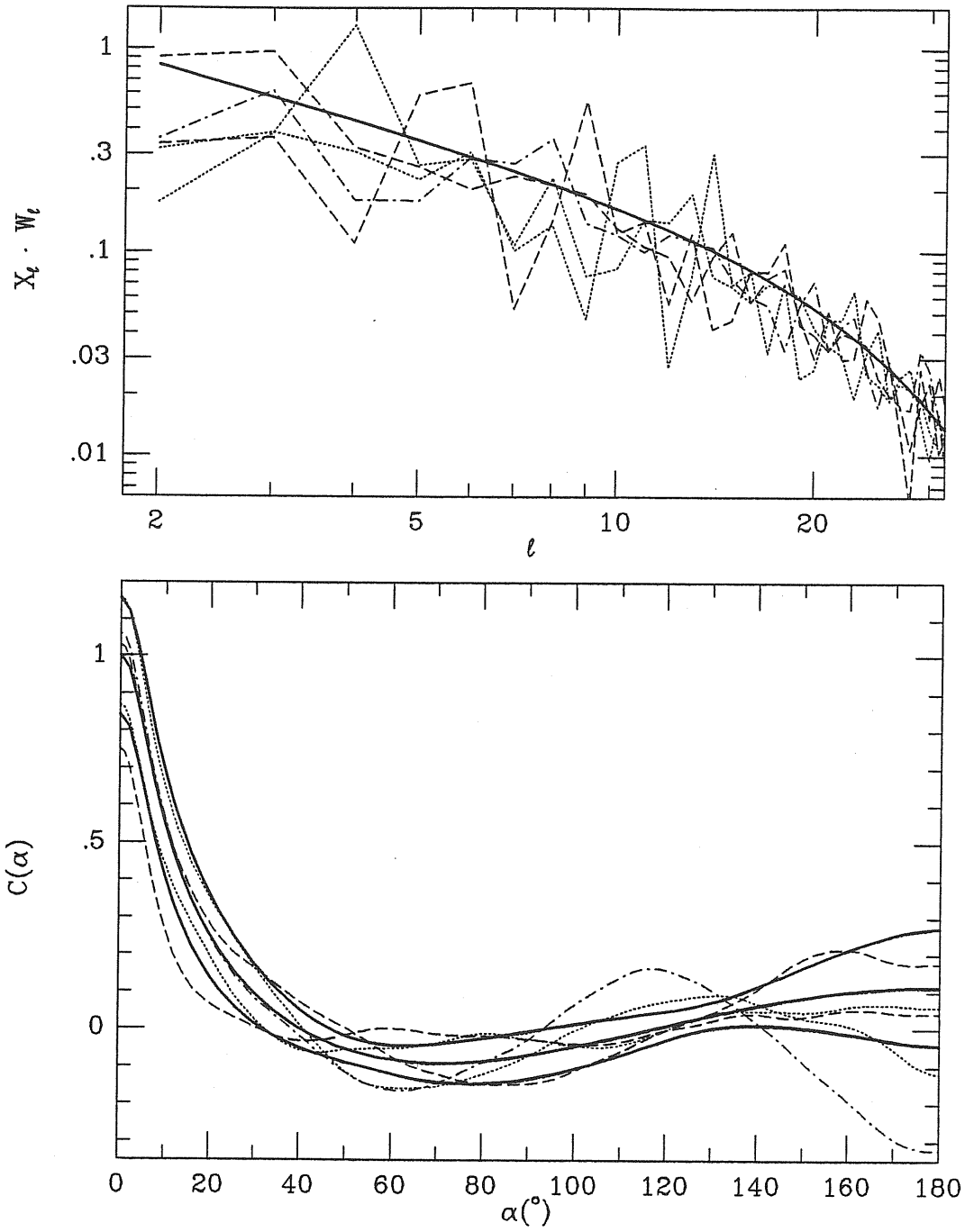

Figure III.10. *Five different random realizations (broken lines) for the product* $X_\ell^2 \cdot W_\ell(\alpha = 0, \sigma = 2^\circ.2, n = 1)$ *are shown in the top panel together with the average value (heavy solid line). The corresponding realizations of* $C(\alpha, \sigma)$ *are shown as a function of the angle* α *(same line types as in the top panel) together with the average value and the* $\pm$ 1 *s.e. band (heavy solid lines).*

primordial fluctuations from the experimental upper limits (see Sect. II.4).

The first who pioneered this approach were Abbott and Wise (1984a, 1984b

hereafter AB). They noted that it was incorrect to derive upper limits (ULs) to the normalization amplitude by direct insertion of the experimental ULs in relations which are valid for ensemble averages only: indeed, as shown in the previous section, the observable quantities can vary quite a bit from observer to observer even when the normalization amplitude is constant. Their discussion concentrated on the statistical uncertainty related to single harmonic components. Here we will enlarge their discussion to the acf and to joint and conditional pdf's and also complete the procedure by the inclusion of a simple but non-trivial point, neglected by AB.

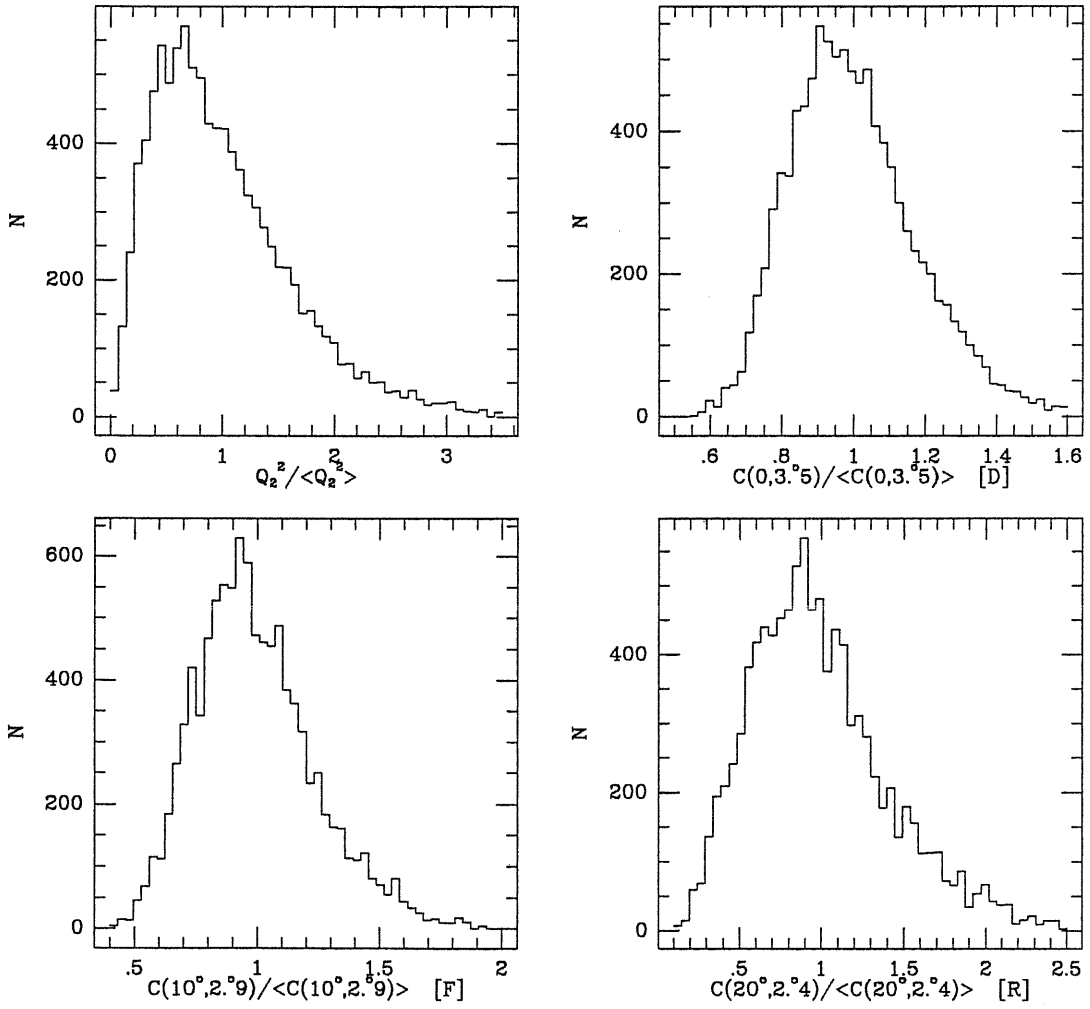

Figure III.11. *The pdf numerically obtained from* 10000 *different simulations is shown for four interesting quantities.*

Before starting to describe the method, we want to present in Fig. III.11 the

pdf obtained for quantities of interest in the following discussion (we remind the reader that D stands for Davies, F for Fixen and R for Relic: the experiments and results are described in Sect. II.4). Of course the only pdf which has an analytical expression is the one for the quadrupole, Q_2^2, and we tried to fit the others through Gaussian or chi-square distributions with poor results (a fit of the quadrupole distribution with a normalized χ_a^2 gave $a = 5.00 \pm 0.02$, which, because of the binning in the histogram and Poisson noise, can be considered to be an excellent result). The shapes and the width of these distributions have a non trivial dependence on the smoothing parameter, σ, and the beamthrow angle, α.

Let us now consider a given observable, y, for which an observational upper limit y_{lim} is available. Let us also assume that this observable is theoretically distributed according to a pdf $P_{th}(y)$ and with an expected value $\langle y \rangle$. It is then possible to define a parameter γ_ϵ such that

$$P_{th}\left(y \leq \gamma_\epsilon \cdot \langle y \rangle\right) = \epsilon \,. \tag{III.28}$$

For $y = y_{lim}$ we obtain $P_{th}(y_{lim} \leq \gamma_\epsilon \cdot \langle y \rangle) = \epsilon$ or, equivalently,

$$P_{th}\left(y_{lim} \geq \gamma_\epsilon \cdot \langle y \rangle\right) = 1 - \epsilon \,. \tag{III.29}$$

Then, at the $(1 - \epsilon)$ confidence level (hereafter c.l.), one has $y_{lim} \geq \gamma_\epsilon \cdot \langle y \rangle$.

This implies at the same c.l. an upper limit on the ensemble average of the observable y :

$$\langle y \rangle \leq \gamma_\epsilon^{-1} \cdot y_{lim} \,. \tag{III.30}$$

For ϵ small, $0 < \gamma_\epsilon \ll 1$. Because of this the upper limit on $\langle y \rangle$ obtained through Eq. (III.30) is weaker than that obtained by limiting $\langle y \rangle$ directly with y_{lim}. For example, as shown by AB, one finds that the upper limit on the expected squared quadrupole is almost one order of magnitude greater than the observational upper limit at the 99% c.l.

The c.l. considered so far take into account only the theoretical probability distribution. On the other hand, *the quoted upper limits y_{lim} have a confidence*

level by themselves, which should also be taken in account (AB treated such experimental limits as 'frozen').

Hence a more realistic approach consists in considering the joint probability with c.l.

$$1 - \epsilon(\langle y \rangle) \;=\; P_{exp}(y_{lim}) \cdot P_{th}(\langle y \rangle \leq \gamma_\epsilon^{-1} \cdot y_{lim}) \,, \qquad \text{(III.31)}$$

where P_{exp} is the experimental pdf from which the UL value y_{lim} has been derived together with its c.l.

Now, a good approximation for experiments with large sky coverage (Kaiser and Silk, 1987) is to consider P_{exp} to be a Gaussian of dispersion σ_{err} for the quantity y_{lim}. Therefore we finally have that

$$1 - \epsilon(\langle y \rangle) \;=\; erf\left[\frac{y_{lim}}{\sqrt{2}\sigma_{err}}\right] \cdot P_{th}(\langle y \rangle \leq \gamma_\epsilon^{-1} \cdot y_{lim}) \,. \qquad \text{(III.32)}$$

Table III.1

Observable y	Experimental limit y_{lim} quoted	adopted (96%)	$\gamma_{0.01}^{-1}$	Ensemble average upper limit (95%)	Upper limit on fluctuations amplitude $\mathcal{A}_{max}$ (95%)
Q_2 [BPG]	$2.5{\cdot}10^{-4}$ (90%)	$3.1{\cdot}10^{-4}$	$\sqrt{9.01}$	$9.3{\cdot}10^{-4}$	$8.3{\cdot}10^{-8}$
Q_2 [R]	$1.1{\cdot}10^{-4}$ (95%)	$1.1{\cdot}10^{-4}$	$\sqrt{9.01}$	$3.3{\cdot}10^{-4}$	$1.0{\cdot}10^{-8}$
$C(10^o,2^o.9)$	$1.4{\cdot}10^{-9}$ (90%)	$1.8{\cdot}10^{-9}$	1.85	$3.3{\cdot}10^{-9}$	$1.4{\cdot}10^{-9}$
$C(20^o,2^o.4)$	$5.5{\cdot}10^{-10}$ (95%)	$5.5{\cdot}10^{-10}$	4.0	$2.2{\cdot}10^{-9}$	$2.0{\cdot}10^{-9}$

Table III.1. *The upper limits derived on the amplitude of primordial fluctuations for the scale-invariant case.*

As an example, let us consider the available limits on the quadrupole and the a.c.f. for the scale invariant spectrum, $n = 1$. The appropriate numbers are reported in Table III.1 . We proceed as follows. We convert published upper limits, quoted to a given c.l., to new limits at the 96% c.l. The limits on the expected values of different observables are then obtained by Eq. (III.32) with

$\gamma_{0.01}^{-1}$. The resulting upper limits on the expected values are therefore at 95% c.l. (see Table III.1). It is then possible also to obtain upper limits at the same c.l. for the overall normalization $\mathcal{A}$ by using the relations of Sect. II.5 .

It is of interest to note that the most stringent upper limits come from those on the acf's and that the acf seems to be the most powerful observable to constrain primordial amplitudes.

We now pass to outlining methods for checking the self–consistency of different experimental results within the framework of the present model, taking proper account of the inherent uncertainties.

The recently claimed detection of CMB temperature anisotropy (Davies *et al.*, 1987) provides in principle a unique tool for determining the amplitude of density fluctuations in a self consistent way, in the framework of the linear theory. Also, it would provide a way of checking the consistency of this experiment with other upper limits. This has been done by taking into account only expectation values (cfr. Sect. II.5 and Scaramella and Vittorio, 1988a). We want here to generalize the argument by properly taking into account the statistical distribution of different observables. Independently of the confirmation of the Davies *et al.* result, we want to stress a method that would provide a self consistency check of the theoretical assumptions, given a set of observations.

As we see from Fig. III.12 , upper limits on the quadrupole value reflects very poorly on limits on the temperature fluctuations under scrutiny, so we will pass to discussing those obtained on the acf itself.

The R experiment (see Sect. II.4) sets an upper limit $C^* = 5.5 \cdot 10^{-10}$ on the amplitude of $C(20^0, 2.4^o)$ (see Table III.1). Then, following the formalism given in Eq. (III.20) an following, we have

$$C^* \geq C(20^o, 2.4^o) = \alpha \langle C(20^o, 2.4^o) \rangle = \alpha \frac{\langle S(20^o, 2^o.4) \rangle}{\langle S(0^o, 3.5) \rangle} \langle C(0, 3^o.5) \rangle \ . \quad \text{(III.33)}$$

Here $\alpha \equiv [C(20^o, 2.4^o) / \langle C(20^o, 2.4^o) \rangle]$ and $\langle S(\alpha, \sigma) \rangle$ is the value of the sum defined in Eq. (III.22) and obtained by direct summation of the appropriate values for

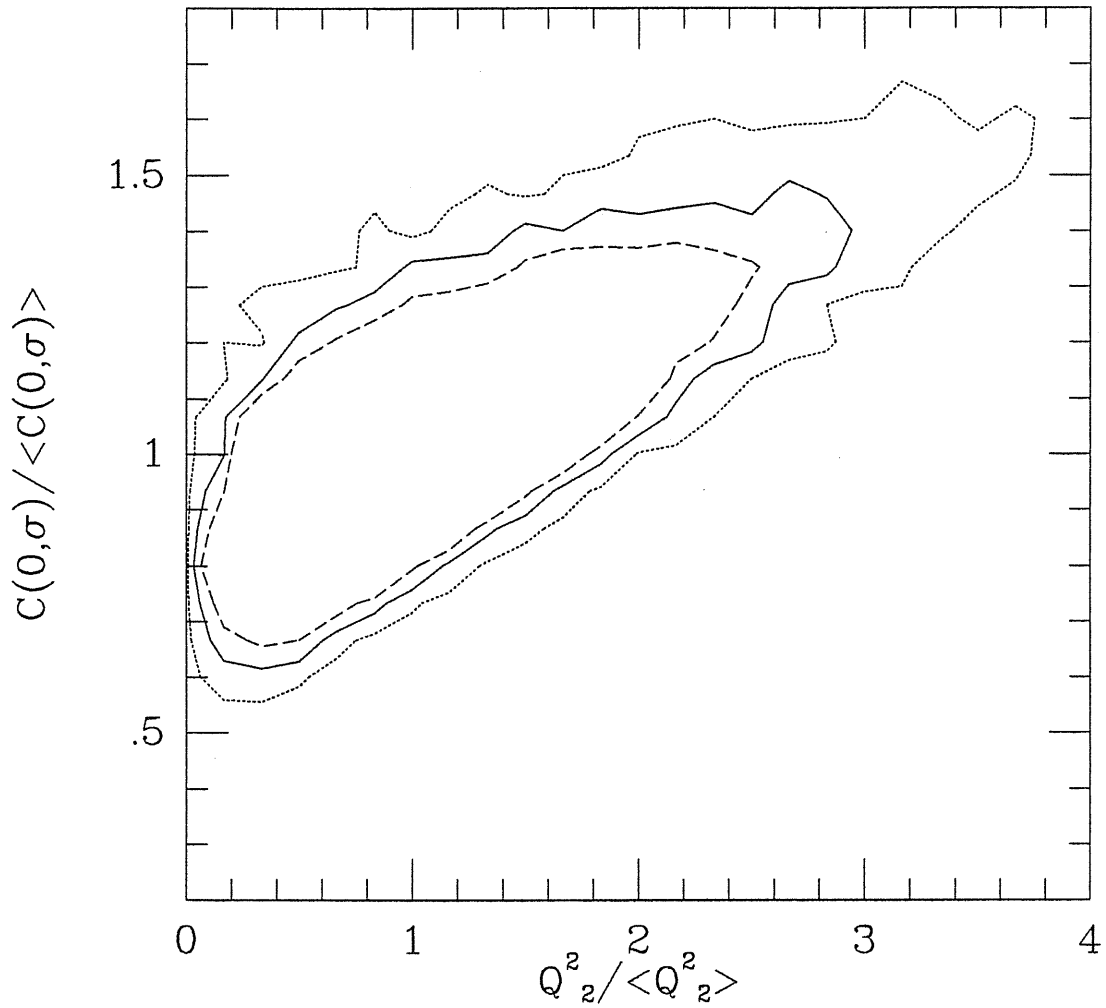

Figure III.12. *Isoprobability contours for the joint distribution of the value of the acf at zero lag with* $\sigma = 3.5^o$ *and the quadrupole value. Dotted line:* 99 %, *solid line:* 95 %, *dashed line:* 90 %.

$W_\ell(\alpha, \sigma)$ (remind that $\langle X_\ell \rangle = 1$). On the other hand, (see Eq. (II.38)), for the D recorded temperature we have that

$$\begin{aligned} \langle \Delta^2 \rangle =& \frac{3}{2} \langle C(0, 3^o.5) \rangle + 2 \langle C(8^o, 3^o.5) \rangle - \frac{1}{2} \langle C(16^o, 3^o.5) \rangle \\ \cong & \; 0.248 \, \langle C(0^o, 3^o.5) \rangle \, . \end{aligned} \tag{III.34}$$

The last factor comes from assuming the appropriate scaling for the $\langle |a_l^m|^2 \rangle$ for the Zel'dovich spectrum. Then by substituing in Eq. (III.33) we have

$$C^* \geq \alpha \, \frac{\langle S(20^o, 2^o.4) \rangle}{\langle S(0^o, 3.5^o) \rangle} \, \frac{\langle \Delta^2 \rangle}{0.248} = \frac{\alpha}{0.248} \, \frac{\langle S(20^o, 2^o.4) \rangle}{\langle S(0^o, 3.5^o) \rangle} \, \frac{\Delta^2}{\beta} \, , \tag{III.35}$$

where Δ^2 is the D measured value and β is the actual measured value in units of the expected value. Substituing the observed upper limit C^*, the measured $\Delta^* = 3.0 \cdot 10^{-5}$ (see Sect. II.5), and the values $[\langle S(20^o, 2^o.4)\rangle / \langle S(0^o, 3.5^o)\rangle]$ one gets

$$\alpha \leq 0.61 \ \beta \left(\frac{\Delta^*}{\Delta}\right)^2 . \qquad \text{(III.36)}$$

A similar result is obtained on using the Fixen upper limit with a similar line of argument. In fact in this case, correcting the F limit upwards to have 95 % c.l., one gets

$$\alpha \leq 0.72 \ \beta \left(\frac{\Delta^*}{\Delta}\right)^2 . \qquad \text{(III.37)}$$

Using our simulation, we find that 1843 and 1139 realizations, out of 10000, satisfy the inequality given by Eq. (III.36) and Eq. (III.37) respectively, for $\Delta^* = \Delta$ and 1094 case satisfy both inequalities at the same time. Therefore we have at this stage that a level of temperature fluctuations $\Delta = \Delta^*$ would be in contrast with the measured upper limits with a low final confidence level: 77.5 % from the R limit, $\sim$ 84 % from the F limit and only $\sim$ 80 % if one considers their union. The cause can be understood by considering the joint distribution of $\Delta^2/\langle\Delta^2\rangle$ and $[C(20^o, 2^o.4)/\langle C(20^o, 2^o.4)\rangle]$, which is given in Fig. III.13 . Note that the distribution of $\Delta^2/\langle\Delta^2\rangle$ is very narrow around the unity value, a fact which implies that different observers should measure an anisotropy which differs from the expected value at most by 20%, quite independently of the actual value of $[C(20^o, 2^o.4)/\langle C(20^o, 2^o.4)\rangle]$.

On the other hand, one can take advantage of the sharpness of the Δ distribution, which is much steeper than the Gaussian of the experimental upper limit: if we consider the values for C^* at 90 % c.l., we obtain that the numbers in the inequalities of Eq. (III.36) and Eq. (III.37) become respectively 0.51 and 0.59. Now only 1149 and 238 cases, respectively, satisfy these constraints, with final confidence levels of $\sim$ 80 % and $\sim$ 88 %. The latter limit shows that the best constraint comes from the F experiment (only one out of the 238 cases does not satisfy the R constraint also), mainly because of its angle, very appropriate for the

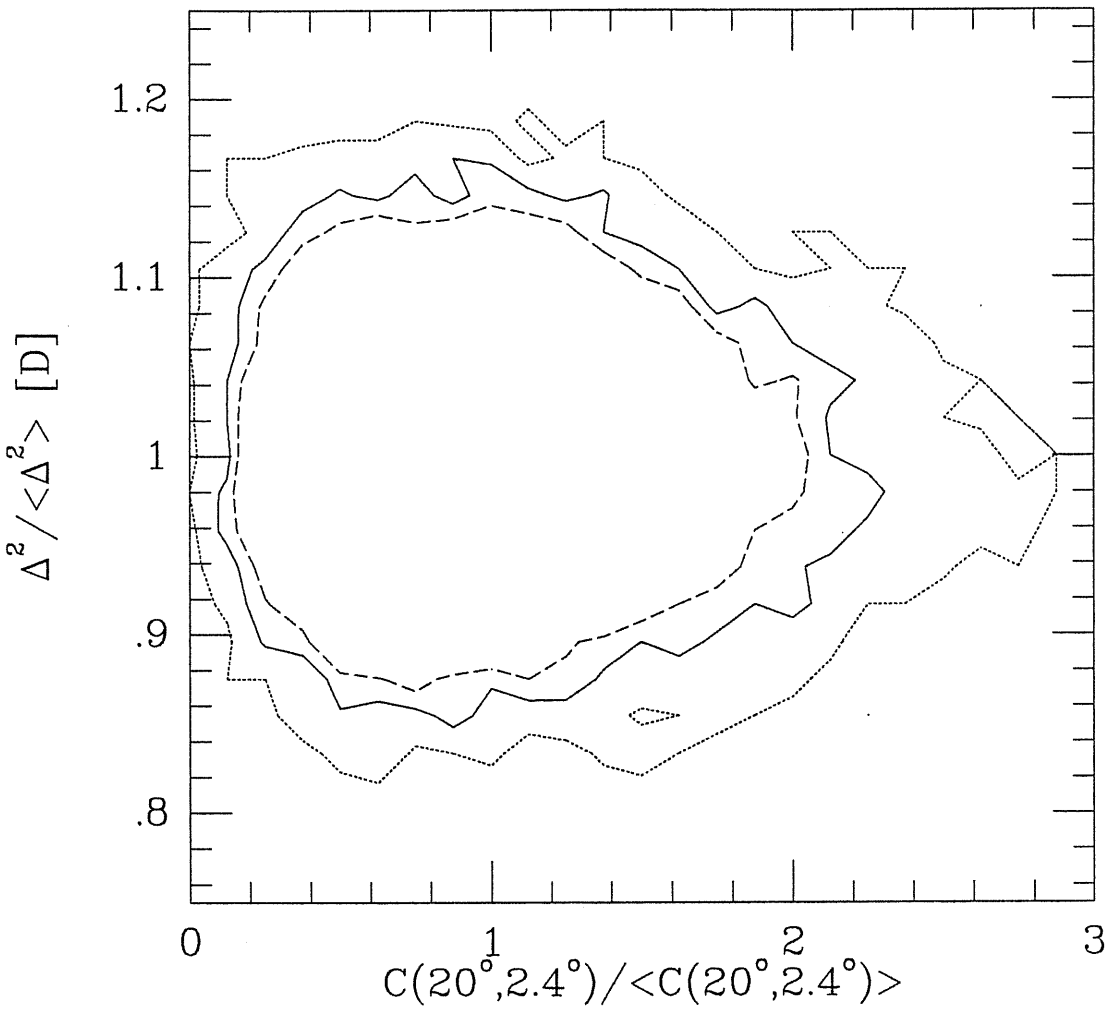

Figure III.13. *Isoprobability contours for the joint distribution of the temperature fluctuations as measured by the D experimental setting and the value of the acf with the F parameters. Dotted line:* 99 %, *solid line:* 95 %, *dashed line:* 90 %. *Note different axes' scaling.*

range of angles used by D. Indeed from Fig. III.14 we can see that, although correlated, there is a large uncertainty in the mutual regression of the acf evaluated for the R anf F cases (e.g. slightly less than a factor of two in the actual value for R if the value for F coincides with its average).

Up to this moment, we have used information on $C(\alpha, \sigma)$ at a given angle α. Results of the simulations (see Fig. III.14) show that $C(20^o)$ and $C(10^o)$ are weakly correlated. On the other hand, for a given observer, $C(\alpha, \sigma)$ is uniquely determined for all $\alpha's$ and we will show the importance of having the full information available. Before starting the discussion of this new kind of approach it is useful to have a

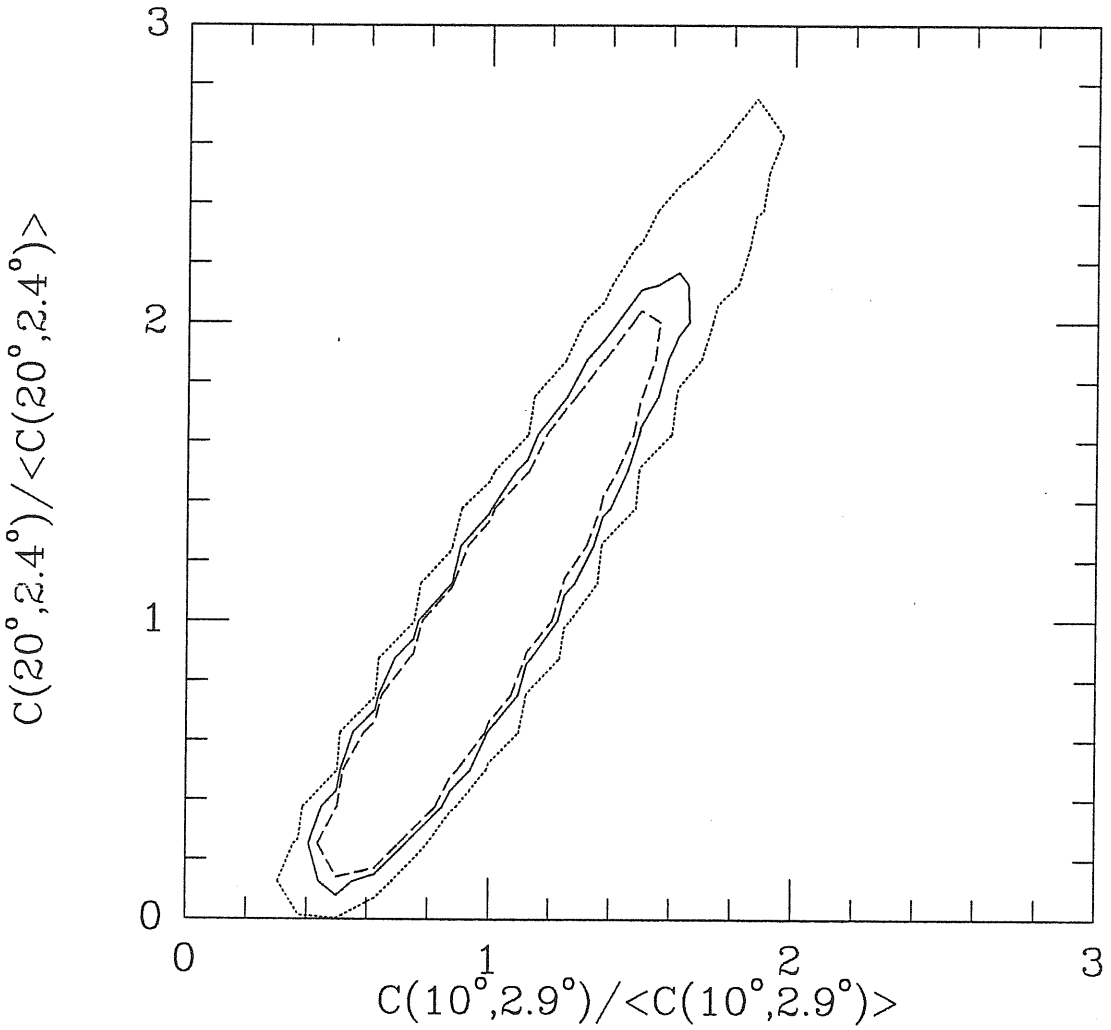

Figure III.14. *Isoprobability contours for the joint distribution of the values for the acf as measured with parameters appropriate for the F and R upper limits. Dotted line:* 99 %, *solid line:* 95 %, *dashed line:* 90 %.

direct comparison of the relative widths of the theoretical distributions considered so far: they are shown in Fig. III.15 . The acf seems to get broader as α increases, but one should remind that the beam dispersions are different, as they are for the Melchiorri *et al.* (M) setting (single subtraction) and the one by D (double subtraction). Hence *detailed computations are needed for each case*. On the other hand, the numerically computed variances are in very good agreement with the analytical estimates (cf. Eq. (III.24)).

We pass now to discussion of the possible use of the known upper limits on the *shape* of the acf. The Relic satellite provides us also with upper limits on

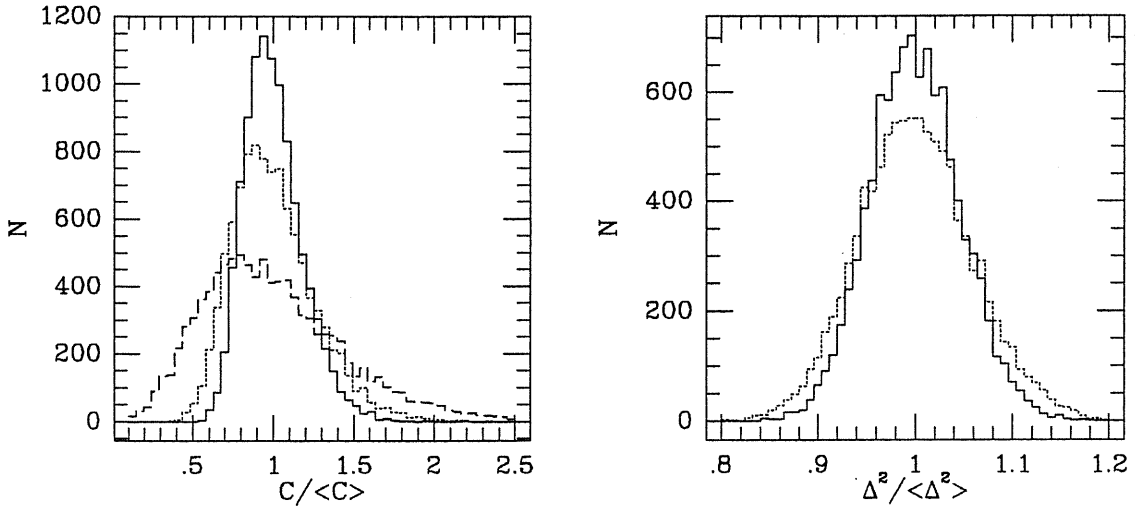

Figure III.15. *A direct comparison of the widths of the pdf's for the values of the acf considered so far, left panel (solid line: D at zero lag; dotted line: F; dashed line: R). The same for two different settings for* $(\Delta T/T)^2$ *measurements (solid line: M; dotted line: D). 10000 simulations.*

the correlation function on angular scales $20^o < \alpha < 150^o$ (Strukov *et al.*, 1986). These new, revised upper limits (the limit on the acf is 5/4 of that quoted by Lukash and Novikov, 1987) are still more stringent than the F ones by at least a factor of two. These limits are plotted in Fig. III.16 .

We have then built up the probability distributions for the quadrupole and the Melchiorri *et al.*, Davies *et al.* experiments, under the condition of normalizing each realization with the maximum amplitude compatible with the R and F upper limits on $C(\alpha, \sigma)$ taken at the 96 % c.l. Two of these cases are shown as an example in Fig. III.16 . This provides us with the maximum amplitude of fluctuations observable for a given observer.

These distributions differ from the ones shown in Fig. III.11 . In that case we plot the intrinsic theoretical distribution, in units of the expected values. Fig. III.17 shows the distribution of the quadrupoles measured by different observers, under the previously discussed assumption. At the 95% final confidence level, we expect that the quadrupole value (99 % of the numerical pdf is below $Q_2^2 \cong 5.0 \cdot 10^{-8} K^2$) is less than the quoted R upper limit ($Q_2^2 \leq 8.2 \cdot 10^{-8} K^2$) by

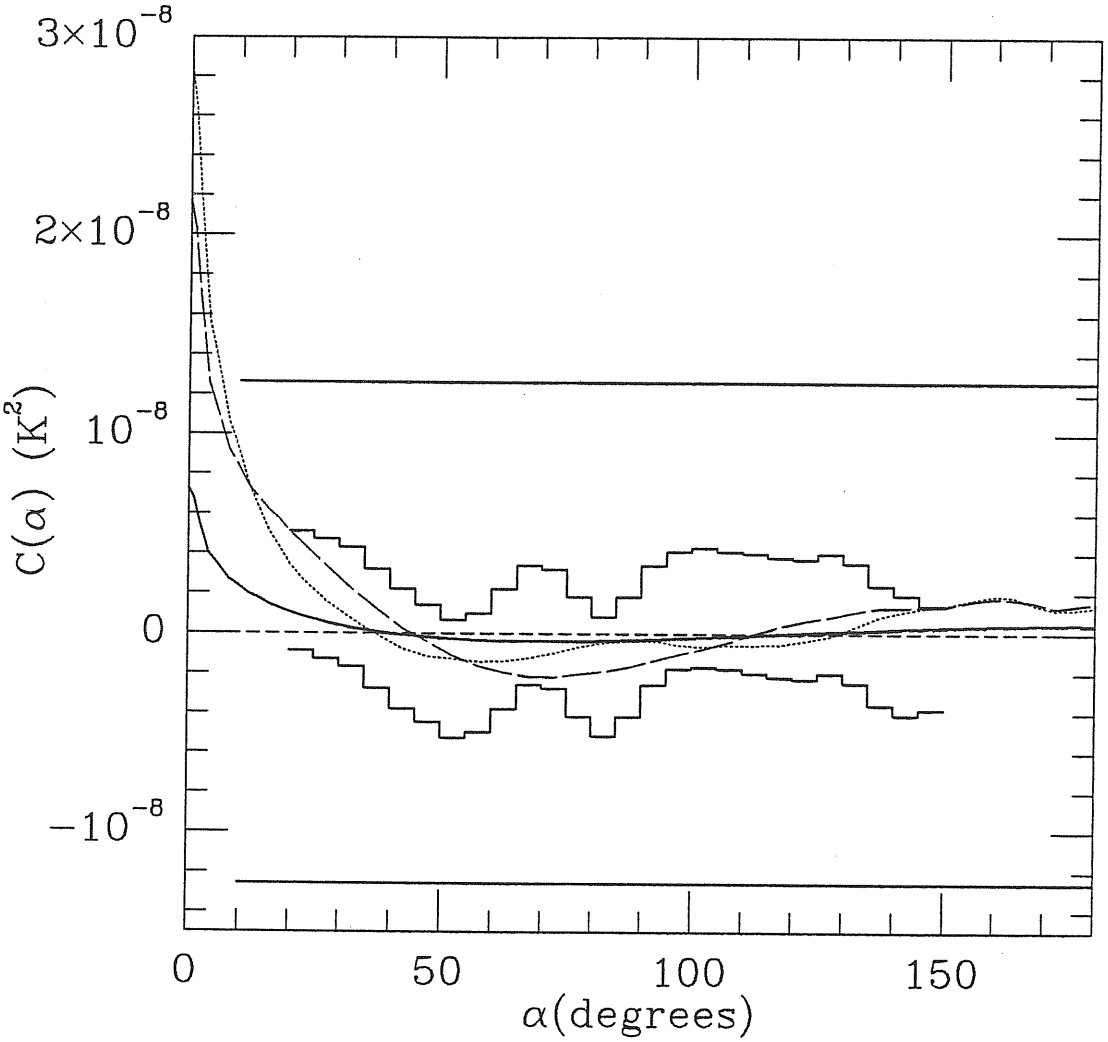

Figure III.16. *Present upper limits on the acf oscillation band are plotted as heavy solid lines: outer straight lines are the F limit, jagged lines are the R limit. Two maximally compatible shapes for the acf, out of 10000 simulations, are shown as dotted and long-dashed line, while the maximally compatible ensemble average acf is shown as heavy solid curve.*

~ 40 %. The same analysis has been applied to the D and to the M experiments. The relative distributions are also shown in Fig. III.17 .

Despite the similarities of the reported upper limit and detection, the two distributions show some differences. In particular, if we compare the distribution with the M upper limit, we find that the quoted upper limit ($\Delta^2 \leq 1.16 \cdot 10^{-8} K^2$) roughly identifies the maximum of the distribution. In other words, it is the value that most of the observers, under the condition of being maximally consistent

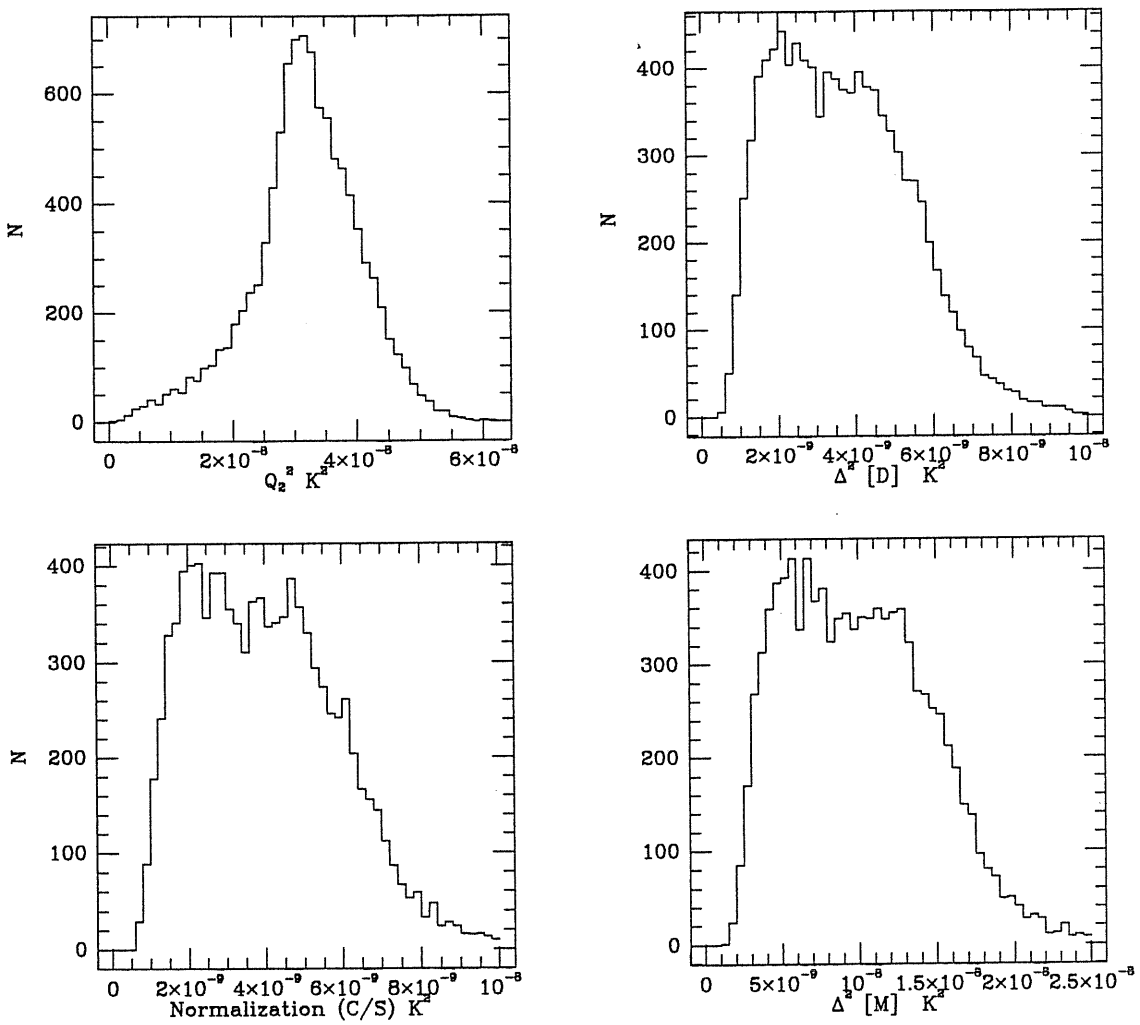

Figure III.17. *Posterior df's obtained for each realization -10000 simulations- from the maximum amplitude compatible with the known upper limits.*

with the R and F upper limit on the $C(\alpha, \sigma)$ would have measured. In the Davies *et al.* case ($\Delta^2 = 6.6 \cdot 10^{-9} K^2$), on the contrary, only $\sim$ 5% of the observers would have measured $\Delta \gtrsim \Delta^*$. Therefore we are led to the conclusion that a level of fluctuation such as the one found by Davies *et al.* cannot be compatible with present upper limits at the overall $\sim$ 91 % c.l. in the theoretical frame we assumed.

It is also of great importance to determine the maximum ensemble amplitude 'safely' compatible with the upper limits on the acf. We found that with an amplitude $\langle \mathcal{A} \rangle = 9.6 \cdot 10^{-10} K^2$ only 1 % of 50000 cases would violate the upper limits at 96 % c.l. Our conclusion is then that with 95 % c.l. such 'safe' ensemble amplitude for a scale-invariant spectrum is: $\langle \mathcal{A} \rangle \leq 1.3 \cdot 10^{-10}$.

We can make the comparison of this value with that quoted as a 95 % c.l. upper limit on the quadrupole for the Zel'dovich spectrum by Lukash and Novikov (1987) and by Strukov *et al.* (1986). In these papers, the values $2 \cdot 10^{-5}$ and $1.6 \cdot 10^{-5}$ are respectively quoted as limits obtained by fitting the spectrum $C_n^2 \propto (2n+1)/[n(n+1)]$. By this description we were led to think that this limit was obtained by fitting the average spectrum. Different to our first understanding, though, the procedure followed in obtaining such a limit was very similar to the one we adopted here. The procedure (Klypin, private communication) consisted in simulating $\sim \mathcal{O}(100)$ theoretical skies and then feeding this pattern into a selection function which contained all the details of the experiments, like the sky areas with different weights due to different sampling, the experimental noise, the receiver response, and so on. Taking into account the different definition of quadrupoles (cfr. Sect. II.4) we have that $Q_2^R \leq 5.7 \cdot 10^{-5}$ while from our limit we find $Q_2 \leq 3.7 \cdot 10^{-5}$ which translates into a decrease of ~ 35 % with respect to the R limit. The R limit is higher because we enforced also the F upper limit on the acf and this constrains $\sim 1/4$ of the possible shapes (e.g. $\sim 1/4$ of the acf simulations 'hit' this limit) and perhaps because of their use of the whole information about the experimental details which could not entirely be represented by the published acf confidence band.

Therefore, by using the whole information stored in the acf shape, we have been able to decrease by one order of magnitude the upper limit on the quantity $\mathcal{A}$ from that obtained by the use of the 'best value' alone (cfr. Table III.1). This conclusion is limited here to flat universes, as discussed in Sect. II.5 . We will leave the application of this method to open universes to future work. In the meantime we want to note that, using standard normalization (e.g. $\Delta M/M(R_s) = 1/b$ for $R_s = 8h^{-1}Mpc$ with b a bias factor) for the cold dark matter (CDM) spectrum and the derived upper limit on $\langle \mathcal{A} \rangle$, one has that $[\mathcal{A}_{CDM}/\langle \mathcal{A} \rangle]^{1/2} \approx (1/2)\, b^{-1}\, h_{50}^{-1}$. Hence we find that the global normalization for the 'standard' CDM model ($\Omega_0 = 1$, $n = 1$, $H_0 = 50\, kms^{-1}Mpc^{-1}$) in the unbiased case ($b = 1$) is only a factor of two below the upper limits: previously it was thought instead that this model allowed plenty of room, almost one order of magnitude. Similarly one

can limit the nonlinearity epoch of a massive neutrino model. With the normalization $\Delta M/M(R_s) \simeq 0.6(1+z_{NL})$ and a neutrino free–streaming length of $\lambda_{fs} \simeq 13\,h^{-2}Mpc$, we find that, for $h = 1/2$, the nonlinearity epoch is severely constrained: $z_{NL} \lesssim 2$ (even lower for anti–biased models). We will leave also to future work the full discussion of these effects on the various cosmological models.

III.5 A recently reported 'bump' in the CMB sky: when could it have originated ?

In a recent meeting, the Tenerife group reported preliminary results (Watson *et al.*, 1988) of the new experiment, which had the same setting as the one described in Davies *et al.* (1987), the only difference being the smaller dispersion σ ($3.5^o \rightarrow 2.4^o$).

Because of the increased resolution, the data now showed to the eye a positive 'bump' which is not explained by known radiosources contribution. Watson *et al.* suggested that the level of anisotropy found in the Davies *et al.* analysis was essentially due to the signal coming from the bump region, $\sim 15^{\rm h}$, as we independently found with our 'jack-knife' analysis of the Davies *et al.* data (see Sect. III.2).

The bump has a span of $\sim 30^{\rm min} \lesssim 6^o$ at the scan declination, and with a signal level of $\sim 0.3mK$. Watson *et al.* noted that in the same direction on the sky lie two interesting astronomical features: the Bootes void and a string of galaxies, suggesting that gravitational effects alone from these features are an unlikely cause for the bump.

Because of the importance of such a finding for its possible cosmological implications, we want to give a more detailed discussion of these points, with the stress put more on the procedure than on the possibility of reaching a definitive conclusion, because of the partial amount of available information.

It is useful for the following discussion to have an estimate of the surveyed

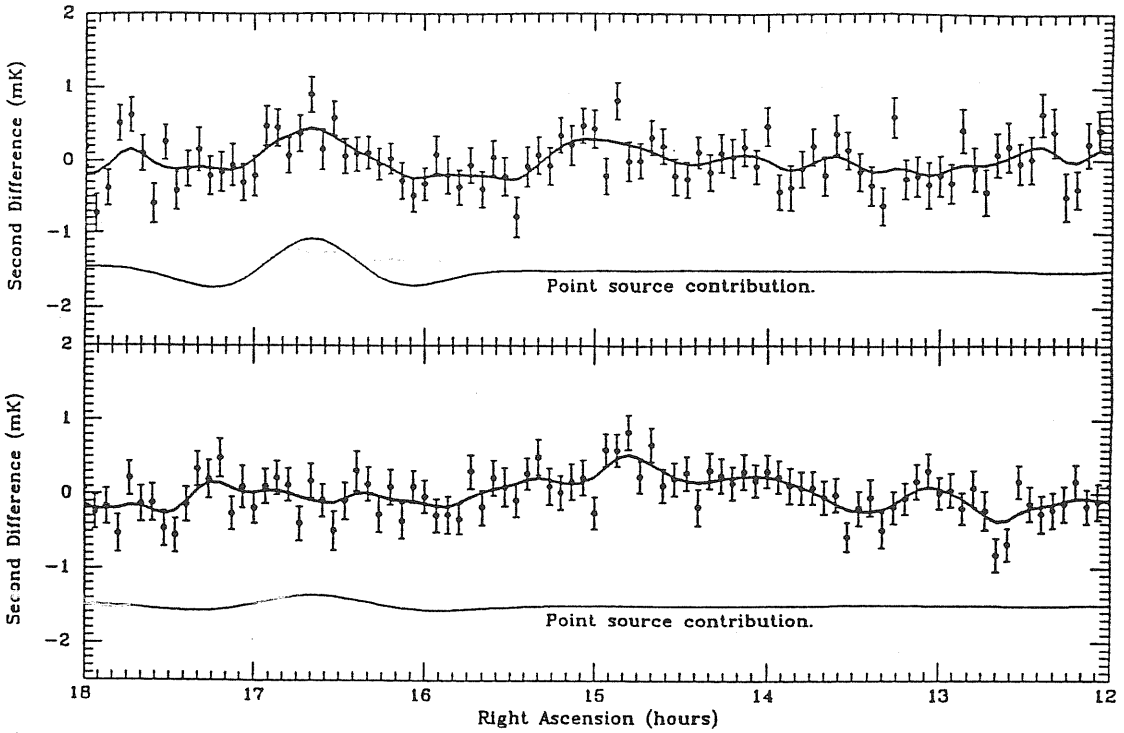

a) The most sensitive part of the scan of 5.6° data, between RA 12^h and 18^h showing 1 sigma error-bars and a line of a running gaussian mean (of width 2.8°) and, below, the predicted point source contribution.
b) Same as (a) but of the original 8.8° system.

Figure III.18. *(adopted from Watson et al., 1988) The scan with the smaller beam dispersion (upper panel) and the one with the larger beam dispersion (lower panel) are shown together with the estimated radiosources point contribution*

area: the experiment scanned the sky at fixed declination, $\delta = 40°$, with Gaussian beams of dispersion $\sigma = 2.4°$, a beamthrow angle $\alpha = 8°$ and double beam subtraction (the same configuration as that given in Davies *et al.*, 1987, only the beam dispersion is different). The best data come from the range in Right Ascension between 12^h and 18^h and a generous estimate for the width of the surveyed strip is $\simeq 10°$ (e.g. a $\sim 4\sigma$ band, up to where the beam response falls off by 90 % from its peak value). With the above values the covered area results $\delta A \simeq 0.21\, sr$, that is only 1.7 % of the sky.

One of the possible causes for the bump is that this signal is directly related to the primordial perturbations at the recombination epoch, and therefore that the position and the characteristics of the bump have a statistical origin. If a fluctuation field is present in the density distribution of the matter on large scales,

this will reflect into temperature fluctuations of the CMB through the Sachs–Wolfe (1967, S–W) effect (see Sect. II.1). Zabotin and Naselski (1985) and Sazhin (1985) explicitly noted that the temperature pattern originated in such a way would of course show peaks and troughs, giving therefore detection chances also to experiments which could come close in sensitivity but not reach the average (e.g. rms) fluctuation level.

The properties of the resulting fluctuation field have been studied in detail by Vittorio and Juskiewicz (1986, hereafter VJ) and Bond and Efstathiou (1987), under the hypothesis that the matter density field in a flat universe has a Gaussian distribution with a scale–invariant (Harrison–Zel'dovich) spectrum (see Sect. III.1). The results given in the previous papers are relative to the expected values taken over the ensemble constituted by all possible observers: unfortunately on the large angular scales, in contrast to smaller ones, it is not possible to justify a spatial ergodicity (see Sazhin, 1985) and hence it seems that the only way to get probability density distributions is to resort to Monte–Carlo numerical simulations. This is essentially due to the fact that temperature fluctuations on large scales are correlated even for directions which differ considerably (see Sect. II.3 , Coles, 1988, Scaramella and Vittorio, hereafter SV, 1988a). With the caution given above, let us then discuss the case for primordial power law density spectra ($|\delta_k|^2 \propto k^n$) which have a Gaussian distribution in a flat universe. For the case $n = 1$, scale–invariant, an application of the theoretical curve for the smoothed temperature autocorrelation function $C(\alpha, \sigma)$ (hereafter acf, where α is the sky separation angle) due to the SW effect (SV, 1988) to the data taken from the same experiment with a larger beam ($\widetilde{\sigma} = 3.5^\circ$) gives (see Sect. III.2 , Vittorio *et al.*, 1989) $\widetilde{t} \equiv [C(0, \widetilde{\sigma})]^{\frac{1}{2}} = 0.16\ mK/T_b \simeq 6 \cdot 10^{-5}$ (T_b is the background temperature).

Following VJ one can evaluate the probability of having a spot which is a peak (or a well) of amplitude ν times the rms level, t. Because the observed hot spot appears to be almost resolved, one cannot take advantage of the subtraction technique and the appropriate probability is here that for an 'absolute' detection. An excursion in temperature of amplitude $\Delta \geq \nu \cdot t$ subtends a mean angle of

$D(\nu) = 2\sqrt{2}\, t/(\nu u)$ degrees, where $u \equiv -\frac{d^2}{d\alpha^2} C(\alpha,\sigma)|_{\alpha=0}$ (see Sect. III.1). On the other hand, for a given intrinsic value, the recorded level of fluctuation is a function of the amplitude of the beam dispersion (Sect. III.1 , SV, 1988a), hence we must convert the above value of $\tilde{t}$ to that appropriate for the smaller beam, finding $t \equiv [C(0,\sigma)]^{\frac{1}{2}} \cong 0.18\, mK/T_b$. Now a fluctuation peak of $\Delta \cong 0.3\, mK/T_b$ is not much above the mean level: $\nu' \simeq 1.7$. We can then get an *approximate* idea of how probable a detection of such a peak would be if we still continue to use the asymptotic expressions given in VJ, although these are fully valid in the limit $\nu \gg 1$. Defining $\theta \equiv 2\,\sigma$, for $n = 1$ one has $D(\nu) \cong 2.8\,\theta\, F(\theta)/\nu \simeq 20^o/\nu$, where $F(\theta) = [\ln(1^o/\theta) + 3.78]^{\frac{1}{2}} \cong 1.5$ (see VJ). Hence we can estimate the average number of hot spots between $\nu_1' = 1.5$ and $\nu_2' = 2$ as

$$N_*(\nu_1') - N_*(\nu_2') = \frac{2600}{[\theta\, F(\theta)]^2} \left[\nu_1' \, e^{-({\nu_1'}^2/2)} - \nu_2' \, e^{-({\nu_2'}^2/2)}\right] \cong 11 \qquad \text{(III.38)}$$

over the whole sky. Therefore one would expect ~ 0.9 of such spots with $\nu \approx \nu'$ per steradian and a ~ 20 % chance of getting one in the surveyed region.

On the other hand the value for $\tilde{t}$ used above seems to depend strongly on the particular hot spot examined here (Sect. III.2 , Vittorio *et al.*, 1989; Watson *et al.*, 1988) and if this is the case the above argument does not apply because the estimated value for $\tilde{t}$ is no longer representative of the mean rms. We can instead try to get an estimate for the value of t: this should be greater than that which would give a very small chance for a positive detection. Indeed if we in principle allow only a 5 % detection probability (only three such spots on the whole sky), this obviously increases the peak height: $\nu \cong 2.8$ (hence a better confidence in the relations used), which would allow a background value for t as low as $t \simeq 0.11\, mK/T_b$.

The previous estimate, though, should be raised somewhat when one takes into account the fact that the spot should at least fill the beam in order not to loose too much of the signal (cf. discussion below) and its chance to be exactly on the axis of the receiver is quite low. Therefore one could still argue in favor of intermediate values for the peak height, $2 \lesssim \nu \lesssim 3$, getting $t \simeq 0.10$—$0.15\, mK/T_b$. To consider a different n for fixed ν would increase (decrease) the average number

of hot spots for $n > 1$ ($n < 1$) while the opposite behaviour is expected for the mean diameter, D (Sect. III.1 , SV, 1988b). On the other hand, we want to stress the fact that in order to make more precise and meaningful estimates one should first have a two–dimensional map of the isotemperature contour of the bump on the sky and then evaluate directly the probability of such an occurrence through specific Monte-carlo simulations.

Large fluctuations in the temperature pattern on the sky, albeit related to primordial effects, are not necessarily due to large scale perturbations such as those considered in the previous paragraph.

If one is willing to abandon the hypothesis of the isotropy of the universe and hence the basic Friedmann–Robertson–Walker (FRW) model, some of the anisotropic homogeneous models (e.g. Bianchi–type) show an effect which can be of great relevance to the observed bump.

As pioneered by Novikov (1968) and then extensively analyzed mainly by the Russian school and by Barrow and collaborators (Barrow *et al.*, 1983; Lukash and Novikov 1985; Barrow *et al.*, 1985; for a review see Barrow, 1986, and references therein) some universe models, because of the anisotropy present in their expansion, show a peculiar feature in the temperature pattern: a cosmological 'hot spot'.

This phenomenon happens in open universes (but not necessarily in all open models) and more specifically in the anisotropic models Bianchi–V and Bianchi–VII$_{h\neq 0}$ (see Mac–Callum, 1979, for a general discussion). The typical quadrupole pattern of axisymmetric Bianchi–I gets focused in a small region of the sky, whose extent increases with Ω_0. In models Bianchi–VII$_{h\neq 0}$ also a spiral pattern is superimposed (Barrow *et al.*, 1986). The size of this focused region is $\approx 80\,\Omega_0$ degrees, therefore for $\Omega \lesssim 0.1$ one would get roughly the right scale of the reported bump.

As stressed by Barrow (1986) the discovery of a *unique* such spot in the sky would prove the universe to be open. The very same uniqueness of this phenomenon, on the other hand, makes its chances of being detected, if present,

inversely proportional to the fraction of the sky covered by the experiment, which in the present case (see above estimates) is very low: ≈ 1—$2\,\%$ (moreover, in an 'unlucky' situation in which by chance the direction of such 'hot spot' is within a few degrees of the galactic plane, we probably would never be able to separate its signal from the galactic emission).

The ulterior effects of the beam smearing and of scattering due to a possible reheating of the universe are discussed in detail by Bajtlik *et al.* (1986). Also, from their Fig. 3b is clearly seen that if the metric is not axisymmetric, both the two hot and the two cold spots are focused in a small region ($\approx 5^{\circ}$ for $\Omega_0 = 0.1$) and integration by the beam would then greatly depress the original signal, hardly giving the observed shape.

Another possible cause for the signal is that of a 'localized' extragalactic origin. We will discuss the likelihood that the signal could be due to nearby ($0 < z \ll 1$) known structures, such as those hypothesized by Watson *et al.*.

In the field of view corresponding to the direction of the recorded signal a string of galaxies is present (Tago *et al.*, 1986). Because of its unusual distribution in space, this structure has been suggested to be a relic of a pancake collapse in which the two smallest among the eigenvalues of the initial deformation tensor (see Zel'dovich and Novikov, 1983) had same value. Here only the number of galaxies and their position on the sky is of interest.

First we note that, for completely unresolved sources, the dilution factor of the present beam is high: $\Omega_A^{-1} \equiv (2\pi\sigma^2)^{-1} \cong 92$. Therefore one needs quite a powerful radiosource to generate the recorded signal: because we are in the Rayleigh–Jeans region (R–J), one has that $S_\nu = 2\,k_B\,T\,\Omega_A/\lambda^2$ (Pacholczyk, 1970) and hence that the required flux density for a single on–axis point source would be $S_\nu \lesssim 10\ Jy$. Such a powerful source would have already been taken into account by Watson *et al.*, who subtracted known sources with $S_\nu \geq 1\ Jy$, listed by Kuehr *et al.* (1981). We can estimate the required average contribution from these galaxies

as follows: the response from the beam is

$$R_\nu(x,y) = \frac{1}{\Omega_A} \int_{-\infty}^{+\infty} dx' \int_{-\infty}^{+\infty} dy' I_\nu(x',y') \exp\left\{ -\frac{[(x-x')^2 + (y-y')^2]}{2\,\sigma^2} \right\}, \quad \text{(III.39)}$$

where the signal from point–like sources can be written as

$$I_\nu(x',y') = \sum_{i=1}^{N} S_{\nu,i}\ \delta(x_i - x')\,\delta(y_i - y')\,. \quad \text{(III.40)}$$

Therefore we have $R_\nu(x,y) \cong \Omega_A^{-1}\,\langle S_\nu \rangle\ f(x,y)$, where $\langle S_\nu \rangle$ is the average flux from these sources and

$$f(x,y) \equiv \sum_{i=1}^{N} \exp\left\{ -\frac{[(x-x_i)^2 + (y-y_i)^2]}{2\,\sigma^2} \right\} \quad \text{(III.41)}$$

From the galaxies listed in Table 2 of Tago etal we find that for the beam center positioned at $\alpha = 14^h\ 55^m$ and $\delta = 40^o$, $f \lesssim 3$. It follows that one would need at least $\langle S_\nu \rangle = \Omega_a\, 2\, k_B T\, \lambda^{-2}/f \gtrsim 3\ Jy$. Obviously at least some of these galaxies would have been well above this average value and therefore would have certainly shown up in the aforementioned catalogue of radiosources.

Let us now examine two possible effects on CMB due to the void *alone*, namely gravitational and inverse Compton (Zel'dovich and Sunyaev, 1969; SZ effect).

The Bootes void, discovered by Kirshner *et al.* (1981), is one of the largest underdensities near us: according to Kirshner *et al.* (1987, KOSS), the greatest sphere that can be fitted to the data has a radius $R = 31\ h^{-1}\,Mpc$ and its center lies at $\alpha = 14^h\,50^m$, $\delta = 46^o$, and at a distance $D = 155\ h^{-1}\,Mpc$ (note that its projected diameter spans $\simeq 23^o$ on the sky !).

This void, which has not been totally surveyed, is not completely empty, but its average number density of galaxies is estimated to be less that 25 % of its surroundings, a result consistent both in optical (KOSS) and in infrared (Strauss and Huchra, 1988).

Effects on the CMB due to nonlinear matter distribution have been studied mainly for clumps of matter through the use of exact spherical solutions (Rees

and Sciama, 1968; Dyer, 1976; Raine and Thomas, 1981). Recently a similar line of approach was used by Thompson and Vishniac (TV, 1987), who gave an approximate solution for the case of a completely empty sphere. They matched an interior Minkowski metric to an exterior pressureless, flat, FRW model. The solution obtained is approximate in that the shell of matter at the void boundary is treated as thin (in reality one needs a 'compensated' hole in order to keep the outer universe Friedmannian, and perhaps the use of an exact solution could modify the results of the following discussion).

Because of its closeness (the void center is at $z = 0.05$) and its smallness on a cosmological scale ($R/cH_0^{-1} \simeq 10^{-2}; H_0 = 100\ h\, km\, s^{-1}\, Mpc^{-1}$ is the present value of the Hubble parameter), it is possible both to consider the void as a sphere (the unphysical sharpness of the boundary makes little difference because it gets severely smoothed by the beam) and to use euclidean geometry as an good approximation.

According to TV the difference in temperature along a line of sight through the void is given by

$$\Delta = \eta^3 cos\psi \left[\frac{8}{9}\alpha - \frac{16}{81} cos^2\psi\right] , \qquad \text{(III.42)}$$

where ψ is an angle defined in their Fig. 1, $\eta \equiv R/(ct_0) = 3R/(2cH_0^{-1}) \cong 1.5 \cdot 10^{-2}$, and α here is the exponent of the assumed growth with time of the void radius in comoving coordinates: $R(t)/(1+z) \propto t^\alpha$. For a void whose boundary is at rest with respect to the Hubble flow $\alpha = 0$, while a typical value for self–similar solutions after a cosmic explosion is $\alpha \approx 0.13$ (TV; Ostriker, 1986; Bertschinger, 1985, and references therein). It is important to note that different from 'lumps' of matter, for which the Rees–Sciama effect gives $\Delta \approx (\delta\rho/\rho)\eta^3$ and the density contrast $\delta\rho/\rho$ can be much greater than unity, for a void the effect is at most of order $\Delta \approx \eta^3 \ll 1$ because, by definition, $|\delta\rho/\rho|_{void} \leq 1$ and the only way of increasing the amplitude of the effect is increasing the size of the void itself, making η grow.

Already at this stage one can see that the gravitational effect from Bootes void is far from reaching the required amplitude for Δ (Watson *et al.*), but we feel

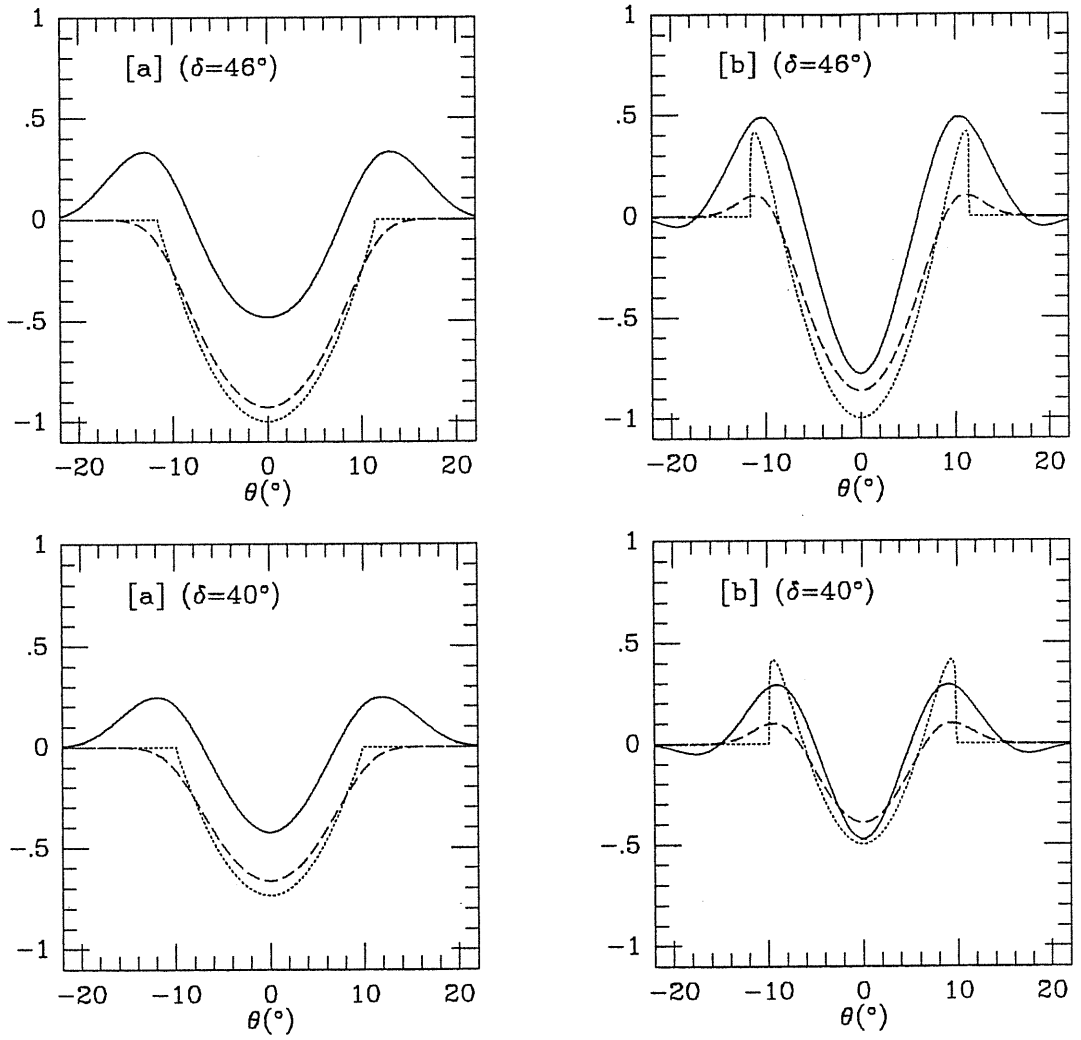

Figure III.19. *Theoretical signals due to the 'empty' void: cases [a] and [b] are respectively for a comoving boundary or one with non-zero peculiar velocity. The upper panels refer to a scan through the void center, the lower ones to the actual declination of the experiment scan. Dotted lines refer to the theoretical assumed signal, dashed lines to the smoothed signal, solid lines to the output of the double subtraction. All curves are normalized to the maximum unsmoothed signal.*

that the results of the following detailed analysis are nevertheless quite instructive, both from the methodological point of view and from the final amplitude levels we derive.

If we define θ as an angle on the sky from the center of the void, we can express ψ as a function of θ through

$$\psi = \theta + tg^{-1}\left[\left(\frac{x_p}{D - x_p\, cotg\theta}\right)\right]$$
$$x_p \equiv \frac{tg\theta}{(1+tg^2\theta)}\left\{D - \left[R^2 - (D^2 - R^2)\, tg^2\theta\right]^{\frac{1}{2}}\right\} . \qquad \text{(III.43)}$$

In Fig. III.19 we present for the two cases $\alpha = 0$ (Fig. III.19 [a]) and $\alpha = 0.13$ (Fig. III.19 [b]), three curves obtained with a theoretical scan through the center of the void ($\delta = 46°$; for simplicity we will also approximate constant declination paths as straight lines on the void projected circle). These curves show the profiles appropriate for the emitted signal (i.e. that seen by a perfect, ideal receiver, dotted line), for that recorded by a single Gaussian beam of dispersion σ (i.e. that seen by an 'absolute' measurement, dashed line), and finally that of interest to us, namely that obtainable by the Watson *et al.* experimental setting (e.g. double beam subtraction, solid line). All the curves have been normalized to the maximum unsmoothed signal and the zero refers to the background level.

It is interesting to note how the original 'cold' signal (which has however a 'hot' ring in the expanding case) gets diluted by the beam smearing (simulated by 2–D FFT) and further modified by the double subtraction, which, although it is capable to produce an 'hot' ring also for the non expanding case, still gives a negative difference at the center of the void.

Moreover the path of the scan of this experiment ($\delta = 40°$) did not pass through the void center, but almost midway between the void center and its boundary: taking into account this fact we get that the profiles shown in upper Fig. III.19 [a,b] are modified to the corresponding ones shown in the lower part. The curves in the latter figure are still normalized to the maximum unsmoothed signal of Fig. III.19 : we see that the original maximum signal for case [a] (nonexpanding boundary) gets diluted in the measurement process by a factor ~ 0.4 to a final $\Delta \simeq -3 \cdot 10^{-7}$, and by a factor ~ 0.5 for the case [b] (expanding boundary), where $\Delta \simeq -1.5 \cdot 10^{-7}$. Therefore the possible gravitational signal not only has the wrong shape (sign and width) but also falls short by $\lesssim 3$ orders of magnitude (vs. only one and a–half order of magnitude given by the simple argument $\Delta \approx \eta^3 \simeq 4 \cdot 10^{-6}$).

In general, one of the most likely source of anisotropies in the CMB is a further electromagnetic interaction between matter and background photons after the recombination epoch. This interaction can be due to various processes, among which are reprocessing by dust or scattering by plasma electrons. The scattering can be due to thermal electrons in hot gas typically in clusters (SZ) or can be coherent and due to bulk flows of ionized matter (Hogan, 1984; Ostriker and Vishniac, 1986), typical for instance of the explosion scenario.

Most of these interactions, though, occur at redshifts greater than unity and their effect can show on typical angular scales of few arcminutes up to $\sim 1^o$, with little hope of being capable of giving birth to a single signal coherent on a scale $\sim 5^o$–10^o (the volume subtended by such an angle at $z \sim \mathcal{O}(1)$ is impressively large).

Here we want to examine the possibility that matter connected to the void could be responsible for such an interaction.

First we note that a coherent scattering given by a possible expanding shell at the void boundary is an unlikely possibility. In fact in order to form the galaxies present on the boundary the shell must have cooled down to $T < 10^4\ K$ (e.g. Wandel, 1985) and cold electrons would have now little effect on the background photons. Moreover for an expanding void the net distortion should be given by the imbalance of the competing effects from the nearby side of the shell and the far one. These boundary shells would indeed have along the line of sight opposite peculiar velocities of slightly different amplitude, an the same would have for temperature and density values, because of the different times for the photons–shell interaction.

We therefore concentrate on a possible non relativistic S–Z effect. The Comptonization parameter, y, which is physically proportional to the integral of the electron pressure along the line of sight, is given by

$$y(z_1, z_2) = \int_{z_1}^{z_2} n_e(z)\, c\, \sigma_T\, \frac{k_B T_e(z)}{m_e c^2} \left(\frac{dt}{dz}\right) dz\ , \qquad \text{(III.44)}$$

where n_e is the electron density, assumed spatially homogeneous, T_e their temperature, σ_T is the Thomson cross–section and m_e is the electron rest mass. In our

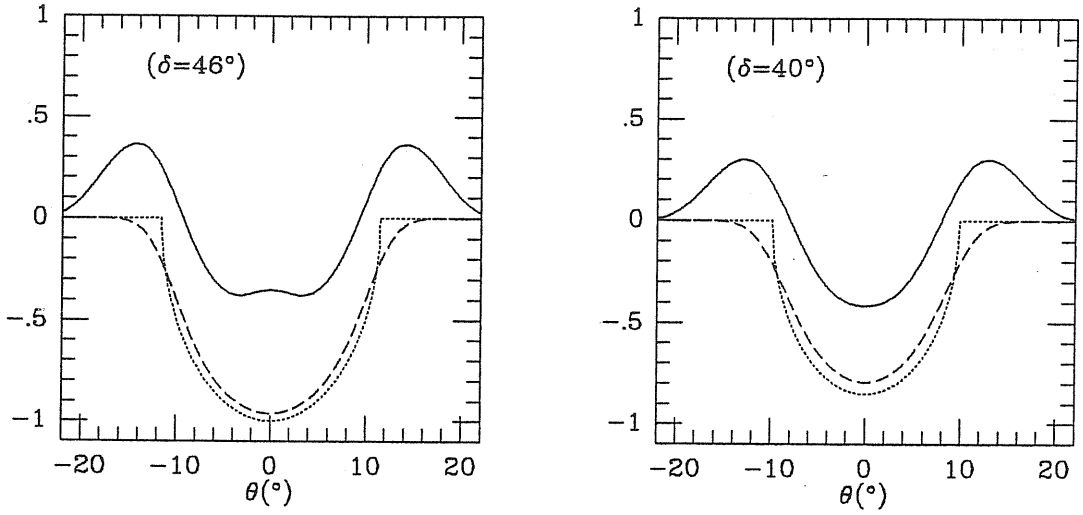

Figure III.20. *Curves analogous to those shown in Fig. III.19 for the signal due to the S–Z effect.*

case, because we are comparing the signal from across the void to that outside, we are dealing with the *difference* in Comptonization parameter, δy, along these different lines of sight. Here, because the void is so close, for simplicity we can approximate the effects of the cosmological expansion, taking as reference values those relative to the center of the void, for which $\bar{z} \cong 5 \cdot 10^{-2}$ (the far side is at $z_2 \cong 6 \cdot 10^{-2}$ and the close one at $z_1 \cong 4 \cdot 10^{-2}$). Assuming adiabatic cooling for the gas we get $\delta y(\bar{z}) \cong (1+\bar{z})^4\, \delta y_0 \simeq (1+4\bar{z})\, \delta y_0 \simeq 1.2\, \delta y_0$, where

$$\delta y_0 \;=\; 2R\, \sigma_T\, \delta n_e(0)\, \frac{k_B T_e(0)}{m_e c^2} \qquad \text{(III.45)}$$

is evaluated at the present. Numerically this amounts to $\delta y_0 \cong 1.20 \cdot 10^{-4}\, h\, T_{40}\, \delta\Omega_b$, where $\delta\Omega_b$ is the the present difference in plasma abundance between background and void in terms of the critical density, and T_{40} is the present gas temperature normalized to $40\, keV/k_B$. Now in the R–J region the effect on the background temperature is $\Delta \cong -2\, \delta y(\bar{z})$, so we get

$$\Delta \simeq\; -6 \cdot 10^{-5}\, h\, T_{40}\, \left(\frac{\delta\Omega_b}{0.2}\right) . \qquad \text{(III.46)}$$

This amplitude is only a factor 2 within the desired level for $h = 1$ and $\delta\Omega_b = 0.2$ (the latter is the maximum value compatible with standard nucleosynthesis, Boesgaard and Steigman, 1985).

We can then try to simulate the signal shape as was done in the previous section. The optical path within the sphere, ℓ, is connected to the previously defined θ by

$$\ell^2 = 4\,\frac{\left[R^2 + tg^2\theta\,(R^2 - D^2)\right]}{(1 + tg^2\theta)}\,. \qquad \text{(III.47)}$$

The relative signal is presented in Fig. III.20 for the unsmoothed, single beam, and double subtraction cases. We again see that there is a lower dilution factor of ~ 0.5 when we consider the final signal at $\delta = 40^o$. Hence, assuming $\delta\Omega_b = 0.2$ as difference for the gas mass density, one would need a gas temperature $T_{40} \simeq 4\,h^{-1}$ to get the right amplitude.

One possible concern at this point would be not to have an X–ray emission level from this gas such as to violate the observed level of isotropy of the X–ray background (XRB). The observed XRB has a spectrum which is well fitted by free–free radiation due to hot gas with $T_{40} = 1$ (Boldt, 1987, and references therein) and is isotrope within few percent of its average value on angular scales of $\sim 5^o$ (Shafer and Fabian, 1983). The measured XRB intensity at $\epsilon^* = 10\,keV$ is $I^b_{\epsilon^*} = 3.2\ keV\,cm^{-2}\,s^{-1}\,keV^{-1}\,sr^{-1}$ (Marshall *et al.*, 1980). The angle–integrated free–free emissivity of the gas associated with the void would then be $\epsilon^{ff}_{\epsilon}(\bar{z}) \cong 1.03 \cdot 10^{-11}\,[\delta n_e(\bar{z})]^2\,T_e^{-\frac{1}{2}}(\bar{z})\,\exp[-\epsilon/k_B T_e(\bar{z})]\,\bar{g}_{ff}\ cm^3 s^{-1} K^{\frac{1}{2}}$, where $\bar{g}_{ff}$ is the velocity averaged Gaunt factor (Rybicki–Lightman, 1979). As we are in an optically thin case the maximum received intensity at $\epsilon = \epsilon^*$ would be $I^{void}_{\epsilon^*} \cong (1+\bar{z})^6\ 2R\ \epsilon^{ff}_{\epsilon^*}(0)/(4\pi)$, so that

$$I^{void}_{\epsilon^*} \simeq 3.95 \cdot 10^{-5}\,h^3\,T_{40}^{-\frac{1}{2}}\,e^{[-0.227/T_{40}]}\,\bar{g}_{ff}\left(\frac{\delta\Omega_b}{0.2}\right)^2\ cm^{-2}s^{-1}sr^{-1}\,. \qquad \text{(III.48)}$$

By requiring $T_{40} \cong 4\,h^{-1}$, $\bar{g}_{ff} \approx 2.5$, and one gets $I^{void}_{\epsilon^*}/I^b_{\epsilon^*} \simeq 1.5 \cdot 10^{-5}\,h^{\frac{7}{2}}$ which is quite satisfactory. On the other hand, looking at Fig. III.20 , we can see that, after having taken into account the double subtraction, there is a sign problem: to get a positive Δ, we would need a negative δy and hence $\delta\Omega_b < 0$. This in turn would imply that an uniform diffuse hot gas is present everywhere but into the void volume. Now, while both gravitational underdensities and cosmic explosions could in principle account for baryonic matter evacuation from the void during its formation (although for dimensions such Bootes' one would need a hierarchy of

explosions, Carr and Ikeuchi, 1985), it is difficult to imagine what mechanism could keep the gas outside the void during recent times. Indeed for a gas with $T \lesssim 10^9\ K$ the sound speed is such that the gas would cross the void within a Hubble time. Also an even hotter remnant gas left behind from cosmic explosions could not prevent the outer gas from filling the void by means of pressure equilibrium because this would result in $\delta y = 0$. Other difficulties are given by energetic constraints on the heating of the gas (Field and Perrenod, 1977) which however would still need to have a higher temperature than that observed for the XRB, and the fact that some such voids without gas would easily induce fluctuations such as to violate the mentioned isotropy limits of the XRB and those of CMB on smaller angular scales.

The presence of a 'hot spot' in the same area of the sky, on the other hand, was already reported in the literature, a fact which adds interest to this particular problem. A 1978 balloon borne experiment (single subtraction, beamthrow of 6^o and dispersion of 2.2^o; see Fabbri *et al.*, 1982, for a complete description) scanned an area which contained the direction $\alpha \sim 13^{\rm h}$ and $\delta \sim +40^o$. This data were used (Ceccarelli *et al.*, 1983) to perform an analysis of the possible SZ effect quite similar to the one made above, from which was derived an upper limit on the rms temperature fluctuation of $0.1\,mK$ (at a different wavelenght, almost at the peak of the CMB spectrum), and consequently a limit on the comptonization parameter of $|\delta y| < 2 \cdot 10^{-2}$ (cf. the limit we get here: $|\delta y| < 10^{-4}$, having taken into account the factor of two which comes from the beam pattern). The data reported in their Figure 2, though, seems to indicate the presence of the characteristic tilted 'S' shape similar to the one expected from a concentrated signal at $\alpha \sim 13^{\rm h}$ in the case of a single subtraction. The problem is that the sign of this signal cannot be determined by the figure, without the essential information about whether signal from the beam trailing in Right Ascension was subtracted from the signal from the other beam or viceversa (the 'S' flips its sign by changing the subtraction order). Moreover the reported data span quite a range of different declinations, making difficult immediate comparisons with the previous discussion.

The same group then reported (Boynton *et al.*, 1983; see their Fig. 1 and

Fig. 3) through data from a second flight, the presence of a large region whose average temperature, as shown in their figures, is $\sim 1\,mK$ higher than its surroundings and should correspond to a gradient of $\sim 0.1\,mK$ as seen by the single subtraction used by this experiment. This very large region (roughly $20^o \times 20^o$) is on the other hand far from the void region and it should probably have been detected also by american balloon experiments and the russian satellite experiment, which covered almost the whole sky (Lubin *et al.*, 1985, see also the comment by Wilkinson, 1983). These experiments could probably have detected also the bump reported by Watson *et al.*: indeed the bump amplitude is $\sim 1/10$ of that of the well detected dipole anisotropy.

Therefore detailed surveys of this zone, made at different wavelengths with enough spatial resolution and coverage, would be a great source of information, albeit not necessarily cosmological (perhaps a galactic cloud could be responsible for the bump –it would be interesting to have a direct cross–check on the IRAS database–; we note that also the existence of very large intergalactic clouds has been suggested by studies of differential optical extinction: see Rudnicki, 1986).

III.6 Brief summary of the chapter.

In this chapter we made applications and extensions of the formalism developed in Chap. II. We generalized the estimates for the average number and diameter of hot spots expected on the sky, through the inclusion of the beam dispersion effects within the formalism. This is an important point which can be exploited in the choice of the best experimental configurations, which have to maximize the detection probabilities expected within a given theoretical model.

Another application was the direct fit to the data of Davies *et al.* of the shapes of the acf appropriate for the scale–free models. The results showed how the final figures are sensitive to the theoretical choice: a fluctuation level ~ 60 % higher than the one quoted by Davies *et al.* was found for the scale invariant spectrum. On the other hand we also discussed in detail the Likelihood Ratio

method and showed how the final results are (of course) sensitive to the signal to noise ratio of the experiment: this statistical approach seems to be, in our present opinion, really more powerful than the method used before, especially because can test properly the assumption of a given set of models (e.g. those which have long range correlations), although care must be exercised in the interpretation of its outputs.

We then extended the formalism to the more general case of a random observer, who can obtain very different values for the same quantities that another observer has measured, and obtained probability distribution functions for the observables of interest through numerical simulations. This resulted in the derivation of much more stringent upper limits on the amplitude of primordial fluctuations than those available in the literature, taking full advantage of the reduced statistical uncertainty of the whole correlation function with respect to that of the only quadrupole component. We also pointed out that proper account should be given to the uncertainty of the experimental upper limits, a fact which reflects heavily in the final confidence levels. We also note that, more than the improvement of almost a factor of nine in the theoretical upper limits, the importance of these results resides in the entirely new method developed, which can be readily implemented to future data (the factor of nine is the square root of the ratio of the upper limit on the value of $\mathcal{A}$ obtained from the the R quadrupole and the value we obtained from constraining the acf shape).

We also examined in detail some of the possible causes of the reported bump in the microwave sky. We think that this kind of signal deserves the maximum attention because of its potential wealth in cosmological information, since, as we discussed above, there are not many mechanisms capable of giving such an ample signal, a lucky, very uncommon situation as far as fluctuations in the CMB are concerned. While more data are necessary to proceed further in the analysis of this particular phenomenon, we showed the necessity of detailed comparisons between theoretical signals and what could be actually recorded from these signals: of importance is not only the amplitude, but also the sign and the shape of the final signal. Indeed, within the limits of the processes examined here, apart from

the low probability of occurrence we estimated for some cases, we can confidently exclude the possibility that the string of galaxies or the Bootes void generated the reported bump: this is of course not an astonishing novelty in the gravitational case because simple back of envelope calculations show the implausibility of such explanation, but we think that the 'overkill' of a factor of $\sim$ 30 with respect to the simple order of magnitude estimate, which we showed results from detailed computations, is a serious warning for future, not so clear-cut cases.

Part of the containts of Sect. III.1 and of Sect. III.4 will appear in the proceedings of two recent congresses (Scaramella and Vittorio, 1988b, 1988c). The material of Sect. III.2 is due for publication in the *Astrophysical Journal* (Vittorio *et al.*, 1989; I want to acknowledge here the people I collaborated with on this specific topic for drawing figures and the numerical work of Sect. III.2 , which, in contrast to the rest of the material presented in this thesis, was essentially carried out in Rome). Finally, the contents of Sect. III.3 and of Sect. III.5 will be soon submitted for publication (Scaramella and Vittorio, 1988d, and Scaramella, 1988, respectively).

References to Chapter III

Abbott and Wise, 1984a, *Physics Letters* **135B**, 279.

Abbott and Wise, 1984b, *Astrophysical Journal (Letters)* **282**, L47.

Abbott, L.F., and Schaefer, R.K., 1986, *Astrophysical Journal* **308**, 546.

Bajtlik, S., Juszkiewicz, R., Prószyński, M., and Amsterdamski, P., 1986, *Astrophysical Journal* **300**, 463.

Barrow, J.D., 1986, *Can.J.Phys.* **64**, 152.

Barrow, J.D., Juszkiewicz, R., and Sonoda, D.H., 1983, *Nature* **305**, 397.

Barrow, J.D., Juszkiewicz, R., and Sonoda, D.H., 1985, *Monthly Notices of the Royal astronomical Society* **213**, 917.

Bertschinger, E., 1985, *Astrophysical Journal Supplement Series* **58**, 1.

Boeesgard, A.M. and Steigman, G., 1985. *Annual Review of Astronomy & Astrophysics* **23**, 319.

Boldt, E., 1987, *Phys.Rep.* **146**, 215.

Bond, J.R., and Efstathiou, G., 1987, *Monthly Notices of the Royal astronomical Society* **226**, 655.

Boynton, P.E., and Partridge, R.B., 1973, *Astrophysical Journal* **181**, 243.

Boynton, P.E., Ceccarelli, C., de Bernardis, P., Masi, S., Melchiorri, B., Melchiorri, F., Moreno, G., and Natale, V., 1983, IAU Symp. 104 *"Early evolution of the Universe and its present Structure,"*, Abell, G.O., and Chincarini, G. eds.

Carr, B.J., and Ikeuchi, S., 1985, *Monthly Notices of the Royal astronomical Society* **213**, 497.

Ceccarelli, C., Melchiorri, F., Pietranera, L., Dall'Oglio, G., and Olivo Melchiorri, B., 1983, *Astrophysical Journal (Letters)* **269**, L27.

Coles, P., 1988, *Monthly Notices of the Royal astronomical Society* **231**, 125.

Davies, R.D., Lasenby, A.N., Watson, R.A., Daintree, E.J., Hopkins, *Nature* **326**, 462.

Dyer, C.C., 1976, *Monthly Notices of the Royal astronomical Society* **175**, 1429.

Efron B., *SIAM Rev*, 1979, **21**, 460.

Fabbri, R., Lucchin, F., and Matarrese, S., 1987, *Astrophysical Journal* **315**, 1.

Fabbri, R., Guidi, I., Melchiorri, F., and Natale, V., 1982, *"Second Marcel Gross-*

mann Meeting on General Relativity,", Ruffini, R. ed., North–Holland.

Field, G.B., and Perrenod, S.C., 1977, *Astrophysical Journal* **215**, 717.

Fixen, D.J., Cheng, E.S., and Wilkinson, D.T., 1980, *Physical Review Letters* **44**, 1563.

Gradshteyn, Rhyzik, 1980, *"Table of integrals, series and Products,"*, Academic Press.

Hogan, C.J., 1984, *Astrophysical Journal (Letters)* **284**, L1.

Kaiser, N., and Lasenby, A., 1987, preprint.

Kaiser, N., and Silk, J., 1987, *Nature* **326**, 529.

Kirshner, R.P., Oemler , A. Jr., Schechter, P.L., and Schechtman, S.A., 1981, *Astrophysical Journal (Letters)* **248**, L57.

Kirshner, R.P., Oemler , A. Jr., Schechter, P.L., and Schechtman, S.A., 1987, *Astrophysical Journal* **314**, 493.

Kühr, H., Witzel, A., Pauliny–Toth, I.I.K., and Nauber, V., 1981, *Astr. & Astrophys. Suppl. Series* **45**, 367.

Lubin, P., Villela, T., Epstein, G., and Smoot, G., 1985, *Astrophysical Journal (Letters)* **298**, L1.

Lubin, P., and Villela, T., 1986, in *Galaxy Distances and Deviations from Universal Expansion*, Madore, B.F., and Tully, R.B., eds. D.Reidel Pub. Co.

Lukash, V.N., and Novikov, 1985, *Nature* **316**, 46.

Lukash, V.N., and Novikov, I.D., 1987, I.A.U. Symp. **127**, Hewitt *et al.* (eds.), D.Reidel Pub. Co.

Mac Callum, M., 1979, *Physics of the Expanding Universe*, Demiańsky, M. (ed.), *Lectures Notes in Physics* **109**, 1, Springer–Verlag.

Marshall, F.E., Boldt, E.A., Holt, S., Miller, R.B., Mushotsky, R.F., and Rose, P., 1980, *Astrophysical Journal* **235**, 4.

Melchiorri, F., Melchiorri, B.O., Ceccarelli, C., and Pietranera, L., 1981, *Astrophysical Journal (Letters)* **250**, L1.

Novikov, I.D., 1968, *Soviet Astronomy* **12**, 427.

Ostriker, J.P., 1986, *"Galaxies Distances and Deviations from the Universal Expansion"*, Madore, B.F., and Tully, R.B. eds., Reidel.

Ostriker, J.P., and Vishniac, E.T., 1986, *Astrophysical Journal (Letters)* **306**, L51.

Pacholczyk, A.G., 1970, *Radio Astrophysics*, W.H.Freeman and Co., San Francisco.

Press, W.H., Flannery, B.P., Teukolsky, S.A., and Vetterling, W.T., 1986, *"Numerical Recipes,"*, Cambridge University Press.

Raine, D.J., and Thomas, E.G., 1981, *Monthly Notices of the Royal astronomical*

Society **195**, 649.

Rees, M.J., and Sciama, D.W., 1968, *Nature* **217**, 511.

Rudnicki, K., 1986, in *"Gamow Cosmology,"*, LXXXVI Enrico Fermi Summer School, Melchiorri, F., and Ruffini, R. eds., in press.

Rybicki, G.B., and Lightman, A.P., 1979, *Radiative Processes in Astrophysics*, J.Wiley and Sons, New York.

Sachs, R.K., and Wolfe, M.A., 1967,*Astrophysical Journal* **147**, 73.

Sazhin, M.V., 1985, *Monthly Notices of the Royal astronomical Society* **216**, 25p.

Scaramella, R., and Vittorio, N., 1988a, *Astrophysical Journal (Letters)* **331**, L53.

Scaramella, R., and Vittorio, N., 1988b, in *Cosmology and Fundamental Physics*, 3^{rd} ESO–CERN Symposium, Bologna, Giacomelli, G.,and Setti, G. (eds.), Reidel.

Scaramella, R., and Vittorio, N., 1988c, in *"The Epoch of Galaxy Formation"*, Frenk, C ed., in press.

Scaramella, R., and Vittorio, N., 1988d, in preparation.

Shafer, R.A., and Fabian, A.C., 1983, *Early Evolution of the Universe and Its Present Structure*, Abell, G.O, and Chincarini, G. (eds.), Reidel Co.

Strauss, M.A., and Huchra, J., 1988, *Astronomical Journal* in press.

Strukov, I.A., Skulachev, D.P., Klypin, A.A, and Sazhin, M.V., 1986, *"Special Astrophysical Observatory, 15–21 September"*, **53**.

Tago, E., Einasto, J., and Saar, E., 1986, *Monthly Notices of the Royal astronomical Society* **218**, 25p.

Thompson, K.L., and Vishniac, E., 1987, *Astrophysical Journal* **313**, 517.

Vittorio N., 1989, *in preparation.*

Vittorio, N., and Juszkiewicz, R., 1987, *Astrophysical Journal (Letters)* **314**, L29.

Vittorio, N., de Bernardis, P., Masi, S., and Scaramella, R., 1989, *Astrophysical Journal* in press.

Wandel, A., 1985, *Astrophysical Journal* **294**, 385.

Watson, R.A., Rebolo, R., Beckman, J.E., Davies, R.D., and Lasenby, A.N., 1988, Proceedings of the *Large Scale Structures and Motions in the Universe*, Trieste, Italy, Reidel Publishing Company, Giuricin, G., Mardirossian, F., Mezzetti, M., and Ramella, F. editors.

Wilkinson, D.T., 1983, IAU Symp. 104 *"Early evolution of the Universe and its present Structure,"*, Abell, G.O., and Chincarini, G. eds., comment at page 148.

Zabotin, N.A., and Nas'elskii, P.D., 1985, *Soviet Astronomy* **29**, 614.

Zel'dovich, Ya.B., and Novikov, I.D., 1983, *"The Structure and Evolution of the Universe"*, Univ. of Chicago Press.

Zel'dovich, Ya.B., ans Sunyaev, .R.A., 1969, *Astr.Sp.Sci.* **4** 201.

IV Two issues on hierarchical clustering and biased theory of galaxy formation.

IV.1 Different perturbation spectra and the Press-Schechter mass function.

Among astronomers there is a general consensus that on cosmological scales most matter is in the form of weakly interacting particles (WIMP's), the so-called dark matter (DM), rather than in the baryonic form we have been familiar with so far. The reasons for this belief are known: foremost for the theorists there is a prejudice stemming from inflation (Guth, 1981; Albrecht and Steinhardt, 1982; Linde, 1982), a concept which solves at once the monopole, flatness, isotropy, initial perturbations and horizon problems. Indeed inflation prescribes for the cosmic density the critical value $\Omega_0 = 1$ (more precisely it requires that the space curvature vanishes; see however Madsen and Ellis, 1988), while the baryonic density, whether estimated from the observation of luminous matter (Oort, 1932 and 1960) or from theory of the primordial nucleosynthesis (Schramm and Steigman, 1981; Yang *et al.*, 1984; for a recent review see Trimble, 1987), is known to be much less abundant, $\Omega_{0B} \ll 1$. It is then obvious to postulate the existence of as much DM as is needed to satisfy $\Omega_0 = 1$. In particle physics (for a review see Turner, 1987) there are so many candidates for this role that it would be very surprising if there were no DM at all or indeed if there were one kind only (Shafi and Stecker, 1984).

One then has the two extra bonuses that DM by itself may solve *i*) some, if not all, of the missing mass problems that exist on smaller scales, from clusters of galaxies to individual galaxies to dwarf irregulars (Aaronson, 1983 and 1987; Faber and Lin, 1983), and *ii*) the problem (Vittorio and Silk, 1984; Bond and Efstathiou,

1984) of the undetected small scale fluctuations in the microwave background (Uson and Wilkinson, 1984) at the the level required by pure adiabatic baryonic models. Incidentally earlier on these two arguments by themselves were considered a sufficient motivation for introducing DM. Only in the solar neighborhood is it likely that the missing matter is in fact subluminous, and therefore unseen, baryonic matter (Bahcall, 1987).

In reality the phase space argument of Tremaine and Gunn (1979; see also Madsen and Epstein, 1985) showing that the light neutrinos that might bind clusters of galaxies (Szalay and Marx, 1976) cannot be trapped in smaller structures, forces us to explore the alternatives roles of two extreme forms of DM, hot (H) and cold (C). These are defined by the fact that the corresponding WIMP's are or not relativistic at radiation-matter equivalence. One understands from the basic theory of gravitational instability of free streaming matter (Bond *et al.*, 1980) and from the pancake theory of Zel'dovich and coworkers (Zel'dovich, 1980; Doroshkevich *et al.*, 1980) that HDM (typically *30 eV* neutrinos) generates the first structure on the scale of superclusters: it is the top-down scenario in which galaxies form later - and unfortunately too late - by fragmentation. On the contrary (Peebles, 1982; Blumenthal *et al.*, 1984), CDM generates structure first on the subgalactic scales and then on the larger ones via hierarchical clustering along the lines of what is known as the bottom-up scenario.

While the latter view appeared more successful than the former for some time, it became clear eventually that it had to be modified in some basic way. The first problem to show up, the so-called Ω-problem, was the fact that dynamical observations (Tamman, 1986; Davis and Peebles, 1983; see the review by Peebles, 1986) stubbornly indicate $\Omega_0 \approx 0.2$ in conflict with the theoretically appealing unit value. Explored solutions range from *biasing* (Kaiser, 1984; Davis *et al.*, 1985; Bardeen *et al.*, 1986) to a cosmological constant (Turner *et al.*, 1984) to WIMP's decaying in recent times to a relativistic component (Dicus *et al.*, 1977; Gelmini *et al.*, 1984; Olive *et al.*, 1985) to the existence of a hot diffuse component (Bludman and Hoffman, 1986). Among these, perhaps bias seems to be the most promising, while the other suggestions have more difficulties .

Recently the existence of a large amount of power on large scales (precisely *i*) in the cluster-cluster correlation function: Bahcall and Soneira, 1983; *ii*) in bubbles: de Lapparent *et al.*, 1986; and *iii*) in large scale streaming motions: Collins *et al.*, 1986; Dressler *et al.*, 1987) casts doubts on the gravitational instability picture in its simplest form for CDM: indeed that much power on the large scales cannot be accounted for by the linear adiabatic or isocurvature (Efstathiou and Bond, 1986) theory of primordial perturbations with the Zel'dovich spectrum, once the amplitude of the perturbations themselves is normalized to fit the observations on small - *i.e.* galactic - scales. Explosive galaxy formation (Ostriker and Cowie, 1981; Ostriker and Ikeuchi, 1983; Carr and Ikeuchi, 1985; Dekel *et al.*, 1987) may be a way out for large scale voids. Alternatively it may be the right time to resurrect HDM (Melott, 1985 and 1986) (which naturally implies large peculiar velocities, Kaiser, 1983; however see Vittorio and Turner, 1987) in combination either with cosmic strings (Vilenkin, 1983; see the review by Turok, 1986) or with double inflation (Silk and Turner, 1986; Turner *et al.*, 1987) to meet the challenge of the timely formation of small scale structure.

For the above reasons and with particular emphasis on the formation of structure, it is worth while pursuing our earlier work (Achilli *et al.*, 1985) where we assume that the basic scenario is bottom-up, but in the presence, for the sake of generality, (see also Umemura and Ikeuchi, 1985) of a free streaming component consisting either of light ($\leq$ 100 eV) or of intermediate ($\approx$ 1 keV) fermions; as usual the latter case will be dubbed warm (W). Concerning the CDM component we will assume that it consists of massive ($\geq$ 1 GeV) fermions. Incidentally the reader may be reminded that it seems now rather unlikely that neutrinos may close the Universe by themselves in view of recent upper limits to their mass (Winter, 1986; Hillebrandt *et al.*, 1987).

We have then considered pure adiabatic scalar perturbations as suggested by inflation and we have numerically integrated the equations for the linearized evolution of density perturbations relative to a cold component, a massive free streaming component and radiation. Our basic parameter is then the abundance

of the CDM component

$$\eta = \Omega_{CDM} \tag{IV.1}$$

under the simplest assumption that either HDM or WDM makes up the remaining $(1-\eta)$ fraction of the Universe in order to satisfy $\Omega_0 = 1$, while baryonic matter is assumed to be dynamically unimportant. In addition to pure models (only hot, or warm, or cold plus radiation) we considered four hybrid models consisting of CDM for a fraction ($\eta = 0.5, 0.1$) and a free streaming component either hot or warm for the remaining part. The hot WIMP was chosen to be a massive neutrino of mass $90(1-\eta)eV$, while the warm WIMP was given a mass of $750(1-\eta)eV$; the former has the canonical "temperature" of $1.9\,K$, while $1\,K$ is assumed for the latter. The redshift of equivalence is determined by the existence of two massless neutrinos for the the hot cases and of three massless neutrinos in all the other cases. The reduced Hubble constant h (in units of $100\,km/sec/Mpc$) is assumed to be unity throughout; likewise an initial $n = 1$ scale invariant Harrison-Zel'dovich spectrum is assumed in all cases. Computations for the linear adiabatic perturbations in other hybrid models (hot plus warm) were performed by Valdarnini and Bonometto (1985a and 1985b); for the hot plus cold hybrid case, detailed considerations for the non linear evolution were given by Umemura and Ikeuchi (1985) and by Ikeuchi and Norman (1987) for a different model, where an isocurvature perturbation is also present.

In Fig. IV.1 we give in the left panel the transmission factor $T(k)$ as a function of comoving wavenumber k and in the right panel we give the rms mass fluctuation $\Sigma(M)$, both quantities being evaluated at the present. The transmission factors, here normalized to unity on large scales, show clearly the following features: *i*) the existence of two knees relative to the horizon scale at equivalence and to the free streaming length; *ii*) the existence of residual power below the free streaming scale in the hybrid cases due to the stunted growth of the cold component prior to the *catch-up* of the free streaming component (see Achilli *et al.*, 1985). The mass variance, given by

$$\Sigma^2(M,z) = A \int d^3\mathbf{k}\, W(kR) P(k,z)\,, \tag{IV.2}$$

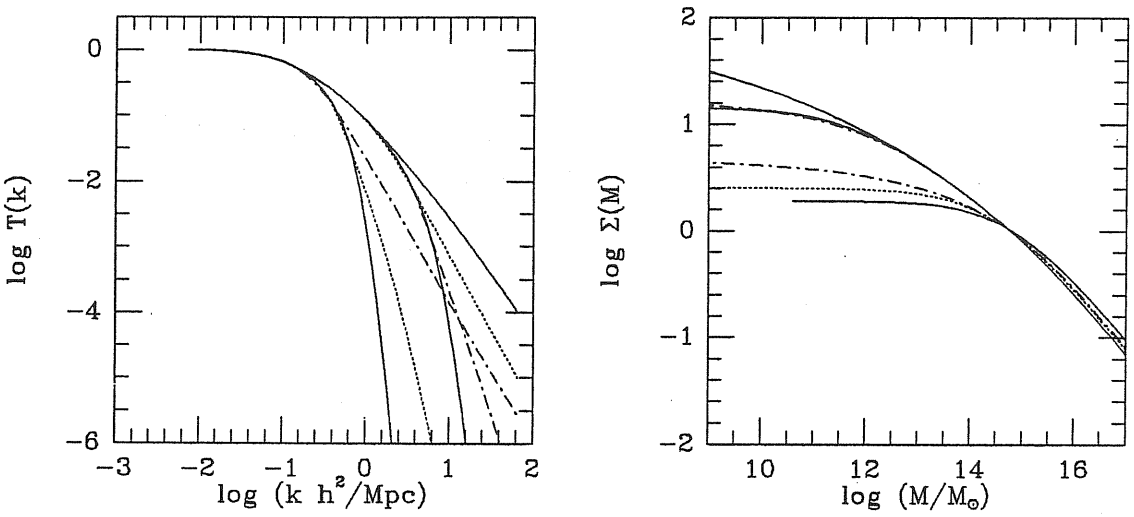

Figure IV.1. *In the left panel a plot of the transmission function $T(k)$ vs. wavenumber k for different cosmological models: from top to bottom full lines refer to the pure CDM model (referred to in the text as C), to the pure warm model (referred to in the text as W), and to the pure hot model. The normalization is chosen to be unity at small wavenumbers. The pure hot model shows the sharp drop due to free streaming, the pure warm model first follows closely the pure cold model, then drops exponentially. Dotted lines refer to the $\eta = 10\%$ hybrids and dashed-dotted lines to the $\eta = 50\%$ hybrids. In the right panel a plot of the variance Σ evaluated at the present for $\nu = 1$ vs. mass M for different cosmological models: as in the left panel, from top to bottom full lines refer to the pure CDM model , to the pure warm model and to the pure hot model (in the latter case the variance is extrapolated below $10^{13} M_\odot$ as the numerical computations become unreliable much below the free streaming mass). Again dotted and dashed-dotted lines refer to the hybrids. The $\eta = 10\%$ warm hybrid is indistinguishable from the pure warm model; on the contrary the hot hybrids are appreciably different from the pure models.*

where $W(kR)$ and $P(k,z)$ are a Gaussian filter and the power spectrum, is normalized in all cases to the galaxy counts (Peebles, 1982) so that $\Sigma(r', z = 0) = 1/\nu$ where ν is a bias factor and $r' \approx 8/1.555\ h^{-1}Mpc$ is the appropriate filtering length. In Fig. 1b we set $\nu = 1$.

Just for comparison purposes we show the variance for the pure hot case, although in reality this normalization is appropriate to the bottom-up scenario only; henceforth we will not treat the pure hot case, but only its hybrids which can give rise to hierarchical clustering, although their variance looks nearly as flat

as in the pure hot cases. For shortness we will label HA the $\eta = 10\%$ hybrid and HB the $\eta = 50\%$ one. As far as WDM is concerned, its $\eta = 10\%$ hybrid does not differ appreciably from the pure case neither in the variance nor in the derived quantities for all the scales of interest, while the $\eta = 50\%$ hybrid is practically equivalent to the pure CDM case; therefore we will limit our discussion to the pure warm case, which we will label shortly W. The pure CDM model will be referred to for comparison simply as C.

Following suggestions by Schaeffer and Silk (1985 and 1988) we use the above results on the mass variance in the Press and Schechter (1976) algorithm to estimate the mass function for the galactic scale and above; the underlying idea of this method is that bound objects grow by pure dissipationless gravitational clustering. In our opinion the simplicity of the method and its predictive power make it worth exploiting it, despite the rigidity of its assumptions and its inadequacy to fully describe the complex physical processes involved.

The basic assumption is that mass fluctuations, $\delta_M = \delta M / \langle M \rangle$, have a Gaussian distribution,

$$\Pi(\delta_M, z) = \frac{1}{\sqrt{2\pi}} \frac{1}{\Sigma(M,z)} exp\left[-\frac{1}{2}\frac{\delta_M^2}{\Sigma^2(M,z)}\right] . \qquad \text{(IV.3)}$$

Accordingly, one can define the fraction of the total density in *bound* objects as

$$F(M,z) = \int_1^\infty d(\delta_M)\, \Pi(\delta_M, z) , \qquad \text{(IV.4)}$$

where we assume that a perturbation becomes bound as soon as its δ_M becomes unity. The factor two which takes in account the secondary infall from adjacent underdense regions disappears when evaluating the distribution of objects per unit mass; hence we neglect it.

It is convenient to introduce Φ, the dimensionless distribution of bound objects per logarithmic mass interval:

$$\begin{aligned} \Phi(M,z) &= -M\frac{dF(M,z)}{dM} \\ &= \frac{1}{\sqrt{2\pi}} \frac{M}{\Sigma^2(M,z)} \left(-\frac{d\Sigma(M,z)}{dM}\right) exp\left[-\frac{1}{2}\frac{1}{\Sigma^2(M,z)}\right] , \end{aligned} \qquad \text{(IV.5)}$$

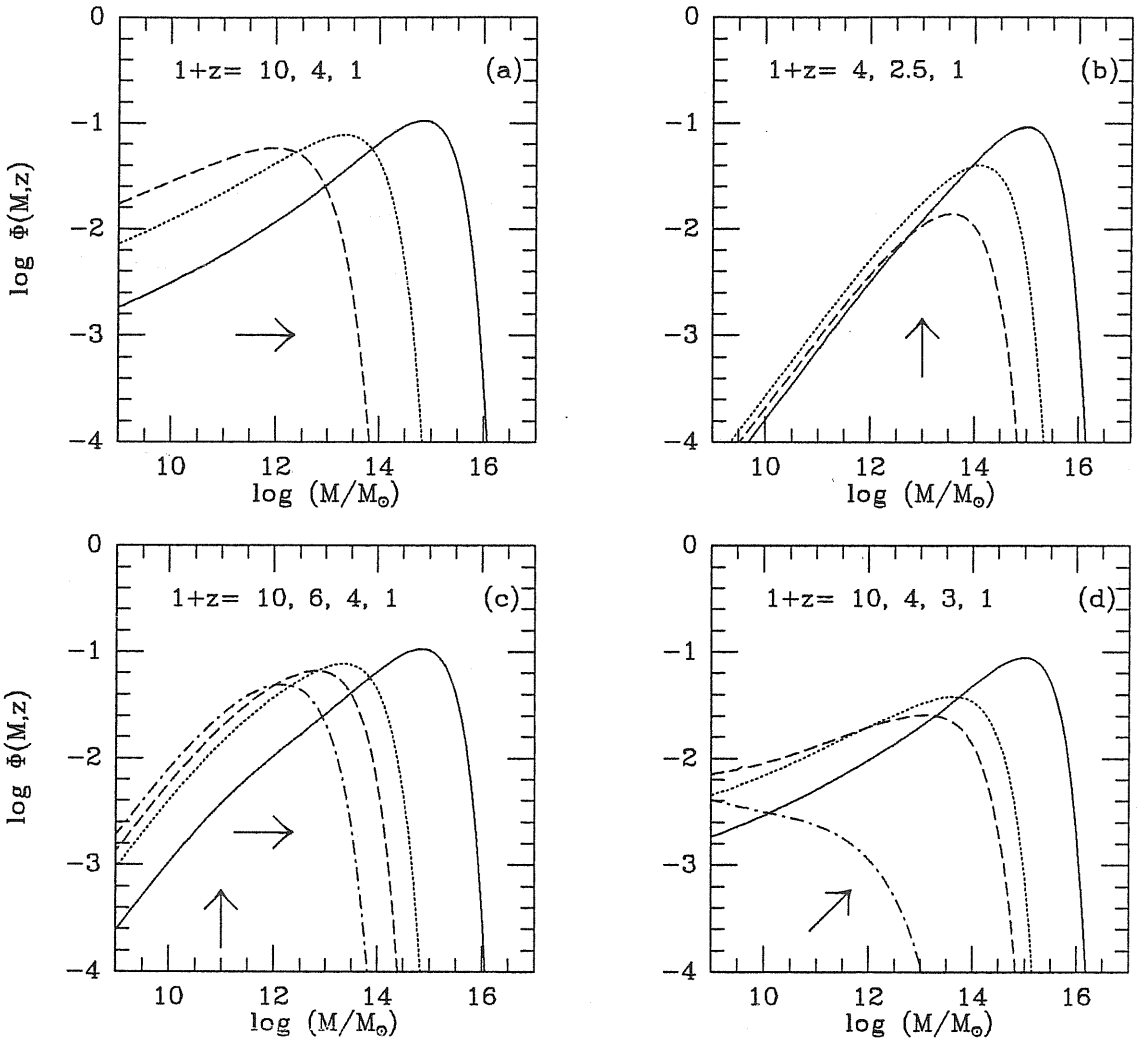

Figure IV.2. *Plot of the dimensionless distribution Φ defined in Eq. (IV.5) for different cosmological models (in different panels) and at different redshifts as indicated: solid lines always refer to the present, dotted and dashed lines to earlier times. On the horizontal axis we give the entire mass range we have explored, $10^9 M_\odot < M < 10^{17} M_\odot$. In panel a) the pure cold case: the arrow underlines how the Press and Schechter scheme describes hierarchical clustering and the gradual shift of power toward the larger scales. In panel b) the HA model ($\eta = 10\%$ hybrid): in comparison with the previous case where curves of almost constant height move to the right with time, here there is an almost vertical increase in amplitude; hence the vertical arrow. In panel c) the pure warm model: the peaks remain at the galactic mass scale over a large redshift interval and only later move to larger masses; hence the vertical and the horizontal arrows. In panel d) the HB model ($\eta = 50\%$ hybrid): its behavior is intermediate between those of panel a) and panel b).*

a quantity already considered by us (Occhionero and Scaramella, 1987).

In Fig. IV.2 we plot Φ at various epochs for different models.

Direct comparison shows very different trends with time: in the pure CDM case the distribution shifts from left to right at almost constant height (a similar plot is given by Couchman, 1987b), indicating how hierarchical clustering displaces power from the small to the large scales. The HA hot model which suffers most from free streaming, behaves in the opposite way, in that while the distribution peaks at nearly constant mass scale, the amplitude rises vertically. The other hot hybrid, HB, shows simultaneously the two features of the above trends: both the peak amplitude and its mass scale increase with time, so that the peak position in the $log\Phi - logM$ plane shifts diagonally. Also the pure warm case W shows the two behaviors, but in a sequence: first there is an almost vertical rise of the peak at galactic scales, then a rightward displacement. It is interesting to note that only in the W case the distribution changes little between $1+z=10$ and $1+z=4$, a range which is likely to encompass the galaxy formation epoch.

To compare with the observed mass distributions, it suffices to multiply Φ by the average background density, $\langle\rho\rangle \approx 3 \cdot 10^{11}\Omega_0 h^2 M_\odot Mpc^{-3}$,

$$\frac{d\rho}{dlnM} = \langle\rho\rangle\ \Phi\ . \qquad \text{(IV.6)}$$

Furthermore we add for comparison two more theoretical pictures to the above one: the first contains a moderate amount of bias, $\nu = 2$, in the same Press and Schechter scheme; the second, as suggested by Schaeffer and Silk (1988), derives galaxy counts from the theory of the number of peaks in the density field above a given threshold, for which we use only an approximate expression. As first shown by Doroshkevich (1970) and then by Bardeen *et al.* (1986), Peacock and Heavens (1986), Couchman and Rees (1986), in the large threshold limit, ($\nu \gg 1$), very simple approximate formulæ can be obtained for the number density of maxima. Of course the identification of a peak with a bound object is a non trivial step, as stressed by Bardeen *et al.* (1986), but the concern lessens somewhat for high thresholds since the region surrounding the peak is then usually simply connected. Indeed it has become widespread in the literature (Bond, 1986, Bardeen *et al.*, 1986, Silk and Vittorio, 1987) to fix the appropriate biasing threshold or the smoothing length by requiring the number density of high peaks to match the

observed number density of objects (i.e. bright galaxies or rich clusters).

In line with these considerations we chose to consider the case $\nu = 3$ as a good compromise: indeed it lies almost at the high end of the canonical range of ν (Blumenthal *et al.*, 1984; Bardeen *et al.*, 1986, Dekel and Rees, 1987) and at the same time is large enough to allow the following approximations. Neglecting terms of order ν^{-2} the number density of peaks is given as (Doroshkevich, 1970; Bardeen *et al.*, 1986)

$$\frac{dN_{pk}}{dV} = n_{pk} \approx \frac{1}{(2\pi)^2} \left[\frac{\langle k^2 \rangle}{3}\right]^{3/2} \nu^2 \, exp\left[-\frac{\nu^2}{2}\right] . \qquad \text{(IV.7)}$$

where $\langle k^2 \rangle$ is an average over the spectrum.

To the same approximation, once ν is related to Σ as described below, the mass distribution becomes

$$\frac{dn_{pk}}{dM} \approx \frac{1}{(2\pi)^2} \left[\frac{\langle k^2 \rangle}{3}\right]^{3/2} \frac{\nu^4}{2\Sigma^2(M,0)} \left(\frac{d\Sigma^2(M,0)}{dM}\right) exp\left[-\frac{\nu^2}{2}\right] \qquad \text{(IV.8)}$$

which we will use below in the form

$$\frac{d\rho}{dlnM} \approx -M^2 \frac{dn_{pk}}{dM} . \qquad \text{(IV.9)}$$

From the observed luminosity distribution one can infer a mass distribution after making appropriate assumptions on the $M(L)$ behavior. Following Schaeffer and Silk (1985 and 1988) we find it convenient to consider a luminosity function of the Schechter type

$$\psi(L) = \psi_* \left(\frac{L}{L_*}\right)^{-\alpha} \exp[-L/L_*] \qquad \text{(IV.10)}$$

(Schechter 1976, Felten 1985) both for galaxies and for clusters (Bahcall, 1979).

The resulting mass distribution is shown in Fig. IV.3 . The differences between the small and the large scales, besides the obvious differences in the values of α, ψ_* and L_* for galaxies and clusters of galaxies, are also due to the assumption of an increasing M/L with the scale. Indeed reasonable values are thought to be

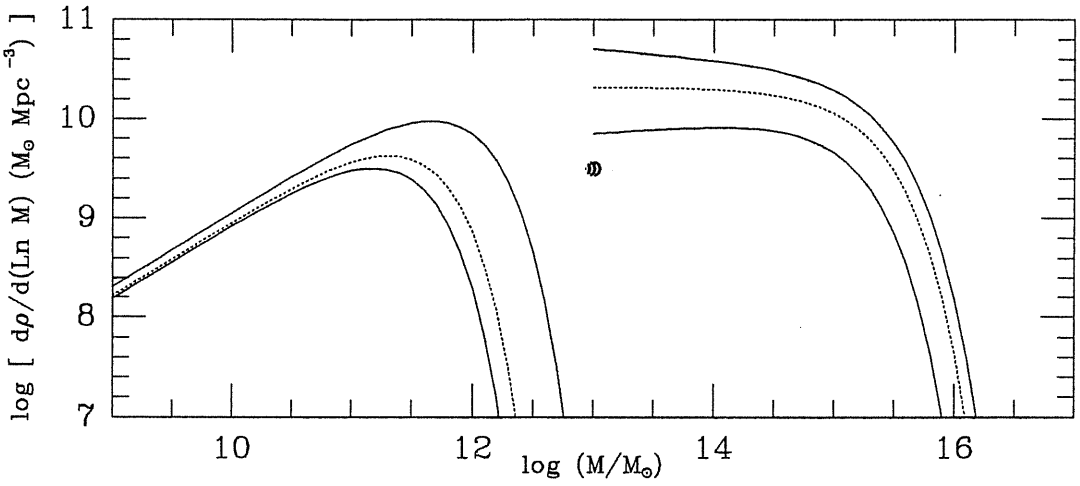

Figure IV.3. *Observational constraints over the mass range we want to explore,* $10^9 M_\odot < M < 10^{17} M_\odot$*; the uncertainty which derives mostly from our poor knowledge of* M/L*, is shown by the solid lines; as an example we show as a solid dot the value of the distribution for* $M/L = 100$ *on the scale of groups.*

$M/L = 80^{+100}_{-20}$ for galactic scales (Faber, 1982) and $M/L = 650^{+100}_{-100}$ for cluster scales (e.g. Coma); we also plot a point corresponding to a value of $M/L = 100$ on the scale of groups to stress the great uncertainty implied on the relative scale (Geller, 1984).

In Fig. IV.4 we plot the theoretical results for the present time and we compare them with the observational constraints of the above paragraph (dotted lines). We use three panels to illustrate three models: the Press and Schechter algorithm, Eq. (IV.5) and Eq. (IV.6) , with $\nu = 1$ in panel a), the same algorithm with $\nu = 2$ in panel b), and finally the approximate peak method, Eq. (IV.8) and Eq. (IV.9) with $\nu = 3$ in panel c). In each panel the C model is shown by a solid line, the W model is shown by a dashed line (practically coincident with the previous one on these scales) and the HA model by a dashed-dotted line.

The C and the W models are indistinguishable because the normalization at $8h^{-1}\,Mpc$ in this gives case identical power on large scales (see Fig. IV.1); the HB model is not shown because it looks quite similar. On the contrary the HA model differs from the others below $10^{15} M_\odot$ mainly because of an appreciable free streaming effect and also because of a slight difference in the equivalence epoch

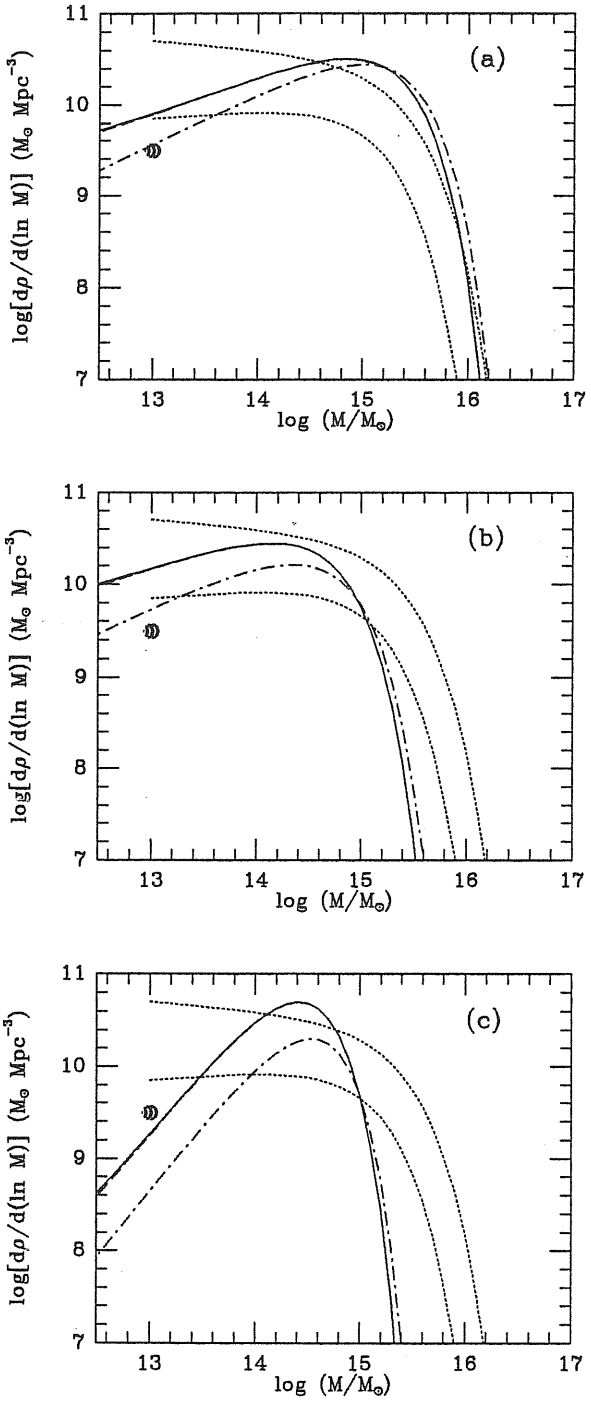

Figure IV.4. *Theoretical predictions on the large scales for three models of formation of condensations: in panel a) the Press and Schechter scheme with $\nu = 1$, in panel b) the Press and Schechter scheme with $\nu = 2$, in panel c) the approximate peak scheme with $\nu = 3$. Solid lines refer to pure CDM models and to pure warm models which give practically coincident results on these scales; dotted-dashed lines refer to the HA hybrids; dotted lines yield the constraints of Fig. IV.3 .*

(two rather than three massless neutrinos).

The overall similar behavior does not allow us to select one model over the others in panels a) and b): in fact the agreement of the theoretical results for $1 < \nu < 2$ with the dotted constraints is remarkable. On the other hand all the models behave rather poorly in panel c).

The main features of this plot can be qualitatively understood in the following way: the sharp drop on the right hand side of each panel is determined by the exponential cutoff which becomes increasingly effective the lower is the value of the variance Σ (hence the progression with the bias factor). On the left hand side of each panel there is instead a rising trend which is independent of bias, but distinguishes markedly between the Press and Schechter approach on one side and the approximate peak formula on the other: in the former case the theoretical counts are proportional to $1/\Sigma$, in the latter to $1/\Sigma^4$ *i.e.* respectively proportional to $M^{(q+3)/6}$ and to $M^{2(q+3)/3}$, where q is the effective spectral index of the power spectrum.

Therefore it seems that the observed large scale mass distribution is in reasonable agreement with the predictions of the Press and Schechter algorithm (almost insensitively of the chemical composition) with a low bias $1 < \nu < 2$, while the high bias peak approximation shows a net deficit on both ends of the large scale range examined here and looks less favorable. Of course these results depend crucially on the adopted normalization; furthermore in the case of moderate thresholds a more precise treatment is of course needed (Bardeen *et. al.*, 1986, Couchman, 1987a, Martinez–Gonzales and Sanz, 1988).

In order to work on this scale we first estimate for each model the average redshift at which a galactic mass becomes bound by the requirement $\Sigma_*(z_b) = 1/\nu$ where $\Sigma_*(z_b)$ is evaluated at $M_* \approx 10^{11-12} M_\odot$. Since for the redshifts of interest for all models $\Sigma \propto (1+z)^{-1}$, then $(1+z_b) \approx \nu\, \Sigma_*(z=0)$. This gives $(1+z_b) \approx 10$, 6, 3, 2.5 for the C, W, HB, HA models respectively. We now make the assumption that galaxies once created are not destroyed (for example we consider mergers to be negligible). Hence the number of galaxies of each cosmological model must be evaluated at the binding redshift of that model. In this way galaxies can

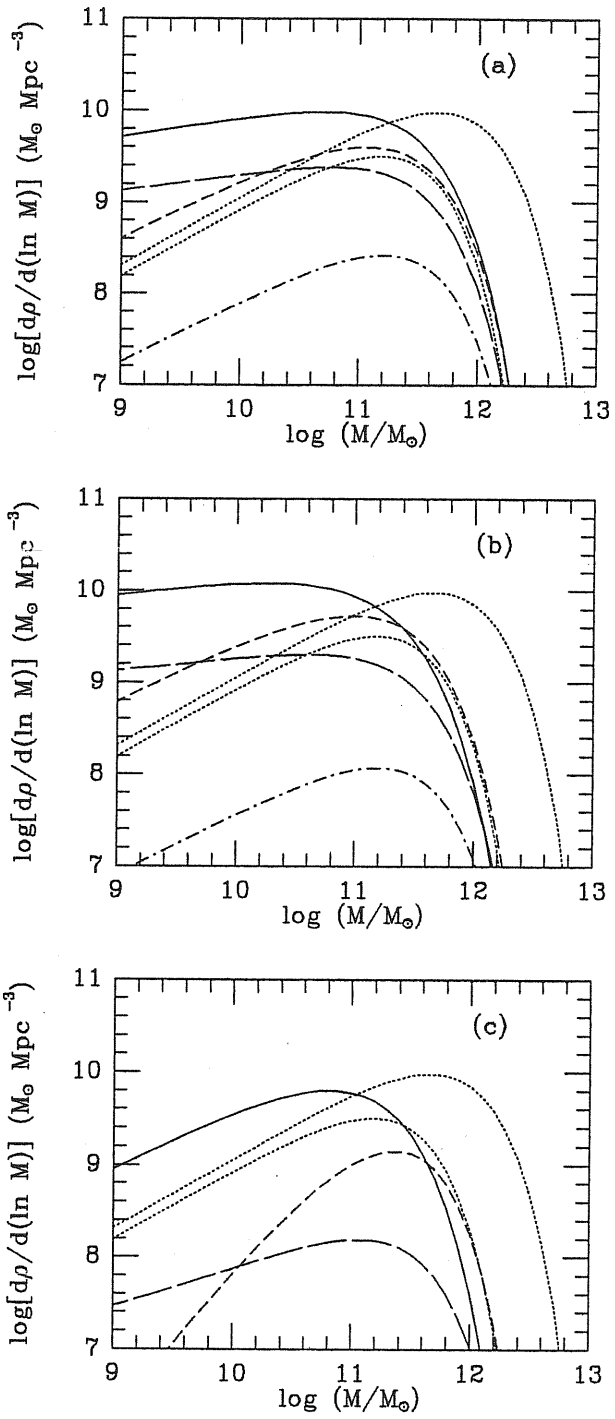

Figure IV.5. *Theoretical predictions on the small scales for three models of formation of condensations of Fig. IV.4 ; again the observational constraints are shown as dotted lines. Solid lines refer to pure CDM model* $(1+z_b = 10)$, *broken lines to pure warm model* $(1+z_b = 6)$, *long dashed lines to to the HB hybrid* $(1+z_b = 3)$, *dotted-dashed lines to the HA hybrid* $(1+z_b = 2.5)$.

be counted as individual objects even when they become part of larger systems. In addition we must take into account the fact that a galaxy actually lights up only

when the rough criterion between cooling and free–fall time $\tau_{cool} < \tau_{ff}$ is satisfied (Gott and Rees, 1977, Blumenthal *et al.* 1984, Silk 1985, Dekel and Silk, 1986). Following the suggestion of Schaeffer and Silk (1985) we crudely mimic the complex underlying physics by imposing an exponential cutoff of the form $exp[-M/M_c]$ where on the basis of cooling considerations $M_c \approx 10^{12}\, M_\odot (\Omega_B/\Omega)^{-3/2}$.

The results of these computations are shown in Fig. IV.5 , where we have three panels in complete analogy to Fig. IV.4 , i.e. with the Press and Schechter algorithm with $\nu = 1$ in panel a), the same algorithm with $\nu = 2$ in panel b), and finally the approximate peak method with $\nu = 3$ in panel c). In each panel the observational constraints are given by dotted lines, the cold C model predictions at $1 + z_b = 10$ by a solid line, the warm W model predictions at $1 + z_b = 6$ by a short dashed line, the hybrid HB model predictions at $1 + z_b = 3$ by a long dashed line, the hybrid HA model predictions at $1 + z_b = 2.5$ by a dotted-dashed line.

In panels a) and b) we note that the C model has an excess of power on the small scales: this circumstance has already been remarked by Schaeffer and Silk (1985) and poses a difficulty for the CDM scenario (which however could be overcome; Dekel and Silk, 1986). On the other hand we note that in the pure CDM scenario the possible feedbacks due to the first condensations are likely to exert a great influence, thereby giving rise to a rich, complicated physical scenario for which the pure hierarchical schemes we examine here can be inadequate (Rees, 1985, Couchman and Rees, 1986, Couchman, 1987b). The latter difficulty should be much lessened, though, for those models – W, HA, HB – which show a less gradual transfer of power from the small scales to the galactic scales (e.g. Fig. IV.2 b, c, and d). In the same panels we see that the free streaming models (W and HA) have the best slopes to fit the observed counts: however the amplitude of the HA model is far too small, while that of the W model is about right given the limits of the present approach. In panel c) model C is in lesser disagreement with the dotted lines only on the low mass side, but not on the high mass side; the other models shows a larger disagreement (in fact model HA disappears from the plot).

In conclusion, we may say that at least from a qualitative point of view the

Press and Schechter algorithm with a moderate amount of bias, $1 < \nu < 2$, gives a remarkably good description of the observations on the large scales, in spite of its simplicity. In fact, the formation of large scale structure in a bottom–up scenario occurs in agreement with the assumptions of a smooth, dissipationless hierarchical clustering upon which the Press and Schechter forecast is based. All this is of course almost entirely insensitive to the chemical composition of the cosmic medium, but occurs when free streaming is important. On the galactic scale, instead, our results do depend on this composition, so that in principle a test is possible: in particular the warm dominated model shows a much closer agreement with the observations than the other models both in the slope and in the amplitude of the theoretical curve, the two relevant quantities after the "external" imposition of the cutoff. Furthermore the warm model looks very attractive also because of its unique feature of exhibiting a peculiar staticity of Φ at the galactic scale for a wide range of redshifts. It should be finally recalled that the free streaming of 1 keV WIMP's naturally yields the galaxy mass (Bond, Szalay, and Turner, 1982).

IV.2 Optical luminosity bias and clustering amplitudes.

It seems quite reasonable to expect that biased theories of galaxy formation (Kaiser, 1984; Politzer and Wise, 1984; Bardeen *et al.*, 1986; Dekel and Rees, 1987) lead to galaxy clustering properties depending on the intrinsic luminosity. A test of such dependence can be performed using the information on intrinsic luminosities L provided by samples of galaxies with known redshift. The 2–point function obtained for a sample of galaxies with $L > L_{lim}$ should keep the form $\xi(r) = (r_o/r)^\gamma$ with $\gamma \sim 1.8$, while r_o should depend on L_{lim} itself. Although the nature and strength of such dependence are related to the specific biasing model adopted, it is reasonable to expect the clustering to be stronger for bright galaxies. We shall discuss this point in more detail at the end of the section.

Starting from a fully different point of view, in a number of recent papers (Calzetti *et al.* 1987, Pietronero 1987), the idea has been pursued that matter

distribution has a fractal nature up to very large scales, possibly exceeding the present horizon scale. These authors show that, if galaxies have a *simple* fractal distribution (we will henceforth drop *simple*) and if a sample occupying a volume of size D is then analyzed according to current methods, the 2–point function will still show the form $\xi(r) = (r_o/r)^\gamma$. However, when another sample with different D is considered, the *clustering length* r_o would also appear to be different, according to the proportionality law

$$r_o \propto D \, . \tag{IV.11}$$

A test of this dependence can be performed using the information on distances furnished by catalogues of galaxies with known redshift.

If we consider all galaxies with $L > L_{lim}$ in a fair sample including galaxies with apparent luminosities $l > l^*$ (or, apparent magnitudes $m < m^*$: magnitude limited sample), this amounts to considering all galaxies of the sample up to a limiting distance

$$D_{lim} = (L_{lim}/4\pi l^*)^{1/2} \, , \tag{IV.12}$$

provided that cosmological and K–corrections can be neglected. Detecting a dependence of r_o on L_{lim} might therefore indicate either an *intrinsic* effect, as is expected in biased models of galaxy origin, or a dependence of r_o on D_{lim}, as is expected within the framework of the above fractal model. However, owing to Eq. (IV.11) and Eq. (IV.12) , the latter model predicts

$$r_o \propto L_{lim}^b \tag{IV.13}$$

with $b = 1/2$. *Biased* models, instead, do not lead to such stringent predictions, although it may be reasonable to expect $b < 0.5$ for them (see below).

In principle one could distinguish between the two above effects by analysing either subsamples of fixed size D down to various L_{lim}, or subsamples with fixed L_{lim} but for various D. Available samples are however quite limited and any subsample whose size $D < 40 \; h^{-1} \; Mpc$ (h is the Hubble constants in units of $100 \; Km \; s^{-1} \; Mpc^{-1}$) is likely to be polluted by local effects. Furthermore the dependence of r_o on L_{lim} is expected to be stronger at larger L_{lim} and the number of objects which may be taken into account then becomes embarassingly small.

Therefore the value taken by b may still be the best indicator of the nature of a possible dependence of r_o on L_{lim}. In the next section we shall discuss the dependence of available outputs on r_o on L_{lim}, coming from the CfA catalog ($m^* = 14.5$).

The value of the correlation length for the galaxies was initially deduced from the correlation *angle* derived from *apparent* magnitude limited samples (see, e.g., Peebles, 1980, and references therein). The value of r_o deduced in this way is based on the validity of the Limber equation. In turn the Limber equation holds provided that r_o does not depend on L.

The dependence of r_o on L_{lim} can be therefore tested only in catalogs of galaxies with known redshifts. An extensive analysis of the data contained in the CfA galaxy sample ($m^* = 14.5$) was carried out by Einasto *et al.* (1986).

Here we shall argue that such analysis leads to $0.17 < b < 0.39$ in Eq. (IV.13) . Before giving more details on the procedure for data analysis, let us outline how it allows us to conclude that the values $b = 0$ and $b = 0.5$ can be excluded at the same confidence level (they lie just outside the 90% confidence level of the χ^2 contour plot). The former value would indicate no dependence of clustering on luminosity. This does not exclude that a constant r_o is, after all, consistent with observational data, but, according to our analysis, the Einasto *et al.* (1986) outputs furnish no more support for a fractal scenario than for constant r_o (see also Jones *et al.*, 1988).

Among the large set of data elaborated by Einasto *et al.* (1986) we selected those of depth $D > 40\,h^{-1}\,Mpc$. At a distance of $40h^{-1}Mpc$ a galaxy of luminosity L^* (L^* is the turning point in the galaxy luminosity function) appears of $m = 14.5$.

Einasto *et al.* (1986) found the values for r_o for subsamples of different L_{lim} in two different directions of the sky (sets A and B). This allows to fit the dependence of r_o on L_{lim} Eq. (IV.13) estimating also an error on b.

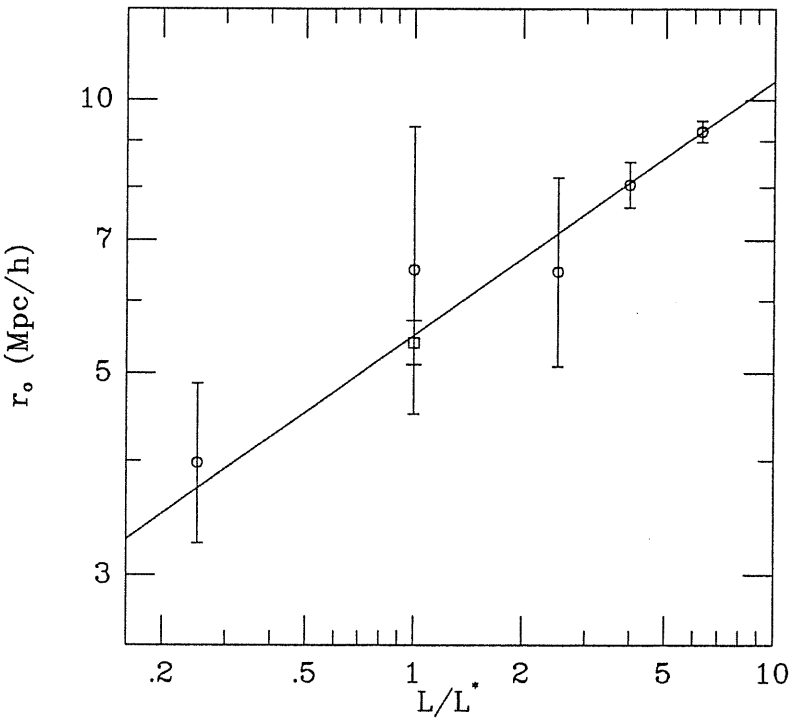

Figure IV.6. *Observational points and error bars obtained from Einasto et al. (1986) -circles; see Table I- and from Davis and Peebles (1983) and Maurogordato and Lachieze-Rey (1987) -square-. Only the former points for distances* $\geq 40h^{-1}Mpc$ *(*$L_{lim} > L^*$*) are used to obtain the best fit line.*

In spite of the limited amount of data a simple least–square fit, performed by suitably weighting the points in different celestial areas by the number of bright galaxies present there, directly yields $b = 0.28 \pm 0.11$ (further details are given in Table I).

Let us also remark that quite similar results on b and its error are obtainable if the points of sets A and B (see Table I) are fitted separately and the different results are then suitably weighted. Results would be most reliable if different L_{lim} data could come from completely independent samples. Here, though, subsamples corresponding to different L_{lim} partially intersect. The effect of any such residual interdependence within the data seems to be maximally diluted in the frame of our former approach. Einasto *et al.*(1986) put together the observed increasing trend of r_o at the distances and luminosities considered here with points obtained from smaller volumes of size $\sim 20\ h^{-1}Mpc$ and with cluster correlation data. This inhomogeneous set of data was then fitted by Calzetti *et al.*(1987) and Pietronero

(1987) with Eq. (IV.13) using $b = 1/2$ as is to be expected within the frame of the above fractal models of matter distribution in space.

Table IV.1

$\log\left(\frac{L_{lim}}{L^*}\right)$	$\log\,(r_0\ h^{-1}\,Mpc)\ [N_{gal}]$		$\log\,(r_0\ h^{-1}\,Mpc)$		
	Subsample A	Subsample B	mean	dispersion	best fit
0.00	0.884 [576]	0.462 [118]	0.812	$1.58 \cdot 10^{-1}$	0.740
0.40	0.905† [238]	0.695 [196]	0.810	$1.04 \cdot 10^{-1}$	0.852
0.60	0.916 [425]	0.841† [65]	0.906	$2.54 \cdot 10^{-2}$	0.908
0.80	0.959 [220]	0.987 [65]	0.965	$1.17 \cdot 10^{-2}$	0.964

Table IV.1. *The above values are directly obtained from Einasto et al.(1986), apart those marked by a dagger which are given by linear interpolation. The weight of the latters is accordingly halved. The value of b obtained from the above table* $[log(r_o) = a + b \cdot log(L_{lim}/L^*)]$ *is* 0.28*; the small resulting* χ^2 ($\simeq 0.38$) *reflects into the large errors.*

However, if we add the data relative to a distance of $20\,h^{-1}Mpc$ to the fair sample ($D > 40\,h^{-1}Mpc$) of data we used in Table IV.1 , the value of b does not change appreciably from the one we obtained. The formal error however decreases, the full error bar being contained in the error bar for b given here (the confidence limit on the values $b = 0$ or $b = 0.5$ becomes accordingly more severe). To consider also data from cluster of galaxies might increase the value of b; within the framework of any biased theory of galaxy formation, cluster data are however not homogeneous with galaxy data being related to different values of the *smoothing scale* R_s and of the *bias parameter* ν .

According to Table IV.1 , the best fit value for r_o –at $L_{lim} = L^*$– is $5.50\ h^{-1}Mpc$. This is to be compared with Davis and Peebles (1983) result yielding $r_o = 5.4 \pm 0.3\ h^{-1}Mpc$. This result was obtained considering 1230 galaxies of the northern emisphere with $L > L^*$. More recently Maurogordato and Lachieze-Rey (1987), analyzing a subset of the CfA sample, including 396 galaxies with $L > L^*$, also finding $r_o = 5.4\,h^{-1}Mpc$. These points are also shown in Fig. IV.6 .

It is important to note that the same value has been obtained from these authors for the *same* L_{lim} but for *different* depths ($D = 40\,h^{-1}Mpc$ for the latter and $D = 100\,h^{-1}Mpc$ for the former), directly in contrast with the above fractal scenarios.

All the above authors note the existence of a possible dependence of r_o on L_{lim}. Analogous suggestions, on different bases, are given by Shaeffer (1987a and 1987b).

In the wide scale range from galaxies up to Abell clusters it is reasonable to associate each scale with a precise value of the smoothing radius R_s . Peaks of different height, but above a critical threshold δ_c , will probably virialize at different times. Clusters which are observable today are peaks which have virialized before the present epoch and have not merged in larger structures yet.

This picture is appropriate to describe hierarchical clustering of collisionless systems which can however merge and loose their own individuality during their subsequent evolution in time. This view, started by Press and Schechter (1974), reflects in the current bias approach, relating volumes (and masses) to R_s^3.

On the other hand, within the framework of biased theories of galaxy formation, the mass/luminosity range occupied by individual galaxies is likely to be selected by precise physical effects.

Individual galactic masses can be related to various different initial conditions and the existence of an appreciable range of *galactic* masses is probably mostly due to the impact of different local geometries on fluctuation evolution rather than to gravitational collapses over different scales R_s.

A tentative way to find the statistical impact of this wide set of variables starts from considering a single *smoothing radius* R_g, related to the typical scale above which primeval fluctuations can hardly cool down into individual galaxies. Different luminosities will then be related to the different residual heights of the individual *smoothed* fluctuation. This is likely to dilute the impact of some initial geometries; however, for large galactic masses, i.e. at the bright end of the lumi-

nosity function, we are probably considering notably high peaks, which differ less in geometrical details.

If one considers the peak distribution

$$\rho_g(x) = \vartheta[\epsilon_{b,R_g}(x) - \nu_g \sigma_{b,R_g}] \qquad \text{(IV.14)}$$

(σ_{b,R_g} is the the background mass variance over the scale R_g), the size S of the volumes where the argument of the step distribution ϑ is positive is not the same for all peaks and can be related to the peak value ϵ_p of the smoothed fluctuation field $\epsilon_{b,R_g}(x)$ in the volume where the threshold value $\nu_g \cdot \sigma_{b,R_g}$ is overcome.

Let us outline the difference between R_g –approximated by a unique value– and S : the actual mass of the final galaxy and its luminosity L will certainly be related to the volume $\sim S^3$ involved within the protogalactic size. Therefore, as S increases with ϵ_p, selecting objects with $L > L_{lim}$ is equivalent to taking peaks with $\epsilon_p > \epsilon_{p,lim} = \nu_{lim}\sigma_{b,R_g}$.

This is equivalent to saying that, on top of a physical bias –allowing only peaks with $\epsilon_p/\sigma_{b,R_g} > \nu_g$ to turn into galaxies—, a further selection (*optical bias*, see Bonometto *et al.*, 1987) occurs, with respect to more severe thresholds $\nu_{lim} > \nu_g$. There can be little doubt that ν_{lim} is an increasing function of L_{lim}. The details of such dependence can be tentatively discussed as follows.

Bardeen *et al.* (1986) and Couchman (1987) considered the question of the relation between s and ϵ_b. In Fig. IV.7 we report the form of $\epsilon_{b,R}(x)$, obtained after averaging over angles, for a standard CDM scenario, in the case of a primeval Gaussian spectrum with spectral index $n = 1$, for different values of the peak density contrast ϵ_p. Such profiles are characterized by a slope which keeps fairly constant, both with respect to ϵ_p itself and for $r \lesssim R_g$. The expression

$$\epsilon_{R_g}(r) \;=\; \epsilon_p - g\left(\frac{r}{R_g}\right)^{1+\delta} \qquad \text{(IV.15)}$$

can therefore furnish an approximation to $\epsilon_{b,R}(r)$ up to $r \gtrsim R_g$. The exponent $\delta \ll 1$ avoids a cusp at $r = 0$.

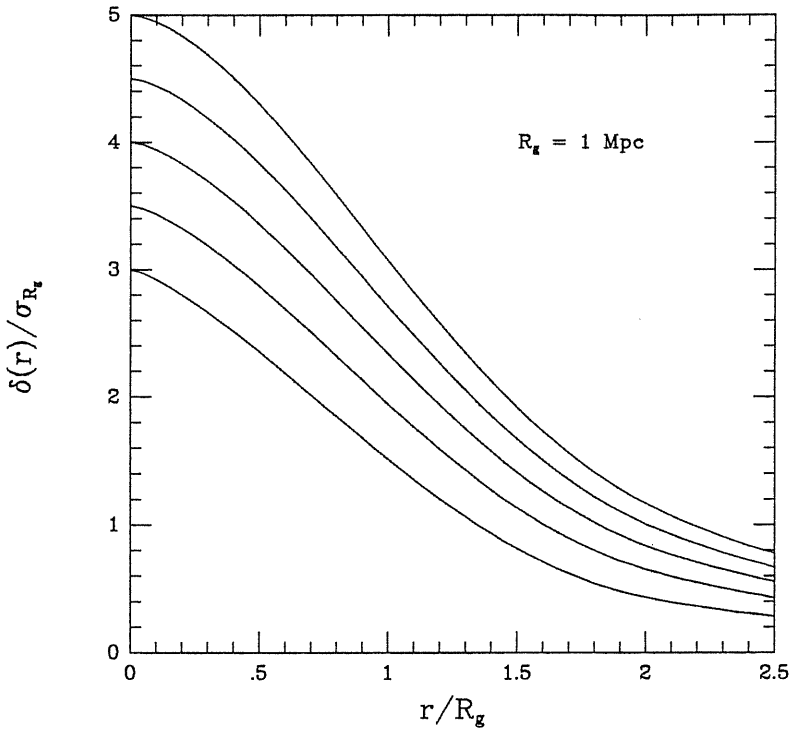

Figure IV.7. *Continuous lines represent angle-averaged mean density profiles of primeval peaks in a standard CDM model (h=1, n=1, $\Omega_o = 1$), for different values of the peak height ϵ_p.*

For large ϵ_p (i.e. for large L) we may therefore take $S \propto \epsilon_p^{1-\delta}$ and therefore $L_{lim} \propto \nu_{lim}^{\beta}$ with $\beta = 3(1-\delta) + \alpha$. The quantity α is enclosed here to allow considering the effects of a secondary infall of matter into a fluctuation of size S (see Hoffman and Shaham, 1985; Hoffman, 1988). For large ν and for a Gaussian spectrum, in the linear regime $\xi_{\nu,R_g}(r) \simeq \nu^2 \xi_{b,R_g}(r)/\sigma_{R_g}^2$. Then, owing to the observed law $\xi(r) = (r_o/r)^{\gamma}$, we expect $r_o \propto \nu^{2/\gamma} \propto L_{lim}^{2/\gamma\beta}$. Comparing this output with Eq. (IV.13) we see that, for $1.7 < \gamma < 1.8$, $0 < \delta < 0.2$ and $\alpha = 0$, $b = 2/\beta\gamma$ falls in the range 0.37–0.49. Considering $\alpha > 0$ would widen the above interval towards smaller values. The observational interval 0.17–0.39 (see above) would suggest $0 \lesssim \alpha \lesssim 1$.

In our opinion the above arguments can be taken at least as an indication that the L_{lim} dependence of r_o, observed at large L, is likely to fit the trend found within the framework of a simple bias model not requiring a fractal scenario. In this context it seems clear that a reliable determination of the dependence of r_o on L_{lim}, based on wider samples, would be helpful in understanding the details of

the bias mechanism and of the process of galaxy formation.

While we agree with Pietronero (1987) that systematic variations of the average number densities with D can be present in data, the most significant dependence of r_o seems to be the possible one on L. In turn this raises a number of technical problems in defining a universal galaxy luminosity function, which would depend on position. Distance calibrations, relevant to possible distortions of the Hubble flow, therefore become more complicated and their neglect certainly increases observational errors above currently accepted values. Furthermore de–projection procedures, such as the ones implied by the Limber equation, become much more involved and a number of results deduced just from angular data should be reviewed in this light.

IV.3 Brief summary of the chapter.

We will comment on the contents of the two sections separately, because the material presented there is self–contained.

In the first section of the Chapter, following a suggestion by Schaeffer and Silk, we attempted to estimate the present distribution of galaxies from the linear growth of primordial adiabatic fluctuations. The latter are studied in flat Universe models dominated by dark matter, in one of its three popular varieties –hot, warm, and cold– or in some mixture thereof.

The mass distributions are derived either from the canonical Press–Schechter (PS) mechanism or from an approximate peak count, within an assumption of high bias. Our theoretical curves are then confronted with those derived from luminosity functions of galaxies and clusters.

On the large scales the PS approach seems to give acceptable agreement with the data for all models, regardless of their chemical composition (*i.e.* the nature and the abundance of the dark matter components); the approximate peak approach seems instead to represent the observations less closely.

On small scales on the other hand the results are so strongly sensitive to the chemical composition that it is possible to draw some conclusions: the pure warm model is the one which overall fits the data best.

This work has been accepted for publication (Occhionero and Scaramella, 1988), and is in the main stream of a renewed theoretical interest in the prediction and evaluation of mass–functions and their application in various astrophysical contexts. Several papers have appeared in the literature or in (yet) preprint form after most of the above material was completed (early 1987) and were not referred to in the text. Among these, just to name a few, are predictions of quasar distribution (Efstathiou and Rees, 1988), consideration of the Sunyaev–Zel'dovich effect from cluster evolution (Cole and Kaiser, 1988), extension of the formalism to non–Gaussian statistics (Lucchin and Matarrese, 1988), estimates on the X–ray luminosity evolution from clusters (Cavaliere and Colafrancesco, 1988), and a more sophisticated peak treatment than the one presented here (Colafrancesco *et al.*, 1988). The most recent review on this important topic that we are aware of is that by Lucchin (1988).

In the second section of the Chapter, available observations on the dependence of the galaxy correlation length r_o on luminosity were discussed. Their trend is not incompatible with a canonical bias model. On the contrary the behaviour expected within a simple fractal model of matter distribution in the Universe finds no more support in data than the assumption of constant r_o does.

This work has been widely circulated last year in a preprint form (Scaramella and Bonometto, 1987), and is currently under the refereing process. After its completion other papers appeared on this issue: while Blanchard and Alimi (1988) argue that the trend observed in the data of Einasto *et al.*(1986) can be due to the numerical estimator used for the computation of the correlation function, a luminosity dependence of the amplitude of the two–point correlation function has been confirmed by studies of the CfA sample by Hamilton (1988) and Davis *et al.* (1988), who use data also from a new survey in the South. These latter authors find a dependence of r_0 on the intrinsic limiting luminosity which translates into a value

for $b \approx 1/4$, which confronts very well with our above estimate of $b = 0.28 \pm 0.11$, and argue that no dependence of r_0 is observed on the physical depth of the sample, again in agreement with our discussion and in contrast with the simple fractal predictions.

From the theoretical side also of relevance are the recent discussions of Hoffmann (1988) and Ryden (1988), who respectively stress a dependence of the mass bound to a proto–peak on the height of the peak itself, and computes explicitly such a dependence, finding a relationship of the type $M \propto \nu^{\alpha}$, where α depends upon the adopted effective spectral index. This supports and is in complete agreement with our basic explanation of the observed trend, that is a dependence of the mass, and hence of the optical luminosity, of large galaxies on the height of their proto–peaks over the general fluctuation background. Indeed we want to remark that the line of reasoning exposed above could lead to important information on the shapes, and therefore on the fluctuation spectrum, of primordial peaks on galactic scale lengths, through an observable quantity (i.e. b).

It is also appropriate to comment, and is useful for considerations discussed in the next Chapter, that such luminosity dependence on the mass of the galaxies (for the most luminous galaxies) is expected to be due to processes related to the formation of the galaxy itself. Other processes, which would for instance trigger bursts of star formation, would not necessarily be correlated with the primordial perturbations, and hence would probably not be reflected in the suggested luminosity dependence of the correlation amplitude. This argument is in fact very appropriate for the IRAS sample galaxies, where the infrared luminosity is very dependent on the present star formation rate. Indeed Davis *et al.* (1988) find that the trend observed in optical luminosity does not show up in a similar sample of IRAS galaxies.

References to Chapter IV

Aaronson, M., 1983, *Astrophysical Journal (Letters)* **266**, L11.

Aaronson, M., 1987, in *"Dark Matter in the Universe"*, IAU Symp. 117, J.Kormendy and G.R.Knapp eds., Reidel Publ. Co.

Achilli, S., Occhionero, F., and Scaramella, R., 1985, *Astrophysical Journal* **299**, 577.

Albrecht, A., and Steinhardt, P.J., 1982, *Physical Review Letters* **48**, 1220.

Blanchard, A., and Alimi, J.M., 1988, *Astronomy & Astrophysics* **203**, L1.

Bahcall, J., 1987, in *"Dark Matter in the Universe"*, IAU Symp.No.117, J.Kormendy and G.R.Knapp eds., Reidel Publ. Co.

Bahcall N., and Soneira, E., 1983,*Astrophysical Journal* **276**, 10.

Bahcall, N.A., and Soneira, R.M., 1983, *Astrophysical Journal* **270**, 20.

Bardeen, J.M., Bond, J.R., Kaiser, N., and Szalay, A., 1986, *Astrophysical Journal* **304**, 15.

Bond, J.R., 1986, in *"Galaxy Distances and Deviations from Universal Expansion"*, F.Madore and R.B.Tully (eds.), Reidel Pub. Co.

Bond, J.R., Efstathiou, G, and Silk, J.,1980, *Physical Review Letters* **45**, 1980.

Bond, J.R., and Efstathiou, G., 1984, *Astrophysical Journal (Letters)* **285**, LL45.

Bond, J.R., and Szalay, A., 1983, *Astrophysical Journal* **274**, 443.

Bond, J.R., Szalay, A., and Turner, M.S., 1982,*Physical Review Letters* **48**, 1636.

Bonometto, S.A., Lucchin, F., and Matarrese, S., 1987, *Astrophysical Journal* **323**, 19.

Bludman, S.A., and Hoffman, Y., 1986, in *"Inner Space/Outer Space"*, E.W.Kolb, M.S. Turner, D.Lindley, K.Olive, and D.Seckel eds., The University of Chicago Press.

Blumenthal, G.R., Pagel, H., Primack, J.R., and Rees, M.J., 1984, *Nature* **311**, 517.

Calzetti, D., Giavalisco, M., Pietronero, L., and Ruffini, R., 1987, preprint.

Carr, B.J., and Ikeuchi, S., 1985, *Monthly Notices of the Royal astronomical Society* ,, 213 497.

Cavaliere, A., and Colafrancesco, S., 1988, *Astrophysical Journal* **331**, 660.

Colafrancesco, S., Lucchin, F., and Matarrese, S., 1988, preprint.

Cole, S., and Kaiser, N., 1988, *Monthly Notices of the Royal astronomical Society* **233**, 637.

Collins, C.A., Joseph, R.D., and Robertson, N.A., 1986, *Nature* ,, 320 506.

Couchman, H.M.P., 1987a, *Monthly Notices of the Royal astronomical Society* **225**, 777.

_____1987b, *Monthly Notices of the Royal astronomical Society* **225**, 795.

Couchman, H.M.P., and Rees, M.J., 1986, *Monthly Notices of the Royal astronomical Society* **221**, 53.

Davis, M., Efstathiou, G., Frenk, C., and White,S.D.M., 1985, *Astrophysical Journal* **291**, 371.

Davis, M., Meiksin, A., Strauss, M.A., da Costa, N., and Yahil, A., 1988, *Astrophysical Journal (Letters)* **333**, L9.

Davis, M., and Peebles, P.J.E., 1983, *Astrophysical Journal* **267**, 465.

Dekel, A., and Rees, M., 1987, *Nature* **326**, 455.

Dekel, A., and Silk, J., 1986, *Astrophysical Journal* **303**, 39.

de Lapparent, V., Geller, M., and Huchra, J., 1986, *Astrophysical Journal (Letters)* **302**, L1.

Dicus, D.A., Kolb, E.W., and Teplitz, V.L., 1977, *Physical Review Letters* **34**, 168.

Doroskevich, A.G., 1970, *Astropysics* **6** 320.

Doroskevich, A.G., Khlopov, M.Y., Sunyaev, R.A., Szalay, SA.S., and Zel'dovich, Ya.B., 1980, in *"Tenth Texas Symp. on Rel. Astrophys."*,

Dressler, A., Faber, S.A., Burstein, D., Davies, R.L., Lynden–Bell, D.,Terlevich, R.J., and Wegner, G., 1987, *Astrophysical Journal (Letters)* **313**, L37.

Efstathiou, G., and Bond, J.R., 1986, *Monthly Notices of the Royal astronomical Society* **218**, 103.

Einasto, J., Klypin, A.A., and Saar, E., 1986, *Monthly Notices of the Royal astronomical Society* **219**, 457.

Efstathiou, G., and Rees, M.J., 1988, *Monthly Notices of the Royal astronomical Society* **230**, 13p.

Faber, S.M., 1982, in *"Astrophysical Cosmology"*, Brück, A., Coyne, G., and Longair, M., eds., Pontificial Scientific Academy.

Faber, S.M., and Lin, D.N.C., 1983, *Astrophysical Journal (Letters)* **266**, L17.

Felten, J.E., 1985, *Comm. on Astrophys.* **11** 53.

Geller, M., 1984, in *"Clusters and Group of Galaxies"*, F.Mardirossian *et al.* (eds.),

Reidel Publ. Co.

Gelmini, G., Schramm, D.N., and Valle, J.P., *Physics Letters* **146B**, 311.

Gott, R., Rees, M., 1975, *Astronomy & Astrophysics* **45**, 365.

Guth,A., 1981, *Physical Review* **D**, 23 347.

Ikeuchi, S., and Norman, C.A., 1987, *Astrophysical Journal* **312**, 485.

Hamilton, A.J.S., 1988, *Astrophysical Journal (Letters)* **331**, L59.

Hillebrandt, W., Hoflich, P., Kafka, P., Muller, E., Schmidt, H.U., Truran, J.W., and Wampler, J., 1987, *Astronomy & Astrophysics* ,, in press.

Hoffman, Y., and Shaham, J., 1985, *Astrophysical Journal* **297**, 16.

Hoffman, Y., 1988, *Astrophysical Journal* **328**, 429.

Kaiser, N., 1983, *Astrophysical Journal (Letters)* **273**, LL17.

_____1984, *Astrophysical Journal (Letters)* **284**, LL9.

Klypin, A., and Kopilov, M., 1983, *Soviet Astronomy (Letters)* **9**, L41.

Jones, B.T.J., Martinez, E., Saar, E., Einasto, J., 1988. *Astrophysical Journal (Letters)* **332**, L1.

Linde, A.D., 1982, JETP Lett. **40** 1333.

Lucchin, F., 1988, in *"Morphological Cosmology,"*, XI Cracow Summer School, *Lectures Notes in Phisics*, in press.

Lucchin, F., and Matarrese, S., 1988, *Astrophysical Journal* **330**, 535.

Madsen, J., and Epstein, R., 1985, *Physical Review Letters* **54**, 2720.

Madsen, M.S., and Ellis, G.F.R., 1988, *Monthly Notices of the Royal astronomical Society* **234**, 67.

Martinez–Gonzales, E., and Sanz, J.L., 1988, *Astrophysical Journal* , in press.

Maurogordato, S., and Lachieze–Rey, M., 1987, *Astrophysical Journal* **320**, 13.

Melott, A., 1985, *Astrophysical Journal* **289**, 2.

Melott, A., 1986, preprint.

Occhionero, F., and Scaramella, R., 1987, in *"LBL workshop on Cosmology and Particle Physics"*, Hincliffe, I., ed., World Scientific.

Olive, K., Seckel, D., and Vishniac, E.T., 1985,*Astrophysical Journal* **292**, 1.

Oort, J.H., 1932, *Bull.Astron. Inst.Netherlands* **6**, 249.

Oort, J.H., 1960, *Bull.Astron. Inst.Netherlands* **15**, 45.

Ostriker, J.P,, and Cowie, L., 1981, *Astrophysical Journal (Letters)* **243**, L127.

Ostriker, J.P,, and Ikeuchi, S., 1983,*Astrophysical Journal (Letters)* **268**, L63.

Peacock and Heavens, 1985, *Monthly Notices of the Royal astronomical Society* **217**, 805.

Peebles, P.J.E., 1980, *"The Large Scale Structure of the Universe"*, Princeton University Press.

_____1982, *Astrophysical Journal (Letters)* **263**, L1.

_____1984, *Astrophysical Journal* **277**, 470.

_____1986, *Nature* **321**, 27.

Pietronero, L., 1987, Physica **144 A**, 257.

Politzer, D., and Wise, M., 1984, *Astrophysical Journal (Letters)* **285**, L1.

Press, W.H., and Schechter, P., 1974, *Astrophysical Journal* **187**, 125.

Rees, M.J., 1985, *Monthly Notices of the Royal astronomical Society* **213**, 75p.

Ryden, B., 1988, *Astrophysical Journal* **333**, 78.

Saarinen, S., Dekel, A., and Carr, B., 1987, *Nature* **325**, 598.

Shaeffer, R., 1987a, *Astronomy & Astrophysics* **180**, L5.

Shaeffer, R., 1987b, *Astronomy & Astrophysics* **181**, L23.

Schaeffer, R., and Silk, J., 1984, *Astrophysical Journal (Letters)* **281**, L13.

Schaeffer, R., and Silk, J., 1985, *Astrophysical Journal* **292**, 319.

Schaeffer, R., and Silk, J., 1988, *Astrophysical Journal* **332**, 1.

Schechter, P., 1976, *Astrophysical Journal* **203**, 297.

Schechter, P., 1976, *Astrophysical Journal* **203**, 297.

Schramm, D.N., and Steigman, G., 1981, *Astrophysical Journal* **243**, 1.

Shafi, Q., and Stecker, F.W., 1984, *Physical Review Letters* **53**, 1292.

Silk, J., 1985, *Astrophysical Journal* **297**, 9.

Silk, J., and Turner, M.S., 1986, *Physical Review* **in**, press.

Silk, J., and Vittorio, N., 1987, *Astrophysical Journal* **317**, 564.

Szalay, A., and Marx, G., 1976, *Astronomy & Astrophysics* **49**, 437.

Tamman, G.A., 1986,in *"Cosmology, Astronomy and Fundamental Physics"*, Proc. Second ESO-CERN Symp., G.Setti and L.Van Hove eds.

Tremaine, S.D., and Gunn, J.E., 1979, *Physical Review Letters* **42**, 407.

Trimble, V., 1987, *Annual Review of Astronomy & Astrophysics* **25**, 425.

Turok, N., 1986,in *"Cosmology, Astronomy and Fundamental Physics"*, Proc. Second ESO-CERN Symp., G.Setti and L.Van Hove eds.

Turner, M.S., 1987,in *Dark Matter in the Universe*, IAU Symp.No.117, J.Kormendy

and G.R.Knapp eds., Reidel Publ. Co.

Turner, M.S., Steigman, G., and Krauss, L., 1984, *Physical Review Letters* **52**, 2090.

Turner, M.S.,Villumsen, J.V.,Vittorio, N., Silk, J., and Juszkiewicz, R., 1987, *Astrophysical Journal* **323**, 423.

Umemura, M., and Ikeuchi, S., 1985, *Astrophysical Journal* **299**, 583.

Uson, J.M., and Wilkinson, D.T., 1984, *Astrophysical Journal* **283**, 471.

Valdarnini, R., and Bonometto, S.A., 1985, *Astronomy & Astrophysics* **146**, 235.

Valdarnini, R., and Bonometto, S.A., 1985, *Astrophysical Journal (Letters)* **299**, L71.

Vilenkin, A., 1985, *Phys.Rep.*, **121**, 263.

Vittorio, N., and Silk, J., 1984, *Astrophysical Journal (Letters)* **285**, L39.

Vittorio, N., and Turner, M.S., 1987, *Astrophysical Journal* **316**, 475.

Winter, K., 1986, in *"Cosmology, Astronomy and Fundamental Physics"*, Proc. Second ESO-CERN Symp., G.Setti and L.Van Hove eds.

Yang, J., Turner, M.S., Steigman, G., Schramm, D.N., and Olive, K.A., 1984, *Astrophysical Journal* **281**, 493.

Zel'dovich, Ya.B., 1980, *Monthly Notices of the Royal astronomical Society* **192**, 663.

V Superclusters and large-scale peculiar velocities.

V.1 Cluster of galaxies catalogues and the new ACO catalogue.

We will briefly review here the basic properties of the currently available catalogues of cluster of galaxies and the main results appearing in the literature on this topic. More detailed information can be found in reviews by Bahcall (1977, 1988), Oort (1983), and Geller (1987).

Currently, four main catalogues of cluster of galaxies are available: Abell's, Zwicky's, Schechtman's, and ACO (from Abell, Corwin and Olowin).

All of them have been optically and visually selected according to different criteria, and therefore have various biases and are not homogeneous among themselves, except for Abell's and ACO. Only Abell's catalogue has been extensively studied from a statistical point of view, with results which have great importance for our definition and comprehension of large scale structures. Most of the information in the following summary is taken from Bahcall, (1988).

The Abell (1958) catalogue of rich clusters of galaxies contains a total of 2712 clusters that are the richest, densest clusters found on the Palomar Sky Survey plates and are identified by a well–defined set of selection criteria.

Of these rich clusters, 1682 constitute Abell's statistical sample, and are distributed over 4.26 steradians of the sky and satisfy the following selection criteria: (a) A cluster must contain at least 50 members, after proper correction for background, in the magnitude range m_3 to $m_3 + 2$, where m_3 is the magnitudeof the third brightest galaxy; (b) the $\gtrsim 50$ members should be contained within a cir-

cle of radius 1.5 $h^{-1}\,Mpc$ around the center of the cluster (this corresponds to the Abell radius $R_A = 1.7'/z$, where z is the cluster redshift; clusters wich have counts between 30 and 50 are still considered rich but do not belong to the statistical sample); (c) the cluster redshift should be in the range $0.02 \lesssim z \lesssim 0.20$; and the cluster should lie north of declination $\delta = -27^o$ and within the completeness region given in Abell (1958).

The clusters' distances were estimated by Abell by the magnitude of the tenth brightest galaxy, m_{10}. For each cluster the catalogue lists the cluster postion on the sky; m_{10}; the distance group D (estimated from m_{10}); and the Richness classification, R. The latter is related to the number of member galaxies brighter than $m_3 + 2$ and located within $R_A = 1.5\,h^{-1}\,Mpc$ from the cluster center, after having corrected for the background by comparison counts in a nearby field. Lucey (1983) gives an assessment of possible incompletness in the Abell catalogue.

Table V.1

Population	# of clusters	Richness class R	Distance class D	mean redshift	m_{10} range
$30-49$	1030	0	1	0.027	$13.3-14.0$
$50-79$	1224	1	2	0.038	$14.1-14.8$
$80-129$	383	2	3	0.067	$14.9-15.6$
$130-199$	68	3	4	0.090	$15.7-16.4$
$200-299$	6	4	5	0.140	$16.5-17.2$
≥ 300	1	5	6	0.180	$17.3-18.0$

Table V.1. *Richness and distance group specifications for the Abell's catalogue.*

The Abell catalogue covers the northern Galactic hemisphere and a part of the southern hemisphere. To complete the sky coverage, the late G.O. Abell, H.G. Corwin and R.P. Olowin compiled a catalogue of clusters of galaxies (Abell *et al.*, 1988, hereafter ACO; because of its recent completion, at the moment we have only a brief preprint version of the catalogue characteristics and will not go

into great detail in its discussion), with the same criterion used to select clusters as for Abell's catalogue.

The ACO catalogue, which lists 1638 clusters south of declination $\delta \leq -17^o$, has some important differences, though, from Abell's catalogue. ACO lists more information, in that it gives for each cluster, besides m_{10}, also the first and third ranked magnitudes, m_1 and m_3, the number of galaxies N_g between m_3 and m_3+2 (Abell's lists only a discrete classification, see Table V.1 ; later Struble and Rood, 1987, listed N_g for Abell clusters), and morphological classification (a five class division from regular to irregular, R–RI–IR–I, and Bautz-Morgan classification, see Bahcall, 1977).

Two other important differences are the quality of the plates from which the catalogue has been compiled and the richness class estimates. While the Abell catalogue was compiled on red band plates, the ACO has been drawn from plates in the J (almost blue) band (survey of United Kingdom's $1.2\,m$ Schmidt Telescope –UKST–) which are of better quality and complete to a deeper magnitude than the ones used for Abell's compilation: this fact makes ACO complete to a deeper distance than its counterpart (the listed magnitudes, though, have been recalibrated and referred to the V band). On the other hand, ACO suffers, in our opinion, from a drawback caused by a different procedure for background estimates: while in Abell's the background was estimated locally, by counts in a nearby field, for ACO the background has been estimated globally, through an assumed galaxy luminosity function. This procedure makes the details of the counts N_g to determine the richness of the cluster less reliable and therefore also the partition in classes of different richness R (see Table V.1), especially because for some of the clusters, the number of galaxies N_g listed is zero or even negative ! This is of course an overcorrection: if the number were less than 30 the "cluster" would have not been classified as such in the first place. We now pass on to summarize, for comparison purposes, the characteristics of the other two catalogues.

The Zwicky *et al.* (1961-68) "Catalogue of Galaxies and Clusters" contains over 30000 galaxies brighter than 15.7^m identified on the Palomar Sky Survey

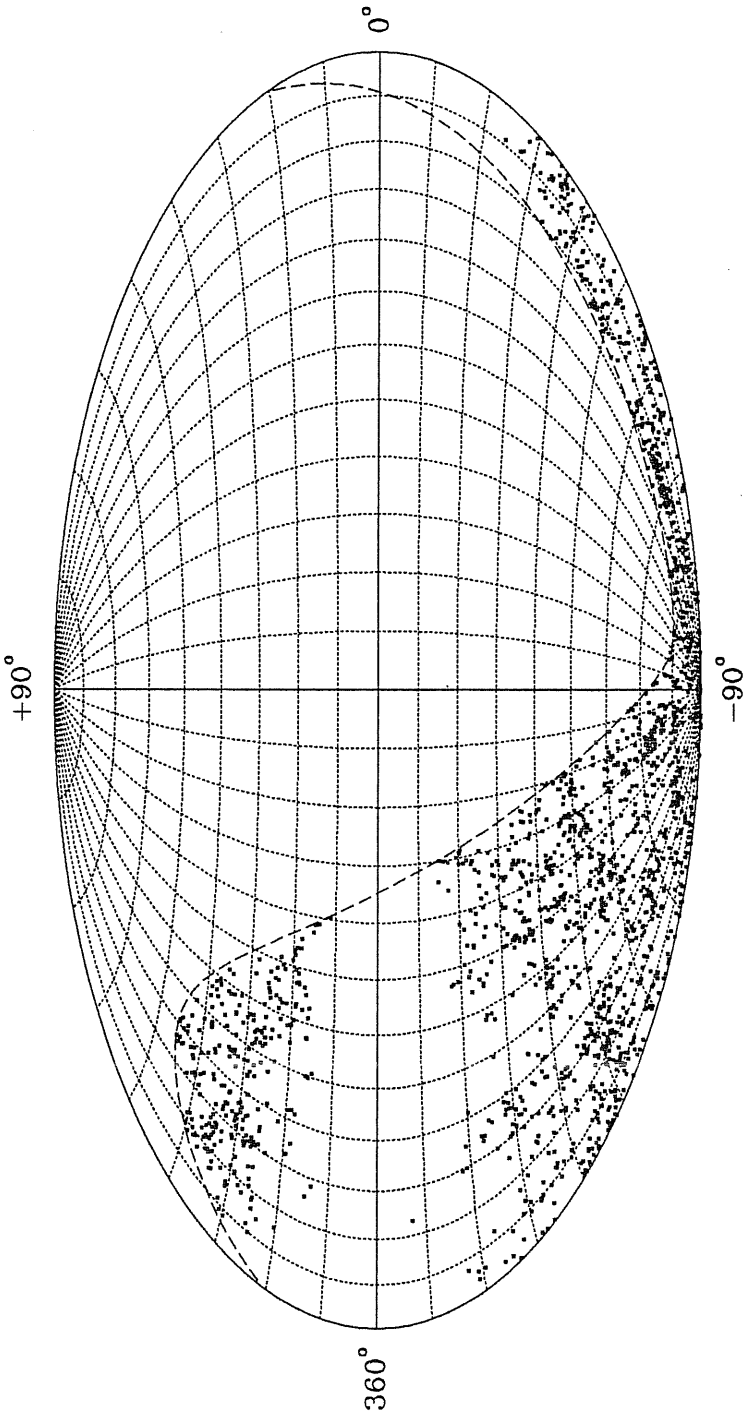

Figure V.1. *Equiarea projection of the ACO clusters in galactic coordinates. While the strong decrement in the number of clusters for* $|b| \lesssim 20°$ *is due to galactic extinction, the absence of clusters in other regions is simply due to the limited sky coverage of the ACO catalogue,* $\delta \leq -17°$*, whose border is shown by the dashed line.*

plates and 9700 clusters of galaxies visible to the limit of plates ($m \cong 20$). The criteria for including a cluster in the catalogue are the following: (a) The cluster must contain at least 50 galaxies in the magnitude range m_1 to $m_1 + 3$, where m_1 is the magnitude of the brightest galaxy; (b) these galaxies must lie within the cluster's contour, defined as the isopleth where the projected galaxy density is about twice that of the neighbouring field; (c) no limit on the cluster redshift is specified, but aggregates such as the Virgo cluter (which cover very large areas of the sky) are not included in the contour maps; and (d) the cluster must lie north of declination -3^o and within certain areas specified in the catalogue. The cluster distances are classified according to estimated redshifts as: near clusters ($z \lesssim 0.10$), medium distant ($z \cong 0.10$—0.15), very distant ($z \cong 0.15$—0.2), and extremely distant ($z \gtrsim 0.2$). Cluster population (richness) is defined as the number of galaxies visible on the red Palomar Sky survey plate, corrected for the mean field count, that are located within the isopleth of twice the the field density. Because of the latter condition from the the field density and the counts are taken to the plate limit, the population in Zwicky clusters depends systematically on the cluster redshift. Other problems are pointed out by Abell (1975).

The Schechtman catalogue is based on an automatic procedure applied to the visual counts of Shane and Wirtanen (1967). The clusters are selected as local density maxima above a given threshold value of the galaxy counts in $10'$ bins. This procedure selects 646 clusters with declination $\delta > -22.5^o$ and Galactic latitude $|b| \geq 40^o$, which are considerably poorer than the Abell's $R \geq 1$ clusters. Scechtman finds that ~ 40 % of his clusters are members of the Abell's catalogue, with a space density which is about 6 times higher than Abell's $R \geq 1$ clusters.

We close this section with the remark that two further catalogues of galaxies (and clusters of galaxies) are being built by means of 'objective' algorithms through automatic scanning of plates (COSMOS in Edinburgh and APM in Cambridge). These catalogues will make a dramatic improvement in the quality of the data and will add much reliability to their statistical analyses.

V.2 Estimates of distance and density of the ACO catalogue, and a percolation algorithm.

As already remarked in the introduction, it is of great importance to be able to assess the distances to given objects. In the case of clusters of galaxies we principally have three different levels of possible knowledge, that we now discuss briefly. The first method is to evaluate the so-called 'distance modulus', that is to estimate the distance from apparent magnitudes, making definite assumptions on a universal luminosity function; we will discuss this method below in more detail for a preliminary analysis of the ACO catalogue. The second method is to measure the mean redshift of the cluster and assign a distance through the assumption of a pure Hubble flow. The third method is the use of distance estimators more sophisticated than the single observed magnitude, like the Tully–Fisher relation for spirals and the Faber-Jackson and similar relationships for ellipticals. These latter methods, together with redshift estimates are used to try to map the peculiar velocity field, as we will see in detail in the next sections.

To have measured redshift for clusters obviously gives much more precise information on the cluster radial distance than estimates through apparent magnitudes but to obtain such redshifts has not been easy (hopefully, with the use of multislit spectroscopy, this will not be the case for new catalogues, ACO included): it took more than 20 years before there appeared in the literature (Hoessel *et al.*, 1980) the measured redshift for a small, nearby subset of the statistical sample of Abell's catalogue ! With this information (104 clusters of $R \geq 1$ and $D \leq 4$) Bahcall and Soneira (1983, and 1984) were able to discuss the clustering of clusters themselves (sometimes called 'superclustering' or 'second order clustering') through a compilation of a supercluster finding chart and the first evaluation of the spatial cluster–cluster two–point correlation function, $\xi_{cc}(r)$ (given also contemporarily by Klypin and Kopilov, 1983). On the other hand, as stressed by Postman *et al.* (1988), to have a reliable mean redshift for the cluster requires at least $\sim 5-10$ measures of z for different galaxies thought to belong to the cluster, both because of the presence of interlopers and because of the spread in radial velocities along the line of sight due to peculiar velocities within the cluster itself

(the 'finger of God' effect; a typical value for a cluster is $\sigma_{rms} \approx 700 - 1000\, km/sec$ along the line of sight).

In the ACO catalogue case we are presently in almost the same position as we were after the Abell catalogue release: scarce redshift information is available. Having as a goal the identification of primary targets for subsequent redshift studies, we will discuss a *preliminary* study of distance estimates for the ACO catalogue, because we are still working on this very recent dataset.

A detailed study of distances estimates through the use of m_{10} for Abell's catalogue is given in Postman *et al.* (1985). These authors found that the use of m_{10} as a distance estimator is very unreliable for $z \geq 0.1$ ($m_{10} \geq 16.5$), because of foreground contamination (the tenth brightest galaxy does not belong to the cluster) and systematics in Abell's magnitude estimates. After corrections for the Scott effect (richer cluster have systematically brighter M_{10}) and K-correction (see below) a calibration on 561 Abell clusters, according to Postman *et al.*, gives a linear relationship between $\log(z)$ and m_{10} which has a standard error of 14 % on the logarithm ($\Delta z/z \cong 32$ %). Part of this observed scatter ($\sigma_{m_{10}} \cong 0.70\ mag$) is estimated to be intrinsic (Postman *et al.* estimate $\sigma_{M_{10}} \cong 0.48\ mag$ from the galaxy luminosity function) and part to be due to errors in the Abell's visual magnitude estimates (they obtain $\sigma_{m_{10}} \cong 0.39\ mag$ by quadrature subtraction, while Abell's own estimate (1958) was $\sigma_{m_{10}} \cong 0.20\ mag$).

In the ACO case we are in a different situation: the catalogue lists only 145 clusters with measured redshifts (plus another 23, which are highly unreliable). We will now discuss the preliminary distance estimator we derived.

In a FRW universe for non-negligible redshifts the simple euclidean relationship $L \propto d^{-2}$, which implies $m - M = 5 \log(d/10\, Mpc)$, does not hold but can be appropriately generalized through Mattig's formulæ (see Sandage, 1961, or Weinberg, 1972, or Peebles, 1980) to the following relationship:

$$5 \log [D_L(z)] \ = \ m - M \ , \qquad \text{(V.1)}$$

where the quantity D_L, the so–called 'luminosity distance', is a function of the

redshift, z, and of the cosmological FRW model (assumed to be pressureless) through the deceleration parameter $q_0 \equiv \Omega_0/2$:

$$\frac{H_0}{c} D_l(z, q_0) \equiv q_0^{-2} \left\{ q_0 z + (q_0 - 1) \left[\sqrt{1 + 2q_0 z} - 1 \right] \right\} . \qquad \text{(V.2)}$$

Proper and comoving distances, r and $d = (1+z)r$ respectively, are then related to the luminosity distance by

$$r = \frac{D_L(z)}{(1+z)^2} \quad ; \quad d = \frac{D_L(z)}{(1+z)} . \qquad \text{(V.3)}$$

The above relationships hold for an ideal situation, i.e. bolometric magnitudes, no extinction, and, when applied to different objects, assumes a common intrinsic magnitude M.

We then applied corrections to take in account the physical effects involved as much as possible (cf. above discussion). These are: galactic extinction (we corrected observed magnitudes with a simple $cosec|b|$ law, where b is the galactic latitude), the Scott effect (we included a logarithmic dependence on the listed number of galaxies, N_g, taking the maximum between N_g and 30 to try to minimize the problems caused by the aforementioned 'global' background correction), and finally the K–correction. The last correction takes into account the fact that the observed magnitudes refer to given spectral bands and are not the bolometric magnitudes assumed by Eq. (V.1) . These facts reflect into two separate modifications, one of which is dependent on the spectrum of the original galaxy, while the other depends only on the redshift. Because of the cosmic expansion, a given observed wavelength interval, $\delta\lambda_0$, corresponds to a narrower interval at the emission redshift, z_{em}, so that $\delta\lambda_0 = \delta\lambda_{em}/(1+z_{em})$. Because $m_{obs} \propto 2.5 \log \left[\int f_\lambda d\lambda \right]$ with f the received flux, this amounts to a correction for the observed magnitude of $\Delta m = -2.5 \log(1+z)$, which is the same for all galaxies at the same z. The other part is also due to the redshift effect, but varies from galaxy to galaxy and from band to band because it is dependent on both the galaxy spectrum and on the actual observation wavelength, λ_0. More precisely if we denote by $S(\lambda)$ the observetional bandpass function and $F(\lambda)$ the spectral flux of the emitting galaxy, we have that what is actually observed, instead of the convolution $\int_0^\infty S(\lambda_0) F(\lambda_0) d\lambda_0$,

is $\int_0^\infty S(\lambda_0)F[\lambda_0/(1+z)]d\lambda_0$, because the redshift means we are sampling a different part of the emitted spectrum.Hence we will write the total K–correction as

$$K(z) \;=\; -2.5\log\left[\frac{\int_0^\infty S(\lambda)F\left[\frac{\lambda}{(1+z)}\right]d\lambda}{\int_0^\infty S(\lambda)F[\lambda]d\lambda}\right] + 2.5\log(1+z)\,. \qquad \text{(V.4)}$$

We took the numerical value from Ellis (1982), as given in Shanks *et al.* (1984), relative to elliptical and S_0 galaxies (the most likely morphological type for the m_3+2 brightest in a rich cluster). This is $K(z) = 4.14z - 0.44z^2$.

We also decided, pending the uncertainty in the value for H_0, to sometimes quote the distances directly in $km\,sec^{-1}$, so that the reader can easily convert to distances in Mpc through his preferred value for H_0 (we will also sometimes use the standard notation $H_0 = 100\,h\,km\,sec^{-1}Mpc^{-1}$ when appropriate for direct comparisons with results given in the literature). To ease comparison with other authors' work we also will assume an Einstein–de Sitter universe (i.e. $q_0 = 1/2$). The latter assumptions has little effect (at most a few percent) at the distances which are of interest here and it is dwarfed by the present uncertainties due to the assumed laws for extinction and K–correction.

We therefore fitted the following relationship to the 145 clusters with measured redshifts, that are listed in the ACO catalogue:

$$f(z) \equiv \log\left[D_L(z)\right] + 0.2\,K(z) \;=\; A + B\,m_{10} + C\log\left(\frac{N_g}{80}\right)\,. \qquad \text{(V.5)}$$

We then defined the sample variance estimate as $\sigma^2_{sample} = \sum_{i=1}^{N_{obj}}[f_{i,meas} - f_i]^2/(N_{obj}-\nu)$, where N_{obj} is the number of calibrating objects and ν (here $\nu = 3$) is the number of degrees of freedom in the fitted functional relationship. We found that two among the 145 original clusters we examined had estimated redshifts which were strongly inconsistent with the derived relationship. These two clusters in fact had measured redshifts which were beyond three sigma's from their estimates, suggesting a spurious redshift or m_{10} attribution. Hence we calibrated Eq. (V.5) on the remaining 143 clusters, obtaining the following values for the

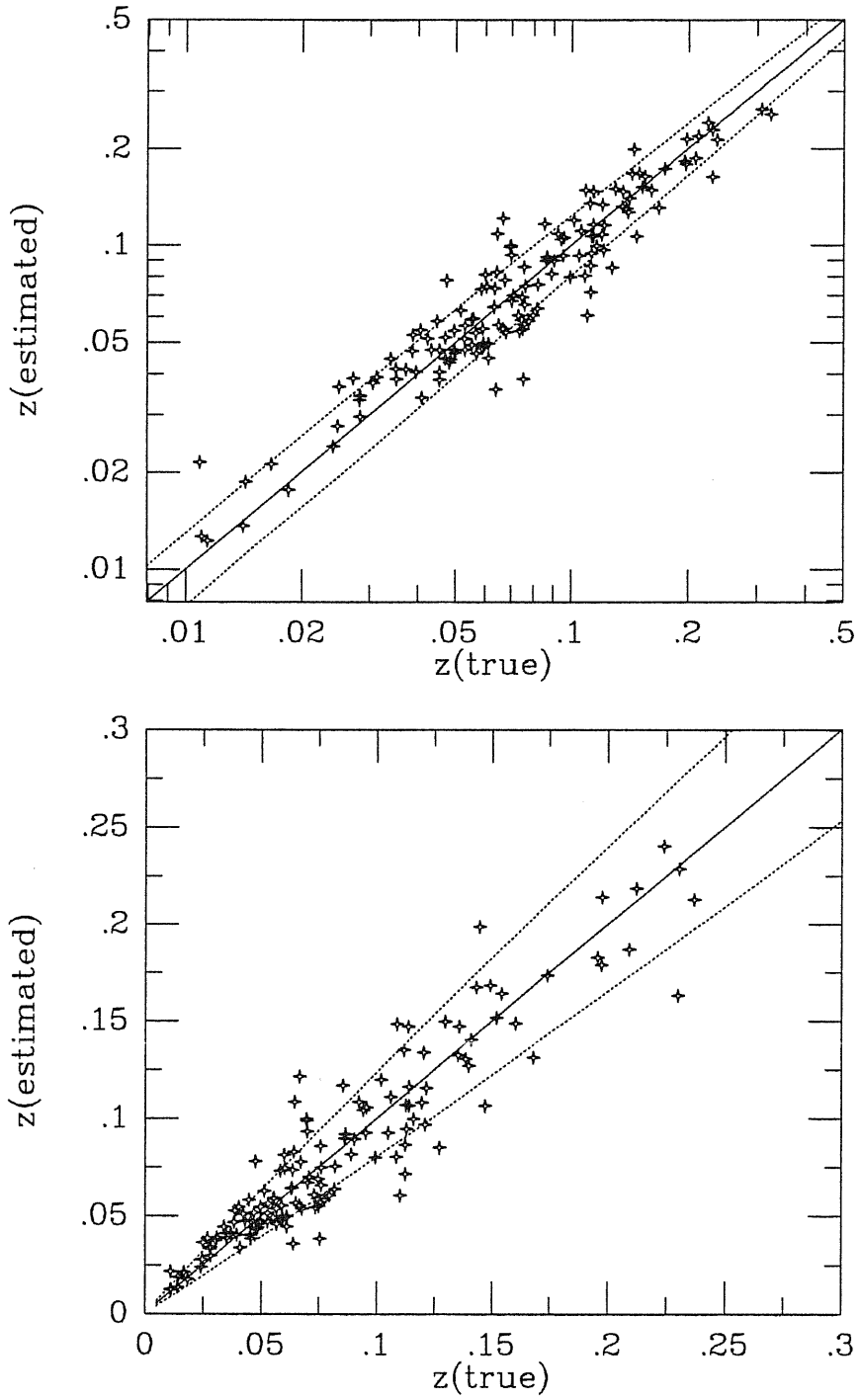

Figure V.2. *Estimated redshifts versus measured redshifts are plotted for the calibrating sample of 143 ACO clusters (log-log plot, upper panel, linear-linear plot, lower panel). Dotted lines denote the* $\pm\sigma_{sample}$ *confidence region (for 'perfect' estimates all points would lie on the solid lines on diagonals). Effects of the non-linearity of the K(z) term can be seen in the upper panel for* $z \gtrsim 0.2$ *(of course for such values of z the distance is no longer simply proportional to the redshift).*

fitted parameters and the estimated sample dispersion:

$$A = -4.45290 \ ; \ B = 0.2085 \ ; \ C = 0.1998 \ ; \ \sigma_{sample} = 0.1136 \ . \qquad \text{(V.6)}$$

In Fig. V.2 we show the data which have been used for the present calibration.

It is opportune now to make some comments on the above relationship. The first comment is that the fitted coefficient of the apparent magnitude term, B, differs only by ~ 4 % from the value $1/5$, which is expected in a 'clean' theoretical universe: if not by a mere chance, this is very a remarkable agreement. The second comment is that we have been very conservative in keeping most of the calibrating objects and that the value for the estimate of the sample dispersion that we found, $\sigma \cong 11.4$ % is in agreement with that derived from Postman *et al.* for the Abell catalogue (~ 14 %): although we fitted a slightly different relationship *on a different catalogue*, for $z \ll 1$ we have that $f(z) \rightarrow \log z$, and then, in the same limit, $\Delta z/z \cong 25$ % (it is perhaps more instructive to make the comparison on the magnitudes: we find $\lesssim 0.60$ *mag*, while Postman *et al.* find $\cong 0.70$ *mag* –but we used a more detailed richness dependence on a better catalogue).

Other authors have also made similar distance estimates based on the same ACO catalogue we used, although very little information is currently available and that only in preprint form, because of the already mentioned novelty of this catalogue. At the present moment (i.e. mid–October 1988) we have available a just published letter from Bahcall *et al.* (1988) in which the use of a $\log z - m_{10}$ is mentioned relationship but no detail is given of the functional form or the values for any parameter, and another preprint by Couchman *et al.* (1988) in which such a relationship is fully discussed. The latter authors fitted a relationship very similar to the one we used in Eq. (V.5) but with some differences. It is not clear to us from their wording if they imposed or found through direct fitting a value for $B = 0.20$, but this is of little importance, as is the fact that they fitted a linear K–correction term, while we took such a term from the literature. The real discrepancy between their results and ours is in their estimate of σ_{sample}: they found a dispersion of only ~ 0.26 *mags* (i.e. $\Delta z/z \cong 13$ %). The good agreement we found instead with the Postman *et al.* estimates, makes us believe

that the discrepancy of a factor two in the dispersion estimate for distances has to be ascribed to their excessive curbing of the calibrating number of clusters N_{obj} down to only 28 from the original $\sim$ 160 listed in the catalogue (i.e. the 145 we started with plus the unreliable 23) from which they find a dispersion of $\sim 1.3\, mag$. Indeed, such a low dispersion is already at the level of the error associated with the visual magnitude estimates alone, without taking into account the much larger contribute from the intrinsic absolute magnitude dispersion. We will accordingly use our relation in the present work, although the effect of a calibration which makes use of all the magnitudes listed in the catalogue (i.e. m_1, m_3, and m_{10}, as was pioneered by Leir and van den Bergh, 1976) is currently under examination and will be discussed elsewhere (Scaramella *et al.*, 1989).

We now pass on to discuss preliminary density estimates for the ACO catalogue. To this end it is useful to have estimates of the solid angle covered by ACO catalogue on the sky. It is convenient also to discriminate among regions at different galactic latitude, b. We computed the following estimates through a simple Monte–Carlo calculation, because of the elaborate geometrical boundaries. This simple algorithm consists in the computation of the fraction of random numbers, drawn uniforimily from a region of known area, which belong to the region whose area is to be computed. Numbers can be drawn from a uniform distribution on the unit sphere according to the following rule: ξ_1 and ξ_2 are drawn uniforimily from the unit interval, and the polar angles θ and ϕ computed by:

$$\phi \;=\; 2\pi\,\xi_1 \quad ; \quad \theta \;=\; \cos^{-1}\left(1 - 2\,\xi_2\right) \;. \tag{V.7}$$

In our case we have drawn random numbers uniformily from the region with declination $\delta \leq -17^o$ and then counted their distribution in shells of given galactic latitude b.

One of the known biases found in the Abell catalogue is a decrease of the number of clusters going towards low latitudes. Bahcall and Soneira (1983) found that this decrement for $R \geq 1$ clusters is well represented for $|b| \geq 30^o$, by the following law: $N(|b|) = N_0\, dex\,[-0.3\,(csc|b| - 1)]$. The value they obtained for the

Table V.2

$\|b\| \leq$	25 ± 5	35 ± 5	45 ± 5	55 ± 5	65 ± 5	75 ± 5	85 ± 5	$\|b\| \geq 20$
Ω	0.75	0.64	0.45	0.35	0.28	0.21	0.09	2.77

Table V.2. *Solid angles for different latitude shells for the ACO catalogue. $|b|$ is the galactic latitude (degrees) and the solid angles are in steradians.*

spatial density of the nearby statistical sample is $n \cong 6 \cdot 10^{-6} (h^{-1}\, Mpc)^{-3}$ from a simple average for $|b| \geq 30^{o}$. The latter value becomes $n_0 \cong 9 \cdot 10^{-6} (h^{-1}\, Mpc)^{-3}$ when corrected for the cosecant decrease.

It is important to note that one would not expect such a decrement for plates which are nominally complete for a magnitude much deeper than $m_3 + 2$. One obvious effect which is present in the data is that due to galactic extinction. This effect, however, should not play an important rôle for intermediate latitudes, at least not at the level of missing many of the galaxies with unreddened magnitude smaller than $m_3 + 2$, so that the cluster is no longer considered rich because it does not meet the minimum threshold of $N_g = 30$. The probable cause of the decrement in the compiled list of clusters lies in possible galaxy–star misclassifications and the fact that the human eye is sensitive to luminosity density contrasts more than to absolute values: hence, by peering into plates, one can easily miss a cluster of galaxies embedded in a crowded star field, while the same cluster would have been noted in an almost empty field. This fact stresses again the great importance of data samples that are automatically selected.

We can proceed to a preliminary estimate of ACO clusters density as follows, stressing the fact that it will be possible to obtain definite values only when a redshift sample is available and complete to reasonable depths (here we have 143 clusters with measured redshift –a number greater than the 104 used by Bahcall and Soneira in their study– but these are not representative of a complete sample, so their space distribution is not significant).

One could naively think of assigning to each cluster the distance estimate

obtained by simply using the listed value of m_{10}, corrected for galactic extinction, into Eq. (V.5) with the parameter values given in Eq. (V.6) and then deriving the comoving distance (we are interested in comoving densities) from the estimated luminosity distance. The problem with the above procedure is that one would then almost use the inverse logarithm of the expected value of the logarithm of the distance, and this is in principle very different from the expected value of the distance itself. We can in fact see that we are facing a situation formally similar to the Malmquist effect: if we ignore for example the K–correction term on the l.h.s. of Eq. (V.5) , we can easily see that, because of the underlying assumption of a Gaussian distribution of dispersion σ_{sample} for the sum of r.h.s. quantities, the luminosity distance has a probability distribution function which is lognormal. Therefore, in the approximation $K(z) \cong 0$, we would have that for the expected value of the luminosity distance: $\langle D_L \rangle = dex\,\{\langle \log(D_L) \rangle + [\ln(10)\sigma^2_{sample}]/2\}$, where $\langle \log(D_L) \rangle$ is obtained by estimating from the values of m_{10} and N_g. Hence we would need to multiply the naive value $dex[\langle \log(D_L) \rangle]$ by the constant factor $dex\left[0.5\ln(10)\sigma^2_{sample}\right] \cong 1.035$, which reflects in $\sim$ 11 % decrease of the initial (too large) density estimate, which is not negligible.

In our case, because of $K(z) \neq 0$, the analytic pdf for the luminosity distance is quite complicated and is a function of z, therefore we adopted the following procedure to obtain what in the following will be referred to as the 'reference catalogue'. We estimated $\langle D_L \rangle$ for each cluster i as the mean taken from 1000 values, obtained by solving the following relation for z_i:

$$D_L(z_i) + K(z_i) = A + B\, m_{10,i} + C \log\left(\frac{N_{g,i}}{80}\right) + \xi_j \cdot \sigma_{sample}\ , \qquad \text{(V.8)}$$

where ξ_j, $j = 1, \ldots, 1000$ is randomly drawn from a Normal distribution with zero mean and unit variance. We can then immediatly evaluate $D_L(z_i)$ for each j, once we have derived z_i, and finally get the estimate for $\langle D_L \rangle$ by a simple average. We then still get an uncertainty of $\lesssim 1$ % on the precise figures for the $\langle D_L \rangle$ estimate ($\sim (\Delta z/z) \cdot 10^{-3/2}$; of course the uncertainty of the real value of D_L is still of the order $\sim \Delta z/z$), so one might think we wasted one hour of CPU time of a Vax–station to get not much improvement; but now we have a random

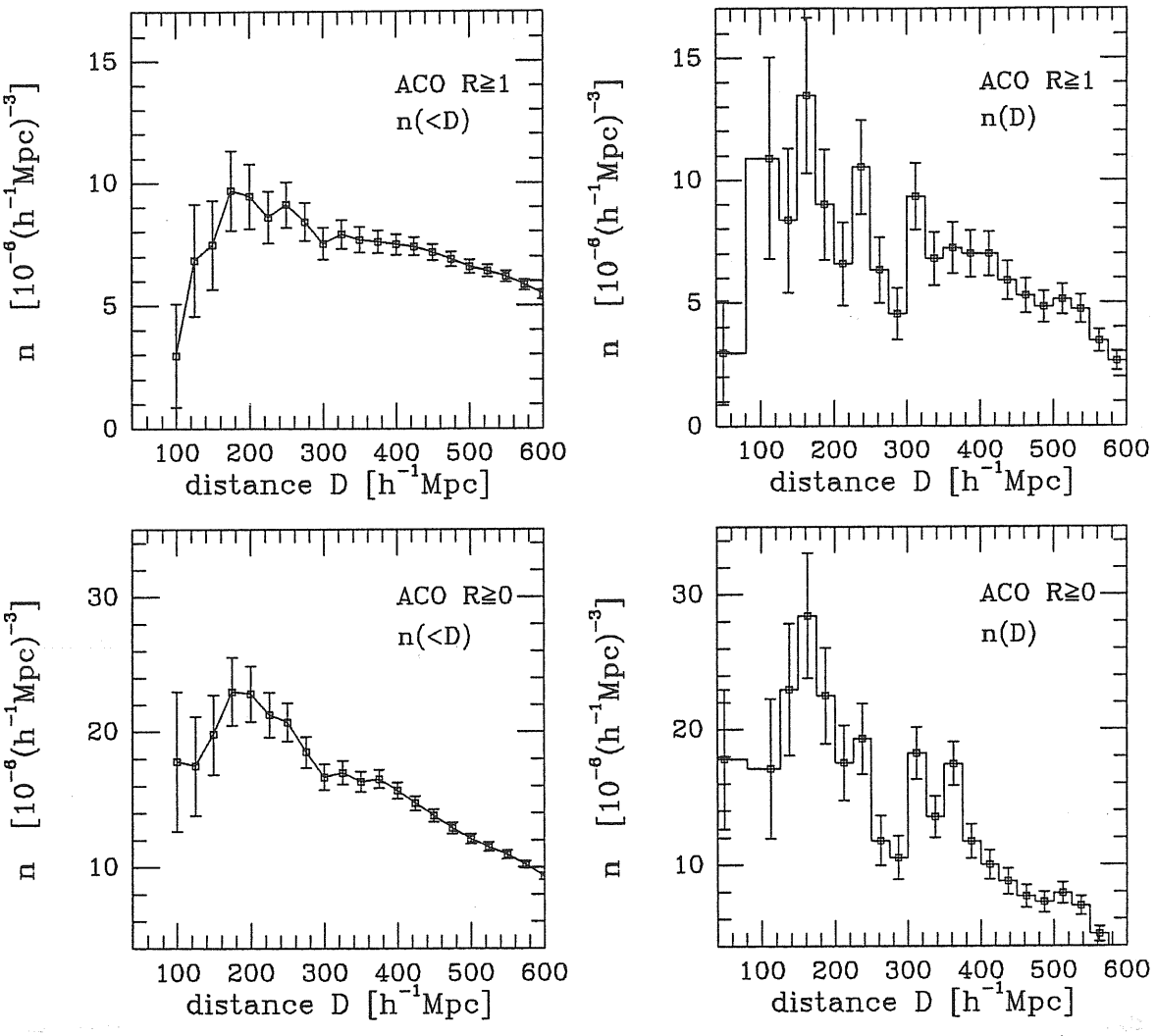

Figure V.3. *Cumulative density (left panels) and differential density (right panels) are plotted for ACO clusters with* $|b| \geq 30^o$. *Upper panels show richness class* $R \geq 1$, *lower ones show all rich clusters. The amplitude of the error bars show uncertainties due to Poisson noise.*

uncertainty on the given $\langle D_L \rangle$ and no longer a systematic one: because of the use of a large number of clusters, this uncertainty should average out in the density computation.

In Fig. V.3 we plot cumulative and differential densities obtained for all the ACO clusters with $|b| \geq 30^o$ and those of richness class $R \geq 1$ (e.g. those with $N_g \geq 50$). For a completely homogeneous distribution we would expect an almost constant density up to a a certain depth, followed by a density decrease due to catalogue incompletness. From the plots of Fig. V.3 we can note instead that two features stand clearly out –see lower right panel of Fig. V.3 – from the

possible uncertainties due to binning and Poisson noise: there is a prominent overdensity situated at a distance of $\sim 175\ h^{-1}\,Mpc$ (the binwidth is $25\ h^{-1}\,Mpc$) and an underdensity at a distance of $\sim 260\ h^{-1}\,Mpc$. These features are particularly noteworthy because they show up in an angle-integrated distribution. Apart from these two features, we can see from the plots of cumulative density that a 'plateau' is present up to $\lesssim 400\ h^{-1}\,Mpc$ (see also the behaviour of differential distributions), a fact which roughly indicates the distance beyond which catalogue incompleteness becomes non-negligible.

We can also try to make quantitative comparisons with the already mentioned results from the Abell's catalogue. However we have to bear in mind that, although in principle the method of compilation is almost the same for both ACO and Abell's catalogue, the differences in original plates, and especially the fact that we are using here estimated distances while the result for Abell's is based on measured redshifts, could have non-negligible effects on this comparison. Last, but not least, there is the theoretical prejudice that the distribution of rich clusters of galaxies should be the same in both the northern and southern galactic emispheres (cf. Tully's arguments (1987, 1988)). We indeed find a density of rich ($R \geq 1$) clusters with $|b| \geq 30^o$ and within $D = 400\ h^{-1}\,Mpc$, which is higher by $\sim 1/4$ than the one quoted by Bahcall and Soneira (1983): their value for the density is $n \cong 6 \cdot 10^{-6}\, h^3 Mpc^{-3}$, while we find $n \cong (7.5 \pm 0.4) \cdot 10^{-6}\, h^3 Mpc^{-3}$. Such a discrepancy initially puzzled us very much. After various checks, though, we noted that part of this difference is due to the already noted 'nearby' high peak in the density distribution, for distances $150 \lesssim D \lesssim 200\, h^{-1}\,Mpc$.

Indeed, if we neglect this huge overdensity and consider the density derived from clusters which have estimated distances in the range $200 \lesssim D \lesssim 400\, h^{-1}\,Mpc$, we find that $n \cong (6.8 \pm 0.4) \cdot 10^{-6}\, h^3 Mpc^{-3}$ which is a value in lesser disagreement with the value from Abell's, given the already mentioned differences, to which we add possible richness misclassifications due perhaps to distance errors and to the already noted problems due to the 'global' background correction. By close inspection of the plots of Fig. V.3 , one can in fact see that the cumulative density for clusters of $R \geq 1$ already has a slightly decreasing slope for $D \gtrsim 330\ h^{-1}\,Mpc$

(although the differential keeps fairly constant between 330 and 400 $h^{-1}\,Mpc$) while the cumulative density for clusters of $R \geq 0$ shows a much more marked transition from a constant to a decreasing slope. This behaviour could suggest that part of the clusters in that distance range are attributed to the richness class $R = 0$ instead of to $R \geq 1$ because of underestimates of the quantity N_g, causing the small difference in slopes. We would indeed expect the opposite behaviour in the absence of richness misclassifications (the completness distance range of $R \geq 1$ clusters should be greater than or at least equal to that of $R = 0$ clusters, because the former are more easily recognized and, having intrinsically brighter magnitudes –cf. the Scott effect– for the third and tenth brightest galaxy, can be selected further away).

Of course all the above estimates are preliminary in that definite comparison can be made only when redshifts are available. Still, at the moment, we can make another comparison which adds confidence to our present results. In their paper, concerned with the estimate of the angular two–point cluster–cluster correlation function $w(\theta)$, Bahcall *et al.* considered ACO clusters of richness $R \geq 1$ wich have galactic latitude $-90° \leq b \leq -45°$, and divided them into a nearby sample with estimated distance D within 300 $h^{-1}\,Mpc$, and a far sample with $300 \leq D \leq 600\ h^{-1}\,Mpc$. These authors find 89 and 456 clusters in the nearby and far sample respectively and only state that they used the tenth brightest galaxy magnitude for the distance estimates, deferring the details of such estimation to a future paper. For the same range in b and distances we find 95 clusters in the nearby sample (+7 % with respect to Bahcall *et al.*), and 461 in the far sample (+1 %), for a total of 556 within $D = 600\ h^{-1}\,Mpc$ (+2 % with respect to their 545). Apart from the discrepancy in the nearby sample, the overall agreement seems to be remarkable, given the lack of information on the characteristics of their procedure. The same authors say that they find two different decreasing trends in the ACO clusters distribution: one with galactic latitude and one with declination. Both are said to be well represented by cosecant laws, the one with the galactic latitude with a less steep exponent than the one found by Bahcall and Soneira for the Abell catalogue (0.2 instead of 0.3). We will leave the discussion of such points to future work

(Scaramella *et al.*, 1989) and just say that, with slightly different parameters for the distance estimator than those we present here which we used for the above and following results, we found a decrese with the galactic latitude which has a steeper slope than the one quoted by Bahcall *et al.*, and in agreement with the one derived from Bahcall and Soneira for Abell's catalogue.

We now pass on to give an outline of a 'percolation' algorithm that we developed in order to find candidate superclusters (SC's): these would be primary targets for the first redshift surveys of the ACO catalogue. Above we put the word percolation between quotes because of its frequent improper use that is in the astrophysical literature. In fact the meaning that astrophysicists usually attach to percolation is that of a 'friend of friends' algorithm, that is to identify 'chains' of clusters which have each member of the chain within a given distance, usually called 'percolation radius', of at least another member of the chain. This is done with the goal of identifying the most prominent features in the spatial distribution of the object under study.

As an example we can consider a one–dimensional case, some beads along a straight string. Assume we have four beads, say A, B, C, and D, and that these beads are respectively located in a given system of coordinates at positions 1, 1.5, 3, and 4. If we decide to consider chains which have percolation length 0.6, we will find only one chain, with A and B as members. For a percolation length of 1.2 there are two chains, one is still composed of A and B, the other of C and D. For percolation lenght of 1.5 or more, a single chain is present, which contains all the beads. This is quite different from the meaning of percolation in statistical physics, where the percolation length has a unique value, the value of a variable at which the physical system under study has a sudden transition in some of its properties (i.e. 'percolates'). Obviously a discussion of this point is irrelevant here: a nice, complete discussion can be found in Stauffer (1979). As we said in the first chapter, this latter interpretation, that is finding the percolation radius at which there forms a chain which connects the opposite sides of a cubic sample of galaxies without interruption, has been proposed as a possible way of discriminating among possible topologies of the galaxy distribution (see Shandarin and Zel'dovich, 1983),

but it does not seems to be very sensitive to differences in the galaxy distribution (see Bhavasar and Barrow, 1983, and Dekel and West, 1985).

In our opinion, as can be seen from the simple example above, one of the disadvantages of this type of approach is its intrinsic pairwise sensitivity: an object which belongs to a given chain, could have been ascribed to it even if just barely lies within the required distance (and the opposite situation could arise). This 'hard' behaviour can also lead to dramatic changes, if the included (or excluded) object happens to be in a such position as to bridgen a gap between two other chains: the result could be the formation (or destruction) of a much larger chain, made from the union of the other two. A possible remedy to this problem is that of having different descriptions derived from considering different values for the percolation length, so studying a sort of hierarchical development of the chains. We also note that, roughly speaking, smaller values for the percolation radius tend to select denser regions.

In the case of clusters of galaxies this method has been used by Bahcall and Soneira (1984) and by Batuski and Burns (1985).

The former authors mainly used the nearby, complete sample that they studied for the cluster–cluster correlation function. They gave a list of superclusters, and its 'evolution' as a function of the value, f, of the density contrast threshold for supercluster (SC) membership. The values that were considered for f spanned a wide range: $20 \leq f \leq 400$. The most interesting result from this work is the fact that the superclusters appear to be highly compact: the authors estimate that the fraction of the volume occupied by SC's in the examined sample is only ~ 3 % for $f = 20$ and ~ 0.3 % for $f = 100$ (this values refer, though, only to SC's composed of clusters with $R \geq 1$). Also, the larger SC's appear to have elongated structures.

Batuski and Burns (1985) extended this kind of work to a sample of Abell clusters composed of 652 members which had measured or *estimated* redshifts $z \lesssim 0.13$. Among these $\sim$ 50 % had measured redshift. These authors gave a list of *candidate* SC's with the main purpose of giving to observers primary targets for future detailed studies. The lists consists of candidate SC's because of

the problem that estimated distances results in a uncertain attribution of cluster membership to given complexes ('chains'). Batuski and Burns used a $\log cz - m_{10}$ relationship to estimate distances, with an uncertainty in the estimated redshifts of $\Delta z/z \cong 30$ %. Their procedure was the following: first a number of 'cores' of SC's candidates were selected through percolation with a value for the percolation radius of $R_p = 3000\, km\, s^{-1}$ (they actually quote $R_p = 40\, h^{-1}\, Mpc$ but use $H_0 = 75\, km\, s^{-1}\, Mpc^{-1}$: therefore we prefer to quote distances directly in $km\, s^{-1}$, taking $H_0 \equiv 1$) for the whole sample. Then they considered the uncertainty in the membership attribution by computing the likelihood of membership of those clusters previously selected as core members. This was a pairwise estimate of the mutual probability of being within distance R_p, that each core cluster has with the other core members. If the maximum among these probabilities was greater than 15 % the cluster was included in the list.

Analysis of the derived list shows the presence of elongated, non–spherical structures of sizes $7500 - 15000\, km\, s^{-1}$ and more spherical voids of similar dimensions. Comparisons made with a random sample constrained to have the same spatial two–point correlation function, derived by Bahcall and Soneira, showed the presence in the data of more structure (i.e. information) than that which could be described by the two–point correlation function alone. This is a quantitative conclusion based on the fact that the large–scale distribution today does not have (at least as described by the observed clusters) an isotropic Gaussian density distribution, even on typical clusters' scale-length. The same authors gave evidence for a filament of clusters which is $\sim 300\, h^{-1}\, Mpc$ across (Batuski and Burns, 1985).

The above mentioned procedure seems to have a potential problem, that is that of not including clusters which can have a non negligible probability of membership, but were not initially selected as core members, as would happen instead, for instance, if the smallest distance from a core member was initially $\gtrsim R_p$.

Having in mind finding a similar list of candidate SC's for the ACO catalogue,

we tried another kind of approach. The procedure is the following. We decided to make use of 100 simulated copies of the catalogue, in which the distance for each cluster without a measured redshift was estimated once for each catalogue by the method of Eq. (V.8) . We also built a percolation algorithm, based on the partition of the given catalogue into different equivalence classes (the equivalence relationship is of course that of having mutual distance smaller than the adopted percolation length, R_p). Then we ran this percolation algorithm on the reference catalogue (i.e. that for which $D_L = \langle D_L \rangle$), finding in this way some complexes with a list of memberships. Up to this point we used a procedure very similar to the selection of cores used by Batuski and Burns.

We then started a different procedure: we did not consider as interesting only those clusters initially selected by membership of the reference catalogue. We instead used the complexes found in the reference catalogue to mark 'interesting volumes': these are defined as those spheres of radius R_p centered on the positions of the complexes themselves. The position of a complex is taken to be the mean value of the positions of its members. We then checked in the 100 random catalogues all those complexes whose position fell into a given interesting volume, and kept track of which clusters belonged to these complexes, so as to finally get the number of times that a cluster was a member of whatever complex had a position which happened to be within the interesting volume.

With this procedure clusters which were not included in the complexes found in the reference catalogue have also the possibility of 'showing up' as candidate members, with a frequency that should be proportional to the probability of their 'true' membership.

Although the interesting volumes found in the reference catalogue refer to the complexes extracted from the most probable position of the clusters, these are not necessarily those of the most probable complexes. We then decided to also try using as starting interesting volumes the average of the union of those found in 5 different random catalogues, where two interesting volumes are considered joint if the distance between their positions is within R_p. However, we were faced

with the overwhelming number of possible complexes, given by all the possible different chains which can form when the clusters are moved around: formally a chain is no longer the same as soon it looses or gains a member ! It is this fact which suggested to us considering interesting volumes: we can expect that usually the position of a chain, being the average of its members, does not change very much unless the chain itself suffers very drastic changes like, for instance, being 'eaten' by a much larger one because of an intervening bridging cluster, or being broken apart into two separate pieces because the usual backbone cluster happens to be further away. In this latter case the situation has changed so much that, correctly, no complex is listed as belonging to the interesting volume for this particular random realization.

The procedures outlined above are of course not exact and involve a number of assumptions which are arbitrary (although these have been derived through much experimentation). On the other hand, at the moment, these procedures seem to be the best we can think of, regarding both the implementation time (it took several months of hard programming to develop and test the software described in these short paragraphs), and the fact that this problem has no intrinsic solution. Another point that we want to stress is that one should not, in the quest for improvement, lose contact with the original goal: the risk would be to get a list of candidate superclusters ready when the cluster redshifts had already been measured in the course of time, so that the list, based on estimated distances and probabilities, would have become useless !

At the moment we are still working on this issue, using different values of R_p , different richness thresholds for the sample, and different distances estimates, so that the actual figures of the complete list SC candidates (actually long, boring computer printouts) will be given elsewhere (Scaramella *et al.*, 1989). We want to discuss below, instead, a preliminary result of this analysis which could be of great importance for Cosmology. Before discussing this –for the present moment– exciting result, we must consider in some detail in the next section the general frame of the discussion, which is that of possible large-scale peculiar motions.

V.3 Large scale peculiar velocities.

One of the milestones of modern Cosmology was the discovery of the Hubble law: redshift $\propto$ recession velocity $\propto$ distance. As we saw in the previous section, in Friedmann models this relationship is no longer linear, but still holds conceptually, because the basic assumption of homogeneity results in the fact that fiducial observers follow geodesics which are orthogonal to equal time hypersurfaces, or, more directly, have null peculiar velocities (see discussion in the first section of Chap. II).

On the other hand, just by considering mass conservation, when an inhomogeneity develops this causes peculiar motions of the matter itself. This inevitably leads to Döppler effects, which reflect into the total amount of the observed redshift (actually for large peculiar velocities and/or no longer expanding regions this can lead to blueshifts, like that of M31). Therefore, because $1 + z_{obs} = (1 + z_{cosm})(1 + z_{pec})$, where $1 + z_{pec} \sim v/c$ for non–relativistic peculiar velocities (as is usually true for motions of galaxies and clusters with respect to their environment), one is led to attribute to such objects the wrong distance $d(z_{obs})$, instead of $d(z_{cosm})$. Of course, if the extent of such discrepancy is small this is not a problem, but there are serious issues related to this phenomenon.

We will discuss very briefly only some of these issues here, both because of their wide range of applications and the recent interest which has arisen around some of them. Indeed, the question of large–scale peculiar velocities (LSPV), on which we will concentrate henceforth, is completely unsettled at the present moment and there are many different conflicting ideas and experimental results on this important topic.

One of the key points of peculiar velocities is how to measure them: apart from obvious distortions in redshift plots (e.g. 'finger of God' effects or systematic differences in two-point correlation amplitudes between radial and projected separation components), one obviously needs a way of estimating distances which is independent of the measured redshift. There are two main techniques used at the moment, which try to estimate the intrinsic luminosity of a galaxy from measurable

quantities (the distance is then derived from the measured apparent magnitude). These are the Tully Fisher relationship, used to estimate the intrinsic luminosity of spiral galaxies from their rotation velocity, as measured by linewidths, and a recent update of the Faber–Jackson relationship used for elliptical galaxies. The latter relationship relates their intrinsic luminosity to the magnitude of the star dispersion velocity.

We now summarize the highlights of this problem. One of the aspects that makes the question of LSPV extremely interesting is that one could in principle measure the value of the cosmic mean density, i.e. the value of Ω_0 from it. In the linear density perturbation theory, in fact, one has that matter density contrasts grow self–similarly and, because the only potential in the game is the curl–free gravitational one, the peculiar velocity is always aligned along the direction of the peculiar acceleration. This latter vector, in turn, had the same direction that it has today and is directly related to (in principle) measurable overdensities. This is possible through the law of growth of linear density perturbation, which is also a function of Ω_0 . The basic formula (see Peebles, 1980) is:

$$\frac{\partial^2 \delta}{\partial t^2} + 2H(t)\frac{\partial \delta}{\partial t} = 4\pi G \langle \rho \rangle \delta , \qquad \text{(V.9)}$$

where $\delta \equiv \delta\rho/\langle\rho\rangle$ is the density contrast, $\langle\rho\rangle$ is the background mean density, and $H(t) = (d/dt)ln[a(t)]$ with $a(t)$ the expansion parameter ($a \propto (1+z)^{-1}$).

Now, Eq. (V.9) has a solution of the form $\delta(\mathbf{x},t) = A_1(\mathbf{x})f_1(t) + A_2(\mathbf{x})f_2(t)$, where the index 1 refers to the growing mode (at most a modest power law because of the cosmic expansion, different from the usual exponential growth of the classical Jean's instability), and the index 2 refers to the decaying mode. The latter mode can usually be neglected. For the matter dominated E.d.S. case one has simply $f_1(t) \propto t^{2/3} \propto (1+z)^{-1}$. The peculiar velocity $\mathbf{v_p}$ associated with the perturbation is given to a good approximation by

$$\mathbf{v}_p(\mathbf{x}) = \frac{2}{3} H_0^{-1} \Omega_0^{-0.4} \mathbf{g}_p(\mathbf{x}) , \qquad \text{(V.10)}$$

where $\mathbf{g}_p$ is the peculiar acceleration, computed through a volume integral of the

matter overdensity. Then one has

$$\mathrm{g}_p(\mathrm{x}) \;=\; G \int d^3r\; [\delta\rho(\mathrm{r})] \left(\frac{\mathrm{r}}{r^3}\right) \;=\; G\,\rho_c\,\Omega_0 \int d^3r\;\delta(\mathrm{r}) \left(\frac{\mathrm{r}}{r^3}\right) \qquad \text{(V.11)}$$

with, as usual, $\langle\rho\rangle \equiv \Omega_0\rho_c$. Substituting for the critical density value, $\rho_c \equiv 3H_0^2/(8\pi G)$, one finds the following relationship, often used in the literature:

$$\mathrm{v}_p \;=\; \frac{1}{3}\,\Omega_0^{0.6}\,H_0\,\mathbf{D}\,, \qquad \text{(V.12)}$$

where the peculiar velocity is expressed in terms of the *dipole of the whole matter density contrast*,

$$\mathbf{D} \;\equiv\; \frac{3}{4\pi} \int d^3r\;\delta(\mathrm{r}) \left(\frac{\mathrm{r}}{r^3}\right)\,, \qquad \text{(V.13)}$$

where the integral, formally extending to infinity (i.e. up to large scales, but less than the horizon scale–length because of the Newtonian approximation used in the above formulæ), should at least encompass a depth such as to guarantee its convergence to a definite value. This is a crucial point, as we will see in the discussion below.

In the highly idealized case of a single, isolated spherical perturbation of radius R, the ratio of the peculiar velocity at the edge of the spere to the unperturbed velocity, $v_H = H_0 R$, is then given by

$$\frac{v_p}{v_H} \;\cong\; -\frac{1}{3}\,\Omega_0^{0.6}\;\langle\delta\rangle\;\left[1+\frac{\langle\delta\rangle}{3}\right]^{-\frac{1}{2}}\,, \qquad \text{(V.14)}$$

where $\langle\delta\rangle$ is the average contrast whithin the sphere and a correction which takes into account mild non-linear regimes has been inserted (Yahil *et al.*, 1986).

The above equation has been widely applied to the Virgocentric infall in order to measure the value of Ω_0 (Davis *et al.*, 1980; see the review by Davis and Peebles, 1983). The answers given by this method in its application to the Virgo case have been recently criticized as inadequate, mainly because of difficulties in the estimating of $\langle\delta\rangle$ due to redshift distortions (see Kaiser, 1987). Indeed a great uncertainty in the values for Ω_0 derived through Eq. (V.14) has been shown in various N-body simulations, while of course the value for Ω_0 assumed in the

simulations is perfectly known (Bushouse *et al.*, 1985; Lee *et al.*, 1986; Melott, 1986).

However, Villumsen and Davis (1986) find in their detailed simulations that the local peculiar velocity tracks both direction and amplitude of the peculiar force extremely well. This happens also in presence of large asphericities in the flow field. These authors conclude that the agreement between peculiar velocity and acceleration vectors, expected in the linear regime, can be extended surprisingly well into the nonlinear perturbations of the developing overdensities, up to density contrasts of order $\langle\delta\rangle \sim 4$ (for such a value for $\langle\delta\rangle$ the alignment is still within $\sim 25^o$).

In the above picture, the observed dipole anisotropy of the cosmic microwave backgroud (CMB) plays a fundamental rôle: this anisotropy is widely believed to be extrinsic (see detailed discussion in Sect. II.1), a Döppler effect caused by a peculiar velocity of the Local Group (LG) of $v_{CMB}^{LG} \sim 600\, km\, sec^{-1}$ with respect to the CMB rest frame (the heliocentric velocity with respect to the CMB is $v/c \sim \Delta T_{dip}/T_{back} \sim 3\ mK/3\ K \sim 300\, km\, sec^{-1}$; to this must be added the sun rotation velocity within the galaxy and our galaxy velocity with respect to the LG barycenter).

As shown in the sketch of Fig. V.4 , one can test for the presence of LSPV as pioneered by Rubin *et al.* (1973, Rubin–Ford effect, although at that time the CMB dipole had not yet been measured). The basic idea is that of composition of velocity vectors: by measuring distances and redshifts (hence peculiar velocities) of a shell of galaxies these authors found that a sample of 96 distant spiral galaxies appeared to have a peculiar motion with respect to the LG (this would result in a peculiar velocity for the shell in CMB frame of $\sim 1000\, km\, sec^{-1}$). This result was regarded by most workers in the field as spurious and perhaps due to incorrect treatment of the Malmquist bias (Fall and Jones, 1976). So, when Hart and Davies (1982), applying the same analysis to a less distant sample of 84 galaxies, found that these were at rest with respect to the CMB frame, people generally assumed the lack of LSPV and a local (within a couple of tens of Mpc) origin for the LG

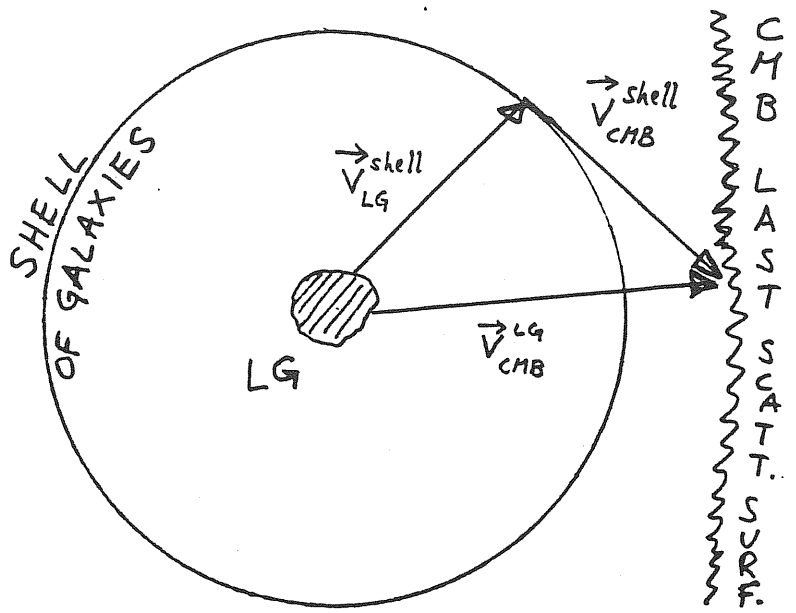

Figure V.4. *A sketch of the different velocity vectors discussed in the text. The peculiar velocity of a shell of galaxies is derived from the subtraction from the peculiar motion of the LG with respect to the CMB (as inferred by the microwave dipole),* v^{LG}_{CMB}*, of the relative velocity between the shell of galaxies and the LG itself,* v^{shell}_{LG}.

peculiar velocity. On the other hand, quantitative information on possible peculiar velocities is very useful in constraining cosmological models of formation of cosmic structure.

The impression of a very quiet universe was reinforced by the work of Aaronson *et al.* (1986), who, measuring Tully–Fisher velocity widths from Arecibo, showed a remarkable linearity in the Hubble flow for 10 distant clusters.

Up to this point, the only flow generally agreed upon was the Virgo infall, with Virgo assumed to be at rest (for brevity we shall drop henceforth the specification 'with respect to the CMB frame').

Then, things started to move and to change this 'idle' picture: Lilje *et al.* (1986) found evidence for a quadrupolar distortion in the Hubble flow in our surroundings, with the major axis pointing towards the Hydra–Centaurus supercluster (SC). Meanwhile, Tamman and Sandage (1985), in their life–long quest for the H_0 value (to measure which one needs accurate intrinsic distance estimates), found that a possible explanation for the LG peculiar velocity was

the following picture: the LG was feeling heavily the gravitational pull from the nearby Virgo cluster, but both were falling towards the Hydra–Centaurus SC, the latter being at rest.

This new picture already involved quite a lot of peculiar motions on large scales (our distance from the Hy–Cen SC is $\sim 3000\, km\, sec^{-1}$).

Just after these arguments appeared in the literature, the whole question of LSPV literally blew off, even reaching newspapers' front pages: at a meeting in Hawaii there appeared the first of several products from a wide collaboration (Burstein *et al.*, 1986), in which, by studying elliptical galaxies, a peculiar, coherent bulk flow of velocity $600 \pm 100\, km\, sec^{-1}$ was reported within a region of $\sim 6000\, km\, sec^{-1}$ (i.e., as early stated, a region of size $\sim 12000\, km\, sec^{-1}$ shared such a flow). The data showed that Hy–Cen SC was also moving and was not at rest as assumed by Sandage and Tamman (think of the amount of gravitational force involved: a SC is not exactly a pebble !).

Contemporarily, an independent confirmation of the existence of LSPC came from Collins *et al.* (1986), who studied throughly 45 of the original 96 spirals observed by Rubin *et al.* and confirmed the presence of LSPV of order $\sim 1000 \pm 300\, km\, sec^{-1}$.

The importance of these results for cosmological models was first considered by Vittorio *et al.* (1986), who pointed out the inconsistency between the usual cosmological models (e.g. CDM, HDM, and alike), the amplitude of the reported bulk flow, and its misalignment angle with respect to the CMB dipole.

The collaboration who studied the sample of ellipticals, for short the 'seven Samurai' (7S) as they have been nicknamed, produced several papers during a short time span, in which they reflected step by step different stages of their understanding of the same set of data. We will briefly sum up some of the heightlights of these papers (Dressler *et al.*, 1987; Dressler *et al.*, 1987; Lynden–Bell, 1986; Lynden–Bell *et al.*, 1986; the original set of data was enlarged and discussed by Faber and Burstein, 1988).

As noted above, the key point is to derive precise, redshift independent distance estimates: to be able to detect peculiar velocities of $\sim 600\,km\,sec^{-1}$ over distances of $\sim 6000\,km\,sec^{-1}$ requires uncertainties as small as 10 %. This explains in part the *large* uncertainties (resulting sometimes even in skepticism) in the observational results.

The 7S results are based on a new relationship used to estimate intrinsic distances for elliptical galaxies. Previously the Faber–Jackson empirical relationship was used, which connects the intrinsic luminosity of an elliptical galaxy to the central dispersion velocity of its stars: $L \propto \sigma^n$, where usually $3 < n \lesssim 4$. This relationship makes use of only two out of the three main quantities (i.e. luminosity, size, and velocity dispersion) of the galaxy and had a large scatter giving large uncertainties in distance estimates, > 40 % for a single galaxy (on the contrary the infrared Tully–Fisher can reach uncertainties of the order $\lesssim 30$ %).

The improvement came by considering a new relationship, $\sigma^{4/3} \propto D_n$, with D_n a given isophotal diameter. This new relationship yields only a $\lesssim 25$ % rms distance uncertainty for the given galaxy. Because of the well known fact that bright ellipticals lie preferentially in clusters of galaxies, such kinds of measures of several ellipticals, under the assumption that those belonging to a nearby cluster are at the same distance, gave a final uncertainty of only $\lesssim 10$ % on *relative* distances between nearby rich clusters (if these had have been uncertainties in absolute distances, one would have had a similar uncertainty in the numerical value for H_0).

This great improvement comes from the fact that the measurable quantity D_n is of course a function of the luminosity/area ratio of the galaxy, and that the elliptical galaxies are well fitted by the de Vaucoleurs' law for the surface brightness profile, $\mu = \mu_0 \exp[-(r/r_e)^{1/4}]$. This leads to a final relation of the form $L \propto \sigma^{8/3}\,\Sigma_e^{-3/5}$, where Σ_e is the integrated surface brightness within the half-light diameter, A_e ($\Sigma_e \equiv B_T + 5\log A_e$ with B_T total magnitude), and use has been made of the relationships $D_n \propto A_e\,\Sigma_e^{4/5}$ and $\Sigma_e = 2L/(\pi A_e^2)$.

The 7S obtained in this way very detailed and almost reliable information on

the 3-D peculiar velocity field within a distance of $\sim 6000\,km\,sec^{-1}$ (some argue that the whole effect could be entirely due to intrinsic differences, for different clusters, in the zero point of the callibrating relationship $\log D_n - \sigma$). The first interpretation was, as said above, that of a bulk flow, and the apparent disagreement with the previous finding of Aaronson *et al.* that clusters were at rest, was argued not to be significant because this latter sample has a very limited sky coverage (such deep observations can be taken only from Arecibo). The flow direction happens to be orthogonal to the 'disk' defined by the clusters observed by Aaronson *et al.* and therefore was not expected to show up in that data.

Then, with a new analysis, the 7S found in the elliptical data that the clusters in the furthest shell of the sphere encompassing their sample appeared to be at rest (i.e. with an unperturbed Hubble flow), while the velocity field of the innermost clusters showed a shear and a convergence towards the direction of the Centaurus cluster. The 7S found that the data were best fitted by a model of general infall towards a single, *unseen* very large spherical mass, nicknamed the "Great Attractor" (GA). The model required the mass of this *single* overdensity to be enormous, $\sim 5 \cdot 10^{16} M_{\odot}$, and this had to lie at very low galactic latitude, in an almost unsurveyed region. The distance of this putative mass, $D_{GA} \sim 4500\,km\,sec^{-1}$, seemed to be consistent with a peak in the radial galaxy density obtained in a sparse redshift survey of the Centaurus region by da Costa *et al.* (1986).

After a short while, Dressler (1988), one of the 7S, published data relative to a low latitude galaxy survey he just made in the same direction, at very low galactic latitudes, and found two peaks in the galaxy number distribution, one at $\sim 3000\,km\,sec^{-1}$, the other at $\sim 4500\,km\,sec^{-1}$. The second one is located at almost the distance predicted by the GA model. He then argued that this overdensity is likely to be the GA itself, and that, through the use of Eq. (V.14) with the assumption $\langle \delta \rangle = \langle [\delta N / \langle N \rangle] \rangle |_{obs}$ (i.e. galaxies trace the mass distribution, no bias is present), the peculiar velocity observed in the sample of ellipticals, which is a LG peculiar velocity component of $\sim 500 \pm 100\,km\,sec^{-1}$ roughly towards Centaurus (more precisely a direction within ten degrees from $\ell \approx 310^{o}$ and $b \approx 10^{o}$), could be accounted for with a low value of the cosmic density: $\Omega_0 \sim 0.1 - 0.2$. We note

also that Lucey *et al.* (1986), had already found that galaxies observed in the Centaurus cluster area formed two clumps, the one at $\sim 3000\, km\, sec^{-1}$ being the proper Centaurus cluster.

There are however two very serious problems with the above conclusions. One problem, as also noted by Dressler himself, is that of the validity of the application of Eq. (V.14) : as discussed above, the assumption of being on the edge of a spherical overdensity embedded in an otherwise perfectly homogeneous universe is likely to be a gross oversemplification of the physical reality under examination. Indeed, the data of 7S show a very complex pattern of peculiar velocities.

The other problem is the estimate for the mean overdensity, $\langle\delta\rangle$. First, only a cone of space is surveyed, and not a volume such as to encompass this entire sphere, so that one has to extrapolate the observed value of the galaxy number contrast to a larger, unsurveyed volume. Second, the estimate of the overdensity is obtained through a rescaling of the result to those from a different survey which covered a larger volume, in order to estimate the biases of the sample used (e.g. to get a reliable estimate for $\langle N\rangle$). This procedure is very coarse, as it is the determination of normalization by rescaling to the overdensity estimated for the Local Supercluster (LSC) through direct comparison of the required peculiar velocity with that estimated for the Virgo infall. As noted (and criticized) by Gunn (1988), the value assumed for the amplitude of the Virgo infall (i.e. $v \sim 250\, km\, sec^{-1}$) is an 'old' value and is inconsistent with the very same picture of the GA. In this scheme, in fact, Virgo is also moving and the LG estimated infall is reduced by a factor of two with respect to the one adopted by Dressler.

Another worry (for us) is the lack of any notable clumpiness in the Dressler data: the overdensity claimed to be the GA is quite smooth and does not contain any rich cluster of galaxies. This fact leads Dressler to speculate about a common yet largely undiscovered class of superclusters (with a size of $\sim \mathcal{O}(50\, h^{-1}\, Mpc)$, and a mass very comparable to a few tens of rich clusters), in which subclustering has been totally ineffective. In our opinion this is in principle not impossible, but

certainly completely novel and difficult to implement with reliably known physical laws.

Utilizing the combined samples of elliptical galaxies used so far, and data coming from other spiral samples (mainly Aaronson *et al.*'s), Faber and Burstein (1988, Burstein, 1988; henceforth FB) fitted a slightly different model, in which the GA is no longer a simple spherical overdensity, but has a pronounced core. This model changes the simple $\sim 1/r$ profile for peculiar velocity amplitudes to a more complicated pattern, almost a 'cylindrical flow'. Also the direction of the peculiar velocity at the LG is raised a bit in galactic latitude ($b \approx 10^o \rightarrow b \approx 20^o$).

FB also discussed a phenomenon dubbed the 'local anomaly'. This refers to –a totally unexpected fact within the picture– which one could call a peculiarity with a possible explanation: there seems to be no distortion of the Hubble flow within a region of $\sim 700\, km\, sec^{-1}$ centered on the LG (for another discussion of this effect and its bearing on the determination of the H_0 value, see Tully, 1988). This means that locally we have no peculiar velocities with respect to the LG, while in general there is a lot of complex streaming. FB argue, on the other hand, that we are within one of several different 'patches' that their data show to have very little internal velocity dispersion within themselves. These patches, however, have large relative peculiar velocities and give rise to the observed complex velocity field. In particular, the smooth flow in the local anomaly would be due to the combined effect of the 'push' from a local void and the 'pull' from a nearby overdensity, which conspire to balance very well the gradient in the velocity field expected from the GA model. Bertschinger and Juskiewicz (1988) recently studied the cylindrical inflow model and found that is very unlikely to happen within the usual models. On the contrary, Kaiser (1987) questioned the effective depth probed by the original sample of the 7S and concluded that the CDM model could not be ruled out from the data.

Further evidence for LSPV has also been recently advocated by James *et al.* (1987). These authors study a sample composed of first-ranked cluster ellipticals, and find from the components of peculiar velocities along the direction of the CMB

dipole a large peculiar flow with amplitude of $\sim 600\, km\, sec^{-1}$. However, Lucey and Carter (1988) find that the hypothesis that the very same sample is at rest cannot be preferred over that of its non zero peculiar motion.

We now pass to illustrate another recent aspect of this area of LSPV: that of local dipoles.

The basic philosophy is quite simple: one computes the dipole in the distribution of some kind of tracers, as in Eq. (V.13) . Then, if the direction of the computed dipole is in good agreement with the direction observed for the CMB dipole, one assumes one has reached the zone of convergence of the peculiar acceleration. So one can use the amplitude of the computed dipole in Eq. (V.12) and read off the value of Ω_0 .

In the simple procedure just outlined, however, there are at least two crucial assumptions that have to be made. These are: i) the assumption that the peculiar acceleration has converged within the effective depth of the studied sample, and ii) the assumption that the distribution of the examined tracers can be somehow well related to the real mass distribution. Three other major dificulties are: a) the estimating of the sample effective depth, necessary to obtain the quantity v_H to be used in Eq. (V.12) , b) the large and uniform sky coverage required to derive a reliable dipole, and c) the actual computation of the dipole itself.

Up to the present time two different kind of tracers have been studied according to the above procedure, that is the distribution of galaxies selected according to their infrared distribution from the IRAS all-sky survey, and that obtained from the merging of different optical galaxy catalogues.

We want to sketch now the main results that have emerged in the past two years from the IRAS data and we stress the fact that the different outputs and different conclusions given initially by different experts in this field, have been obtained starting from *the same original database*. The differences arise only from different methods followed in this very difficult analysis, and can contemporarily give a feeling for the reliability of the final conclusions.

Initially very few of the IRAS galaxies had measured redshifts, but the situation is now improving fast, so that point a) is likely to soon no longer be a difficulty for IRAS. The same comment applies in the case of having a reliable evaluation of the IRAS galaxy infrared luminosity function, which is of relevance to point c).

The first papers on this topic which appeared in a very short sequence were those of Yahil *et al.* (1986) and Meiksin and Davis (1986).

Both groups followed the above outlined procedure, but their final estimates for the value of Ω_0 were different by almost a factor of two ! ($\Omega_0 \cong 1$ and $\Omega_0 \cong 1/2$, respectively, with misalignments IRAS dipole–CMB dipole of $\sim 30^o$). The difference probably arose from different estimates for the effective depth of the sample, derived through the computation of the IRAS galaxy angular two–point correlation function and use of the Limber equation, from different criteria for selecting galaxies among IRAS sources (misclassification with stars and galactic clouds are possible), and from different treatment of sky areas which were unsurveyed or excluded because of contamination.

Other subsequent studies of the IRAS dipole are those of Harmon *et al.* (1987), Villumsen and Strauss (1987), Kaiser and Lahav (1988), and Strauss and Davis (1988). We want to give here only few comments on the results from these papers. As noted above, for samples of IRAS galaxies which have no measured redshifts (after the identification of the optical counterpart) the sample effective depth is estimated through an infrared luminosity function, on which there has not been complete agreement. Even for the same sample and in the same paper, several different solutions for the amplitude and direction of the dipole have been listed. Differences arise from the treatment of unsurveyed areas (some authors extrapolate the signal to these areas, some fill them uniforimily) and from the possible weighting schemes used. The weighting is not a trivial issue at all because of the great range of infrared luminosities. This fact introduces also the problem of the relationship –if any– between the IR luminosity and the mass of a galaxy. Then there is also what is considered to be a major issue: how well do IRAS galaxies

trace the density inhomogeneities ? The weak point in the IRAS' results come from the fact IRAS galaxies do not 'see' clusters of galaxies. This is related to the fact that elliptical galaxies have little infrared emission and, as is well known, clusters of galaxies are mainly composed of early type galaxies. Now, while in high bias scenarios this would not be a problem, we find very disturbing the fact of not being able even to identify deep potential wells, easily recognizable in both optical and X–ray bands, given that one is just looking for important signatures of the gravity field. At the present, there is some tentative taking of this fact into account by 'boosting by hand' the weight given to regions which show prominent optical features (Strauss and Davis, 1988), but this is not regarded by some workers as the best way to obtain reliable results on this delicate issue. Many other difficulties have been pointed out and discussed in detail by Villumsen and Strauss (1987), who estimate a factor of two uncertainty in values of Ω_0 due to possible systematic errors.

The most recent paper on the IRAS galaxy distribution we know of at the moment, is that of Strauss and Davis, in which they give results from a sample of IRAS galaxies with measured redshifts. This allows a good determination of the depth of their sample, which extends up to $\sim 5000\, km\, sec^{-1}$. These authors compute the peculiar acceleration directly, and estimate the peculiar velocity at a point $\mathbf{r}_P$ as

$$\mathbf{v}_P = \frac{H_0 \Omega_0^{0.6}}{4\pi \langle n \rangle} \sum_i \frac{1}{\phi(r_i)} \frac{\mathbf{r}_i - \mathbf{r}_P}{|\mathbf{r}_i - \mathbf{r}_p|^3} , \qquad \text{(V.15)}$$

where ϕ is the selection function of the sample, and $\langle n \rangle$ is the mean galaxy density. Eq. (V.15) is obtained from Eq. (V.10) by considering $|\mathbf{g}_p| = G \sum_i m_i s_i^{-2} = G \langle m \rangle \sum_i s_i^{-2}$, and with $\Omega_0 \rho_c = \langle n \rangle \langle m \rangle$ and $s_i = |\mathbf{r}_i - \mathbf{r}_p|$. This is different from considering the dipole of an observed electromagnetic flux and then, under the usual assumption that the emitters trace the mass distribution well, equating it to the density contrast dipole –both gravitational force and observed luminosity decrease as the distance squared– of Eq. (V.13) , as was done for most other dipole studies. Strauss and Davis initially assign to each of the $\sim$ 2300 galaxies they examined, the position according to the measured redshift, then move the galaxy according to its estimated peculiar velocity, through the use of Eq. (V.15) .

By iteration they get a self-consistent distribution of the examined galaxies and hence a map of the peculiar velocity field. One obvious problem is that one should be able to extend the sum of Eq. (V.15) to large distances, while the sample has a limited spatial extension (this could cause possible problems for galaxies which are in the outer regions).

Strauss and Davis find that the peculiar acceleration computed with this method for the LG converges *within* a distance of $\sim 4000\,km\,sec^{-1}$, and that $v_p\,\Omega_0^{-0.6} \approx 500\,km\,sec^{-1}$. Hence they claim that their result is not consistent with the GA model because of the 'local' convergence of the peculiar acceleration. They find, however, an overdensity of $\delta N/N \sim 0.4$ in the sphere centered on the putative GA position. They also find a qualitative agreement for the peculiar velocity field as measured by the 7S, but the quantitative agreement seems to us to not be very encouraging (the linear correlation coefficient between peculiar velocities of given galaxies as predicted by this work and those measured, is $\lesssim 0.6$ for the 7S sample and ~ 0.25 for a sample of spirals studied by Rubin. Of course a perfect agreement would have given unit value). Moreover, Vittorio (1988) argued about the real achievement of convergence within the surveyed sample, while we simply note that in an open universe with $\Omega_0 = 0.2$, as suggested by most dynamical studies (see Peebles, 1986), the fraction of the peculiar velocity explained by IRAS galaxies within $\sim 5000\,km\,sec^{-1}$ would be less than half that observed by the 7S.

Related to the IRAS galaxies distribution, the existence of a galactic north–south anisotropy was also noted by Rowan-Robinson *et al.* (1986), who argued that this was due to non uniformities on scales $\sim 50 - 100\,h^{-1}\,Mpc$, and therefore of cosmological relevance. On the contrary, Clowes *et al.* (1988) argued from a sample with measured redshifts, that such an anisotropy exists but is of very local origin, at a median distance of $\sim 16\,h^{-1}\,Mpc$. This fact shows how observed disparities in IRAS fluxes reflect poorly into distance inhomogeneities.

Apart from IRAS galaxies, the other flux–computed dipole was obtained by Lahav (1987), who merged different optical catalogues to obtain a large sky coverage. He used ~ 15000 galaxies and obtained a dipole with a difference of $\sim 40^o$

from the CMB dipole and $\sim 10^o$ from the IRAS dipole (one of the earliest directions), and an amplitude such as to derive $\Omega_0 \sim 0.3$ from an estimated sample depth of $50\,h^{-1}\,Mpc$. The greatest problem with such an analysis was the great differences in the merged samples (ESO, UGC, MCG). A recent reanalisys of the optical data (Lahav *et al.*, 1988), using only two catalogues (ESO and UGC), finds a convergence of the dipole signal within $4000\,km\,sec^{-1}$. Now the direction agrees with that of the CMB dipole within 10^o, and the amplitude of the optical dipole is such as to give $\Omega_0 = 0.16 \pm 0.07$. In the same paper another analysis of the IRAS dipole is discussed, whose derived vector agrees with the CMB and the optical ones, but has an amplitude such as to give $\Omega_0 = 0.8 \pm 0.1$. Also this latter dipole seems to be due to clustering at distances within $4000\,km\,sec^{-1}$, in agreement with the results of Strauss and Davis, mentioned above. The only serious discrepancy between the optical and IRAS dipole seems to be the amplitude. This fact, however, could perhaps be explained, according to Lahav *et al.*, in a picture of strong bias for early–type galaxies, which shows up only in the optical, and a much milder bias for late–type ones. These authors consider also contributions to the optical dipole from different sky zones, and find that, for a velocity of the LG of $600\,km\,sec^{-1}$, the contribution to the velocity from a zone of radius 15^o centered on Centaurus cluster is $\sim 250\,km\,sec^{-1}$, while that due to Virgo cluster is $\sim 100\,km\,sec^{-1}$. They note that the ratio of these two velocities is the same as in the GA model, but the velocities here are a factor 2 smaller than those in the GA ($\sim 570\,km\,sec^{-1}$ and $\sim 250\,km\,sec^{-1}$ respectively).

We want to mention that an overdensity of quasar at low redshifts, $z \lesssim 0.5$, has also been claimed (Shaver, 1987). This overdensity in the number of quasars, $\delta \sim 1 - 2$, has an angular diameter of $\sim 30^o - 40^o$ and should have a size of $\sim 400\,h^{-1}\,Mpc$ at the distance of $\sim 800\,h^{-1}\,Mpc$.

As can be seen from the above summary, the situation is not clear at all, both from an observational and from a theoretical view (there are also very recent studies of velocity autocorrelations and derivations of complicated expressions for theoretical window functions which take into account the fact that only the peculiar radial velocities are measurable; see Szalay, 1988, Gorsky, 1988). Moreover, the

'bandwagon' effect makes it very hard to have a complete update of the evolution of the overall picture: ideas and results on this topic, have recently changed so fast that it has become essential to have quick access to preprints and this, unfortunately, is not always the case. Therefore we expect that most of what we have summarized above (i.e. that we are aware of in mid-October 1988) will change on a time-scale of a few months. On the other hand this is one of the peculiarities of an extremely rich and fast evolving field of research, so we do not complain at all !

V.4 A large concentration of clusters beyond Centaurus: can this be the origin of peculiar flows ?

We want to present in this section the most intriguing output we have obtained from a preliminary application of the methods and results discussed in the previous sections of this Chapter.

Recent results from a study Dressler *et al.* (1987) of the distances and velocities of 400 elliptical galaxies out to $\sim 6000\, km\, sec^{-1}$ have shown that the peculiar motions of these galaxies with respect to the Hubble expansion, are best fitted in the Cosmic Microwave Background (CMB) rest frame by a flow induced by a large mass (Lynden-Bell *et al.*, 1988), a Great Attractor of about $\sim 5.4 \cdot 10^{16}$ solar masses centered on $l = 307^o$, $b = 9^o$ at a distance of $R_m = 4350 \pm 350\, km\, sec^{-1}$. A redshift survey of about 900 galaxies in this direction (Dressler, 1988) shows that the excess in galaxy number counts in this area is due to a substantial concentration of galaxies with peaks at $v \sim 3000\, km\, sec^{-1}$ and $v \sim 4500\, km\, sec^{-1}$. In this section we show that in approximately the same direction there is also a unique, very rich concentration of clusters of galaxies which could have important dynamical effects. The estimated redshift distance of these clusters ranges from $v \sim 3000\, km\, sec^{-1}$ to $\sim 20000\, km\, sec^{-1}$, with a main complex at $v \sim 14000\ kms$. The barycenter of this concentration lies $\simeq 25^o$ away from the CMB dipole (Lubin and Villela, 1987) and $\simeq 10^o$ away from the latest reported position of the Great Attractor (Faber and Burstein, 1987, Burstein, 1988).

The analysis of the distribution of clusters of galaxies is of fundamental importance in understanding the matter distribution. Moreover, it is a powerful tool in explaining the origin of the observed peculiar velocity field (Collins *et al.*, 1987; Lynden-Bell *et al.* 1988), and in estimating both the local peculiar acceleration vector and the distance at which the Hubble flow becomes unperturbed (Aaronson *et al.*, 1985). Although their number is relatively small, the clusters, being peaks of the density field, might avoid the problems that some other all-sky density tracers (e.g. IRAS galaxies: Yahil *et al.*, 1987; Meiksin and Davis, 1987; Villumsen and Strauss, 1988; Harmon *et al.*, 1988;, Strauss and Davis, 1988) have in describing the large–scale density field.

To this end we have analyzed the southern part of the new Catalogue of Rich Clusters of Galaxies (Abell *et al.*, 1988; hereafter ACO), which lists 1638 clusters with $\delta \lesssim -17^{o}$. This catalogue lists *bona fide* redshifts for 145 clusters. Because of the absence of completeness in the sample of clusters with measured redshifts, it is obvious that, contrary to what has been done in the Northern Hemisphere (Bahcall and Soneira, 1984), it is not sufficient to use these few clusters with known velocities to map the large scale distribution of clusters in the Southern Hemisphere.

Therefore we have used 143 redshifts to estimate a linear relation between $\log[D_L(z)] + K(z)$ and the magnitude of the 10^{th} brightest member, including also a correction for the cluster richness (Scott effect). $D_L(z)$ is the luminosity distance assuming $q_0 = 1/2$ and $K(z)$ is the K-correction for E and S0 galaxies (Shanks *et al.*, 1984). We find that the relation has a dispersion $\sigma_{sample} \simeq 0.11$ in $\log[D_L(z)] + K(z)$, corresponding to $\Delta z/z \approx 0.25$ for small z. In deriving this relation two clusters have been excluded because their redshift appeared to be inconsistent (beyond three sigma's in the relationship) with the magnitude given in the catalogue. Hereafter comoving distances $d = D_L(z)/(1+z)$ will always be scaled by the value of $H_0 = 100\, km\, s^{-1} Mpc^{-1}$ and therefore quoted in $km\, s^{-1}$. For a detailed discussion of this relationship see Sect. V.2 .

We have proceeded then to a *preliminary* identification of candidate super-

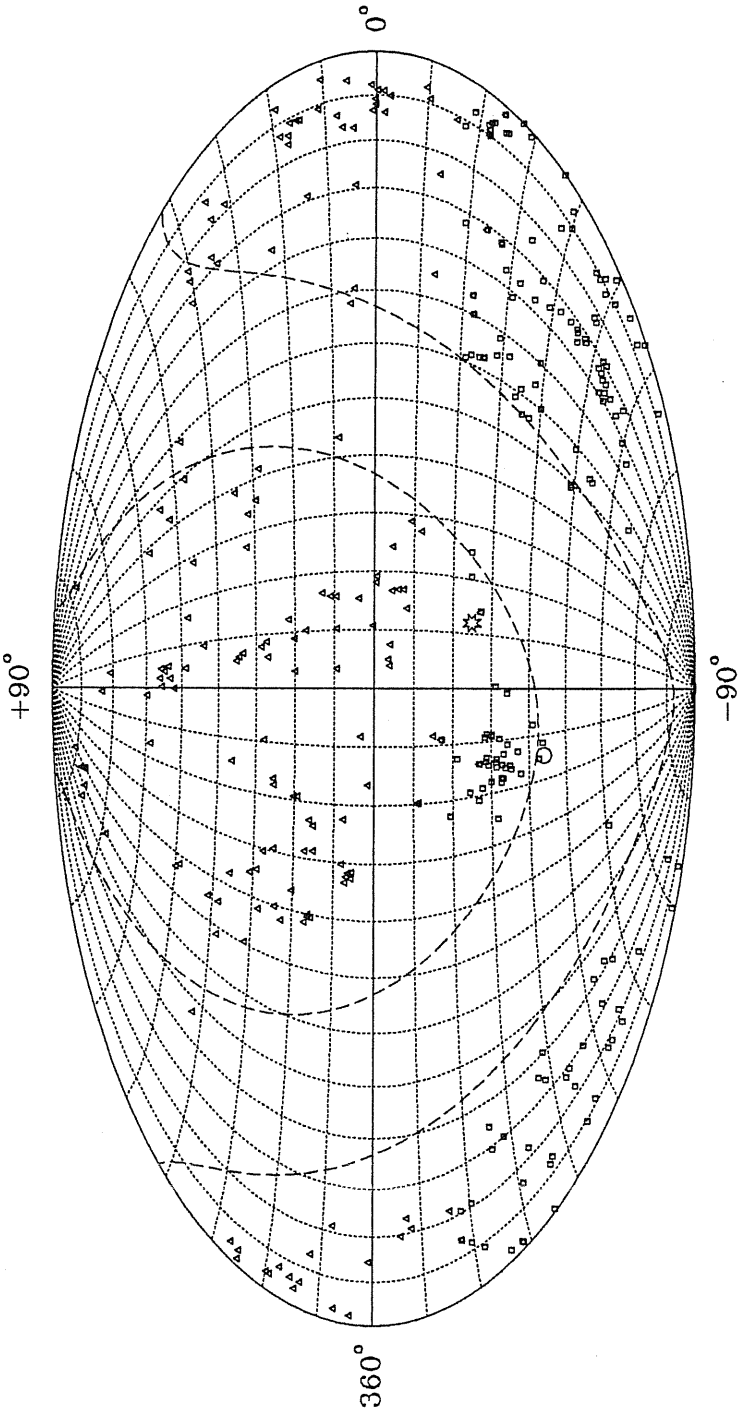

Figure V.5. *Equi-area projection in Right Ascension and Declination of all the rich clusters with measured or estimated distances within* $20000\,km\,sec^{-1}$. *Triangles and squares represent Abell and ACO clusters respectively (some clusters are listed in both catalogues). The star shows the direction of the cosmic microwave dipole and the empty circle shows the latest direction of the Great Attractor. Close to the latter is clearly visible the cluster concentration discussed in the text. Dashed lines indicate the avoidance zone due to our galaxy plane* ($|b| \leq 20°$).

clusters through a percolation algorithm on the reference catalogue, that is the catalogue with distances $d = \langle d \rangle$, where the average is derived from a Gaussian distribution in $\log[D_L(z)] + K(z)$ with variance σ^2_{sample}. The statistical robustness of these structures has been later verified on 100 random catalogues in which the estimated redshift for each cluster was drawn according to the previous distribution. (see see Sect. V.2).

A detailed description of the z estimates and of the supercluster candidates from the ACO catalogue, as well as of their robustness, membership *etc.* will be given elsewhere(Scaramella *et al.*, 1988). Of course, because of the uncertainty in our distance estimates, some numerical details in the following discussion may change slightly after observed redshifts become available.

In this section we discuss the existence (Vettolani *et al.*, 1988) of a remarkable concentration of clusters in the direction of Centaurus. This concentration (28 clusters within an area of about 0.1 steradian) is clearly evident in Fig. V.5 . This figure shows an all sky projection of all the ACO and Abell clusters with a measured or estimated distance smaller than $20000\, km\, sec^{-1}$. A distance cut at $20000\, km\, sec^{-1}$ causes little loss of information due to the incompleteness in the original catalogues and to the errors introduced by the redshift estimates, both in the northern (Bahcall and Soneira, 1984) and in the southern (Scaramella *et al.*, 1989 see Sect. V.2) hemispheres. This concentration, in a volume of $\simeq 2.7 \cdot 10^{11}\, (km\, s^{-1})^3$, corresponds to a cluster density which is a factor ≈ 10 higher than the estimated mean volume density of all the other ACO clusters with $\langle d \rangle \leq 25000\, km\, s^{-1}$ and at comparable galactic latitude.

The complex formed by the clusters denoted by among those listed *'a'*, is noteworthy and will be very interesting for future, detailed studies of supercluster dynamics. This candidate supercluster consists in fact of a number of members similar to that of the Corona Borealis supercluster (Postman *et al.*, 1988), but has the advantage of being almost a factor 2 closer and a factor 2 denser in clusters with richness $R \geq 1$ than the Corona Borealis.

We now discuss the relevance of the listed clusters to the large scale peculiar

Table V.3

I.D.#	α	δ	$\langle d \rangle$	N^{gal}
1736	201.07	−26.90	10225	104
3526	191.53	−41.03	3271	33
3528	192.90	−28.75	15922	70
3530	193.23	−30.08	13494	34
3532	193.65	−30.10	14892	36
3535	193.77	−28.22	16902	30
3537	194.57	−32.17	4945	35
3542	196.48	−34.30	17108	45
3553[a]	199.10	−36.92	15141	36
3554	199.18	−33.22	17220	59
3555	199.50	−28.72	17645	61
3556	200.33	−31.40	16916	49
3557	200.53	−28.62	16628	36
3558[a]	201.27	−31.23	13948	226
3559[a]	201.78	−29.27	13641	141
3560[a]	202.25	−32.97	12349	184
3562[a]	202.67	−31.42	14422	129
3564[a]	202.88	−34.97	12406	53
3565	203.45	−33.72	3241	64
3566[a]	204.02	−35.30	15361	100
3570	205.98	−37.67	10851	31
3571[a]	206.15	−32.62	15259	126
3572[a]	206.32	−33.13	12992	49
3574	206.57	−30.05	4183	31
3575[a]	207.43	−32.63	13597	49
3577[a]	207.88	−27.60	15152	103
3578	208.67	−24.48	9969	52
3581	211.15	−26.78	11931	42

Table V.3. *Clusters within the region delimited by* $190^o \lesssim \alpha \lesssim 212^o$, *and* $-41^o \lesssim \delta \lesssim -25^o$, *with a mean comoving distance* $\langle d \rangle \leq 20000\ km\, s^{-1}$. *Clusters with I.D.# in boldface have redshifts listed in the ACO catalogue. Clusters denoted with the letter 'a' tentatively belong to the main complex cited in the text (value of the percolation radius* $R = 1500\, km\, sec^{-1}$*).*

motions. Being wary of the use of the spherical infall model, in order to estimate the effects due to this region, we have computed the acceleration g induced on the Local Group by the clusters listed in Table V.3 as:

$$\mathrm{g} = G \sum_i \frac{M_i}{r_i^2} \hat{r}_i \,, \tag{V.16}$$

where the mass of each cluster

$$M_i \equiv M_{(R=2)} \left(\frac{N_i^{gal}}{106} \right) \qquad \text{(V.17)}$$

is weighted by the number of galaxies in the cluster, N_i^{gal}, and is expressed in terms of the typical values of an $R = 2$ Abell cluster (*e.g.* Coma, for which $N_i^{gal} = 106$); we also assume pure Hubble flow for the proper distance, $r_i = d_i H_0/(1+z)$, and obviously this can introduce systematic errors because of the presence of coherent peculiar flows.

About 50% of the total computed acceleration is due to the nearest chain of 4 clusters ($\langle d \rangle \simeq 4000\ km\, s^{-1}$, consistent with the quoted distance of the Great Attractor) and the remaining 50% is due to the combined pull by the more distant complexes, which are dominated by the one at $\langle d \rangle \approx 14000\ km\, s^{-1}$ (eleven clusters denoted by '*a*' in Table V.3). This fact could help in explaining part of the 'large' peculiar velocity of Centaurus cluster (Burstein, 1988) and is consistent with the present lack of detection (Lynden-Bell *et al.*, 1988) of a reversed sign for the peculiar flow beyond 4500 kms^{-1}. From 1000 simulations, in which the estimated redshifts of the clusters were randomized around their nominal value, we see that the standard error of the modulus of g is $\lesssim 5$ %, while the direction is always within one degree from $\alpha \simeq 201^o$ and $\delta \simeq -33^o$. This direction is in excellent agreement with one ($\alpha = 200^o, \delta = -33^o$) of the two possible directions for the Supergalactic Center (Lynden-Bell *et al.*, 1988) It is also close to a previously reported quadrupolar distortion of the peculiar flow (Lilje *et al.*, 1986), while most of the optical dipole signal is due to a patch of sky also centered on the same zone (Lahav *et al.*, 1988). Indeed, although the close agreement of the latter dipole with that of the CMB favours a 'local' (e.g. within $\sim 4000\ km\, s^{-1}$) convergence of the peculiar acceleration, its contribution to the infall towards Centaurus (Lahav *et al.*, 1988), $v_p^{dip} \sim 250\ km\, s^{-1}$, seems to account for only half of the observed one, again in good agreement with our above estimate.

The peculiar acceleration $\mathbf{g_p}$ is then obtained by subtraction from g of the acceleration expected from the mean density of clusters in the same volume. Using the relation (Peebles, 1980) $\mathbf{v}_p = \frac{2}{3} H_0^{-1}\, \Omega_0^{-0.4}\, \mathbf{g}_p$ and requiring that the compo-

nent of our peculiar velocity, $v_p \simeq 570\ km\,s^{-1}$, toward this direction is entirely due to the $\vec{g}_p$ derived above, we have:

$$M_{(R=2)} \approx 5\,M_{15}\,h^{-1}\left(\frac{\Omega_0}{0.2}\right)^{0.4}\left(\frac{v_p}{570\,km\,s^{-1}}\right), \qquad \text{(V.18)}$$

where $M_{15} \equiv 10^{15}\,M_\odot$.

The above relation shows that in an open universe it would be possible to ascribe the required peculiar velocity to the *observed* clusters if the mass overdensity related to an $R = 2$ cluster were $\sim 5\,M_{15}$. Recent estimates (Merritt, 1987) of the mass of the Coma cluster give $M_{Coma} \lesssim 3\,M_{15}$. The value of the masses we require is undoubtedly high. But it can be lowered if the overdensity of clusters reported here extends into the avoidance region. Moreover, the required mass is not simply the mass confined within the Abell radius, but can be associated with larger galaxy aggregates in which the clusters are imbedded as suggested by the galaxy–cluster cross–correlation (Seldner and Peebles, 1977), Similarly, if we divide the mass estimates (Postman *et al.*, 1988) for the Corona Borealis Supercluster, $M_{SC} \simeq 26M_{15}$, by the number of members ($N_{cl} = 6$) and weighted as above by the number of galaxies (Struble and Rood, 1987) we obtain $M_{(R=2)} \simeq 6.6\,M_{15}$, which is in good agreement with the value derived from Eq. (V.18) . Of course, this is not the end of the story because a biased distribution of matter would not be consistent with our assumption of clusters as tracers of the mass distribution, although recent estimates (Kaiser and Lahav, 1988) seem to indicate a global biasing factor which is not very far from unity.

A value of $\Omega_0 = 1$ could still be made consistent with the constraints found from Eq. (V.18) , either by boosting up the estimate for $M_{(R=2)}$ or, more realistically, by not requiring that the peculiar velocity be entirely due to a 'forward' gravitational pull. Underdensities and other great, comparable aggregates (e.g. Perseus–Pisces, or another new candidate supercluster similar to the one we present here but at larger distance) could have a relevant dynamical rôle.

Before definite conclusions can be drawn one obviously needs the most complete possible picture of our surroundings given by all of the available tracers.

Ultimately such an effort can also be rich in information on the physics of the tracers themselves. Indeed it would be of great interest to determine if clusters of galaxies are responsible for the overall dynamics or, more unlikely, if we are led to assess the existence of very large mass condensations ($M_{GA} \cong 54\, M_{15}$) in which no very rich clusters are seen (Dressler, 1988). This implies the existence of a physical process which would have coherently prevented cluster formation on scales of $50 - 100\, h^{-1}\, Mpc$.

In summary a detailed study of this region is of great importance, not only because no similar *nearby* concentration of clusters exists over the rest of the sky, but also because of its direction. It is hard to interpret as a mere coincidence the fact that such a concentration of clusters of galaxies is so close on the sky to both the direction of the CMB dipole and that derived from the peculiar motions of galaxies with respect to the Hubble flow.

Further studies of clusters in this area based on intrinsic distance estimates (Dressler *et al.*, 1987b) should eventually find the distance at which the peculiar flow reverses its sign thus delineating the region within which the bottom of a great potential well lies (assuming that this is the major cause of the reported peculiar velocities; Starobinsky, 1988). The concentration '*a*', discussed here, appears to be the best candidate for the bottom of such a well because of both the number of clusters present and their particular richness.

V.5 Brief summary of the chapter.

In this chapter we have discussed some aspects of the large–scale structure which refer to the present (in a cosmological sense) epoch.

We mainly examined the important topics of the largest known aggregates in the Universe, the Superclusters, and of very recent developments in their large scale kinematics and dynamics. We showed the preliminary results of an analysis of distances and density estimates of the new ACO catalogue of rich clusters. Then we discussed a possible way to derive a list of candidate superclusters, making our

best effort to squeeze the maximum information from the present available data.

From this analysis we presented what we think will be a very wealthy source of cosmological information: the richest among nearby superclusters. This identification will allow in future very detailed studies of this complex, which should be able to determine its dynamical status and all the other relevant informations. Indeed, one of the most intriguing questions at the moment is if these aggregates are bound (or even already virialized) and what –if any– is the typical peculiar velocity of rich clusters of galaxies. The answers to such question are of enormous relevance for the dark matter problem for the possible cosmological scenarios (what kind of perturbation spectrum can give these structures ? is a hierarchical scenario still viable ?). In this context in fact Bahcall *et al.* (1985) suggested the presence of large peculiar motions among rich clusters, while Bahcall and Burgett (1986) proposed a possible spatial correlation among superclusters. The suggestion of strong inhomogeneities on very large scales has also been put forward by Tully (1986, 1987, 1988), who find that clusters of galaxies lie preferentially in the supergalactic plane or in planes parallel to it. Tully's suggestion is that there is structure on scales $\sim 0.1z$, that is on scales which, roughly speaking, are one tenth of the present causal horizon ! The importance for cosmology of gathering as much information as possible on the physics of the superclusters is obvious, and the closer they are, the better they can be studied.

Apart from being close and very rich, the supercluster that we have discovered is of extreme importance because of its striking position: its barycenter lies within a few degrees of the most recent determination of the peculiar velocity of the LG (almost within the error of the latter; see also Fig. V.5). Can this fact just be a coincidence ? We think that this is a possibility, but it is noteworthy that the agreement has been 'a priori'. This is so, because the direction of the LG velocity was independently determined without any knowledge of our finding and we, at the beginning, had no idea of where this cluster overdensity would be in the sky. We started to note this concentration among all the others we found, and to realize its possible significance to the peculiar velocity problem, only after having seen its reliability after many simulations. We then checked where this

concentration was and had quite a surprise.

Of course, the above arguments have no relevance at all on the scientific issue on whether this huge cluster overdensity has a great effect on the LG dynamics or not, and if the source of the acceleration is entirely local. But, whether our hypothesis is true or not, we will gain very valuable information in both cases, for the reasons discussed in the previous section.

Before ending this Chapter we want to give a very preliminary estimate for the answer to the obvious question: 'What is the effect of such a big overdensity on the CMB ?' Because the values we found are more likely in an open universe (e.g. $\Omega_0 = 0.2$), this aspect is particularly important (temperature fluctuations, for a given density contrast, usually scale inversely with Ω_0).

We therefore make the following argument, with the caution that, until redshift are known, the results have to be taken as indicative. From the values of Table V.3 , one sees that within within the specified boundaries there are 28 rich clusters, with an average value of $\langle N_g \rangle \simeq 72$. We would expect roughly 3 such clusters within the same volume at low galactic latitude, hence the overdensity is $\delta N_c \approx 25$. This translates (see Sect. V.4 for the notation) into a mass overdensity of

$$\begin{aligned} \delta M \; &\approx \delta N_c \, \frac{\langle N_g \rangle}{106} \, M_{(R=2)} \; \approx \; 17 \, M_{(R=2)} \; \approx \\ &\approx 1.7 \cdot 10^{17} \, M_\odot \, h^{-1} \, \Omega_0^{0.4} \left(\frac{v_p}{570 \, km \, s^{-1}} \right) , \end{aligned} \tag{V.19}$$

where we used the result of Eq. (V.18) . Now the mean mass expected within the same volume is $M_b \cong 8.5 \cdot 10^{16} \, M_\odot h^{-1} \Omega_0$, so we get for the mass density contrast the following value:

$$\frac{\delta M}{M_b} \; \approx \; 2 \, \Omega_0^{-0.6} \left(\frac{v_p}{570 \, km \, s^{-1}} \right) . \tag{V.20}$$

This value for the mass density contrast is almost in the linear regime, so we can tentatively apply the following simple estimates (we are aware, though, of its enormous value: three times the mass required from the GA model).

From the values given in Sect. II.1 (see Kaiser and Silk, 1986), we see that the present angular extent of the horizon length at $z_i \cong 10^3$ is $\Delta\theta_{hor} \lesssim 1^\circ$,

and that of the last surface scattering thickness is $\Delta\theta_{thick} \lesssim 7'\ \Omega_0^{1/2}$. A difficult quantity to assess is the typical size to attribute to the overdensity we consider, because of its shape. The cubic root of the region's volume would give a typical length of $\sim 65\, h^{-1}\, Mpc$, while the same volume corresponds to a sphere of radius $\sim 40\, h^{-1}\, Mpc$. On the other hand the region we are considering has a thin conical shape, with an half–opening angle of $\lesssim 10^o$. Therefore, also having in mind the pancake theory, one could argue that a smaller length, typical of the transverse size, would be more appropriate. If we consider the transverse size at the position of the *'a'* concentration, i.e. at a distance of $\sim 140\, h^{-1}\, Mpc$, we get $\approx 44\, h^{-1}\, Mpc$. We therefore will normalize the perturbation scale length to a value of $\lambda \approx 50\, h^{-1}\, Mpc$, bearing in mind the great uncertainty (~ 50 %) of this value. Such a scale on the last scattering surface subtends an angle of $\Delta\theta_\lambda \approx 30'\, \Omega_0 (\lambda / 50\, h^{-1}\, Mpc)$. We see that, because of $\Delta\theta_\lambda \gtrsim \Delta\theta_{thick}$, any perturbation in the temperature fluctuation is likely to be partially erased by photon diffusion. This is of course a crude statement. However, one can argue as follows that not necessarily any anisotropy should have already been seen because of such an overdensity. It is convenient to evaluate the density contrast at $z = z_i$,

$$\begin{aligned} \left(\frac{\delta M}{M}\right)_{z_i} &= \left[\frac{D(z_i)}{D(z=0)}\right] \left(\frac{\delta M}{M}\right)_{z=0} \cong \\ &\cong 1 \cdot 10^{-3}\, \kappa(\Omega_0) \left(\frac{\delta M}{M}\right)_{z=0} \cong 2 \cdot 10^{-3} \nu^{-1}\, \Omega_0^{-0.6}\, \kappa(\Omega_0)\,, \end{aligned} \tag{V.21}$$

where we used the growing solution for an universe with normalization for the case $\Omega_0 = 1$ ($\kappa(\Omega_0 = 1) = 1$, $\kappa(\Omega_0 = 0.2) \simeq 3$) (Peebles, 1980) and took explicitly in account that the fluctuation we are dealing with could easily be ν times higher than the mean rms density contrast at the same scale. Now, Kaiser and Silk give an expression for simple estimates of $\Delta T/T$ due to perturbations which have a scale comparable with the scale of the last scattering surface. From this we get

$$\frac{\Delta T}{T} \approx \frac{1}{30} \left(\frac{\delta M}{M}\right)_{z_i} \approx 1.5 \cdot 10^{-4}\ \nu^{-1}\, \Omega_0^{-0.6}\, \kappa(\Omega_0)\,. \tag{V.22}$$

In a flat universe ($\kappa = 1$) this level is smaller, even if $\nu = 1$, than the current upper limits on angular scales of a few arc seconds, which are a few in ten-thousandths (see Partridge, 1988). For an open universe the estimated level of temperature

anisotropy would be much higher, but this fluctuation is very likely to be well above the rms value (i.e. $\nu \gg 1$), so one could argue that there is no necessarily a violation of present upper limits. Also, because in the open case ΔL_{thick} increases its value, the damping by photon diffusion becomes more severe. We conclude here this very simple e crude argument, stressing again the uncertainties involved in the above estimates.

As a general conclusion, while we think that the the great mass overdensity here considered will not easily fit within the general picture (it is likely a downward revision of its value), we cannot resist speculating that, perhaps, we have entered into the phase of considering cosmological *'Giant Attractors'*...

... and then, what else ?

Part of the containts of this Chapter have been or will be submitted for publication, e.g. Sect. V.4 (Vettolani *et al.*, 1988;, and Scaramella *et al.*, 1988), and Sect. V.2 (Scaramella *et al.*, 1989), respectively.

References to Chapter V

Aaronson, M., Huchra, J., Mould, J., Schommer, R., and Cornell, M, 1986, *Astrophysical Journal* **302**, 536.

Abell, G.O., 1958, *Astrophysical Journal Supplement Series* **3**, 211.

Abell, G.O., 1975, in *"Stars and Stellar Systems IX,"*, Sndage, A *et al.* eds., UNiv. Chicago Press.

Abell, G.O., Corwin Jr., H.G., and Olowin, R.P, **ACO** catalogue, to be published.

Bahacall, N.A., 1977 *Annual Review of Astronomy & Astrophysics* **15**, 505.

Bahcall, N.A., 1986, *Astrophysical Journal (Letters)* **302**, L41.

Bahacall, N.A., 1988, *Annual Review of Astronomy & Astrophysics* **26**, in press.

Bahcall, N.A., and Soneira, R.M., 1982, *Astrophysical Journal* **262**, 419.

Bahcall, N.A., and Soneira, R.M., 1983, *Astrophysical Journal* **270**, 20.

Bahcall, N.A., and Soneira, R.M., 1984, *Astrophysical Journal* **277**, 27.

Bahcall, N.A., and Burgett, W.S., 1986, *Astrophysical Journal (Letters)* **300**, L35.

Bahcall, N.A., Soneira, R.M, and Burgett, W.S., 1986, *Astrophysical Journal* **311**, 15.

Bahcall, N.A., Batuski, D.J., and Olowin, R.P., 1988, *Astrophysical Journal (Letters)* **333**, L13.

Bardeen, J.M., Bond, J.R., Kaiser, N., and Szalay, A.S., 1986, *Astrophysical Journal* **304**, 15.

Batuski, D.J., and Burns, J.R., 1985, *Astronomical Journal* **90**, 1413.

Batuski, D.J., and Burns, J.R., 1985, *Astrophysical Journal* **299**, 5.

Bhavsar, S.O., and Barrow, J.D., 1983, *Monthly Notices of the Royal astronomical Society* **205**, 61p.

Bertschinger, E., and Juszkiewicz, R., 1988, preprint.

Burstein, D. 1988, in *Large Scale Structure and Motions in the Universe*, Mardirossian, F., *et al.*eds., D.Reidel Pub. Co.

Burstein, D., Davies, R.L., Dressler, A., Faber, S.A., Lynden–Bell, D.,Terlevich, R.J., and Wegner, G., 1986, in *"Galaxy Distances and Deviations from Universal Expansion"*, F.Madore and R.B.Tully (eds.), Reidel Pub. Co.

Bushouse, H., Melott, A.L., Centrella, J., and Gallagher, J.S., 1985, *Monthly No-*

tices of the Royal astronomical Society **217**, 7p.

Collins, C.A., Joseph, R.D, and Robertson, N.A., 1986 *Nature* **320**, 506.

Couchman, H.M.P., Mc Gill, C., and Olowin, O., 1988, CITA preprint.

da Costa, L.N., Nunes, M.A., Pellegrini, P.S., Willmer, C., Chincarini, G., and Cowan, J.J., 1986, *Astronomical Journal* **91**, 6.

Clowes, R.G., Savage, A., Wang, G., Leggett, S.K., Mc Gillvray, H.T., and Wolstencroft, R.D., 1988, preprint.

Davis, M., Tonry, J., Huchra, J., and Latham,D.W., 1980, *Astrophysical Journal (Letters)* **238**, L113.

Davis, M., and Peebles, P.J.E., 1980, *Annual Review of Astronomy & Astrophysics* **21**, 109.

Dekel, A., and West, M.J., 1985, *Astrophysical Journal* **288**, 411.

Dressler, A. 1988, *Astrophysical Journal* **329**, 519.

Dressler, A., Faber, S.A., Burstein, D., Davies, R.L., Lynden–Bell, D.,Terlevich, R.J., and Wegner, G., 1987, *Astrophysical Journal (Letters)* **313**, L37.

Dressler, A., Faber, S.A., Burstein, D., Davies, R.L., Lynden–Bell, D.,Terlevich, R.J., and Wegner, G., 1987, *Astrophysical Journal* **313**, 42.

Ellis, R.S., 1982, in *"The Origin and the Evolution of Galaxies,"*, Jones, B.T.J., Jones, J.E., Reidel Pub. Co.

Faber, S.M., and Burstein, D., 1988, *"Large Scale Motions in the Universe,"*, Proceedings of the Pontificial Academy of Science Study Week # 27, in press.

Fall, S.M., and Jones, B.T.J., 1976, *Nature* **262**, 457.

Geller, M.J., 1987, in *"The Large Scale Structure of the Universe"*, Saas–Fee course, in press.

Górski, K., 1988, *Astrophysical Journal (Letters)* **332**, L7.

Gunn, J.E., 1988, in *"ASP Workshop on the Distance Scale"*, Victoria, B.C., preprint.

Harmon, R.T., Lahav, O., and Meurs, E.J.A., 1987 *Monthly Notices of the Royal astronomical Society* **228**, 5p.

Hoessel, J.G., Gunn, J.E., and Thuan, T.X., 1980, *Astrophysical Journal* **241**, 486.

James, P.A., Joseph, R.D., and Collins, C.A., 1987, *Monthly Notices of the Royal astronomical Society* **229**, 53.

Kaiser, N., 1987, *Monthly Notices of the Royal astronomical Society* **227**, 1.

Kaiser, N., and Lahav, O., 1988, *"Large Scale Motions in the Universe,"*, Proceedings of the Pontificial Academy of Science Study Week # 27, in press.

Kylpin, A.A., Kopylov, A.I., 1983, *Soviet Astronomy (Letters)* **9**, L41.

Lahav, O., 1987, *Monthly Notices of the Royal astronomical Society* **225**, 213.

Lahav, O., Rowan–Robinson, M., and Lynden–Bell, D., 1988, preprint.

Lee, H., Hoffmann, Y., and Fctalas, C., 1986, *Astrophysical Journal (Letters)* **304**, L11.

Leir, A.A., and van der Bergh, S., 1977, Ap.J.Suppl. **34**, 381.

Lilje, P., Yahil, A., and Jones, B.T.J., 1986, *Astrophysical Journal* **307**, 91.

Liljie, P., and Efstathiou, G., 1988, *Monthly Notices of the Royal astronomical Society* **231**,, 635.

Lubin, P., and Villela, T., 1986, in *Galaxy Distances and Deviations from Universal Expansion*, Madore, B.F., and Tully, R.B., eds. D.Reidel Pub. Co.

Lucey, J.R., 1983, *Monthly Notices of the Royal astronomical Society* **204**, 33.

Lucey, J.R., Currie, M.J., and Dickens, R.J., 1986, *Monthly Notices of the Royal astronomical Society* **221**, 453.

Lucey, J.R., and Carter, D, 1988, *Monthly Notices of the Royal astronomical Society* **231**, 15p.

Lynden–Bell, D., 1986 *Quarterly Journal of the Royal astronomical Society* **27**, 319.

Lynden–Bell, D., Faber, S.M., Burstein, D., Davies, R.L., Dressler, A., Terlevich, R.J., and Wegner, G., 1988, *Astrophysical Journal* **326**, 19.

Meiksin, A., and Davis, M., 1986, *Astronomical Journal* **91**, 191.

Merritt, D., 1987, *Astrophysical Journal* **313**, 121.

Oort, J.H., 1983, *Annual Review of Astronomy & Astrophysics* **21**, 373.

Partridge, R.B., 1988, *Rep.Progr.Phys.* **51**, 647.

Peebles, P.J.E., 1980, *"The Large Scale Structure of the Universe,"*, Princeton Univ. Press.

Peebles, P.J.E., 1986, *Nature* **321**, 27.

Postman, M., Huchra, J.P., Geller, M.J., and Henry, J.P., 1985, *Astronomical Journal* **90**, 1400.

Postman, M., Geller, M.J., and Huchra, J.P., 1988, *Astronomical Journal* **95**, 88.

Rowan–Robinson, M., Walker, D., Chester, T., Soifer, T., and Fairclough, J., 1986, *Monthly Notices of the Royal astronomical Society* **219**, 273.

Rubin, V.C., Ford, W.K., and Rubin, J.S., 1973, *Astrophysical Journal (Letters)* **183**, L111.

Sandage, A., 1961, *Astrophysical Journal* **133**, 355.

Scaramella *et al.*, 1989, in preparation.

Seldner, M., Peebles, P.J.E., 1977, *Astrophysical Journal (Letters)* **215**, L1.

Shandarin, S.F., and Zel'dovich, Ya.B., 1983, *Comments Astrophys.* **10**, 33.

Shane, C.D., and Wirtanen, C.A., 1967, *Pub.Lick.Obs* **22**, 1.

Shanks, T., Stevenson, P.R.F., and Fong, R., 1984, *Monthly Notices of the Royal astronomical Society* **206**, 767.

Shaver, P.A., 1987, *Nature* **326**, 773.

Starobinsky, A.A., 1988, preprint.

Stauffer, D., 1979, *Physics Reports* **54**, 2.

Strauss, M.A., and Davis, M., 1988, *"Large Scale Motions in the Universe,"*, Proceedings of the Pontificial Academy of Science Study Week # 27, in press.

Struble, M.A., and Rood, H.J., 1987, *Ap.J.Suppl.Series* **63**, 555.

Szalay, A.S., 1987, in *"The Large Scale Structure of the Universe"*, Saas–Fee course, in press.

Tamman, G.A., and Sandage, A., 1985, *Astrophysical Journal* **294**, 81.

Tully, R.B., 1986, *Astrophysical Journal* **303**, 25.

Tully, R.B., 1987, *Astrophysical Journal* **323**, 1.

Tully, R.B., 1988, in *"Large Scale Structure and Motions in the Universe,"*, Mardirossian, F., *et al.*eds., D.Reidel Pub. Co.

Vettolani, G., Baiesi–Pillastrini, G., Scaramella, R., Zamorani, G., and Chincarini, G., 1988, in *"Large Scale Structure and Motions in the Universe,"*, Mardirossian, F., *et al.*eds., D.Reidel Pub. Co.

Villumsen, J.V., and Davis, M., 1986, *Astrophysical Journal* **308**, 499.

Villumsen, J.V., and Strauss, M.A., 1987, *Astrophysical Journal* **322**, 37.

Vittorio, N., 1988, in *"Large Scale Structure and Motions in the Universe,"*, Mardirossian, F., *et al.*eds., D.Reidel Pub. Co.

Vittorio, N., Juszkiewicz, R., and Davis, M., 1986, *Nature* **323**,, 132.

Yahil, A., Walker, D., and Rowan–Robinson, M., 1986, *Astrophysical Journal (Letters)* **301**, L1.

Weinberg, S., 1972, *"Gravitation and Cosmology"*, New York: Wiley.

Zwicky, F., Herzog, E., Wild, P., Karpowicz, M., Kowal, C.T., 1961-1968, *"Catalog of Galaxies and Clusters, 6 Volumes,"*, Pasadena: CALTECH.